WSRC-TR-96-0037

Groundwater Flow and Tritium Migration from the SRS Old Burial Ground to Four Mile Branch

by

G. P. Flach

Westinghouse Savannah River Company
Savannah River Site
Aiken, South Carolina 29808

DOE Contract No. **DE-AC09-89SR18035**

WSRC-TR-96-0037

Groundwater Flow and Tritium Migration from the SRS Old Burial Ground to Fourmile Branch (U)

G. P. Flach, L. L. Hamm, M. K. Harris, P. A. Thayer, J. S. Haselow and A. D. Smits

Westinghouse Savannah River Company
Savannah River Site
Aiken, SC 29808

SAFETY • RESPONSIBILITY • SECURITY
SRS
SAVANNAH RIVER SITE

DISCLAIMER

WSRC-TR-96-0037

Groundwater Flow and Tritium Migration from the SRS Old Burial Ground to Fourmile Branch (U)

G. P. Flach, L. L. Hamm, M. K. Harris, P. A. Thayer, J. S. Haselow and A. D. Smits

Publication Date: April, 1996

Westinghouse Savannah River Company
Savannah River Site
Aiken, SC 29808

Groundwater Flow and Tritium Migration from the SRS Old Burial Ground to Fourmile Branch (U)

Authentication and Approvals:

G. P. Flach, Author — 4/3/96 Date

W. R. Sadler, Technical Reviewer — 4-3-96 Date

D. B. Moore-Shedrow, Manager, Environmental Sciences Section — 5/6/96 Date

Executive Summary

The objectives of this investigation are twofold. The initial goal is to devise and demonstrate a technique for directly incorporating fine-scale lithologic data into heterogeneous hydraulic conductivity fields, for improved groundwater flow and contaminant transport model accuracy. The ultimate goal is to rigorously simulate past and future tritium migration from the SRS Old Burial Ground towards Fourmile Branch, to better understand the effects of various remediation alternatives such as no action and capping.

Large-scale variability in hydraulic conductivity is usually the main influence on field-scale groundwater flow patterns and dispersive transport, following the relative locations of recharge and discharge areas. Incorporating realistic hydraulic conductivity heterogeneity into flow and transport models is paramount to accurate simulations, particularly for contaminant migration. Sediment lithologic descriptions and geophysical logs typically offer finer spatial resolution, and therefore more potential information about heterogeneity, than other site characterization data.

In this study, a technique for generating a fine-scale, heterogeneous, three-dimensional hydraulic conductivity field from sediment lithologic descriptions is presented. The approach involves creating a three-dimensional, fine-scale representation of mud (silt + clay) fraction using a "stratified" interpolation algorithm. Mud fraction is then translated into horizontal and vertical conductivity using direct correlations derived from measured data and inverse groundwater flow modeling. Lastly, the fine-scale conductivity fields are averaged to create a coarser grid for use in groundwater flow and transport modeling.

The approach is demonstrated using a variably-saturated, finite-element groundwater flow model of the SRS Old Burial Ground. For this application, the technique improves estimates of large-scale flow patterns and dispersive transport, compared to a conventional approach for generating conductivity fields. The conductivity fields mimic actual lithologic data providing a more realistic picture of subsurface heterogeneity. Field-observed, preferential pathways for contaminant migration are replicated in the simulations without the need to artificially create zones of high conductivity.

In addition, a detailed, three-dimensional contaminant transport model of tritium migration from the Old Burial Ground to Fourmile Branch is developed. The transport model uses the groundwater velocity field from the flow model, and a detailed tritium source term. The tritium source varies spatially and temporally, and is reconstructed from burial and operations

records. The model rigorously tracks and accounts for all tritium from burial through ultimate discharge to Fourmile Branch or decay. Transport simulations reproduce historical tritium discharges to Fourmile Branch and provide a more reliable forecast of future migration compared to previous analyses.

The total amount of tritium buried in the Old Burial Ground from approximately 1955 through 1972 is estimated to be 288 grams or 2.8 million Curies (decay-uncorrected). As of 1995, we estimate that 49% of this amount has decayed within waste forms, 45% has been released to the vadose zone, and 6% remains in waste forms. The estimated peak release rate to the vadose zone occurred in 1961 and has declined to 4% of the maximum in 1995. Spent melt crucibles appear to release tritium to the vadose zone at a much higher rate than other waste forms, on average. In the context of a first-order leaching and decay model, the leaching constant for spent-melts is about 0.341 yr^{-1} compared to 0.029 yr^{-1} for other waste forms, on average. Overall, 61% of the tritium inventory recorded in the COBRA database is buried in the west end of the Old Burial Ground and 39% in the east end. However, 97% of the spent melts lie in the east end.

The peak amount of tritium in the groundwater likely occurred in about 1972 (600,000 Ci) and has declined to 41% of this maximum in 1995. The tritium flux to Fourmile Branch is estimated to have peaked at about 4500 Ci per year in 1992 (see figure below). A significant decline is expected in the near future without remediation. Simulated tritium plumes indicate that the source of tritium discharge to Fourmile Branch to-date is entirely from sources buried in the west end of the burial ground. The overall behavior of the predicted plumes is reasonably consistent with monitoring data.

The effects of capping the Old Burial Ground with a hypothetical, very low permeability cover are also shown in the figure. Code simulations indicate that tritium discharge to Fourmile Branch will be reduced by no more than about 300 Curies per year compared to uncapped conditions. The effect is small compared to the present discharge rate of about 4500 Curies per year. The reason is that most of the tritium originally present in solid radioactive waste burials has either decayed or migrated to groundwater below the water table. Tritium already in the groundwater is largely unaffected by capping.

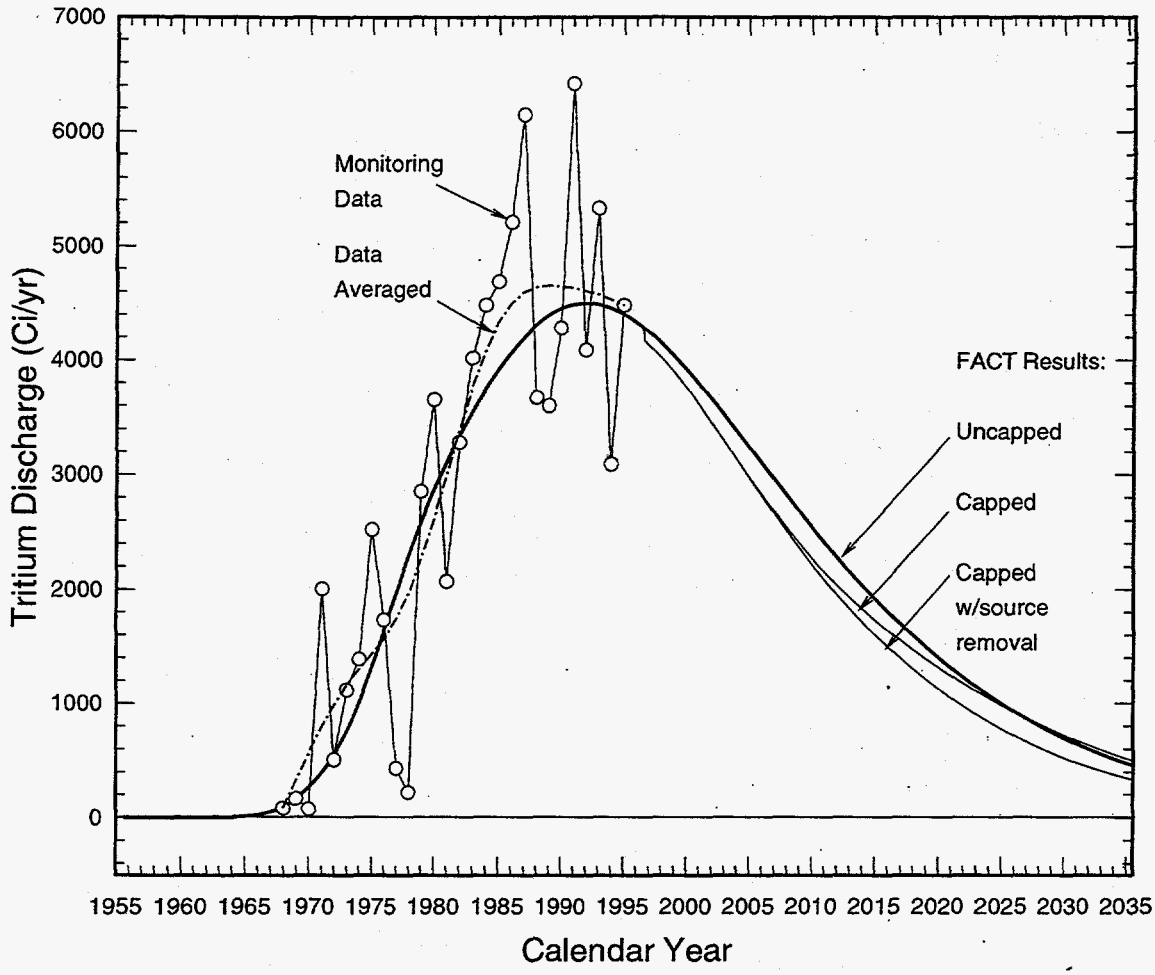
Tritium Discharge (Ci/yr)
7000
6000
5000
4000
3000
2000
1000
0
Monitoring
Data
Data
Averaged
FACT Results:
Uncapped
Capped
Capped
w/source
removal
1955 1960 1965 1970 1975 1980 1985 1990 1995 2000 2005 2010 2015 2020 2025 2030 2035
Calendar Year

Contents

List of Figures

List of Tables

Introduction

The objectives of this investigation are twofold. The initial goal is to devise and demonstrate a technique for directly incorporating fine-scale lithologic data into heterogeneous hydraulic conductivity fields, for improved groundwater flow and contaminant transport model accuracy. The ultimate goal is to rigorously simulate past and future tritium migration from the SRS Old Burial Ground towards Fourmile Branch, in order to better understand the effects of various remediation alternatives such as no action and capping.

The first phase of the project involves groundwater flow simulation using a fine-scale heterogeneous conductivity field, and is a feasibility study. Based on the success of the initial phase, tritium migration from the Old Burial Ground is then simulated in a second phase, using the groundwater flow field from the first phase.

Characterizing hydrogeologic heterogeneity using lithologic data

Groundwater flow and contaminant transport can be affected by many physical, chemical and microbiological factors. After the relative locations of recharge and discharge areas, large-scale variability in hydraulic conductivity is the dominant influence on field-scale groundwater flow patterns and dispersive transport, with other factors introducing second-order effects (Brusseau, 1994). Incorporating hydraulic conductivity heterogeneity into flow and transport models is paramount to accurate simulations in most situations, particularly for contaminant migration. For example, Poeter and Gaylord (1990) show how large-scale aquifer heterogeneity can influence, and in some cases dominate, contaminant transport at the DOE Hanford site through a series of computer simulations. They illustrate how a small but continuous geologic feature having one order magnitude higher conductivity than the surrounding media can have a dramatic effect on contaminant transport behavior (i.e., greatly reduced transport times due to preferential pathways for groundwater flow).

Sediment lithologic descriptions and down-hole geophysical logs offer finer spatial resolution, and therefore more potential information about heterogeneity, than most other site characterization data. However, these data do not provide direct information about hydrogeologic properties and are viewed as "soft" hydrogeologic information. The emergence of powerful computing resources has enabled the routine use of spatially-dense, three-dimensional (3D) "soft" hydrogeologic data in 3D flow and transport models. Methods for supplementing "hard" hydrogeologic data (e.g., pumping tests,

slug tests, laboratory conductivity data), conventionally used to develop flow and transport models, with spatially-dense, 3D "soft" hydrogeologic data are a focus of this study. The integration of hard and soft data should reduce model uncertainty and the amount of field-scale hydrogeologic data required, because the available data is more fully utilized.

The SRS Old Burial Ground was selected as the waste site for development of a non-traditional groundwater flow and transport model that can guide ongoing RCRA and CERCLA surface and groundwater investigations (Fig. 1). The burial ground received solid radioactive and hazardous waste from approximately 1952 to 1972. Primary groundwater contaminants include tritium, trichloroethylene (TCE) and tetrachloroethylene (PCE). The area is undergoing intense hydrogeological characterization for RCRA and CERCLA investigations (Westinghouse Savannah River Co., 1995). Hydrogeological characterization indicates that contaminant plumes emanating from the burial ground are migrating primarily to the south toward Fourmile Branch within the Upper Three Runs aquifer (Fig. 2). Although contaminant transport takes place mainly within this single hydrostratigraphic unit, the aquifer exhibits considerable field-scale heterogeneity, as indicated by a wide-ranging lithology and physical characteristics depicted in Figure 3. This heterogeneity and the present site focus on contaminant transport provide strong motivation for applying a technique that incorporates spatially-dense, 3D, "soft" hydrogeologic data into model conductivity fields.

Lithologic foot-by-foot descriptions of continuous drill core from 135 boreholes are available in the vicinity of the Old Burial Ground (Fig. 1). The fine vertical resolution of these data provide a great deal of information about aquifer heterogeneity. Tritium contamination provides an ideal tracer for assessment of the methodology (tritium is a conservative and unretarded contaminant). Three decades of tritium monitoring data are available in the form of groundwater concentrations and discharge rates to Fourmile Branch.

Simulating past and future Old Burial Ground tritium migration

Effective assessment of various remediation alternatives requires the capability of accurately and rigorously forecasting future tritium releases to Fourmile Branch. Existing models and analyses do not fully provide this capability due to deficiencies in modeling the source of tritium.

GeoTrans (1992) divided the Old Burial Ground into four zones, and within each zone applied a constant mass flux to the water table from 1952 to 1990. After 1990 the source was assumed to decay and the flux declined accordingly. The initial mass flux was derived by multiplying the maximum observed concentration in point of compliance (POC) wells over 15 quarters by the prevailing recharge rate. The assumed source results in grossly

underestimated forecasts of tritium discharge rates to Fourmile Branch. For example, the predicted 1994 release to Fourmile Branch is only 13 Curies, two orders of magnitude lower than the monitoring data (3090 Curies; Arnett, et al., 1995). The effects of capping or other remedial alternatives were not assessed.

Looney et al. (1993) observed that annual Old Burial Ground tritium releases to Fourmile Branch between 1982 and 1992 were approximately constant with an average value of about 4500 Curies. They postulated that annual discharges would remain at about 4500 Ci until at least the year 2010. The basis for this estimate appears to be an assumption that the roughly constant annual discharges are the result of a steady flux to the water table from the burial ground vadose zone. In a follow-up study, Ref. 6 estimated the average annual tritium release since 1984 to be 5300 Ci and the travel time between the burial ground and outcrop point to be 10 years. They assumed the relatively constant discharge rate to be the result of a constant tritium flux to the water table. Capping was predicted to essentially eliminate tritium releases to Fourmile Branch after 10 years had elapsed. Relative to the earlier forecast for no-action (4500 Ci/yr.), capping was therefore predicted to have a large impact. Ref. 2 supported this prediction with an 87% tritium flux reduction as a result of capping the Old Burial Ground. However, they did not predict tritium releases to Fourmile Branch with or without capping. The main weakness of these studies is the assumption of a constant tritium flux to the water table. More likely, leaching and radioactive decay continually deplete the source and result in a decreasing flux to the water table with time (burials ceased in 1972).

A detailed reconstruction of tritium burials and fine-scale, three-dimensional, finite-element modeling are performed in the present study. By explicitly modeling the tritium inventory and associated waste release mechanisms, significantly improved and defensible forecasts are achieved for evaluating remedial alternatives.

Report organization

The remainder of this report, 1) summarizes the lithologic, hydrogeologic, topographic and hydrologic data used to construct a groundwater flow model of the Old Burial Ground, 2) details the development of the Old Burial Ground flow model through incorporation of detailed lithologic data, 3) develops a detailed tritium source model from burial records, operational history, and lysimeter tests, 4) summarizes tritium monitoring data, and 5) develops a transport model simulating past and future tritium migration from the Old Burial Ground to Fourmile Branch for no remedial action and two bounding capping scenarios.

Geology

The study area is located in the Upper Atlantic Coastal Plain physiographic province in southwestern South Carolina (Fig. 1). The SRS is underlain by a southeast-dipping wedge of unconsolidated and consolidated sediment consisting of sand, mud, limestone, and gravel, which range in age from early Late Cretaceous (Cenomanian) to Holocene (Fallaw and Price, 1995). This study involves the Tertiary-aged sediment, principally the Eocene to Miocene sequence (Fig. 2). The Gordon aquifer, the Gordon confining unit and the Upper Three Runs aquifer are the hydrostratigraphic units of interest (Fig. 2).

The Gordon aquifer consists of unconsolidated sand and clayey sand of the Congaree Formation and, where present, the sandy parts of the underlying Williamsburg Formation. The sand is yellowish to grayish orange in color and is subrounded to well-rounded, moderately to poorly sorted, and medium to coarse-grained. The Gordon confining unit separates the Gordon and Upper Three Runs aquifers and is lithostratigraphically equivalent to the Warley Hill Formation. This unit is composed of fine-grained, silty and clayey sand, sandy clay and clay. The clay is stiff to hard and sometimes fissile. Zones of silica-cemented sand and clay, and calcareous sediment are common.

The Upper Three Runs aquifer includes all sediment from the ground surface to the top of the Gordon confining unit. Lithostratigraphically, the Upper Three Runs aquifer includes the Upland unit, Tobacco Road Sand, Dry Branch Formation, and Santee Formation (Fig. 2). The Upper Three Runs aquifer is divided by the "tan clay" confining zone into a "lower" aquifer zone and "upper" aquifer zone. The "lower" aquifer zone consists of a variety of lithologies including terrigenous sand and clay, calcareous skeletal sand, and sandy limestone. The "tan clay" confining zone contains light-yellowish tan to orange clay and sandy clay interbedded with clayey sand and sand. The "upper" aquifer zone is characterized by sand and clayey sand with minor intercalated clay layers. Gravelly layers are common.

Lithologic data

Data from detailed, foot-by-foot descriptions of continuous drill core from 84 boreholes are utilized in this study to define hydrologic properties. Figure 1 shows the areal distribution of the data in relation to the burial ground and Table 1 provides a listing. The core descriptions include data on core recovery; degree of induration; color; sedimentary structures; volume percent terrigenous gravel, sand, and mud; maximum and modal size of the terrigenous fraction; volume percent carbonate gravel, sand, and mud; volume percent cement; volume percent total carbonate sediment; sediment/rock name; grain sorting; volume percent porosity and dominant

type; fossil types; and volume percent accessory constituents, including muscovite, glauconite, lignite, sulfides, and heavy minerals (Ref. 9). Rock/sediment name is deduced from down-hole geophysical logs for intervals of no recovery. The core description for OFS-3SB is provided in the appendix as a typical example (Table A1). From the overall core description, volume-percent terrigenous mud data are used to generate 3D conductivity fields.

For intervals of no core recovery, mud fraction values are defined as part of this investigation for sand (SD), clayey sand (CLSD), sandy clay (SDCL) and clay (CL), based on a statistical analysis of the intervals for which core was recovered. Mud content is first estimated based on gamma ray response (i.e., no recovery intervals are designated SD, CLSD, SDCL or CL). The cores listed in Table 2 are then used to generate a probability distribution function for mud content as shown in Figure 4. Table 3 lists the average mud fraction within the mud fraction ranges 0-25% (SD), 25-50% (CLSD), 50-75% (SDCL) and 75-100% (CL) for the distribution shown in Figure 4. Note that the averages differ somewhat from the midpoints of the intervals. The values in Table 3 define mud fraction in no recovery intervals.

At least 135 core descriptions were available within the General Separations Area at the beginning of the study. These included the 127 cores listed in Ref. 8 and recent cores OFS-2SB through OFS-5SB, BGO-3A and BGO-51AA. Core descriptions known to be of good quality are listed in Table 1. Of these, 84 were used to grid mud fraction as indicated in the table. Those not used were too distant from the Old Burial Ground or not available in electronic form. Note that 30 cores lie within the groundwater flow model domain.

Hydrostratigraphic unit boundaries

Hydrostratigraphic surfaces are used to define the vertical discretization of the finite-element mesh and to compute the average properties of a unit. Ref. 8 produced an extensive series of hydrostratigraphic maps of the General Separations Area. The hydrostratigraphic unit boundaries or "picks" contained in Ref. 8 are adopted for the present study and listed in Table 4.

Hydrostratigraphic surfaces in this study are created by triangulating the scattered data in Table 4 using the optimizing algorithm of Renka (1984) and choosing a linear basis function for each triangle. The two-dimensional interpolated surface honors each hydrostratigraphic pick and is continuous, but its derivatives are generally discontinuous along triangle edges and corners. Higher order basis functions, up to fifth order, were tested. Due to the irregularly distributed locations of the data, linear basis functions produce the best overall results from a physical perspective. The structure contour

map for the top of the "tan clay" confining zone is presented in Figure 5; Figure 6 shows the thickness of the "tan clay" confining zone. The top of the "tan clay" confining zone appears to crop out near the confluence of the F-area outfall and Fourmile Branch based on the elevations of these features (dots in Fig. 5). Analogous plots are presented in Figures 7 and 8 for the Gordon confining unit. The structure contour map of the top of the Meyers Branch confining system is presented in Figure 9.

Topography

Ground elevations are available from U. S. Geological Survey Digital Elevation Model (DEM) data (U. S. Geological Survey, 1993a) and site topographic maps (Map 3302 and Environmental Restoration Dept. drawing GB0599). The Old Burial Ground lies within the New Ellenton SW 7.5-minute series quadrangle. The associated DEM file contains ground elevation data in feet above mean sea level in Universal Transverse Mercator (UTM) coordinates on a uniform 30 meter by 30 meter grid. The data are transformed to site coordinates as follows:

- DEM import: Use Earthvision® v.1.2 (Dynamics Graphics Inc.) to import the USGS file into an EarthVision® binary 2D grid file.
- Grid export: Using the ev_export module of Earthvision®, create an ASCII file of columnar (x,y,z) data.
- UTM to geographic coordinates transformation: Use Earthvision® to convert the (x,y) data from UTM coordinates to geographic coordinates (latitude-longitude).
- Geographic to site coordinates transformation: Use the SRPCOOR algorithm (Looney et al., 1987b) to convert the (x,y) data from geographic to site coordinates.

Ground elevation is used to define the top surface of the finite-element mesh and thereby the head elevations at which surface drainage occurs. Therefore, accurate topography is especially important at seepage faces and stream channels. Interpolation of DEM data that straddle a stream channel typically results in an over-estimated elevation at the stream. To remedy this problem, the DEM data are augmented with (x,y,z) stream coordinates digitized from site topographical maps to ensure the surface elevation grid is consistent with stream elevations. Stream coordinates and elevations for Fourmile Branch are taken from Map 3302 using the digitizer module of Earthvision®. Because the map contour interval is 2 feet, stream elevations are available in 2 foot increments. Elevations for stream coordinates not on a contour line are defined by linear interpolation. Data for the F-area old and

new outfalls are taken from Environmental Restoration Department drawing GB0599, which has a one foot contour interval. Again, elevations for stream coordinates not on a contour line are defined by linear interpolation. Stream elevation data resulting from this process are given in the appendix (Table A2).

A two-dimensional surface defining ground elevation in SRS site coordinates is created by approximating the scattered data using the minimum tension gridding algorithm implemented in EarthVision® v2.0. Figure 10 illustrates the resulting contour plot. The grid resolution is 100 feet by 100 feet, which is approximately the spacing of the DEM data.

Hydrologic data

Hydrologic data utilized for constructing the Old Burial Ground flow model are presented in this section. The hydrologic data needed include hydraulic conductivities, effective porosity, specific storage, soil characteristic curves, recharge, surface discharge and hydraulic head.

Hydraulic properties

Aadland et al. (1995) summarize the results of slug and pumping tests performed within the General Separations Area. Laboratory measurements of horizontal and vertical conductivity for sediments at the SRS are available from a number of sources (Bledsoe et al., 1990; Riha, 1993; Kegley et al., 1994; Aadland et al., 1995; Ref. 1). The conductivity data most useful to this study are those having an accompanying mud fraction measurement (e.g., sieve data). These data are listed in Table A3 (appendix) and used to correlate horizontal and vertical conductivities to mud fraction.

Effective porosity measurements for SRS soils range from 10 to 30% (Looney et al., 1987a) for the range of sand to clay, respectively. Looney et al. (1987a) recommend an average value of 20%. Ref. 3 assumed a 20% effective porosity for aquifers and 30% for aquitards in their groundwater flow model of the General Separations Area.

Specific storage has no effect on steady-state groundwater flow, the focus of this study, but is required code input. Specific storage is defined as $S_s = \rho g(\alpha + \eta\beta)$ where α is soil compressibility, η is porosity and β is fluid compressibility. Based on Freeze and Cherry (1979, Table 2.5), a soil compressibility of 10^{-8} m^2/N may be assumed for sand and 10^{-7} m^2/N for clay. The resulting specific storages become 3×10^{-5} ft^{-1} for sand and 3×10^{-4} ft^{-1} for clay.

Soil characteristic curves for relative permeability and water retention are needed to model unsaturated groundwater flow above the water table. A small set of water retention data from nearby M-area is available for defining the water retention relationship (O'Brien and Gere Engineers, Inc., 1991). The data for M-area sediment samples composed mainly of sand and gravel are plotted in Figure 11; Figure 12 shows the data for clayey sediment samples. Relative permeability data were not acquired by O'Brien and Gere Engineers, Inc. (1991). During technical review of this report, we became aware of soil property data for General Separations Area sediment samples (Ref. 10). These data are not used in the present study.

Groundwater recharge and discharge

Looney et al. (1987a) recommend an average annual recharge rate of 15 in/yr for the SRS. This value is supported by Parizek and Root (1986).

Stream baseflow can be estimated from U. S. Geological Survey monitoring station data at the locations shown schematically in Figure 13. Assuming runoff is negligible during low flow periods, baseflow between stations is the difference between station flow rates during these periods. Table 5 lists the stream flow rates for the date of the minimum flow rate at station 3 for the water year shown (U. S. Geological Survey, 1980-1993). Between stations 3 and 4, the difference in average flow rate is 1.22 ft^3/s or 2.71×10^{-4} ft^2/s over the 4500 ft distance between stations. However, the uncertainty in this estimate is very large; the sample standard deviation is 1.1 ft^3/s. The difference in average flow rates between stations 3 and 4 for all times (not just low flow) from water years 1973 through 1992 is 0.92 ft^3/s for a linear rate of 2.04×10^{-4} ft^2/s. The uncertainty in this estimate is not stated by the U. S. Geological Survey (1980-1993) but is relatively small because many years of daily values have been averaged. This latter result includes the effects of runoff in addition to baseflow, and yet is smaller than the previous estimate based on minimum flows. This nonphysical relationship is presumably a reflection of the large uncertainty in the 1.22 ft^3/s value that must be too high. Actual baseflow should not exceed 0.92 ft^3/s between stations 3 and 4.

Hydraulic head data and potentiometric surfaces

Well hydraulic head data and contour maps are needed to define boundary conditions and calibrate the groundwater flow model. Well inventory and field measurement data are available electronically from the Environmental Monitoring Section (EMS) database. The data are periodically published; for example see ESH-EMS-930261 "Environmental Protection Department's Well Inventory (U)" and ESH-EMS-930097 "The Savannah

River Site's Groundwater Monitoring Program; Second Quarter 1993 (U)". Well coordinates and screen top and bottom elevations are contained in the well inventory database. Head data are taken from the EMS field measurement database. Head data from Burial Ground grid wells south of the Old Burial Ground taken in June 1994 are also available (Amidon, 1994a). The data are assigned to an aquifer unit based on the hydrostratigraphic picks summarized in the GSAWELLS.XLS file received from M. Amidon (1994b) (Ref. 8). Time-averaged well head data for the "upper" aquifer zone, "lower" aquifer zone and Gordon aquifers are tabulated in the appendix (Tables A4 through A6).

In the appendix, Tables A7 through A9 summarize the time-averaged data used to create head contour plots for the "upper" aquifer zone, "lower" aquifer zone and Gordon aquifers, respectively. Stream elevation data (Table A2) supplement well head data (Tables A4 through A6) wherever an aquifer zone or unit is exposed at the ground surface. Pseudo data were created for the "upper" and "lower" aquifer zones to correct deficiencies in the contour plots on the south side of Fourmile Branch which resulted from a lack of data in that region. Specifically, data were added on the south side of Fourmile Branch to raise hydraulic head to the point where the contour lines are approximately symmetric about the stream. Head contour plots created using EarthVision® are presented in Figures 14 through 16.

Groundwater flow model

Methods for generating a heterogeneous, 3D hydraulic conductivity field from estimated mud fraction (silt + clay sized material) are presented in this section. The techniques are then demonstrated for a finite-element groundwater flow model of the SRS Old Burial Ground. Model results are presented and discussed, and the methodology is assessed.

Methods

Figure 17 outlines the methodology used to generate heterogeneous hydraulic conductivity fields from lithologic descriptions. Mud fraction data are initially interpolated onto a 3D grid using an algorithm that preserves sharp vertical contrasts. The mud fraction grid is translated into horizontal (K_h) and vertical conductivity (K_v) fields using direct "correlations" of conductivity to mud fraction. Laboratory conductivity measurements on whole core and quantitative grain-size distribution data from sieve analyses are utilized as a guide for the development of the correlations. On the first pass, the correlations are based strictly on laboratory conductivity data. On subsequent passes, inverse flow modeling also influences the correlations through a feedback loop; that is, the correlations are adjusted to achieve better

flow model results when compared to hydraulic head data and other targets. The fine-scale conductivity fields are transferred to the coarser groundwater flow model grid through arithmetic (K_h) and harmonic (K_v) averaging. The process is discussed below in more detail. Figure 18 illustrates the process for creating the overall groundwater flow model, including the steps shown in Figure 17.

Three-dimensional interpolation of mud fraction data

Boman et al. (1995) have demonstrated that relatively simple interpolation concepts can be used to successfully generate heterogeneous 3D conductivity fields for flow and transport models. They employed what can be termed successive inverse distance weighting (IDW) interpolation by horizontal layer, or "stratified IDW" in their terminology. The idea is to conceptually divide the subsurface into horizontal layers of uniform thickness. These layers are arbitrary and do not necessarily conform to formation boundaries or other geologic features. Within each layer, two-dimensional inverse distance weighting is independently applied using only the subset of borehole data lying within that layer. With this stratified IDW approach, smoothing occurs in the horizontal plane while sharp vertical contrasts (if present) are preserved.

A similar effect can be achieved using the minimum-tension spline interpolation algorithm implemented in the EarthVision® software package (Version 2.0, Dynamics Graphics, Inc., Alameda, CA), by selecting a very small "vertical influence factor." The vertical influence factor is applied to data lying above and below the horizontal plane passing through the interpolation node of interest. By choosing a very small value, almost no weight is given to data above or below each interpolation node relative to data in the horizontal plane of that node. EarthVision® is chosen to generate a 3D mud fraction field from scattered core lithologic data.

Mud fraction values from the 84 boreholes depicted in Figure 1 are interpolated onto a $23 \times 23 \times 251$ grid of dimensions 11,000 ft × 11,000 ft × 250 ft. The areal dimensions correspond to the solid line box in Figure 1. The areal resolution is uniformly set to 500 ft while the vertical resolution is uniformly set to 1 ft, the same as the raw data. In all, 12,626 mud fraction data points are employed. A vertical influence factor of 0.01 is selected to preserve vertical contrasts. Interpolated values of mud fraction are constrained to fall within the physical range of 0 to 1 to remedy under- and over-shoots between or beyond data. In a few locations lacking measured data, pseudo-data are added as control points to minimize extrapolation errors. Figure 19 illustrates the portion of the resulting 3D mud fraction representation contained within the flow model areal domain (dashed box in Figure 1) and cropped by the ground surface. The lithologic heterogeneity of the subsurface

hydrostratigraphic units is easily recognized and corresponds with hand-contoured lithofacies maps and cross-sections (e.g., Fig. 3) (Ref. 8). Note that the interpolation process preserves horizontal stratification of the sediments.

Correlation of mud fraction to hydrologic properties

Laboratory measurements of horizontal and vertical conductivity for sediments at the SRS (Table A3) are plotted as a function of mud fraction in Figures 20 and 21. The data show an overall trend of decreasing conductivity with increasing mud percentage, but exhibit a great deal of scatter. Estimated mud fractions are available for the entire length of all cores, whereas, sieve data are available primarily for transmissive well screen zones (10 to 30 ft). In order to utilize the most data, a direct correlation between conductivity and estimated mud fraction is chosen instead of a grain-size distribution data correlation. Kegley et al. (1994) and Lahm et al. (1995) demonstrated success using this approach. The initial conductivity-mud fraction correlations are developed based solely on the laboratory conductivity data. However, the resulting flow simulation does not generally match hydraulic head, average recharge and stream gain targets adequately. As such, the correlations are iteratively perturbed to improve flow results while maintaining consistency with the laboratory data. The stair-step functions shown in Figures 20 and 21 are the final outcome of this iterative flow model calibration process.

A stair-step functional form is chosen for two reasons. The interpolated mud fraction field shown in Figure 19 contains numerous regions where under- and over-shoots in the initial fit have been clipped by EarthVision® to lie within the specified physical range of zero to one. These initial under- and over-shoots are located between sparsely distributed data and at the fringes of the data (i.e., extrapolation errors). As a result the interpolated mud fraction field contains an artificially large number of values at or near zero and one. The flat portions of the stair-step functions tend to alleviate this problem by assigning the same conductivity to all mud fraction values in the vicinity of zero and one, respectively. Secondly, the stair-step functions provide the analyst very simple and direct control over conductivity values during model calibration when compared to other potential functional forms. A disadvantage of the correlations is the presence of unrealistically abrupt changes in conductivity. This deficiency is not serious however, because the abruptness is effectively smoothed out when the conductivity fields are translated to the coarser flow model grid through the averaging process discussed below.

In order to reduce the degrees of freedom during calibration to a reasonable number, restrictions are invoked early in the process. For the SRS burial ground application, the correlations were constrained such that the ratio of horizontal to vertical conductivity is three. This conductivity

anisotropy ratio is suggested by the laboratory data of Bledsoe et al. (1990). Also, the junctions between steps of 0.1, 0.25, and 0.50 were held constant during final calibration. These choices yield four independent horizontal conductivity parameters spanning the ranges of 0.0 to 0.1, 0.1 to 0.25, 0.25 to 0.50, and 0.50 to 1.0. The flow model calibration process in this study is analogous to that performed for a conventional "layer cake" model, with horizontal conductivities within mud fraction ranges taking the place of hydrostratigraphic unit conductivities (or zonal conductivities within a unit).

Initially, properties were assigned throughout the model domain based solely on mud fraction, without regard to hydrostratigraphic unit or zone or depth of the sediments. However, preliminary groundwater flow simulations exhibited insufficient head differences across the Gordon confining unit in comparison to field data. Also, this approach does not account for known variations in properties with depth for the same mud fraction. For example, sand in the Gordon aquifer tends to be coarser-grained than in the Upper Three Runs aquifer, and therefore more permeable (Ref. 8).

The three-dimensional mud fraction representation presented in Figure 19 apparently does not have enough horizontal continuity in the collection of clay layers at the elevation of the Gordon confining unit to produce a competent confining unit. Some of the core locations shown in Figure 1 do not have data at the depth of the Gordon confining unit. The areal data density may be insufficient to properly connect clay layers between cores. Accounting for dip would probably result in better continuity. Because fitting was done with a one foot vertical resolution, the dip would have to be known accurately to achieve a significantly better mud fraction representation. Another contributing factor may be that clay in the Gordon confining unit has a lower conductivity than clay at other depths. This idea is suggested by the Ref. 3 model. In the Ref. 3 model encompassing the F- and H-area seepage basins, the Gordon confining unit is about an order of magnitude less conductive than the "tan clay" confining zone. Assuming the average mud fraction is similar for both confining units, the Gordon confining unit would have a lower conductivity.

To accommodate these deficiencies, a hybrid approach is taken. Above the Gordon confining unit, conductivities are assigned by lithology (mud fraction). Below the top of the Gordon confining unit, conductivities are assigned by hydrostratigraphic unit (i.e. Gordon confining unit or Gordon aquifer). Porosity and specific storage are assigned by mud fraction everywhere. This approach accounts for property variation with depth by having separate functions above and below the top of the Gordon confining unit. Basically, detailed lithologic data is being employed in those areas where complex heterogeneities are known to exist, while the layered modeling approach is applied to areas suspected to be fairly uniform in the areal directions. It also compensates for insufficient continuity in Gordon

confining unit mud fraction by assigning properties by unit rather than mud fraction at that depth.

Code selection

FACT, a variably-saturated 3D finite-element flow and transport code developed by SRTC, is chosen for flow simulation. FACT is a derivative of the SAFT3D and VAM3DCG codes developed by HydroGeoLogic, Inc. (Huyakorn et al., 1991; Huyakorn and Panday, 1992). The code solves Richard's equations. FACT assumes the hydraulic conductivity tensor is aligned with the principle axes of the porous media and its diagonal values are specified at the element centroids. In this study the porous media is assumed to be isotropic in the two horizontal directions, but anisotropic with respect to its vertical direction.

Flow model grid

To demonstrate the methodology, a finite-element mesh is selected that differs in extent, orientation, and spatial resolution from that of the mud fraction grid generated above. The extent of the flow model and its orientation relative to the mud fraction grid are shown in Figure 1 (dashed versus solid boxes). The mesh is rotated clockwise by an angle of $\theta = 36.48°$ relative to SRS site coordinates. The origin of the model coordinate system is located at 74,150 N and 50,000 E in SRS site coordinates. The coordinate transformation from model coordinates (x,y) to site coordinates (N,E) is

$$N = -x\sin\theta + y\cos\theta + 74{,}150 \text{ ft} \quad (1a)$$

$$E = x\cos\theta + y\sin\theta + 50{,}000 \text{ ft} \quad (1b)$$

This domain captures the entire groundwater flow field from the Old Burial Ground to surface discharge at Fourmile Branch (Fig. 1), and aligns model boundaries with monitoring well clusters for increased boundary condition accuracy. The areal dimensions are 6760 ft × 5070 ft. Eight-noded rectangular "brick" elements, that are restricted to deformations only in the vertical direction, are used. The elemental dimensions in the areal extent are uniformly set to 130 ft per side. The top of the mesh conforms to the ground surface while the bottom of the mesh conforms to the top of the highly competent Meyers Branch confining system (Fig. 2). In addition, two of the intermediate elemental surfaces coincide with the top of the "tan clay" confining zone and the top of the Gordon confining unit, respectively. Mesh nodal elevations for these stratigraphic surfaces are computed using linear triangular interpolation, while bicubic spline interpolation is used for the topographic surface. Vertical mesh refinement between adjoining surfaces is

performed by quadratic vertical interpolation at each areal grid point. Element heights range from about 1 to 20 ft with an average value around 10 ft. The overall nodal dimensions of the flow grid are $53 \times 40 \times 30$ ($52 \times 39 \times 29$ elements). The selected flow grid is much coarser than the mud fraction grid in the vertical direction, but finer in the areal directions.

Transfer of hydrologic properties to flow model grid

The process for translating the 3D mud fraction grid shown in Figure 19 into "composite" elemental conductivity defined over the 3D flow grid involves three steps and the creation of a fine-scale intermediate grid. First, while maintaining the 0.3 m (1 ft) vertical resolution of the mud fraction grid, mud fraction values are interpolated onto an intermediate grid whose areal grid points coincide with the element areal centroids of the flow grid. A natural bicubic spline interpolation is performed for each horizontal layer, independently. In the next step, mud fraction values defined on the resulting fine-scale intermediate grid are translated into "local" horizontal and vertical conductivities using the correlations shown in Figures 20 and 21. In the final step, these local conductivities on the fine-scale intermediate grid are vertically averaged over each finite-element (typically ten fine-scale layers per element). Figure 22 depicts the multi-step process discussed above starting from the fine-scale grid. During this last stage, composite conductivities (horizontal and vertical) are computed based on appropriate averaging (arithmetic and harmonic, respectively) where the local conductivities are assumed to reflect horizontal layering of aquifer materials that extend over the entire areal extent of each element. For a given finite-element these composite (horizontal and vertical) conductivities are expressed by

$$K_h^{comp} = \frac{\sum_{i=ib}^{i=it} (K_h \xi \Delta z)_i}{\sum_{i=ib}^{i=it} (\xi \Delta z)_i} \qquad (2a)$$

$$K_v^{comp} = \frac{\sum_{i=ib}^{i=it} (\xi \Delta z)_i}{\sum_{i=ib}^{i=it} (\xi \Delta z / K_v)_i} \qquad (2b)$$

where

ib ≡ bottom fine-scale layer contained within element

$it \equiv$ top fine-scale layer contained within element

$\Delta z_i \equiv$ vertical height of i^{th} fine-scale layer

$\xi_i \equiv$ fraction of i^{th} fine-scale layer contained within element

$K_{hi} \equiv$ local horizontal conductivity of i^{th} fine-scale layer

$K_{vi} \equiv$ local vertical conductivity of i^{th} fine-scale layer

$K_h^{comp} \equiv$ composite horizontal conductivity of element

$K_v^{comp} \equiv$ composite vertical conductivity of element

The resulting horizontal and vertical conductivity fields are shown in Figures 23 and 24. In these figures, a wire-frame mesh outlines the finite-element flow grid and the finite-element centroidal conductivity values have been linearly interpolated. Both conductivity fields are highly heterogeneous in the upper part of the aquifer system. At the ground surface low conductivity zones in the top layer of elements in the upper far corner of each grid are defined in order to model low infiltration zones corresponding to industrial and capped areas.

Recharge and drain boundary conditions

The present methodology permits low permeability zones to crop out at the surface as shown in Figure 19 at several locations and reflected in Figures 23 and 24. These detailed features, together with a complex, *a priori* unknown seepline, make conventional manual specification of model recharge and drainage conditions a complicated and tedious process. Where low permeability zones crop out, a lower infiltration rate should be specified compared to the average recharge to prevent model hydraulic heads from significantly exceeding ground elevation. Physically, most rainfall runs off these low conductivity areas resulting in low infiltration and heads not exceeding ground elevation. Drain boundary conditions are needed wherever hydraulic head exceeds the ground elevation so that groundwater may properly discharge at the surface under these head conditions. Conversely, recharge boundary conditions should be specified wherever hydraulic head is below the ground surface. Because surface hydraulic heads are not generally known beforehand, a manual trial-and-error process is conventionally required to determine whether a drain or recharge boundary condition is appropriate, and if a recharge condition is needed, the appropriate local infiltration rate.

Huyakorn et al. (1986) implemented an automated process for selecting a drain versus recharge boundary condition following Neuman et al. (1974) and Rulon (1984). The procedure involves a Picard iteration strategy imbedded in the flow code that switches between boundary condition types and also reduces infiltration as a seepline is approached. With this method convergence difficulties may arise for complex terrain and additional computational overhead is required to update boundary conditions during the iteration process.

The deficiencies expressed above can be eliminated by combining the concepts of recharge and drainage into a single boundary condition. The basic idea is that locally the surface is either recharging or draining the subsurface, and there should be a continuous transition between these conditions. Infiltration should occur for negative pressure head (water level below the ground surface) and aquifer discharge should occur for positive pressure head. Also, to be consistent with the continuity needs of the Newton-Raphson iterative solver employed in FACT, the overall function representing this "combined" recharge/drain boundary condition should also be continuous in its first derivative.

Figure 25 presents a combined recharge/drain boundary condition that meets the above criteria. When the water level is well below the ground surface, recharge occurs at the maximum rate permitted locally through user specification. As the pressure head approaches zero, recharge is smoothly reduced to zero. For positive pressure head, the surface drains the aquifer at a rate proportional to the pressure head. To the left of the transition zone, the combined recharge/drain boundary condition is exactly the same as the conventional recharge boundary condition. To the right of the transition zone, the combined recharge/drain boundary condition is identical to a typical drain boundary condition. The transition zone reflects a non-linear region connecting two limiting linear boundary conditions. The mathematical formulation for this function, as shown in Figure 25, is

$$Q_c = \begin{cases} Q_R & \text{for} \quad \psi \le \frac{3}{2}\hat{\psi} \\ \frac{Q_R}{8}\left[7 - 2x - x^2\right] & \text{for} \quad \frac{3}{2}\hat{\psi} < \psi < \frac{1}{2}\hat{\psi} \\ -M_D\psi & \text{for} \quad \frac{1}{2}\hat{\psi} \le \psi \end{cases} \tag{3}$$

where

$$\psi = h - z_c \tag{4}$$

$$Q_R = A_D R_{max} \tag{5}$$

$$M_D \equiv A_D\left(\frac{K_v}{b}\right)_D \tag{6}$$

$$x \equiv 2\left(\frac{\hat{\psi} - \psi}{\hat{\psi}}\right) \tag{7}$$

$$\hat{\psi} \equiv -\frac{Q_R}{M_D} \tag{8}$$

and

$h \equiv$ hydraulic head

$z_c \equiv$ elevation of combination boundary condition

$Q_c \equiv$ volumetric source or sink from combined effects of recharge and drainage

$R_{max} \equiv$ maximum local recharge (17 in/year in this study)

$\psi \equiv$ pressure head

$A_D \equiv$ area available for recharge and drainage (geometric area)

$(K_v/b)_D \equiv$ leakance coefficient (18.2 yr^{-1} in this study)

Equation (3) represents a two parameter model requiring the specification of the maximum local recharge rate (R_{max}) and the surface leakance coefficient $(K/b)_D$. The level of ponding along a seepage face can be adjusted by varying the magnitude of the surface leakance coefficient. Equation (3) is applied at every node over the entire top surface of the flow model in the present study. Seepage faces are automatically established during the iterative solution of the non-linear flow and boundary condition equations.

Prescribed head and no flow boundary conditions

Hydraulic head boundary conditions are derived from the head contour maps presented in Figures 14 through 16. Head is prescribed over each of the four vertical faces of the flow mesh, except for the ground surface nodes to avoid a conflict with the recharge/drain boundary condition just described. First, the head in each aquifer is defined at each node along all four edges of the areal flow mesh. This step is performed using Figures 14 through 16 and bicubic spline interpolation. Then, the hydrostratigraphic surfaces presented in Figures 5 through 9 are used to assign a specific head value to each node

along the four vertical faces. For nodes residing completely within an aquifer (or aquifer zone), the head is assigned directly. For nodes within a confining unit, the head is interpolated between adjoining aquifer units and/or zones.

Monitoring wells indicate that groundwater flow through the burial ground starts at the east end and flows westward. Approaching the west end, the flow turns southward and discharges to the old F-area effluent ditch and Fourmile Branch near their confluence. The water table beneath the eastern end of the Old Burial Ground is relatively flat making it difficult to reproduce the known groundwater flow direction near the prescribed head boundaries in the model. No flow boundary conditions replace prescribed heads at selected "upper" aquifer zone nodes near the northeast corner of the mesh, to ensure westward flow at the east end of the burial ground. Specifically, these nodes are those on the east side with $j \geq 25$ and those along the north side with $i \geq 45$. Without these modifications, groundwater tends to flow out the northeast corner of the model domain in conflict with the monitoring data. Ideally, the boundaries of the model would extend well beyond the east end of the Old Burial Ground in order to reduce the detrimental near-field effects of prescribed head boundary conditions. However, the main focus of this study is the southwest corner tritium plume and creating a fine-scale conductivity field. Expanding the model while keeping the number of computational nodes fixed would result in a coarser mesh and compromise modeling of the southwest plume.

Soil characteristic curves

The van Genuchten (1980) models for soil characteristic curves have a relatively strong physical basis and have been widely used. The equations for water retention-capillary suction and relative permeability are

$$S_e = \frac{1}{\left[1+(-\alpha\psi)^{\frac{1}{1-m}}\right]^m} \tag{9}$$

$$k_r = S_e^{1/2}\left[1-\left(1-S_e^{\frac{1}{m}}\right)^m\right]^2 \tag{10}$$

where S_e is the effective saturation defined by

$$S_e = \frac{S_w - S_{wr}}{1-S_{wr}} \tag{11}$$

and

$\psi \equiv$ pressure head (negative in the unsaturated zone)

$k_r \equiv$ relative permeability

$S_w \equiv$ liquid saturation

$S_{wr} \equiv$ residual saturation (may be empirically determined)

$\alpha, m \equiv$ additional empirical parameters

Figures 11 and 12 show a fit of the M-area data of O'Brien and Gere Engineers, Inc. (1991) using the van Genuchten (1980) functional form. In Figure 11 for sandy samples, $S_{wr} = 0.15$, $\alpha = 3.68\ ft^{-1}$ and $m = 0.183$. For the clayey sample data in Figure 12, $S_{wr} = 0.614$, $\alpha = 1.28\ ft^{-1}$ and $m = 0.14$.

The van Genuchten form for water saturation as a function of capillary suction is continuous, but extremely abrupt at the transition between saturated and unsaturated conditions (Figures 11 and 12). This feature prevents or seriously hinders FACT code convergence to a reasonable head tolerance for this Old Burial Ground study. In addition, the relative permeability variation is also extremely abrupt and likewise contributes to convergence problems. As a remedy, the van Genuchten functional form for water retention is abandoned in favor of the less abrupt variation shown in Figures 11 and 12. Although the chosen function lacks the physical basis of the van Genuchten form, the widely scattered data are reasonably fit using this "pseudo-soil" property function. The equation defining the function is

$$S_w = S_{wr} + (1 - S_{wr})e^{\alpha\psi} \tag{12}$$

where

$S_w \equiv$ liquid saturation

$\psi \equiv$ capillary suction pressure (negative in unsaturated zone)

$S_{wr} \equiv$ residual saturation (0.4)

$\alpha \equiv$ empirical parameter ($0.07\ ft^{-1}$)

Likewise, the van Genuchten expression for relative permeability is discarded in favor of a less abrupt variation given by

$$k_r = S_e^3 \tag{13}$$

where S_e is as defined by equation (11) with $S_{wr} = 0$ (i.e. $S_e = S_w$). Equation (13) has been proposed by Fatt and Klikoff (1959) and Verma et al. (1985) (Pruess, 1987). Site specific data would be needed to assess its validity for the present study.

Results

FACT groundwater flow simulation results for the Old Burial Ground are shown in Figures 26 through 36. The results were generated from the optimal conductivity fields depicted in Figures 23 and 24 and other hydrologic properties summarized in Table 6. Figure 26 illustrates the 3D distribution of hydraulic head simulated by the flow model. Figures 27 through 29 show average hydraulic head within the "upper" aquifer zone, "lower" aquifer zone and Gordon aquifer, respectively. The root-mean-square residual between steady-state model and time-averaged measured hydraulic heads is 3.4 ft. Figures 30 through 32 illustrate head residuals in the "upper" aquifer zone, "lower" aquifer zone and Gordon aquifer, respectively. Table 7 presents summary statistics for each aquifer or aquifer zone. The appendix lists those wells inside the model domain which are used as targets (Table A10). Agreement in the Gordon aquifer is excellent. Residuals in the "upper" aquifer zone are increased, and show some spatial bias. Residuals in the central portion of the model tend to be low, and residuals in the northeast corner near the no flow boundaries are high. These biases are partly the result of an effort to achieve flow patterns more consistent with the conceptual model at the expense of higher head residuals, as discussed previously. The "lower" aquifer zone has an average head residual similar to the "upper" aquifer zone and also exhibits bias, especially in the vicinity of the H-area seepage basins and Fourmile Branch. Here the model head is low at the basin and high at Fourmile Branch.

Water saturation is shown in Figure 33 along the external faces of the mesh. A three-dimensional perspective was chosen to highlight the seepage face regions surrounding Fourmile Branch and the F-area outfall. The predicted seepline compares favorably with measured locations along Fourmile Branch.

The model recharge distribution is shown in Figure 34. Positive values represent infiltration while negative values represent drainage. The average recharge is 13.9 in/year, which is less than the specified local maximum of 17 in/year because of the presence of seepage faces. This value is close to the 15 in/year recommended by Looney et al. (1987a). Areas of low recharge can be seen near the F- and H-area seepage basins, because they were capped with low permeability materials. An area of low recharge can also be seen within the F-area separations complex due to the presence of engineered surfaces accounted for in the model.

The total surface discharge is 1.5 ft^3/s. The model domain contains about 5100 ft of Fourmile Branch and the perennial portion of the F-area outfall is about 1400 ft. Assuming 2.04×10^{-4} ft^2/s is a reasonable average linear rate based on monitoring data, baseflow does not exceed about 1.3 ft^3/s or 115,000 ft^3/day. Groundwater discharge along seepage faces goes towards both stream gain and evapotranspiration. Therefore, aquifer discharge should exceed stream gain and this is the case with the model.

Figure 35 shows 3D pathlines originating from the burial ground that have been projected onto a two-dimensional horizontal plane overlaying water saturation at the top surface. The pathlines start in the vadose zone at an elevation of 270 ft, corresponding to a burial depth of 20 ft or less. The seeplines surrounding Fourmile Branch conform closely to field-observed locations. As illustrated, groundwater pathlines originating from the burial ground converge into a preferred pathway that terminates at the old F-area effluent ditch, consistent with contaminant monitoring data. In addition, local convergence of pathlines is observed in Figure 35 indicating the presence of finer-scale preferred pathways. Figure 36 shows similar 3D pathlines projected onto the cross-section B-B' in Figure 35 with mud fraction as the background. This cross-section coincides with the preferred pathway for groundwater flow from the burial ground and highlights vertical flow patterns. The example pathlines reveal a complex flow field resulting from heterogeneities incorporated into the conductivity field. Figure 36 shows that contaminant migration from the burial ground can be expected to follow multiple distinct pathways within the same aquifer, corresponding to regions of low mud content.

In a parallel effort, a conventional "layer-cake" flow model was created by assigning a uniform conductivity to each hydrostratigraphic unit. Comparison of the models revealed two advantages of the heterogeneous model. First, the models produced different large-scale flow patterns, despite yielding a similar average hydraulic head residual. As shown in Figure 35 for the heterogeneous model, groundwater flows westward in the eastern portion of the burial ground and flows southward at the west end. Westward flow through the burial ground in the heterogeneous model is caused by high mud content beneath the east end of the burial ground. Contaminant monitoring at perimeter wells confirms this overall flow pattern. The conventional "layer cake" model could not be made to behave in a similar manner using uniform layer properties, and indicated that groundwater flow is southward throughout the entire burial ground. The desired overall flow pattern could be achieved with the layer cake model by adding sufficient spatial variation to unit properties during model calibration. However, this process may be time-consuming compared to generating heterogeneity directly from mud fraction data.

A second apparent benefit of the heterogeneous model is the presence of multiple parallel pathways available for contaminant transport, as noted above and shown in Figure 36. As discussed by Brusseau (1994) for example, contaminant dispersion is enhanced by aquifer heterogeneities at all scales. Heterogeneity produces a spatially varying velocity field that transports portions of the contaminant plume at different rates. Heterogeneity not explicitly incorporated into the flow and transport model must be accounted for through a separate mechanical dispersion term. The dispersivity value in this term is empirical and scale-dependent, and requires extensive monitoring data to define accurately. Fine-scale flow and transport models that capture as much aquifer heterogeneity as possible can reduce the magnitude and importance of the empirical dispersion term, leading to more accurate and reliable predictions. A direct, quantitative comparison of the conventional and heterogeneous models on this point was not possible, due to the significant differences in large-scale flow patterns between the models. That is, the large differences in advective behavior precluded a straightforward comparison of dispersive behavior. Qualitatively however, the heterogeneous model appeared to yield greater contaminant dispersion.

Assessment of methodology

The methodology presented here has proven effective in generating a heterogeneous conductivity field for an SRS burial ground flow and transport model. The conductivity fields mimic the actual lithologic data providing a more realistic picture of subsurface heterogeneity compared to traditional layered modeling approaches. The approach improves large-scale flow patterns and dispersive behavior compared to conventional methods. Field-observed, preferential pathways for contaminant migration are replicated in the model without the need to artificially create zones or channels of high conductivity. The concepts are general and can be applied to other sites. The resulting conductivity fields may be used with other finite-element or finite-difference groundwater codes. Nevertheless, improvements and extensions can and should be considered.

As evidenced by large data scatter in Figures 20 and 21, there is much room for improvement in translating lithologic information into hydraulic conductivity. Utilizing additional information about grain size distribution would help, but the experience of Riha (1993) suggests that additional factors such as cementation, pore size distribution, bedding type, etc. should be considered as well.

It would be beneficial to incorporate laboratory conductivity measurements more directly into the process for generating a conductivity field. Presently, these data have only a weak influence on the final conductivity field through the conductivity versus mud fraction correlation

(i.e., individual data points in Figures 20 and 21 have little effect on the correlation). The same can be said of other conductivity information, such as derived from slug and pumping tests. One solution would be to omit the mud fraction interpolation step, translate borehole mud fraction data to conductivity, augment these data with laboratory and *in situ* conductivity measurements, and interpolate the composite conductivity data set onto a 3D grid. Then laboratory and *in situ* conductivity measurements would have a strong local effect on the interpolated conductivity field, in addition to a global effect. Statistical weighting of the data based on estimated uncertainties would also improve the process.

A better understanding of the "stratified" EarthVision® interpolation algorithm is needed with regard to formation interconnectedness or continuity. We suspect, based on the groundwater flow modeling, that the interpolated mud fraction field displayed in Figure 19 underestimates confining zone continuity. There are many interpolated clay intervals in adjacent cores that appear to be slightly offset vertically but are actually connected. The "stratified" interpolation algorithm tends to not connect these intervals because they lie within different horizontal gridding layers. This problem is alleviated to some extent by vertical averaging during the transfer of fine-scale conductivity to the flow model grid. Also, harmonic averaging of vertical conductivities assumes perfect horizontal continuity within a grid element and slightly counteracts underestimation of continuity between elements. The conformal gridding option in EarthVision® could be used to achieve higher confining zone continuity by incorporating known variations in dip of strata into the gridding process. Selecting a coarser vertical resolution for the interpolated grid would increase interconnectedness, as would a larger vertical influence factor. These options would tend to blur vertical contrasts however, leaving conformal gridding as the preferred approach over changing the resolution.

Hydraulic head residuals within the Upper Three Runs aquifer are higher than desired. An objective of the study is to achieve noticeably lower head residuals in comparison to more traditional modeling approaches. One reason for some residuals being high is that all available head data are used as targets. These data include heads from the "SRL" grid wells south of the Old Burial Ground (CC, GG, M, Q, S, U and Y wells). Some of the SRL grid well heads appear to be inconsistent with surrounding data and produce very large residuals (e.g., U-13, Q-17, S-15). These data could be eliminated from the list of targets with justification. Eliminating these questionable targets would reduce the r.m.s. head residual. The large uncertainty in translating mud fraction into conductivity is undoubtedly another reason for some high residuals. Also, a global correlation between mud fraction and conductivity is used. Within the "lower" aquifer zone there is a bias to the distribution of residuals as noted above. In this case, the correlation should perhaps vary spatially to alleviate the bias. A spatially-varying correlation was not used in

order to test the hypothesis that the correct spatial conductivity trends would be a natural outcome of basing conductivity on mud fraction data. While the hypothesis appears to be largely true, improvements can obviously be made.

Flow modeling conclusions

Based on the flow modeling results of this study we conclude:

- Fine-scale, heterogeneous, hydraulic conductivity fields can be successfully generated directly from lithologic data using the methods described herein.

- These hydraulic conductivity fields provide a more realistic picture of subsurface hydrologic heterogeneity than conventional "layer cake" modeling approaches.

- The approach improves large-scale flow patterns and dispersive behavior in groundwater flow and transport models. For the SRS burial ground application, field-observed, preferential pathways for contaminant migration are replicated without the need to artificially create zones of high conductivity.

Tritium source characterization

An extensive search for information relevant to Old Burial Ground tritium transport was conducted from approximately December 1994 to February 1995. This effort included a computerized literature search. Many site personnel were also "interviewed" for information and data including

E&CSD: Mark Amidon, Joe Kanzleiter

SRTC/CPT: Lee Hyder

SRTC/ESS: Ken Dixon, Brian Looney, Chas Murphy, Ralph Nichols

SRTC/IWT: Jim Cook, Steve Serkiz, Elmer Wilhite

SW&ER: Steve Mentrup, Joette Sonnenberg

among others. Table 8 lists the documents collected during the literature search and Table 9 outlines the overall knowledge base gained from the search. The works of Hyder (1993), Ref. 7 and Holcomb (1992) were especially useful starting points. Highlights of the information summarized in Table 9 are presented below.

Burial ground operations

Figure 1 illustrates the study area and surroundings. The original site burial ground comprising 76 acres (Old Burial Ground) was designated in 1954 and probably received the first significant tritiated waste in late 1955 or early 1956 (Bebbington, 1990; Fenimore, 1964) coinciding with large-scale tritium production. The date of the first burial is uncertain and may be as early as 1952. The last recorded burials were in 1972. Fenimore (1964) describes burial ground operations during the first 10 years. The COBRA burial records provide the best record of operations between 1961 and 1972 (Hyder, 1993). A potentially important event associated with the burial ground plumes is the repair to the eroded F-effluent ditch in 1980. This effort was designed to restore the tritium discharge point to its original location farther south from the burial ground.

Inventory

Tritium occurs in many buried waste forms such as spent melt crucibles, magnesium beds, equipment such as pumps and other hardware, and off-site sources (Hyder, 1993). Spent melt crucibles or "spent melts" were the main waste byproduct of the tritium extraction process. Lithium-aluminum target tubes and control rods were melted in steel crucibles to release tritium gas from the solid matrix. The gas was extracted under vacuum. Following the recovery of tritium gas, the molten material was considered "spent". The melts were allowed to cool and solidify in the crucible. A crust of tritium-rich impurities typically formed at the top surface of the spent melt. Spent melts were then buried with no containment in the Old Burial Ground.

The COBRA database constitutes the main source of information about tritium burials. Hyder (1993) discusses the merits and problems (significant) of the database. The earliest COBRA tritium burial records begin in about March 1961. Therefore, there is a great deal of uncertainty about burials during the first several years of operation. Bebbington's (1990) descriptions of early reactor and tritium facility operations can be used to estimate early tritium burials as shown in Figure 37. Even for those years for which burial records were kept, there is considerable uncertainty in the buried inventory, because the recorded amounts are probably little more than guesses (Hyder, 1993; Wilhite, 1995). The estimated tritium content of spent melt crucibles is based on analysis and is probably within plus or minus 25%. An estimate of total annual tritium burials based on Figure 37 and the COBRA records is shown in Figure 38 for the period of burial ground operation. Normalized spatial variations of tritium buried annually from 1961 through 1970 are shown in Figures 39a-j.

Waste form release mechanisms and rates

Except for spent melts, the physical phenomena controlling tritium release from the various waste forms following burial are not known, much less quantified. For spent melt crucibles, a burial ground lysimeter study conducted over a 10 year period from 1974 to 1983 can be used to quantify the tritium release rate under past burial ground conditions. Figure 40 shows the cumulative tritium released from three Line 2 spent melt crucibles and lids with an estimated initial activity of 300-450 Ci (Ref. 5; Ref. 4). The physical phenomena involved in tritium release to the unsaturated zone (e.g. diffusion, dissolution, etc.) have not been identified, although some hypotheses have been advanced by Ref. 5 and Hyder (1993).

A release rate model for spent melts is constructed from the data shown in Figure 40 as follows. Because the physical phenomena controlling tritium release in the lysimeter study have not been identified, a simple first-order leaching model accounting for radioactive decay (also a first-order process) is adopted for data interpretation. The model is consistent with the assumption that the limiting step for mass transfer out of the waste form occurs across the boundary layer (film resistance). Under such conditions concentration gradients within the waste form are considered negligible. Defining the waste form as a control volume, the mass transfer equation for tritium reduces to the release model

$$C_t = -kC - \lambda C \tag{14}$$

where tritium reduction within the waste form is by either first-order radioactive decay or mass transfer into the water phase contained within the neighboring aquifer unit. Assuming a constant mass transfer coefficient (i.e. leaching constant) the analytical solution of equation (14) becomes

$$C = C_0 e^{-(k+\lambda)t} \tag{15}$$

where

$C \equiv$ average concentration in waste form

$C_0 \equiv$ initial concentration in waste form

$k \equiv$ leaching constant (yr^{-1})

$\lambda \equiv$ radioactive decay constant (0.0564 yr^{-1} for tritium)

Based on this model, the cumulative quantities of tritium remaining in the source, lost through decay, and leached to the groundwater through time are, respectively,

$$Q_{source} = Q_{initial} e^{-(k+\lambda)t} \tag{16}$$

$$Q_{decay} = Q_{initial} \frac{\lambda}{k+\lambda}\left[1 - e^{-(k+\lambda)t}\right] \tag{17}$$

$$Q_{leached} = Q_{initial} \frac{k}{k+\lambda}\left[1 - e^{-(k+\lambda)t}\right] \tag{18}$$

where $Q_{initial}$ is the initial quantity of buried tritium. The data shown in Figure 40 are reasonably well fit using parameter settings of $Q_{initial}$ = 400 Ci and k = 0.341 yr^{-1}. Figure 41 illustrates the relative release rate and cumulative released amount for these parameter settings. Note that less than 86% of the initial inventory is ever released. The remainder decays within the spent melt. Also note that approximately 90% of the ultimate release occurs within the first 6 years.

The release rate for non-spent melts is assumed to take the same functional form as for spent melts for lack of a better alternative. Transport model calibration to tritium discharge data at Fourmile Branch indicates that non-spent melts release tritium at a much slower rate than spent melts. A value of k = 0.029 yr^{-1} is chosen for non-spent melts based on model calibration for the base case (defined later). Figure 42 illustrates the relative release rate and cumulative released amount for non-spent melts. For non-spent melts about 34% is ultimately released, while 66% decays within the waste form. More than 25 years are required to reach 90% of the total eventual release.

Source term model

Buried contaminants may be modeled in the variably-saturated FACT code as either point or distributed sources, with either concentration or mass flux prescribed. Tritium-bearing waste forms were buried throughout the Old Burial Ground from approximately 1955 through 1972. Therefore, the Old Burial Ground source term must vary spatially in accordance with the burial records, and temporally in accordance with burial times and the release rate model just described. The spatial variation is handled by assigning buried waste forms to the nearest FACT grid point. For the present application, a source term specified in terms of mass flux rather than concentration is convenient.

A tritium source model defining the release rate from waste forms to the vadose zone as a function of time and space is constructed as follows. Tritiated waste forms are first segregated into spent melts and non-spent melts (i.e., all burials other than spent melts). Figures 43 and 44 show the estimated annual tritium burials for each type of waste and represent a subdivision of Figure 38. Likewise, Figures 45a-j and 46a-j illustrate the normalized spatial variation in tritium burials for spent melts and non-spent melts in burial ground coordinates, respectively. These figures are analogous to Figures 39a-j. For each waste form, the cumulative release rate for all sources buried at FACT areal node x_j for years τ_1 through τ_n is

$$\begin{aligned} H(t,x_j) &\equiv \sum_{i=1}^{n} F(\tau_i,x_j)\cdot G(t-\tau_i) \\ &= \sum_{i=1}^{n} T(\tau_i)\cdot S(\tau_i,x_j)\cdot G(t-\tau_i) \end{aligned} \tag{19}$$

where

$$T(\tau_i) \equiv \text{total annual buried amount in year } \tau_i,\ i = 1,\ \ldots,\ n \tag{20}$$

$$S(\tau_i,x_j) \equiv \text{normalized spatial distribution at node } x_j \text{ for year } \tau_i$$
$$\sum_{j=1}^{N} S(\tau_i,x_j) = 1 \text{ for } i = 1,\ \ldots,\ n \tag{21}$$

$$F(\tau_i,x_j) \equiv T(\tau_i)\cdot S(\tau_i,x_j),\ \text{amount buried at node } x_j \text{ in year } \tau_i \tag{22}$$

$$G(t) \equiv \begin{cases} ke^{-(k+\lambda)t} & t > 0 \\ 0 & t \le 0 \end{cases} \text{ relative release rate for source buried at time } t = 0 \tag{23}$$

Figures 43 and 44 provide $T(\tau_i)$, Figures 45 and 46 essentially provide $S(\tau_i, x_j)$, and Figures 41 and 42 provide G(t) for the spent melt and non-spent melt wastes, respectively. The total release rate is the sum of the contributions from spent melts and non-spent melts. Burial trenches are nominally 20 feet deep. The source term defined by equation (19) is applied to the second layer of nodes from the ground surface. Because the average FACT element height is 10 feet, this corresponds to a simulated burial depth of about 20 feet. The simulated source is therefore a few feet deeper than the actual source, because the average burial depth would be less than 20 feet.

An overall account of the fate of tritium following burial is shown in Figure 47. The cumulative amount of tritium estimated to have been buried in the Old Burial Ground between 1955 and 1972 is 288 g or 2.8 million Curies. This estimate is deduced from COBRA records for the years 1961 to 1972 and from general descriptions of reactor and separation facility operations for earlier years as discussed earlier. Spent melt waste forms are estimated to account for 34% of the total decay-uncorrected tritium inventory. As of 1995, an estimated 49% of the tritium inventory has decayed within waste forms and 45% has been released to the vadose zone, leaving only 6% remaining within waste forms for the base case source term model. As can be seen from Figure 47, an estimated 47% of the initial tritium inventory will ultimately be released to the vadose zone. Because 45% has already been released through 1995, only an additional 2% will be released in the future.

Figure 48 shows the predicted rate of tritium release to the vadose zone, along with the discharge rate to Fourmile Branch at seeps to be discussed below. The peak release to the vadose zone is estimated to have occurred in about 1961 and has declined to only 4% of this maximum value in 1995. Therefore, most of the initial buried tritium has either decayed in place or is migrating with groundwater toward Fourmile Branch.

Tritium monitoring data

Tritium monitoring data take two main forms: groundwater concentrations in monitoring wells and annual release amounts to Fourmile Branch. These are further discussed below.

Groundwater concentrations

Tritium concentration data are available from several sources. The Environmental Monitoring Section (EMS) electronic database contains concentrations for well series such as BG, BGO and HSB, and many of the OBG grid wells, as far back as 1979. Mark Amidon supplied data for the remaining OBG grid wells in electronic form. These data are published in various annual reports (see Table 8). All of the data are concentrated within the Old Burial Ground or its immediate vicinity. Valuable data taken at the F-effluent ditch seepline and between the burial ground and seepline discharge point have recently become available (Dixon and Rogers, 1993; Dixon et al., 1994; Dixon and Cummins, 1994; Ref. 1). All the data show considerable spatial and temporal variability, even within a single calendar year, making data interpretation difficult. To eliminate some of this noise, the data were annually averaged. The resulting number of annual average data from each source is listed below

3770	EMS database
868	IWT annual reports
157	Cone Penetrometer data (Ref. 1)
33	HydroPunch data (Ref. 1)
7	Seepline (Dixon and co-workers)
4835	TOTAL

The nearly 5000 annual average concentration data points were displayed in EarthVision® three-dimensional and Tecplot® two-dimensional images for various years, groups of years, and aquifer units during model development. Despite the large number of concentration data, the information appears to be insufficient to produce well defined plumes using computer interpolation. For example, the calendar year with the most spatial information is 1994. Figure 49 shows the location of "upper" aquifer zone tritium concentration data for 1994. A contour map of 1994 "upper" aquifer zone concentration is shown in Figure 50. The monitoring data alone are insufficient to fully define tritium plumes within the "upper" aquifer zone, as Figure 50 shows only isolated pockets of tritium contamination. Even less spatial resolution is available for the deeper aquifer zones. In addition, an attempt was made to generate meaningful tritium break-through curves using transient data from various individual wells. Figure 51 shows the results for BG-56, a typical example. The data exhibit too much variability to be effectively used on an individual basis for model calibration.

Instead, the data as a whole are used to ensure that predicted tritium plumes are more or less consistent with the data. The total quantity of tritium in the groundwater can be estimated from monitoring well data using the three-dimensional plume images mentioned above and the "Volumetrics" feature of EarthVision®. Table 10 summarizes EarthVision® volumetrics calculations for various calendar years. The selected years offer more spatial information about the extent of plumes than earlier years. However, even the annually averaged concentration data from these years do not fully envelop the entire plume. For example, all of the wells within the Old Burial Ground are screened across the water table, but higher concentrations are probably now present at deeper elevations. The "Data" values in Table 10 probably underestimate the true mass because the full plume has not been considered due to an absence of data. Note that the data estimates show considerable variability from year to year. This behavior is a reflection of the large variability in individual well data mentioned above.

Discharge rate at Fourmile Branch

Fourmile Branch and its tributaries have been continuously monitored for tritium from 1968 to present. Annual monitoring reports (Table 8) summarize and interpret the data. The amount of tritium discharged to

Fourmile Branch, which originated in the Old Burial Ground, can be estimated from these data as shown in Figure 52. The data represented in Figure 52 are a key target for the tritium transport model.

Tritium transport model

Once the tritium source term is defined, and given the velocity and water saturation fields from the flow model, development of a transient transport model is relatively simple as discussed next. Then, transport results for no action and two capping scenarios are presented.

Transport parameters and calibration

Based on model calibration the following transport parameter values are chosen for the base case:

Porosity (effective), ϕ	0.23
Longitudinal dispersivity, α_L	65 ft
Release rate constant for non-spent melts, k	0.029 yr^{-1}
Half-life of tritium	12.3 yr
Time step size	0.1 yr

Following standard transport modeling practice, an "effective" instead of total porosity is used for the base case to account for regions of relatively immobile groundwater that are not effectively penetrated by the solute plume (de Marsily, 1986; Fetter, 1993). The value chosen is well within the guidelines set by Looney et al. (1987a). The dispersivity is relatively low compared to the recommendation of Looney et al. (1987a) probably because the highly heterogeneous hydraulic conductivity field employed in the present flow model alleviates the need for a large mechanical dispersion term. A dispersivity of 65 ft also corresponds to a cell Peclet number of 2. For maximum accuracy, the cell Peclet number should be less than or equal to 2 ($v\Delta x/D = \Delta x/\alpha_L \leq 2$), and this condition is satisfied with the present model. The release rate constant for non-spent melts was selected based primarily on comparison of predicted and measured tritium discharge to Fourmile Branch. This data reflects the overall system behavior. Preliminary simulations were performed at time step sizes of 1 year and 0.1 years. A time step of 0.1 years is judged sufficiently small to minimize the effects of time truncation errors.

Base case results and discussion

Three future scenarios are considered: 1) no action, 2) capping with a hypothetical low permeability cover in mid-1996, and 3) capping and removal of the remaining source in mid-1996. Each simulation begins with a reproduction of past tritium migration from the first significant tritium burial (1955) to present (1996). The simulation continues 40 years into the future (2035) according to the selected remedial alternative. For the first capping scenario, the release rate of tritium to the vadose zone is assumed to be unaffected by capping (i.e., same as the no action case); tritium migration through the vadose zone is slowed by reduced infiltration however. For the second capping scenario, the tritium release rate is zero after capping. The actual tritium release rate after capping is bounded by these two cases.

No action results (reproduce past and predict no action future)

Figure 53 shows an overall accounting of tritium released to the vadose zone as a function of time based on FACT results. Tritium released to the vadose zone either decays in transit, discharges to surface water, migrates outside the model domain (negligible amount) or resides within the groundwater. In the simulation, the peak amount of tritium in the groundwater occurred in about 1972 and has declined to 41% of this value by 1995. Table 10 compares the predicted amount of tritium in groundwater shown in Figure 53 with estimates based on monitoring data and EarthVision® volumetrics calculations. The estimates based on well monitoring data are roughly half the code predictions. The discrepancy is most likely due to the fact that well monitoring data are not available below the water table within the burial ground where the bulk of tritium may be located. The values based on data may be missing a significant portion of the actual plume leading to a low estimate.

Figure 54 shows simulated tritium discharge to Fourmile Branch compared to monitoring data. The model predictions agree with the overall trend, but, do not reproduce the fine structure of the data. The cause of the data "noise" is unknown. The peak discharge is predicted to have occurred in 1992. A substantial decline in discharge to Fourmile Branch is predicted to occur over the next decade.

Figure 55 shows a cut-away of the three-dimensional tritium concentration for calendar year 1995. Tritium descends straight down through the vadose zone from buried waste to the water table at an average rate of about 12 ft/yr (17 in/yr local recharge divided by 23% porosity and 50% average saturation in the model). The plumes then move laterally toward Fourmile Branch (see Figure 36 too). From the southwest corner of the Old Burial Ground the total travel time to the seepline averages approximately 10

to 15 years based on three-dimensional particle tracking. Two-dimensional contour maps of concentration within each aquifer zone/unit can be created from the three-dimensional results through vertical averaging.

Figures 56a-56l illustrate tritium concentrations in the "upper" aquifer zone on a 5 frequency from 1960 to 2015. Two distinct plumes are identified corresponding to burials predominantly in the west and east ends of the Old Burial Ground. Observe that the plume emanating from the southwest corner of the Old Burial Ground contributes solely to the discharge at the Fourmile Branch seepline. This discharge is biased towards the west side of the F-effluent ditch. The east end plume contains more tritium than the southwest plume, but, is mostly confined to the areal bounds of the Old Burial Ground as it migrates slowly westward. Horizontal velocities in the eastern end of the Old Burial Ground are generally low.

Figures 57a-57l show tritium concentrations in the "lower" aquifer zone. Concentrations are lower as expected. The peak concentration lies beneath the Old Burial Ground in the mid-section. The plumes are slowly migrating toward Fourmile Branch.

Figures 58a-58l show Gordon aquifer concentrations, which are extremely low compared to the "lower" and "upper" aquifer zones (note the change in scale). Peak concentrations occur near the west end of the Old Burial Ground. The plumes are dispersing and slowly migrating west to northwest towards Upper Three Runs.

Finally, 1995 seepage face concentrations near the confluence of the F-area effluent ditch and Fourmile Branch are shown in Figure 59. Figure 59 illustrates concentration data at the surface of the three-dimensional concentration field depicted in Figure 55. Note that the scale has been reduced in Figure 59 to highlight the results in this area. The predicted values are consistent with the corresponding monitoring data.

Effect of capping

The second scenario involves placing a certain low permeability cover over the entire Old Burial Ground in mid-1996. The cap is created by changing the conductivity in the top layer of burial ground finite elements to 10^{-5} ft/d, and reduces infiltration by a factor of 85 from 17 in/yr to about 0.2 in/yr. Figure 60 shows the impacted surface elements. The figure also illustrates other engineered surfaces that are present throughout all three scenarios. The modeled cap is purely hypothetical and does not simulate any proposed design, but does offer significant insight into the general effect of capping. Tritium release rates from waste forms to the vadose zone are conservatively assumed to be unaffected by capping.

The simulated effect of capping in mid-1996 is illustrated in Figure 61. As shown, tritium discharge to Fourmile Branch will be reduced by less than 300 Curies per year compared to uncapped conditions. The effect is small compared to the present discharge rate of about 4500 Curies per year. This outcome follows from the fact that most of the tritium originally present in solid radioactive waste burials has either decayed or migrated to groundwater below the water table. Tritium already in the saturated zone is largely unaffected by capping.

The immediate reduction in tritium discharge at the time of capping is the result of a slight reduction in average recharge over the entire model domain when burial ground infiltration is reduced from 17 in/yr to about 0.2 in/yr. The reduced infiltration immediately slows groundwater flow towards Fourmile Branch in the simulation, reducing the tritium flux. The smaller groundwater flow rate also causes additional radioactive decay while tritium is transported in the saturated zone. Reduced infiltration initially decreases the tritium flux from the vadose zone to the water table. As the tritium concentration builds in the vadose zone, the tritium flux to the water table increases and eventually exceeds that for the no action case. As a result, the discharge matches and then slightly exceeds tritium releases for the no action scenario some 30 years in the future.

Effect of capping and source removal

For the previous simulation, the tritium source term in the vadose zone is assumed to be unabated by a reduction in infiltration. Tritium release rates to the vadose zone may be affected by the infiltration rate. Reduced recharge would presumably decrease the release rate. To explore this possibility, the tritium release rates are set to zero coincident with capping as a second case. This assumption is equivalent to assuming the source is dug up and removed prior to capping. The present scenario and the preceding one bound the possible effects of capping. The former case maximizes the potential tritium source term while the present minimizes the source. The results of capping and source removal are shown in Figure 61. The two capping scenarios yield essentially identical results for the first 15 years while saturated zone groundwater presently between the burial ground and Fourmile Branch flushes through. From about 2010 onward, the present scenario continues to yield tritium discharges below the no action case.

Sensitivity case results and discussion

Unconnected pore space and dead-end pores are typically cited as the motivation for defining an effective porosity to be used instead of total porosity in solute transport modeling (de Marsily, 1986; Fetter, 1993).

Unconsolidated Savannah River Site sediment probably contains very little unconnected pore space. Significant dead-end pore space is likely, but its mere presence does not justify using an effective porosity. For the natural groundwater flow rates at the Old Burial Ground, tritium has sufficient time to diffuse into relatively immobile water in dead-end pores. Therefore, water occupying dead-end pores participates in the transport of tritium. Unconnected pore space and dead-end pores cannot be used to justify use of an effective porosity well below total porosity for unconsolidated sediment beneath the SRS. However, larger scale heterogeneities do offer justification. The average vertical finite-element height in the model is about 10 feet. Interbedded sand and clay layers within the resolution of an average cell may effectively isolate portions of the groundwater from a passing tritium plume. In this case, a porosity value significantly less than the total porosity is appropriate for the base case considered above. Nevertheless, a second simulation using total porosity is now considered in case the 23% porosity value used for the base case is too low. The exercise also provides important information about the sensitivity of model results to calibration parameters.

The parameters selected for the sensitivity case following model calibration are

Porosity (total)	0.45
Longitudinal dispersivity	300 ft
Release rate constant for non-spent melts	0.17 yr^{-1}
Half-life of tritium	12.3 yr
Time step size	0.1 yr

Total porosity for SRS sediments ranges from about 0.4 to 0.6 (Looney et al., 1987a) with sands tending to have lower porosity than clays. A value of 0.45 is chosen because sands dominant the distribution of sediments (Figure 4). A larger dispersivity and release rate are needed to match the monitoring data at Fourmile Branch when compared to the base case. The reason is that the Darcy velocity from the flow simulation is the same for the base and sensitivity cases. The tritium mass flux near Fourmile Branch is the Darcy velocity times the solute concentration. The same concentration at the seepline is required regardless of specified porosity in order to preserve mass flux between the base and sensitivity cases. More tritium must be released to the vadose zone for a porosity of 45% to maintain the up-gradient concentration of tritium. This effect is accomplished by increasing the release rate of tritium from non-spent melt waste forms ($k = 0.17\ yr^{-1}$ compared to $0.029\ yr^{-1}$). As indicated by Figure 62, the higher release rate for non-spent melts results in significantly higher releases of tritium to the vadose zone with less decay within the waste form, in addition to earlier release (see Figure 47 for the base case). Figure 63 shows the increased average release rate from all waste forms when compared to the base case (Figure 48). In addition,

a larger dispersivity is needed to achieve the correct elapsed time for tritium break-through following burial.

The same three remediation scenarios considered for the base case are considered for the sensitivity case: 1) no action, 2) capping with a hypothetical low permeability cover, and 3) capping and removal of the remaining source. As before, each simulation begins with a reproduction of past tritium migration from the first significant tritium burial (1955) to present (1996), and continues 40 years into the future (2035) according to the selected remedial alternative.

Figures 64 and 65 summarize the "bottom line" results of the sensitivity study. The total amount of tritium in groundwater is significantly higher for the sensitivity case as illustrated by Figure 64 in comparison to Figure 53. Concentrations are roughly the same between the base and sensitivity cases. The higher inventory of tritium in groundwater is due to larger porosity rather than concentration. Figure 65 shows predicted discharges to Fourmile Branch for no action, capping, and capping with source removal. The sensitivity case results are very similar to the base case (Figure 61) for no remedial action. Capping is predicted to reduce tritium discharges by less than 150 Ci compared to less than 300 Ci for the base case. The reason is that virtually no tritium remains in the waste forms in 1996 compared to a small amount for the base case. Therefore capping has even less effect for the sensitivity case. The similarity of results for the base and sensitivity cases is the result of model calibration to 40 years of monitoring data in both cases. The monitoring data severely constrain the overall model and suggest the results for tritium discharge to Fourmile Branch have low uncertainty, despite large uncertainties in the source term.

Transport modeling conclusions

Based on the base case tritium source term and transport modeling results of this study we estimate:

- The total amount of buried tritium is approximately 288 g or 2.8 million Ci (decay uncorrected).

- Of this amount, 61% is buried in the west end of the Old Burial Ground and 39% in the east end. The east end contains 97% of the spent melts however.

- As of 1995, 49% of buried tritium has decayed within waste forms, 45% has been released to the vadose zone, and 6% remains in waste forms.

- Spent melts release tritium to the vadose zone at a much higher rate than other waste forms, on average. In the context of a first-order leaching and decay model, the leaching constant for spent-melts is about 0.341 yr^{-1} compared to an average of 0.029 yr^{-1} for non-spent melts.

- The peak release rate to the vadose zone occurred in 1961 and has declined to 4% of the maximum in 1995.

- The peak amount of tritium in the groundwater occurred in 1972 (600,000 Ci) and has declined to 41% of this maximum by 1995.

- The source of tritium discharge to Fourmile Branch to-date is entirely from sources buried in the west end of the burial ground. Groundwater velocities are low beneath the east end.

- The tritium flux to Fourmile Branch peaked at about 4500 Ci per year in 1992.

- Tritium discharges to Fourmile Branch will significantly decline in the near future without remediation (Figure 61).

- Capping the Old Burial Ground with a hypothetical, very low permeability cover will reduce tritium discharge to Fourmile Branch by no more than about 300 Curies per year (Figure 61).

A sensitivity analysis using total porosity instead of effective porosity in the transport model suggests:

- The predictions of tritium discharge to Fourmile Branch appear to have low uncertainty. Despite large uncertainties in the source term, the calibrated model is tightly constrained by 40 years of monitoring data.

- The base case tritium source term model may over-estimate the amount of tritium remaining in waste forms. When the source term model is calibrated for transport with a porosity of 45% instead of 23%, the release rate constant for non-spent melts is about 0.17 yr^{-1} instead of 0.029 yr^{-1}. For 1995, 22.2% of buried tritium has decayed within waste forms, 77.7% has been released to the vadose zone, and only 0.1% remains in waste forms for the higher release rate.

- The base case may under-estimate the amount of tritium in the groundwater. For the sensitivity case, the maximum groundwater inventory is 1,330,000 Ci and occurs in 1973. However, groundwater concentrations are similar for both cases.

References

Aadland, R. K., J. A. Gellici, and P. A. Thayer, 1995, Hydrogeologic framework of west-central South Carolina, South Carolina Department of Natural Resources, Water Resources Division Report 5, 200 p. + 47 plates.

Arnett, M. W., A. R. Mamatey and D. Spitzer, eds., 1995, Savannah River Site environmental report for 1994, WSRC-TR-95-075.

Amidon, M. B., 1994a, personal communication.

Amidon, M. B., 1994b, personal communication.

Ref. 1 (deleted reference; contact an author for more information).

Bebbington, W. P., 1990, History of duPont at the Savannah River Plant, duPont, Wilmington, Delaware.

Bledsoe, H. W., R. K. Aadland and K. A. Sargent, 1990, Baseline hydrogeologic investigation - summary report (U), WSRC-TR-90-1010, 40 p. + appendices.

Boman, G. K., F. J. Molz and O. Guven, 1995, An evaluation of interpolation methodologies for generating three-dimensional hydraulic property distributions from measured data, Ground Water, v. 22, p. 247-258.

Brusseau, M. L., 1994, Transport of reactive contaminants in heterogeneous porous media, Reviews of Geophysics, v. 32, p. 285-313.

Ref. 2 (deleted reference; contact an author for more information).

de Marsily, G., 1986, Quantitative Hydrogeology, Academic Press, Orlando.

Dixon, K. L. and V. A. Rodgers, 1993, Results of the fourth quarter tritium survey of the F- and H-area seeplines: March 1993 (U), WSRC-TR-93-526, Rev. 0.

Dixon, K. L., V. A. Rodgers and B. B. Looney, 1994, Results of the quarterly tritium survey of Fourmile Branch and its seeplines on the F- and H-areas of SRS: September 1993 (U), WSRC-TR-94-0286-E, Rev. 1.

Dixon, K. L., and C. L. Cummins, 1994, Quarterly sampling of the wetlands along the old F-area effluent ditch: May 1994 (U), WSRC-TR-94-365, Rev. 1.

Fatt, I. and W. A. Klikoff, 1959, Effect of fractional wettability on multiphase flow through porous media, AIME Transactions, v. 216, p. 246.

Fallaw, W. C. and V. Price, 1995, Stratigraphy of the Savannah River Site and vicinity, Southeastern Geology, v. 35, p. 21-58.

Fenimore, J. W., 1964, Land burial of solid radioactive waste during a 10-year period, Health Physics, v. 10, p. 229-236.

Fetter, C. W., 1993, Contaminant Hydrogeology, MacMillan, New York.

Freeze, R. A. and J. A. Cherry, 1979, Groundwater, Prentice-Hall, Englewood Cliffs, New Jersey.

GeoTrans, 1992, Groundwater transport modeling of constituents originating from the Burial Grounds Complex, WSRC-TR-92-521 (WSRC author W. W. Pidcoe), October 30.

Ref. 3 (deleted reference; contact an author for more information).

Ref. 4 (deleted reference; contact an author for more information).

Ref. 5 (deleted reference; contact an author for more information).

Ref. 6 (deleted reference; contact an author for more information).

Holcomb, H. P., 1992, Transcription of a presentation by Dr. E. L. Albenesius, 'SRS Burial Ground Operation From a Historical Perspective' (U), WSRC-RP-92-349.

Huyakorn, P. S. and S. Panday, 1992, VAM3DCG - variably saturated analysis model in three-dimensions with preconditioned conjugate gradient matrix solvers; documentation and user's guide; version 2.4, HydroGeoLogic, Inc., Herndon, Virginia, 274 p.

Huyakorn, P. S., S. Panday and T. Birdie, 1991, SAFT3D; Subsurface analysis finite element model for flow and transport in 3 dimensions; version 1.3; documentation and user's guide, HydroGeoLogic, Inc., Herndon, Virginia, 288 p.

Huyakorn, P. S., E. P. Springer, V. Guvanasen and T. D. Wadsworth, 1986, A three-dimensional finite-element model for simulating water flow in variably saturated porous media, Water Resources Research, v. 22, p. 1790-1808.

Hyder, M. L., 1993, Tritium in the burial ground of the Savannah River Site (U), WSRC-TR-93-316.

Ref. 7 (deleted reference; contact an author for more information).

Kegley, W. P., W. C. Fallaw, D. S. Snipes, S. M. Benson and V. Price, Jr., 1994, Textural factors affecting permeability at the MWD well field, Savannah River Site, Aiken, South Carolina, Southeastern Geology, v. 34, p. 139-161.

Lahm, T. D., E. S. Bair and F. W. Schwartz, 1995, The use of stochastic simulations and geophysical logs to characterize spatial heterogeneity in hydrogeologic parameters, Mathematical Geology, v. 27, p. 259-278.

Looney, B. B., M. W. Grant and C. M. King, 1987a, Estimation of geochemical parameters for assessing subsurface transport at the Savannah River Plant, DPST-85-904.

Looney, B. B., J. S. Haselow, C. M. Lewis, M. K. Harris, D. E. Wyatt and C. S. Hetrick, 1993, Projected tritium releases from F & H Area seepage basins and the Solid Waste Disposal Facilities to Fourmile Branch (U), WSRC-TR-93-459.

Looney, B. B., J. T. Marsh, Jr. and D. W. Hayes, 1987b, Development of accurate standardized algorithms for conversion between SRP grid coordinates and latitude/longitude, DPST-87-724.

Neuman, S. P., R. A. Feddes and E. Bresler, 1974, Finite element simulation of flow in saturated - unsaturated soils considering water uptake by plants: Report for Project ALO-5WC-77, Hydrodynamics and Hydraulic Engineering Laboratory, Technion, Hafia, Israel, 104 p.

O'Brien & Gere Engineers, Inc., 1991, M Area Post Test Characterization Geotechnical Testing, File: 4998.007 #2.

Parizek, R. R. and R. W. Root, Jr., 1986, Development of a groundwater velocity model for the Radioactive Waste Management Facility, Savannah River Plant, South Carolina, DPST-86-658.

Poeter, E. P. and D. R. Gaylord, 1990, Influence of aquifer heterogeneity on contaminant transport at the Hanford site, Groundwater, v. 28, p. 900-909.

Pruess, K., 1987, TOUGH user's guide, Report No. LBL-20700, Lawrence Berkeley Laboratory.

Renka, R. J., 1984, Algorithm 624: Triangulation and interpolation at arbitrarily distributed points in a plane, ACM Trans. Math. Softw. v. 10, p. 440-442.

Riha, B. D., 1993, Predicting saturated hydraulic conductivity for unconsolidated soils from commonly measured textural properties, M. S. Thesis, Clemson University, Clemson, S.C., 87 p.

Rulon, J., 1984, The development of multiple seepage faces along heterogeneous hillsides, Ph.D. Thesis, University of British Columbia, Vancouver, Canada, 161 p.

Ref. 8 (deleted reference; contact an author for more information).

U. S. Geological Survey, 1980-1993, Water Resources Data for South Carolina, Water Years 1980 and 1985-1993.

U. S. Geological Survey, 1993a, New Ellenton SW DEM file dated FEB-16-93 in header.

van Genuchten, M. T., 1980, A closed-form equation for predicting the hydraulic conductivity of unsaturated soils, Soil Sci. Am. J., v. 44, p. 892-898.

Verma, A. K., K. Pruess, C. F. Tsang and P. A. Witherspoon, 1985, A study of two-phase concurrent flow of steam and water in an unconsolidated porous media, Paper presented at the 23rd ASME/AIChE National Heat Transfer Conference, Denver, Colorado, August.

Ref. 9 (deleted reference; contact an author for more information).

Westinghouse Savannah River Company, 1995, RCRA Part B permit renewal application (U), WSRC-IM-91-53, v. 7, Mixed Waste Management Facility (MWMF) postclosure, 530 p. + appendices.

Wilhite, E. L., 1995, personal communication, January 30.

Ref. 10 (deleted reference; contact an author for more information).

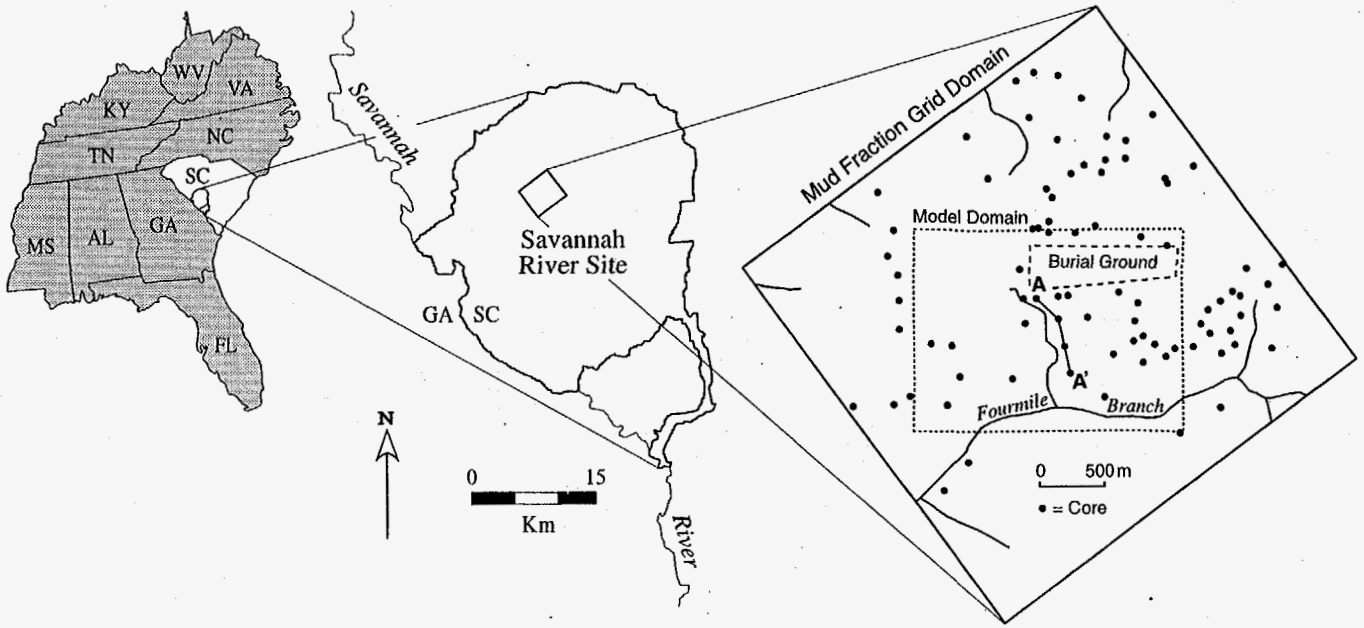

Figure 1. Location map of the Old Burial Ground showing the flow model domain and available sediment lithologic descriptions from 84 wells.

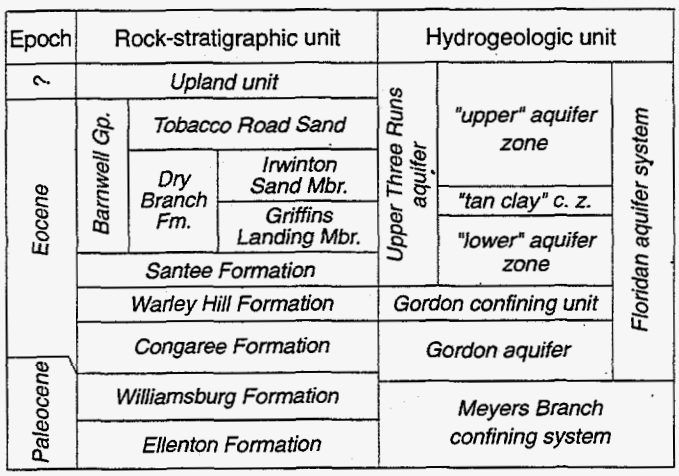

Figure 2. Lithostratigraphic and hydrostratigraphic nomenclature at the SRS (modified from Aadland et al., 1995).

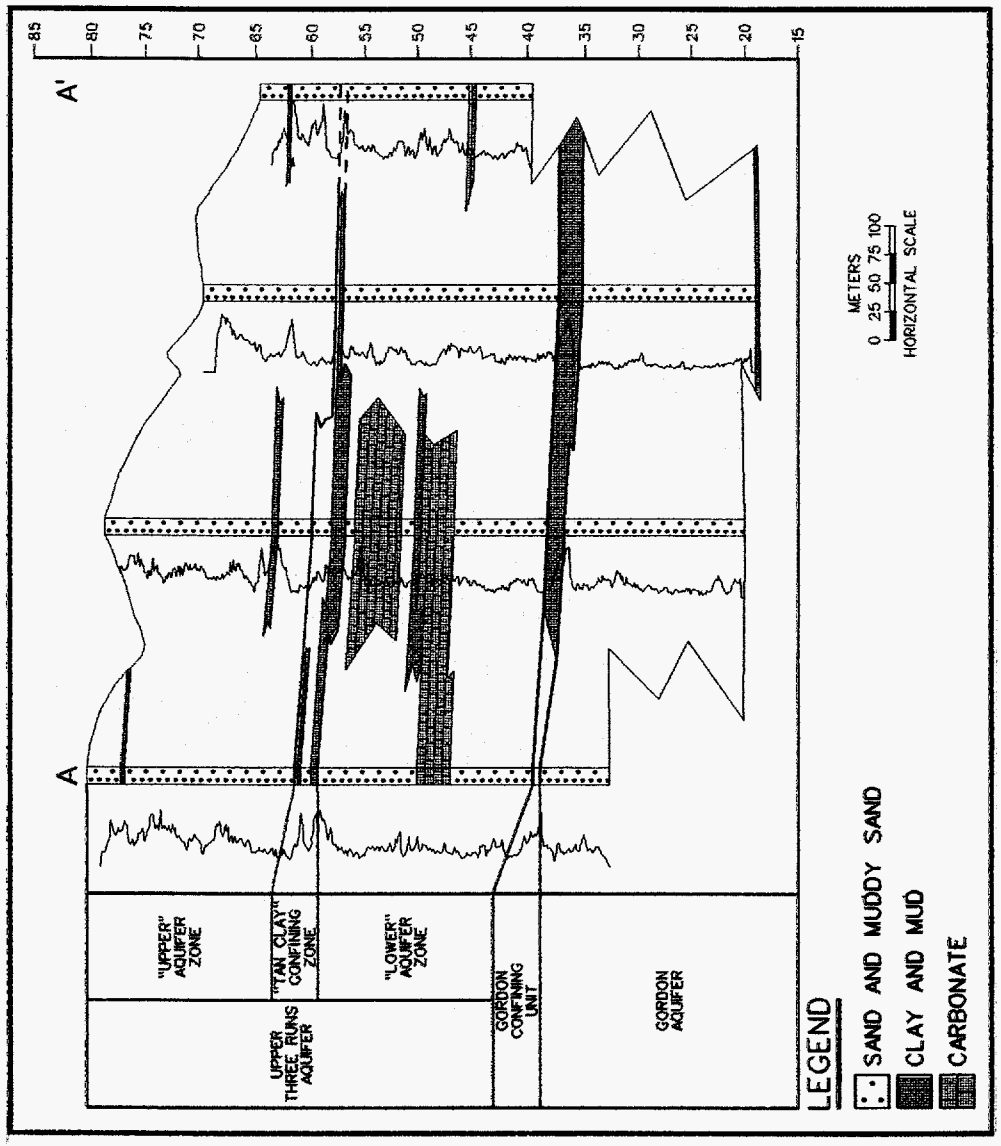

Figure 3. Lithostratigraphic and hydrostratigraphic cross-section A-A' (Fig. 1).

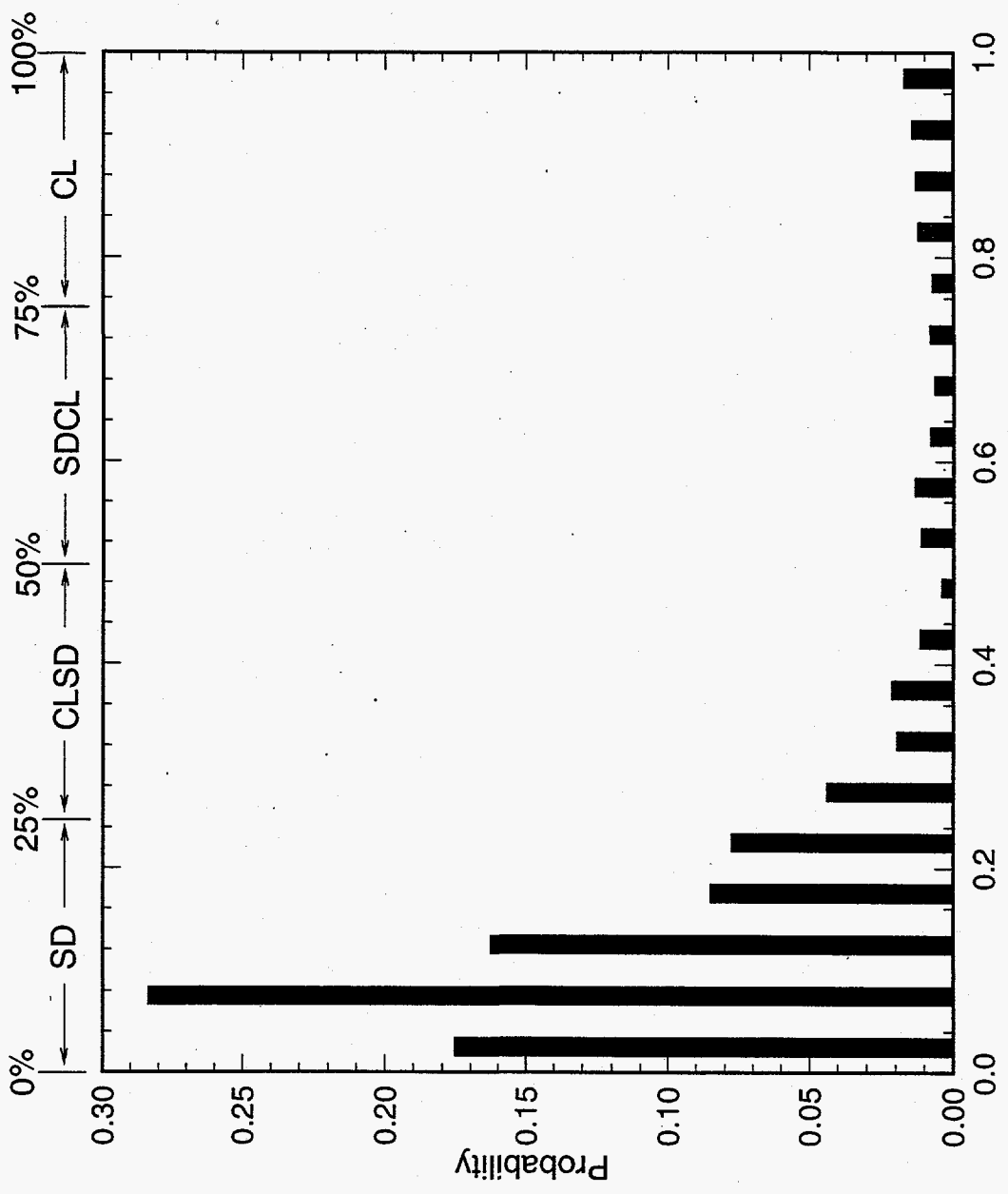

Figure 4. Mud fraction probability distribution based on the cores listed in Table 2.

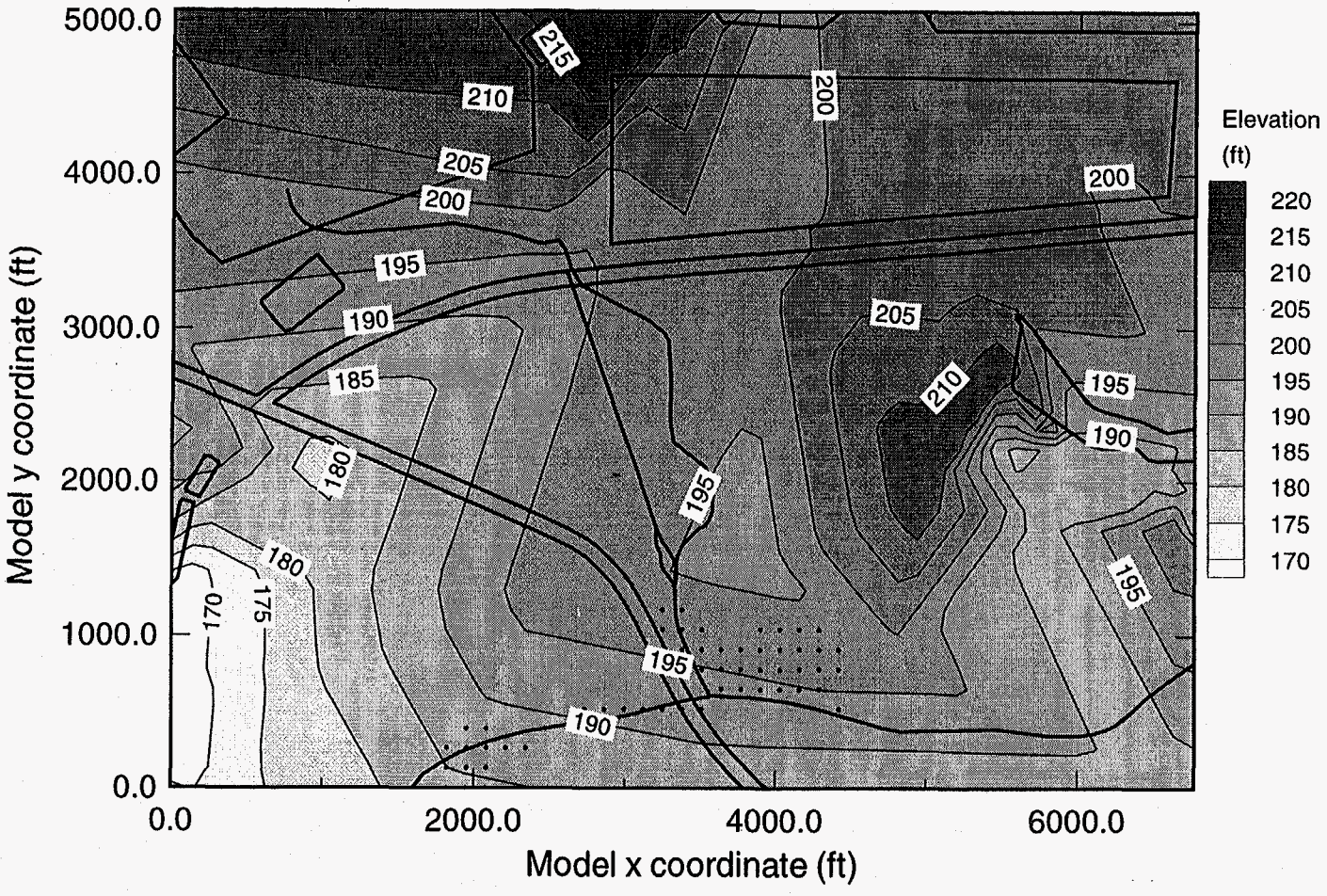

Figure 5. Structure contour map for the top of the "tan clay" confining zone (feet above mean sea level); dots indicate locations where the "tan clay" confining zone is inferred to crop out.

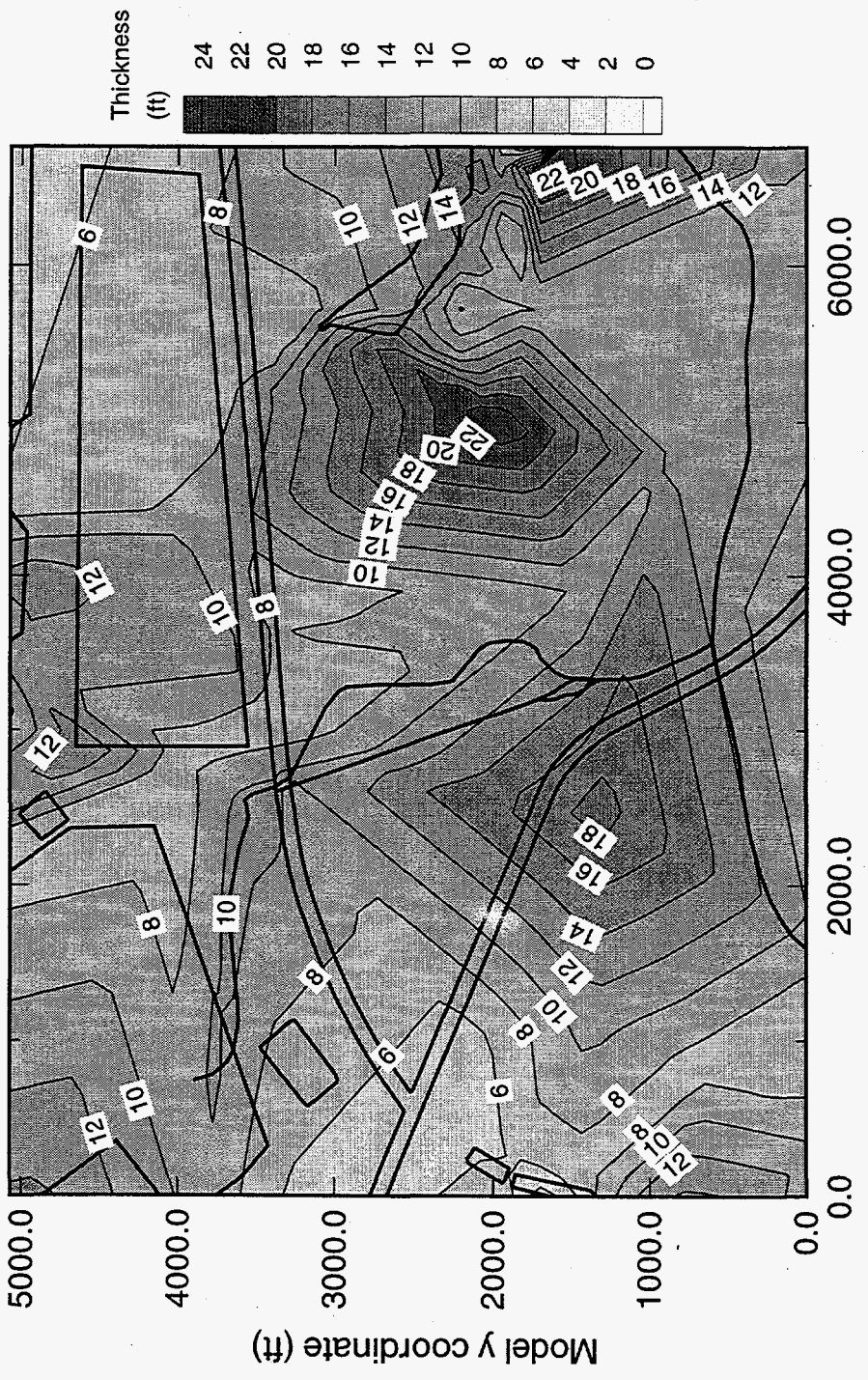

Figure 6. Thickness map for the "tan clay" confining zone (feet).

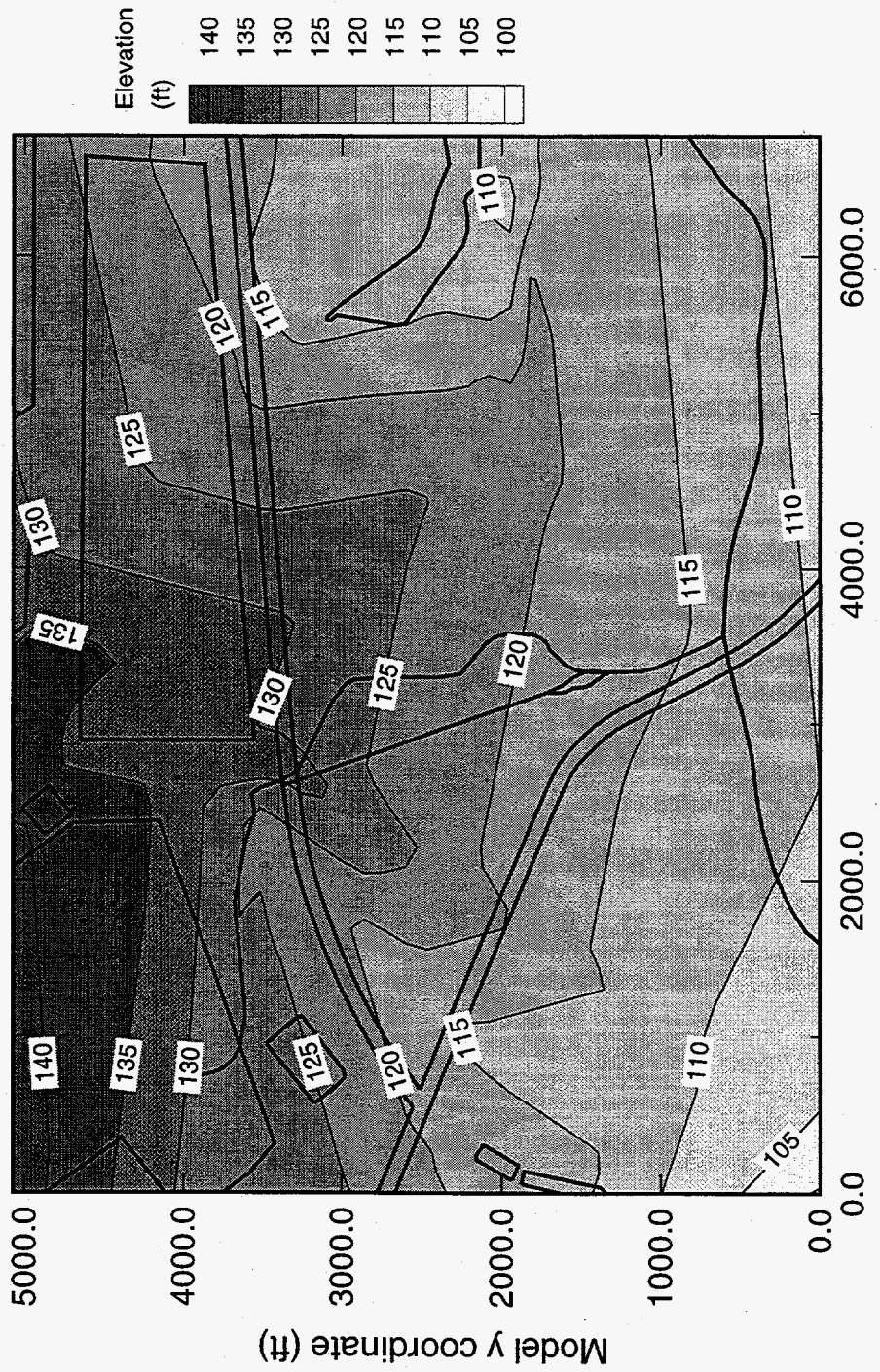

Figure 7. Structure contour map for the top of the Gordon confining unit (feet above mean sea level).

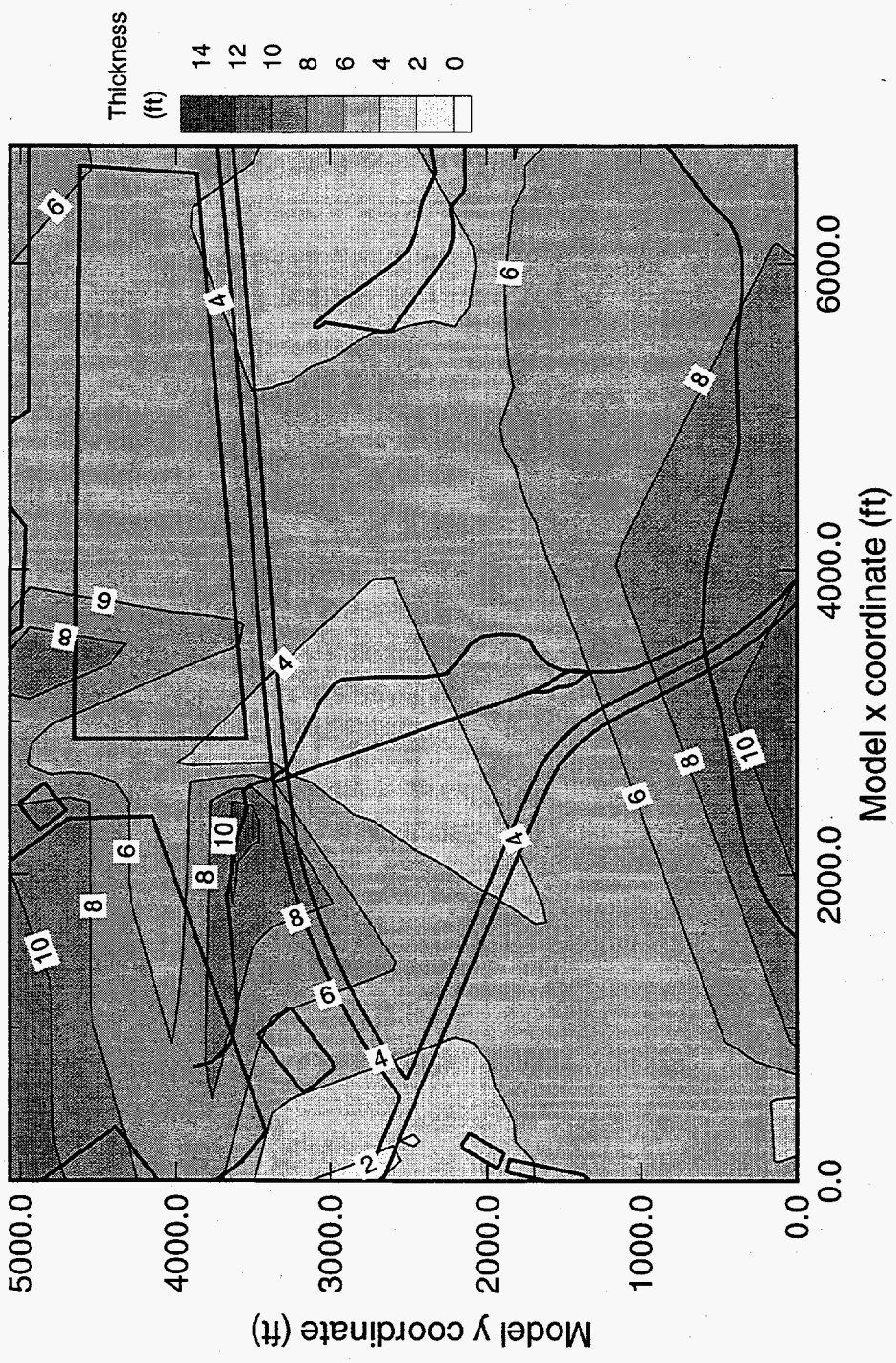

Figure 8. Thickness map for the Gordon confining unit (feet).

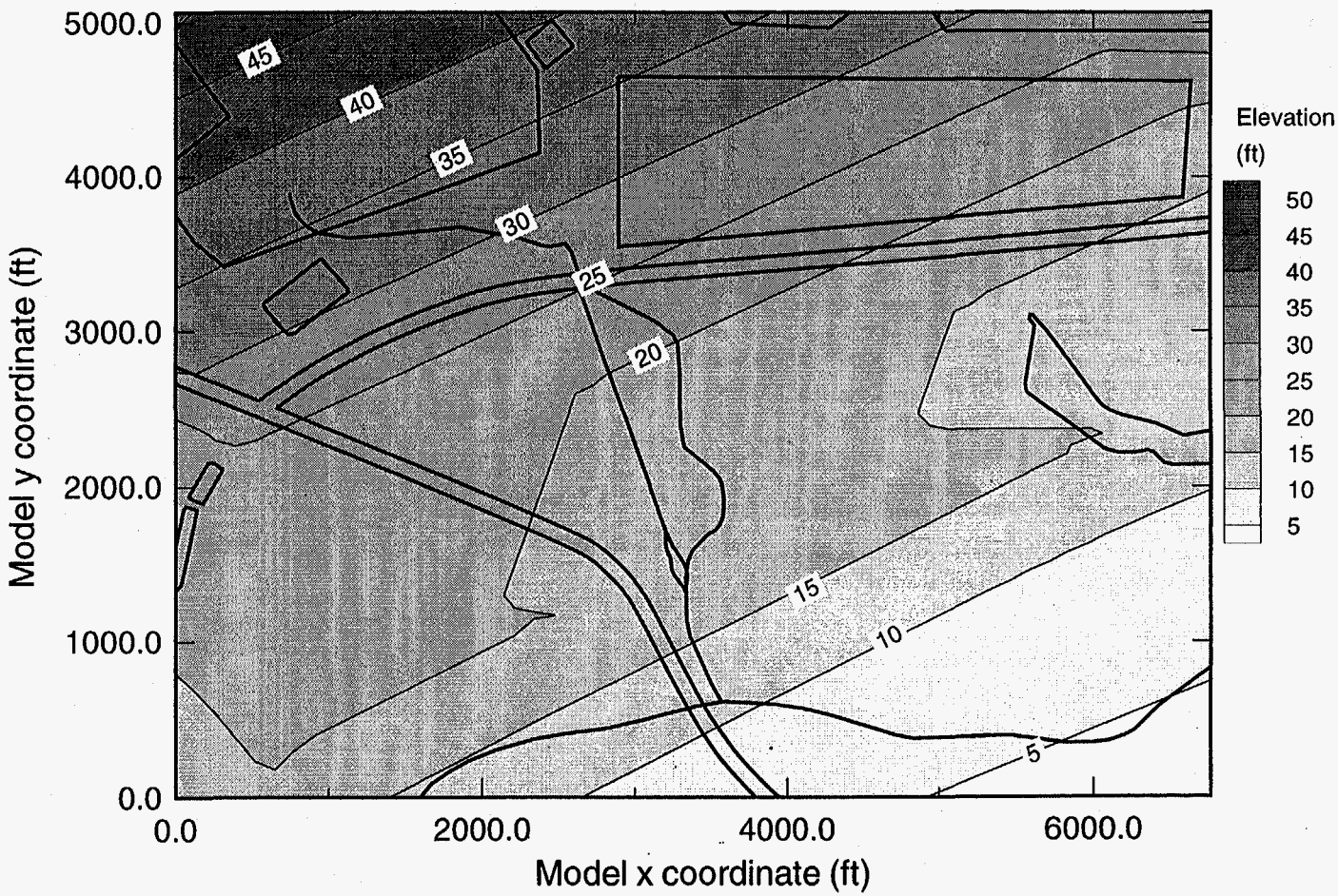

Figure 9. Structure contour map for the top of the Meyers Branch confining system (feet above mean sea level).

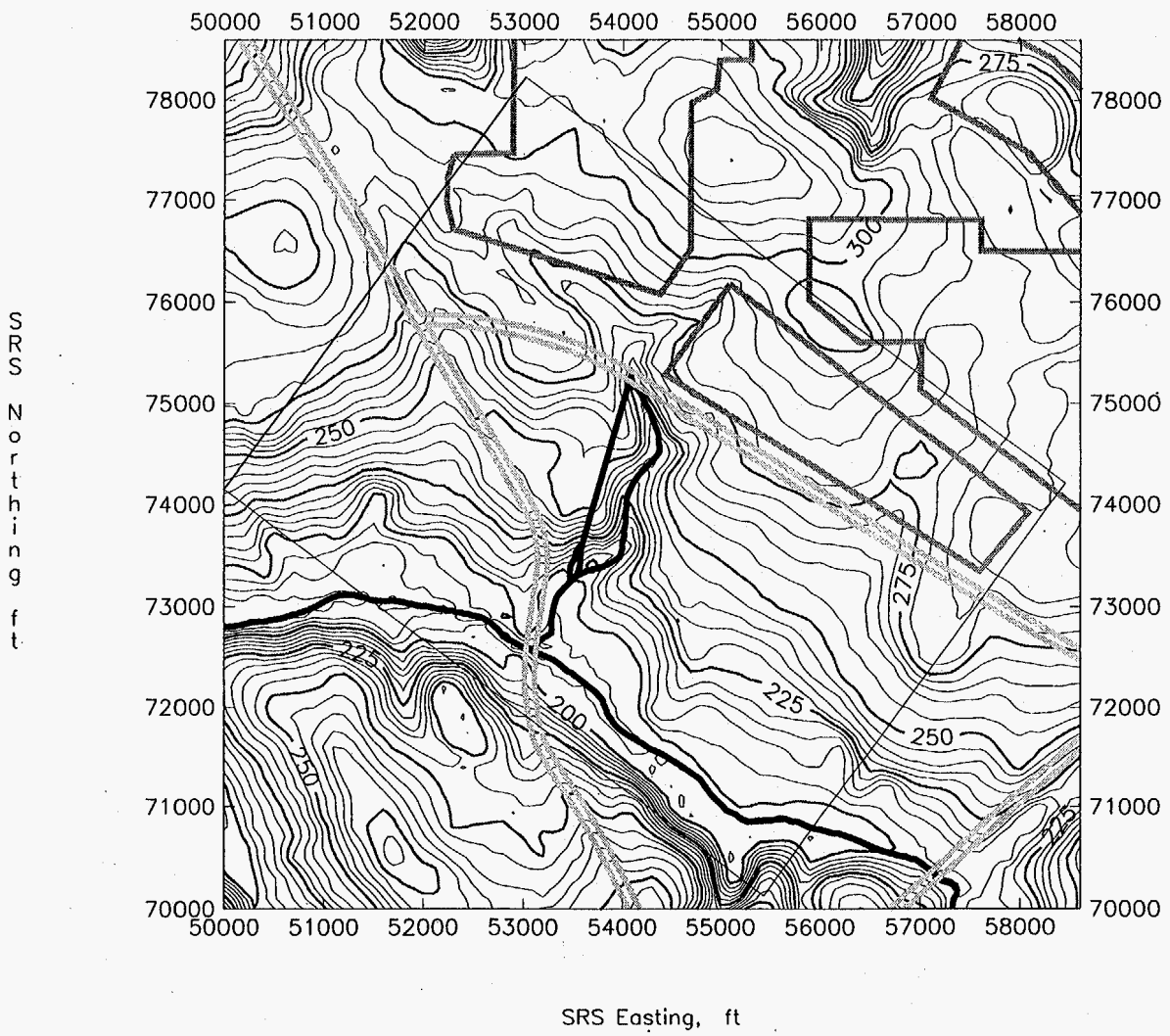

Figure 10. Contour plot of ground elevation (feet above mean sea level).

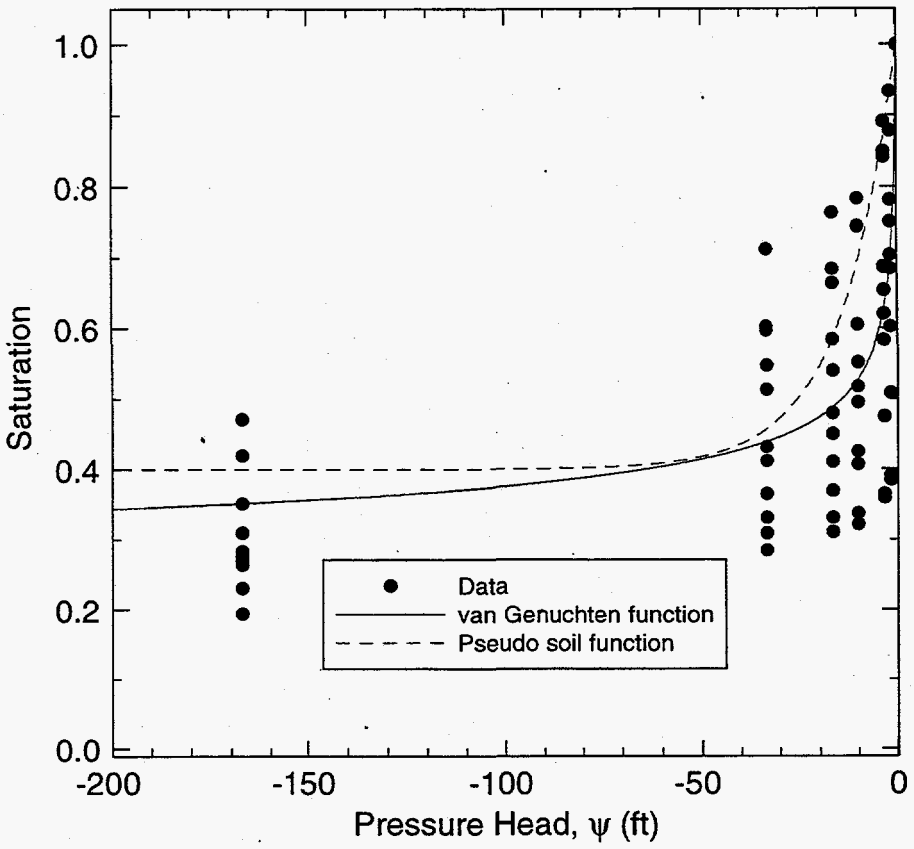

Figure 11. Water retention data and models for sandy sediment.

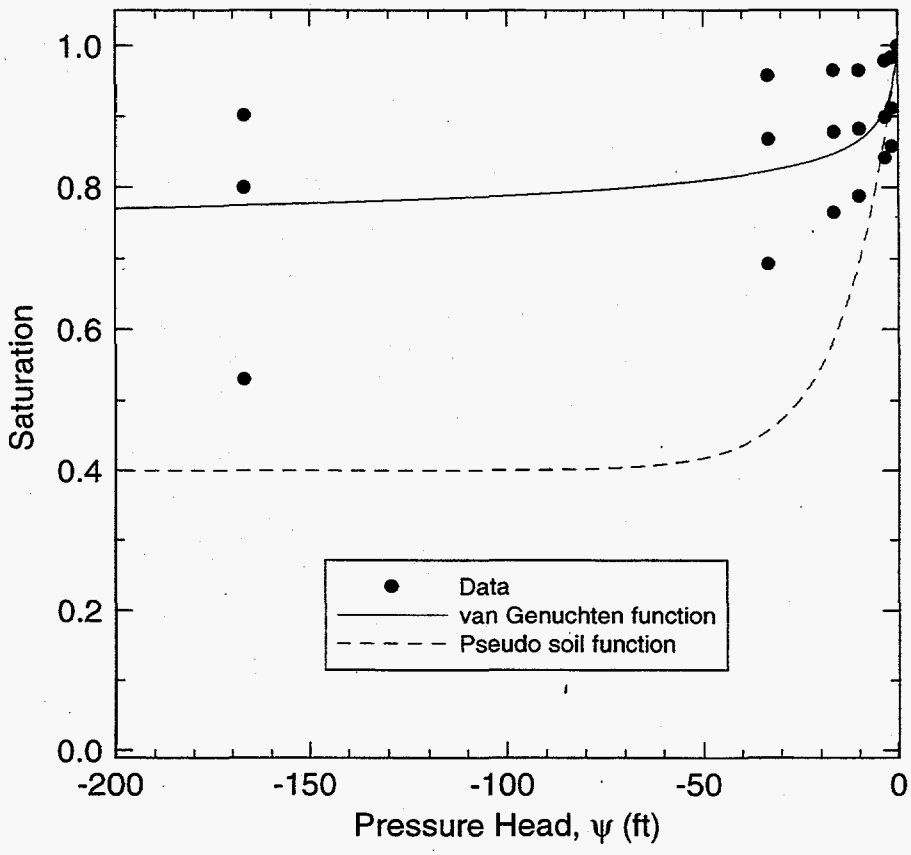

Figure 12. Water retention data and models for clayey sediment.

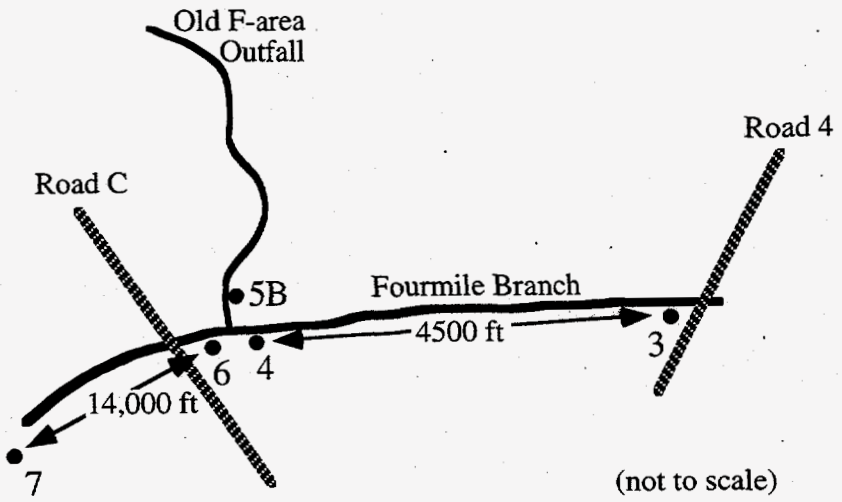

Figure 13. U. S. Geological Survey stream flow rate monitoring stations on Fourmile Branch.

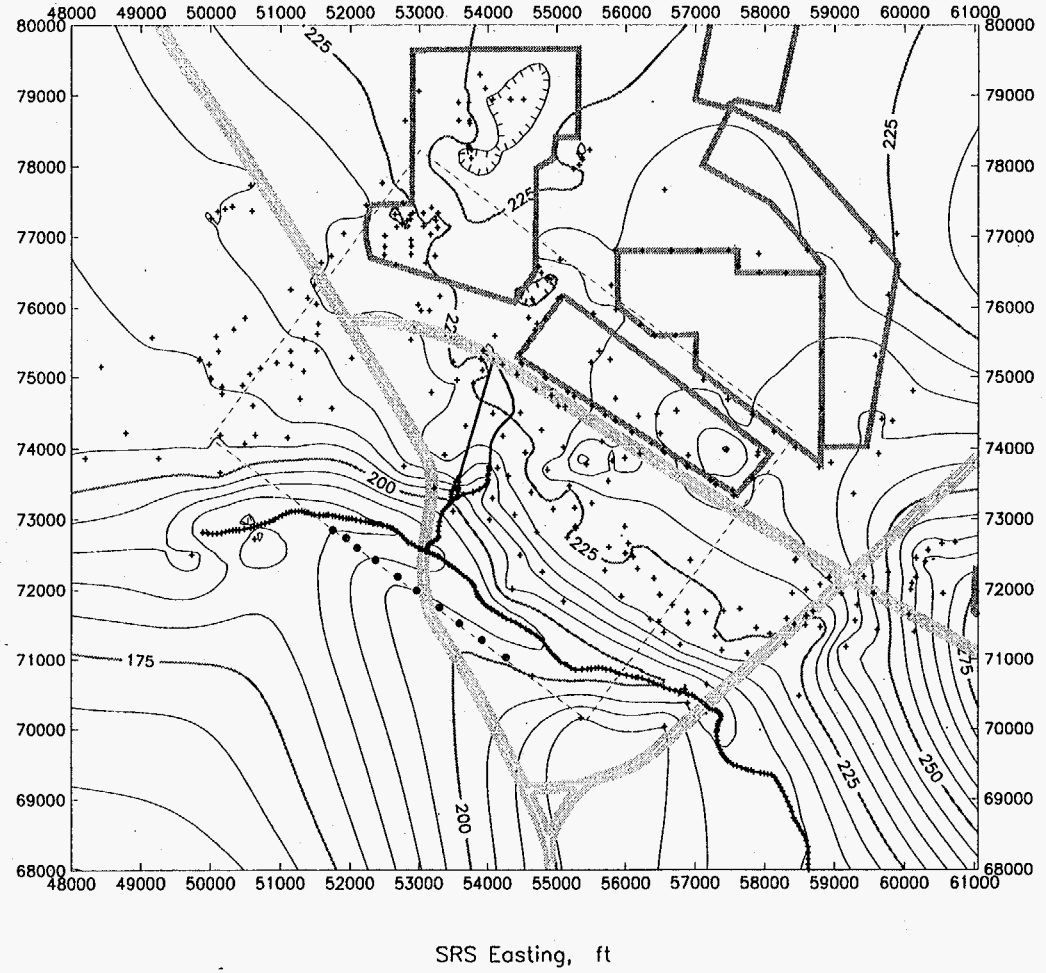

Figure 14. Head contour map for the "upper" aquifer zone within the Upper Three Runs aquifer (feet above mean sea level). + denotes data, ⊕ pseudo-data.

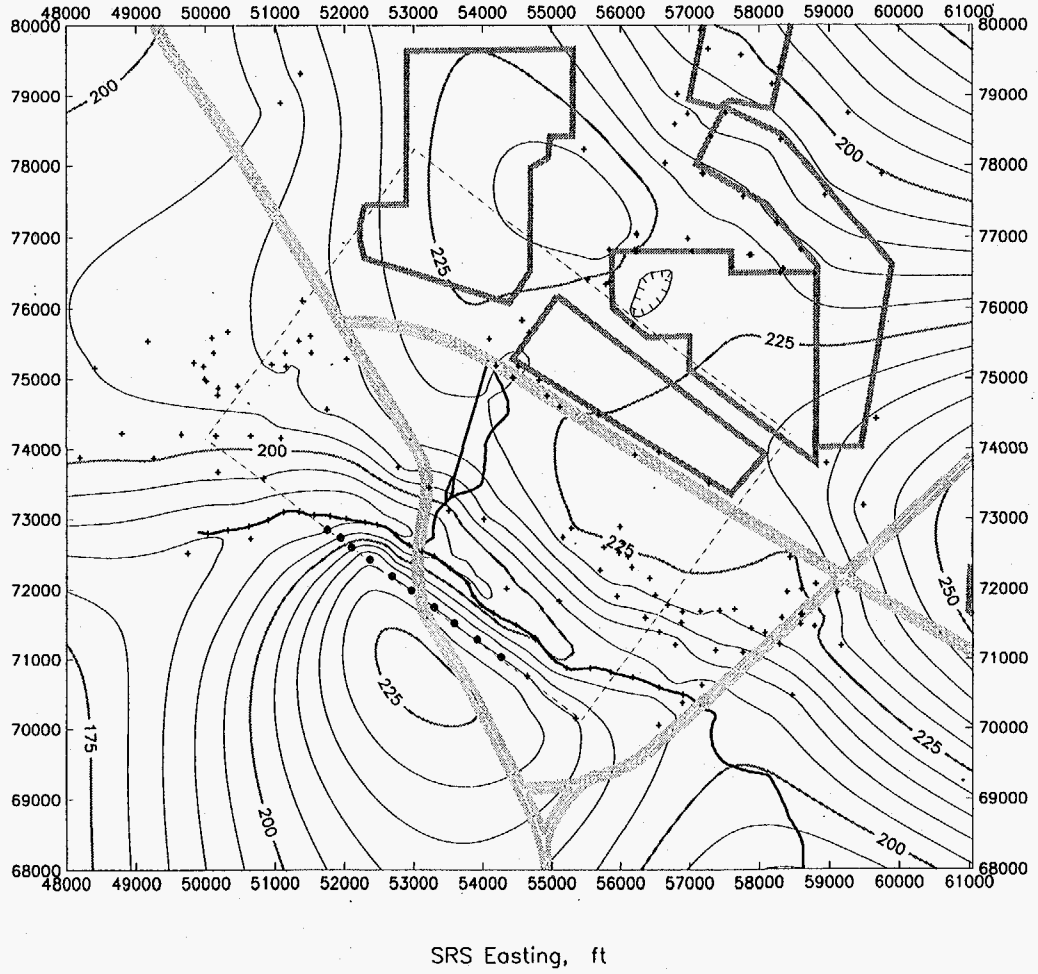

Figure 15. Head contour map for the "lower" aquifer zone within the Upper Three Runs aquifer (feet above mean sea level). + denotes data, ⊕ pseudo-data.

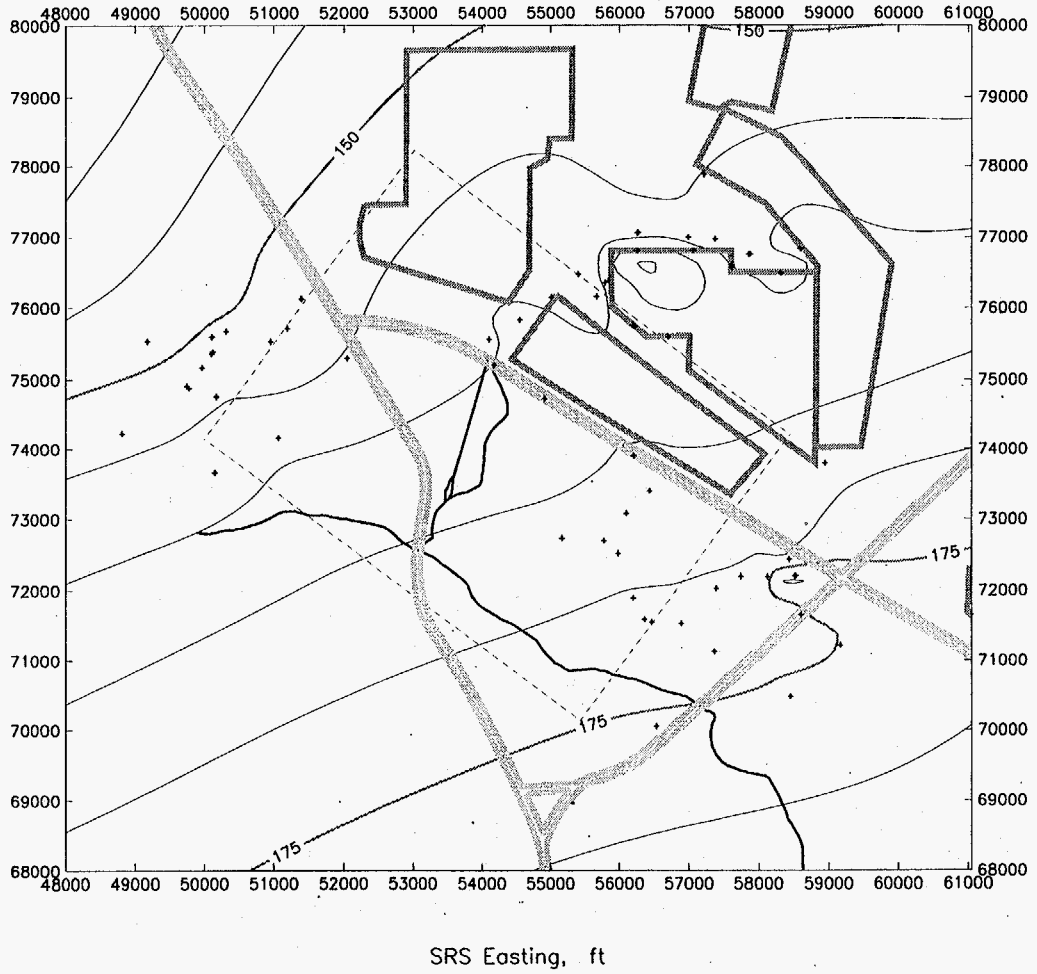

Figure 16. Head contour map for the Gordon aquifer (feet above mean sea level). + denotes data, ⊕ pseudo-data.

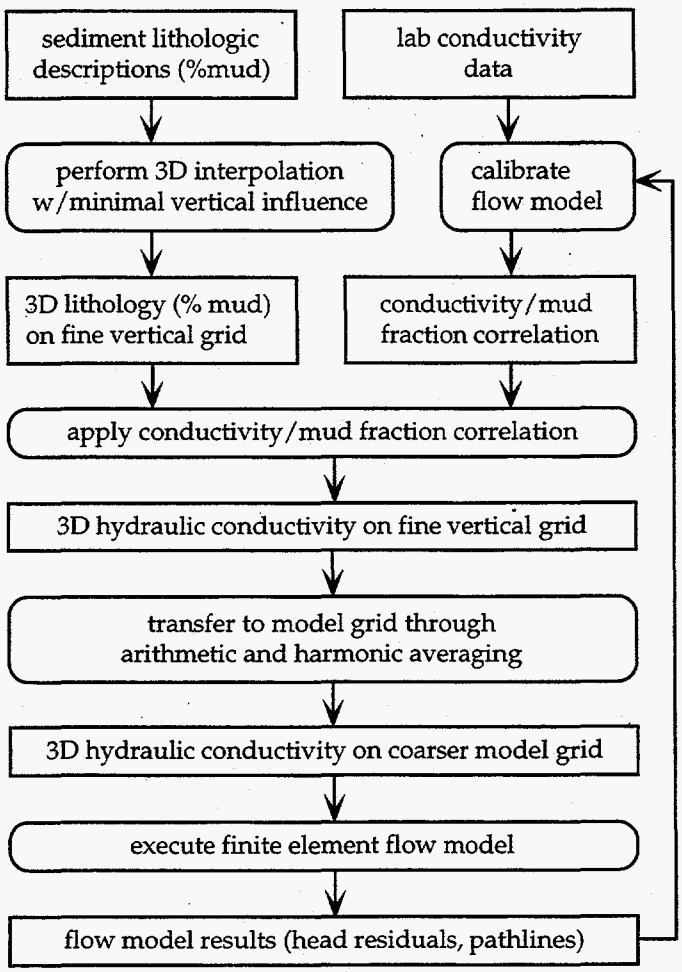

Figure 17. Flowchart summarizing the methodology for creating a heterogeneous conductivity field from sediment lithologic descriptions.

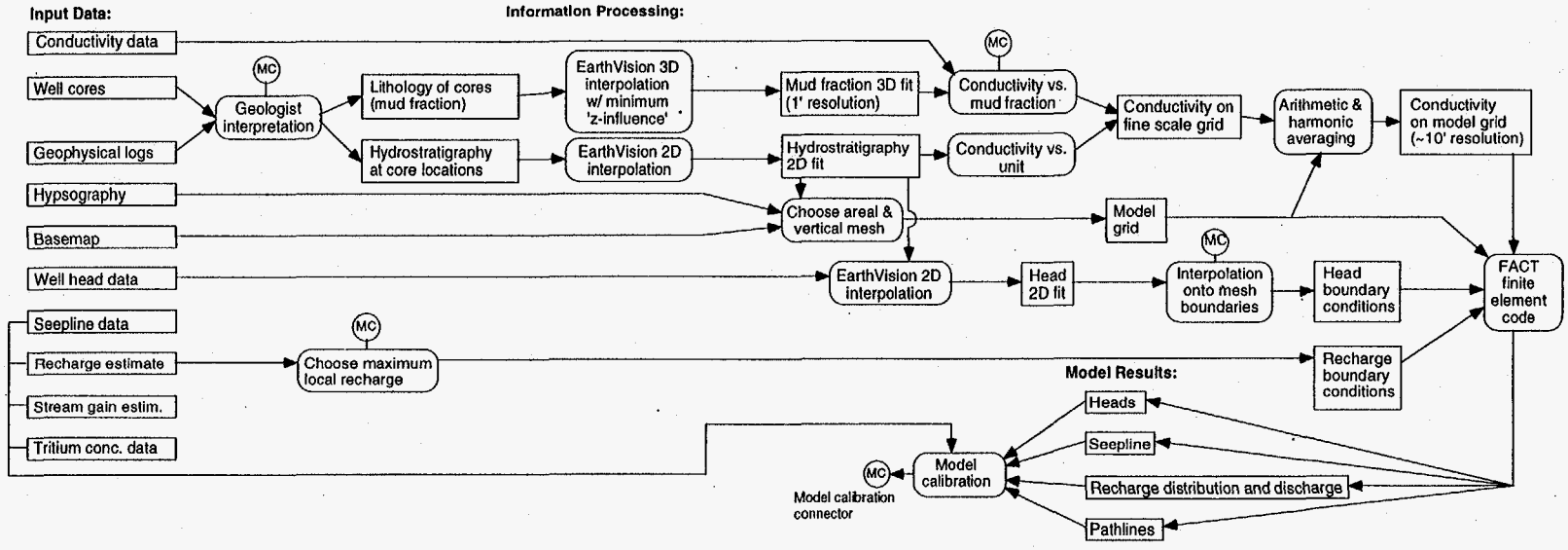

Figure 18. Flowchart summarizing the process chosen for creating a groundwater flow model using sediment core lithologic descriptions.

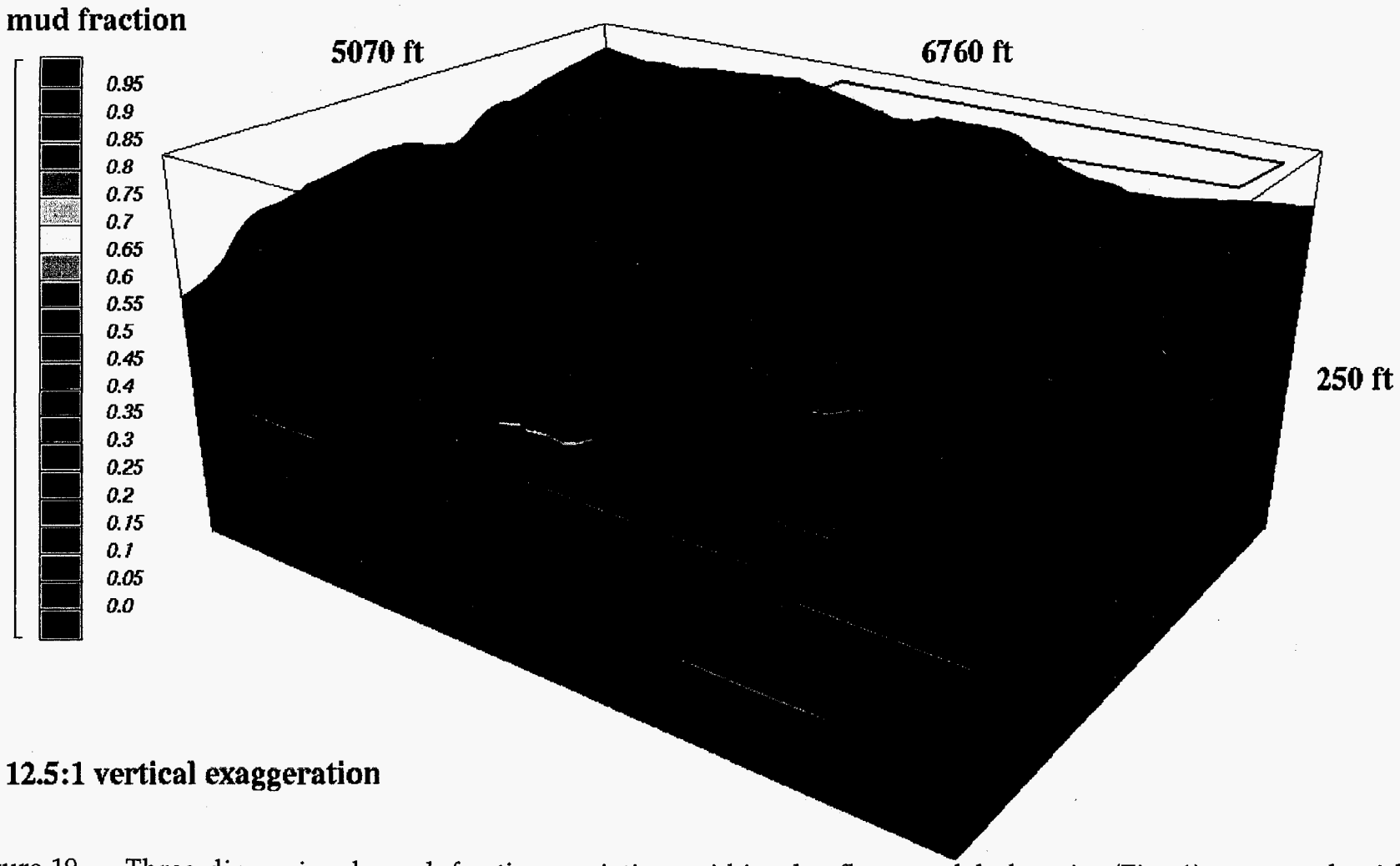

Figure 19. Three-dimensional mud fraction variation within the flow model domain (Fig. 1) generated with EarthVision®'s minimum tension 3D gridding algorithm and a vertical influence factor of 0.01. A total of 12,626 mud fraction values from the 84 cores depicted in Figure 1 were interpolated.

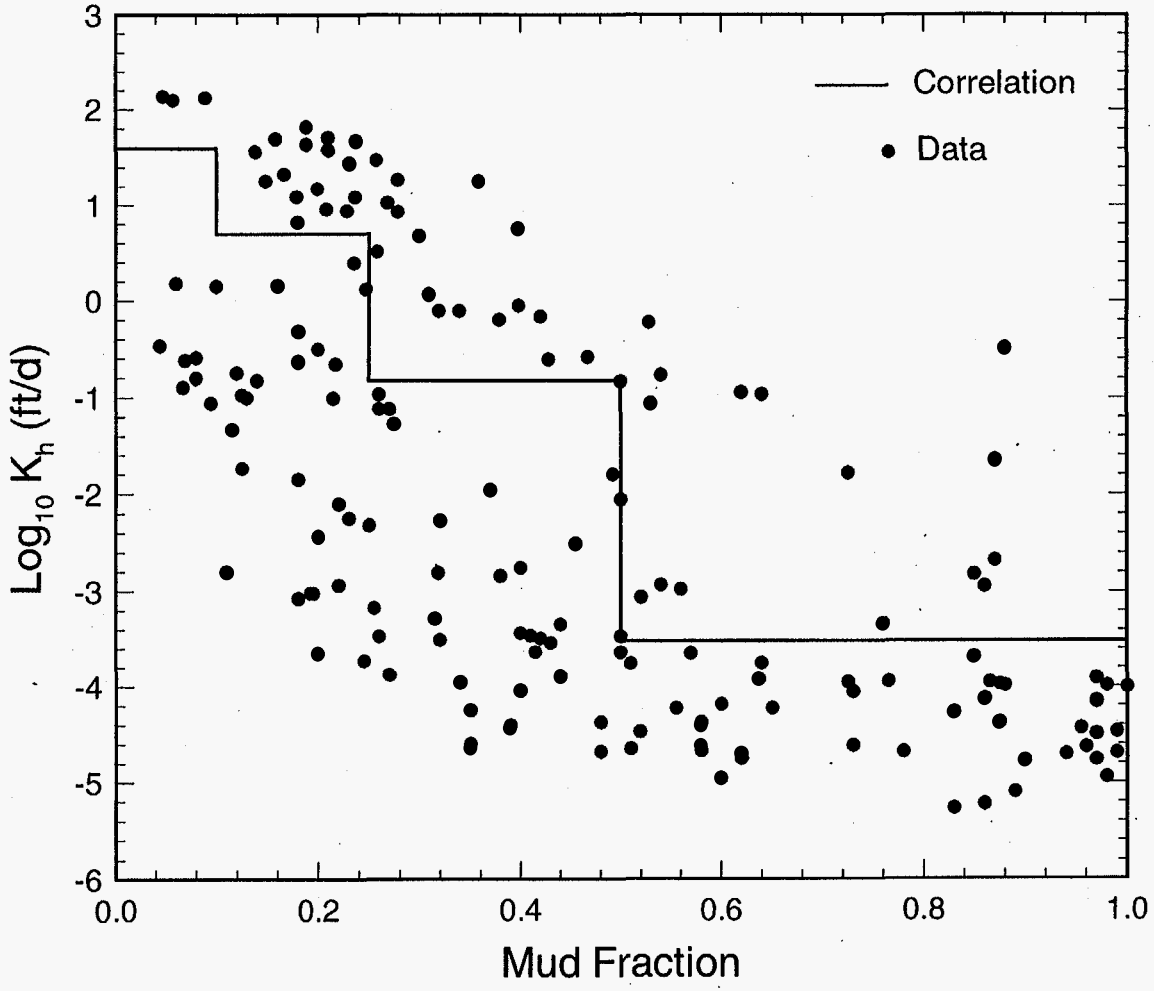

Figure 20. Horizontal conductivity as a function of mud fraction. The data represent laboratory measurements of conductivity from undisturbed core samples and mud fraction measured by sieve analysis. The stair-step correlation line is the result of comparison to the data shown and inverse flow modeling.

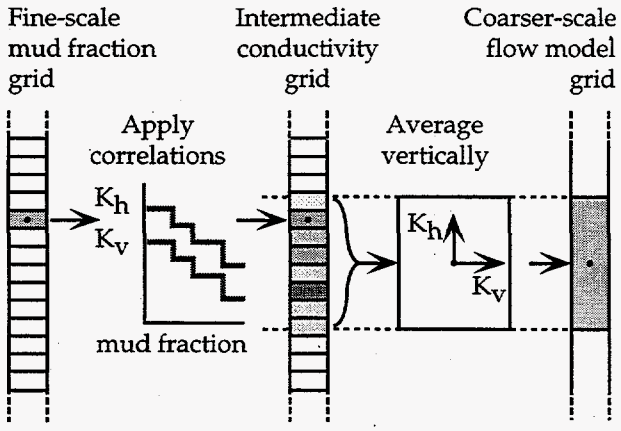

Figure 22. Process for translating the fine-scale mud fraction grid into the coarser-scale flow model conductivity grid.

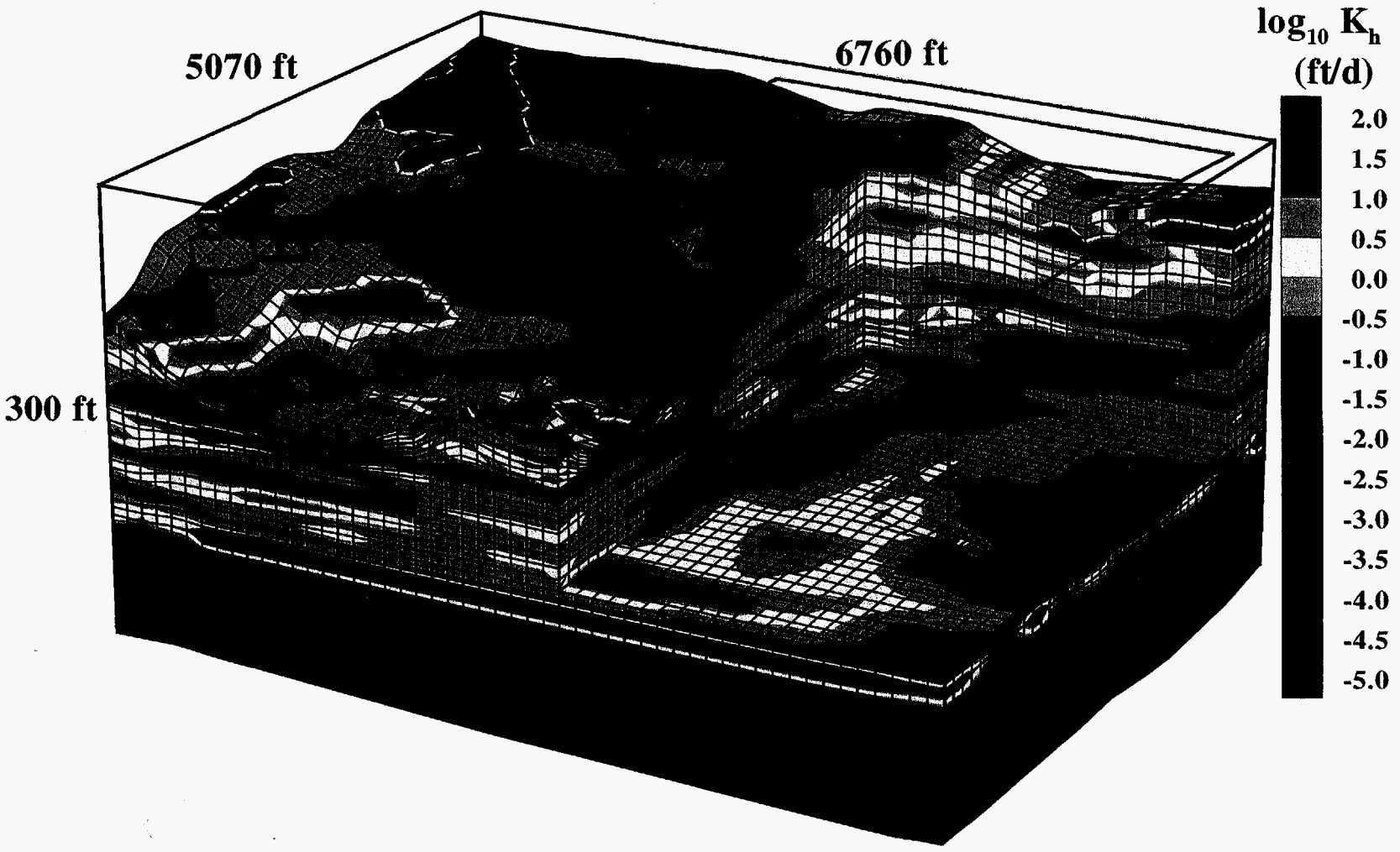

Figure 23. Three-dimensional horizontal conductivity distribution on the flow model finite-element mesh.

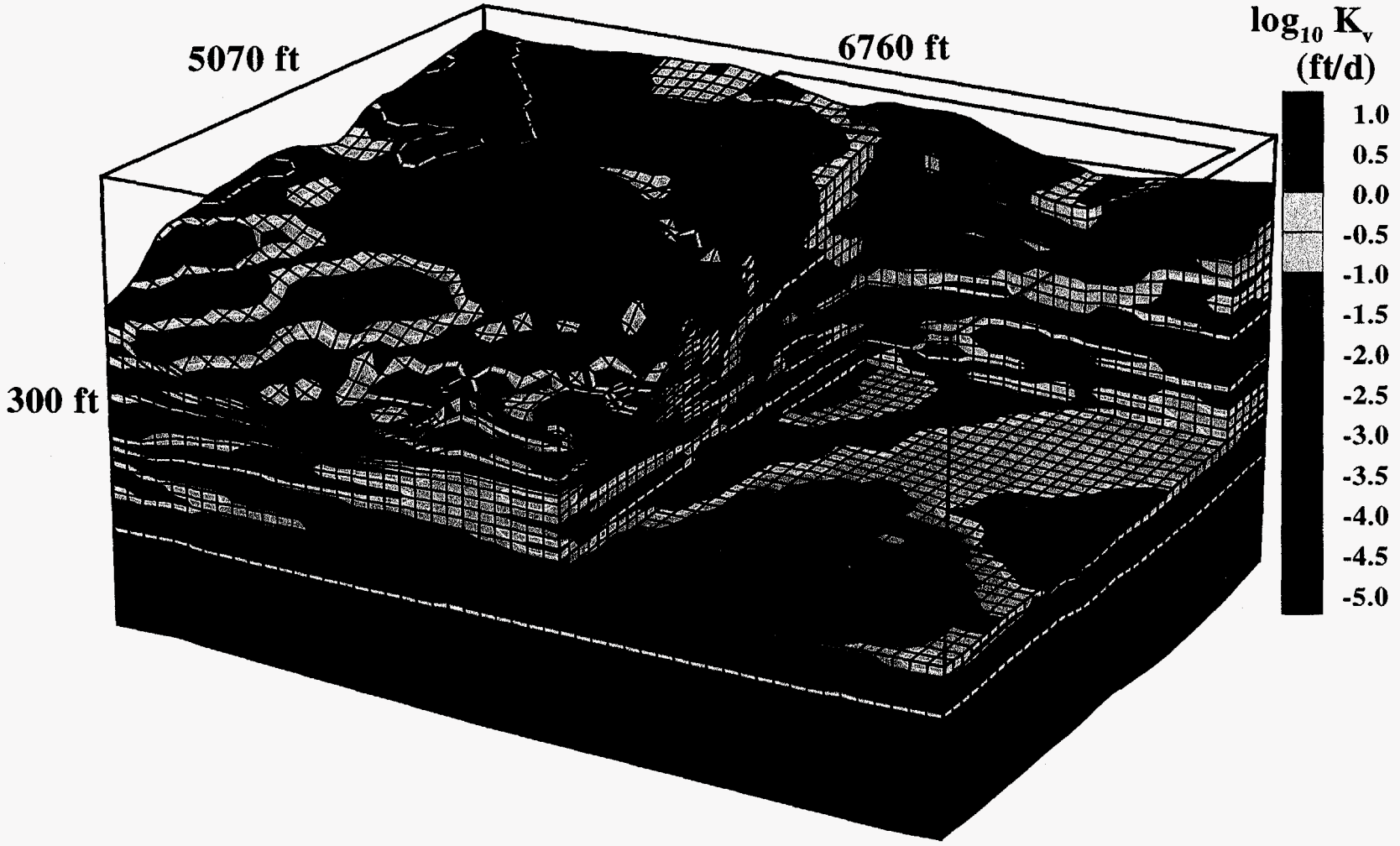

Figure 24. Three-dimensional vertical conductivity distribution on the flow model finite-element mesh.

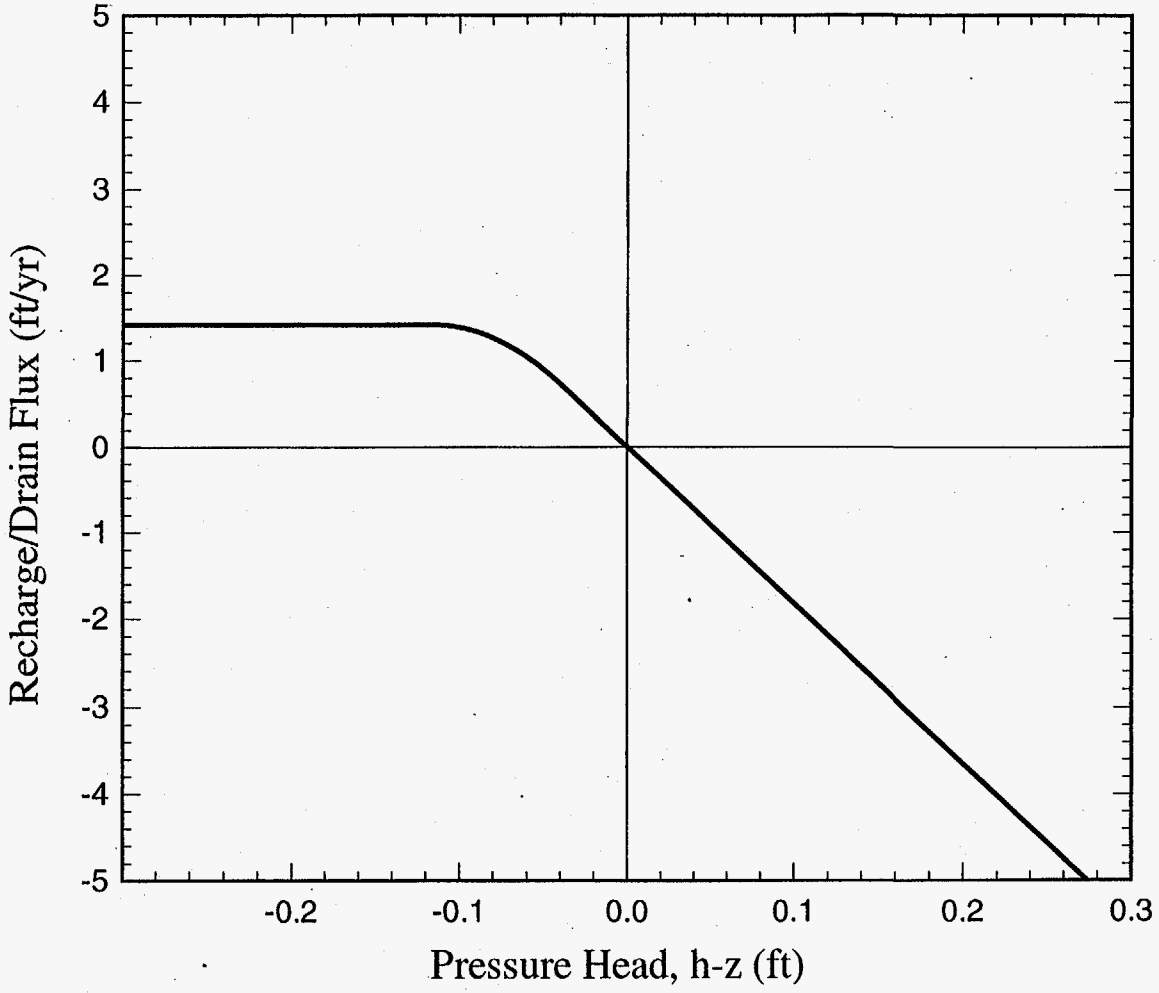

Figure 25. Combined recharge/drain boundary condition applied over the entire top surface of the flow model finite-element mesh.

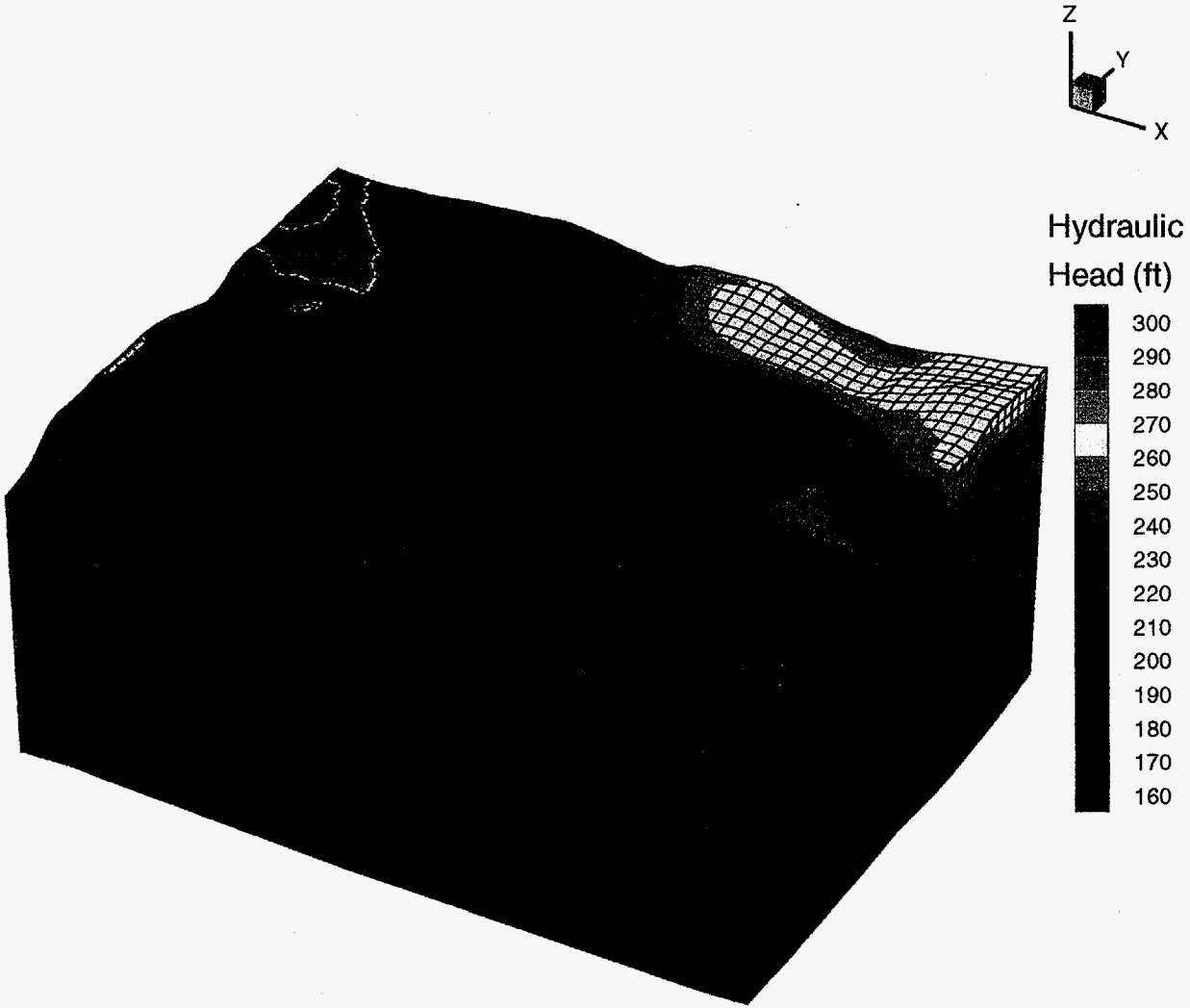

Figure 26. Simulated three-dimensional hydraulic head distribution.

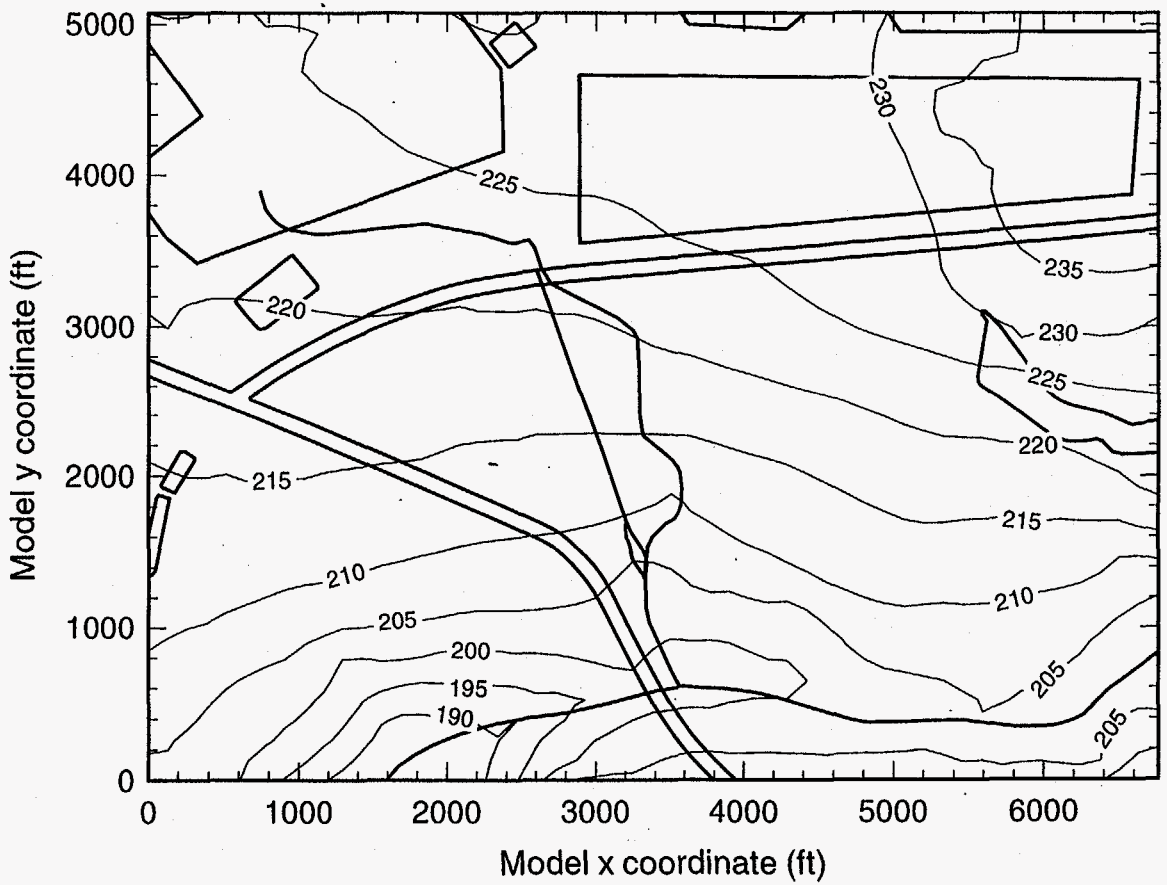

Figure 27. Contour map of vertically-averaged "upper" aquifer zone hydraulic head.

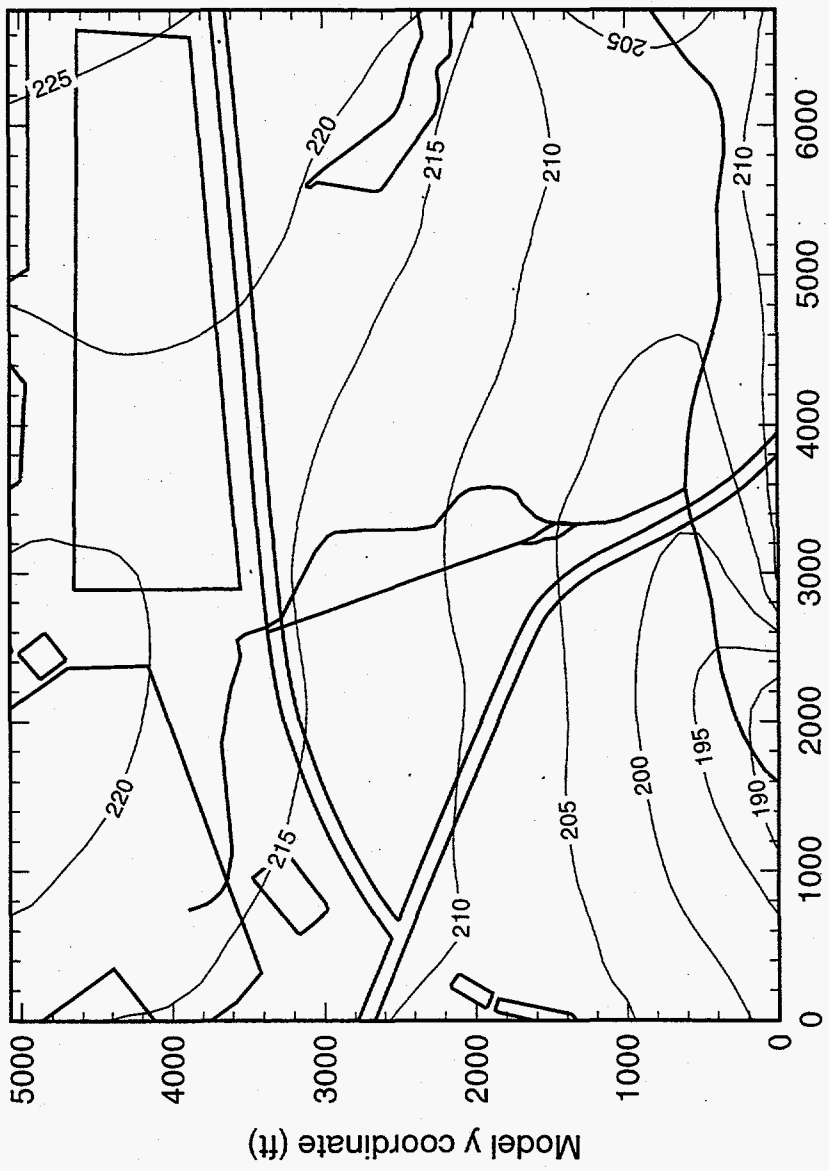

Figure 28. Contour map of vertically-averaged "lower" aquifer zone hydraulic head.

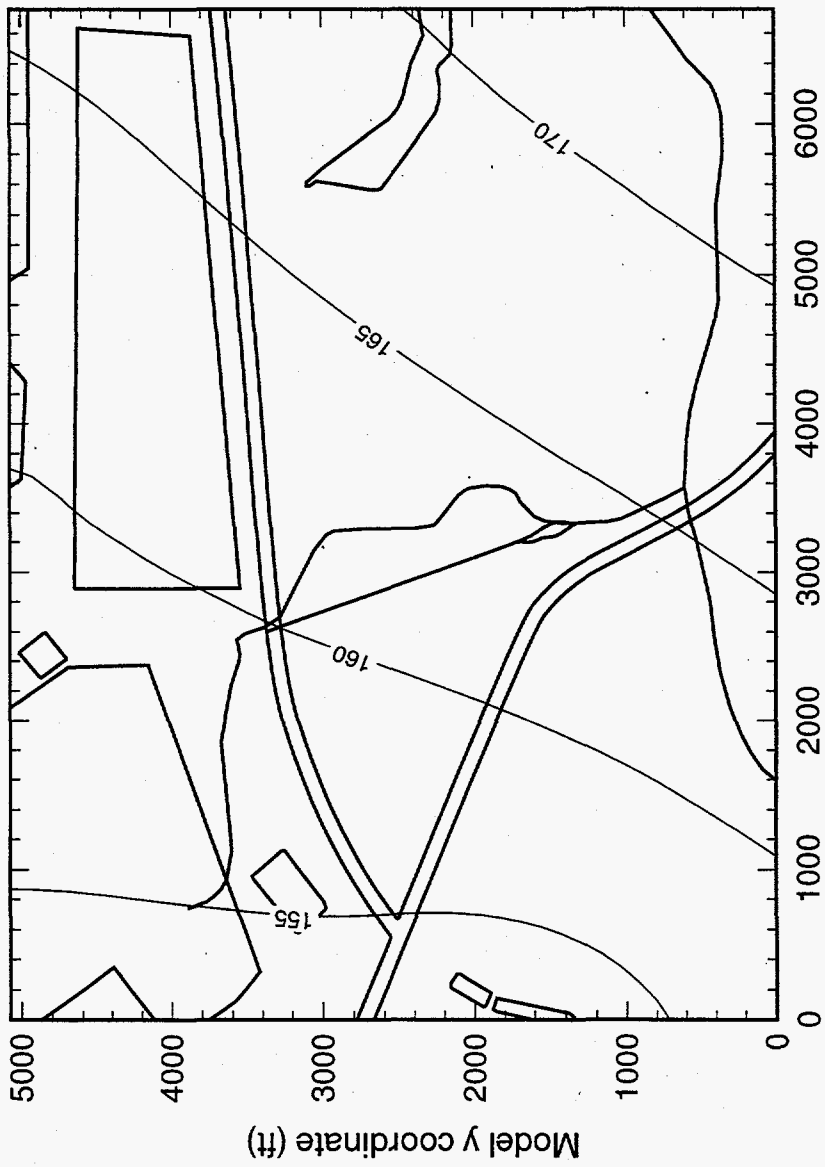

Figure 29. Contour map of vertically-averaged Gordon aquifer hydraulic head.

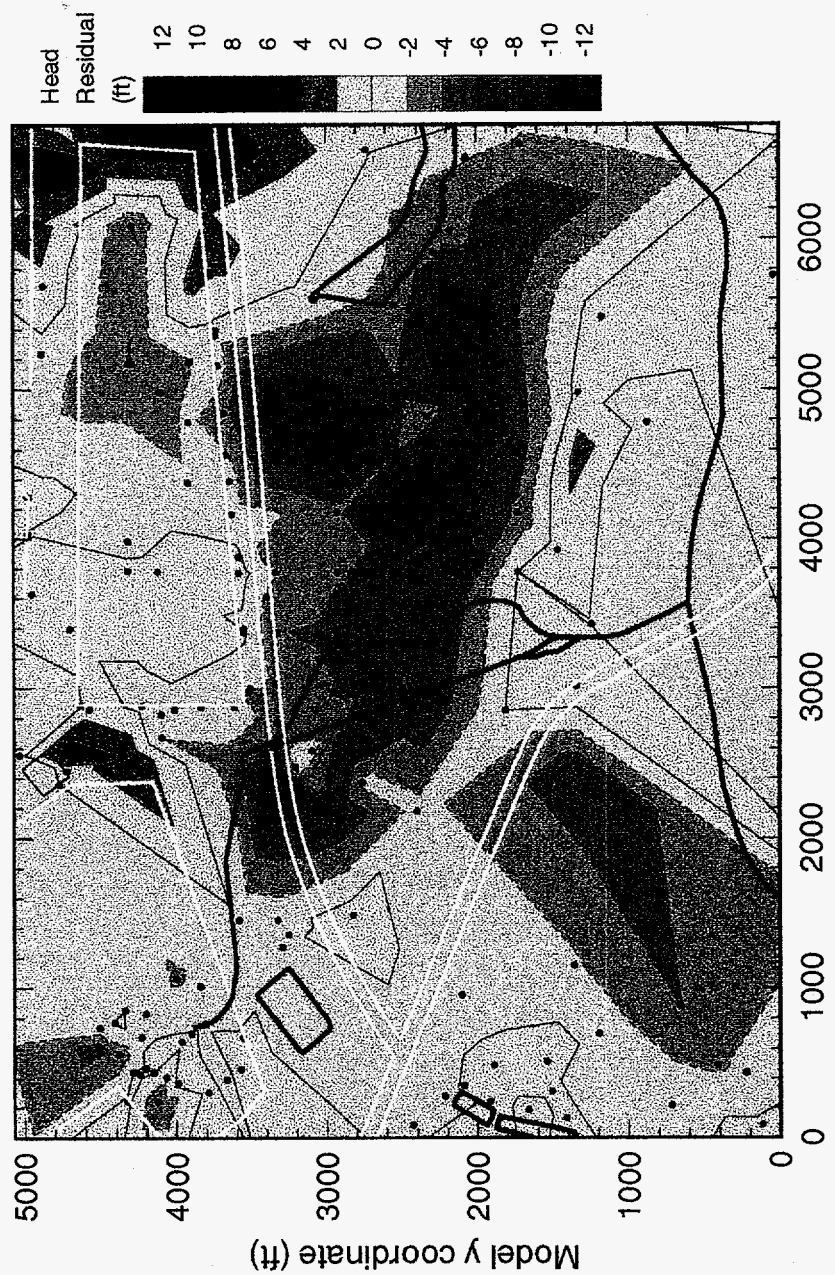

Figure 30. Contour map of "upper" aquifer zone head residuals.

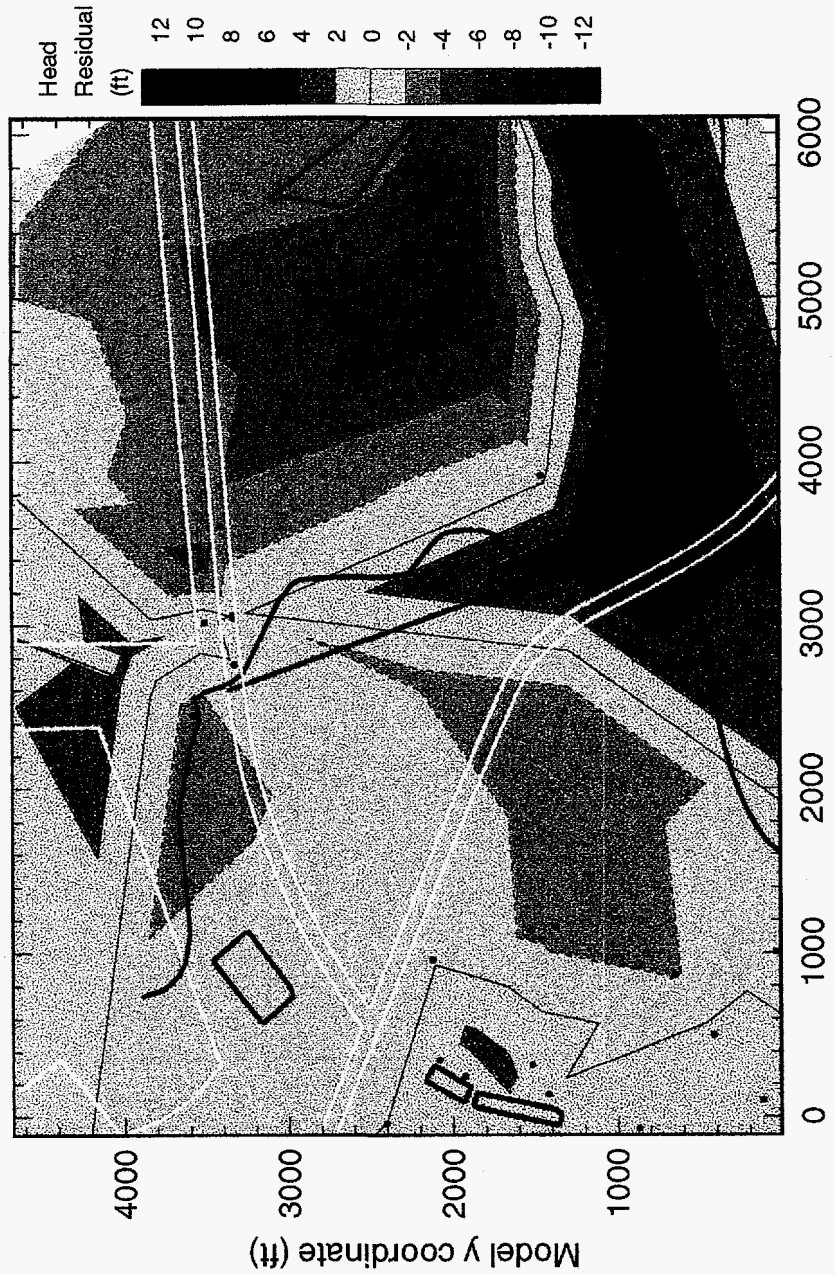

Figure 31. Contour map of "lower" aquifer zone head residuals.

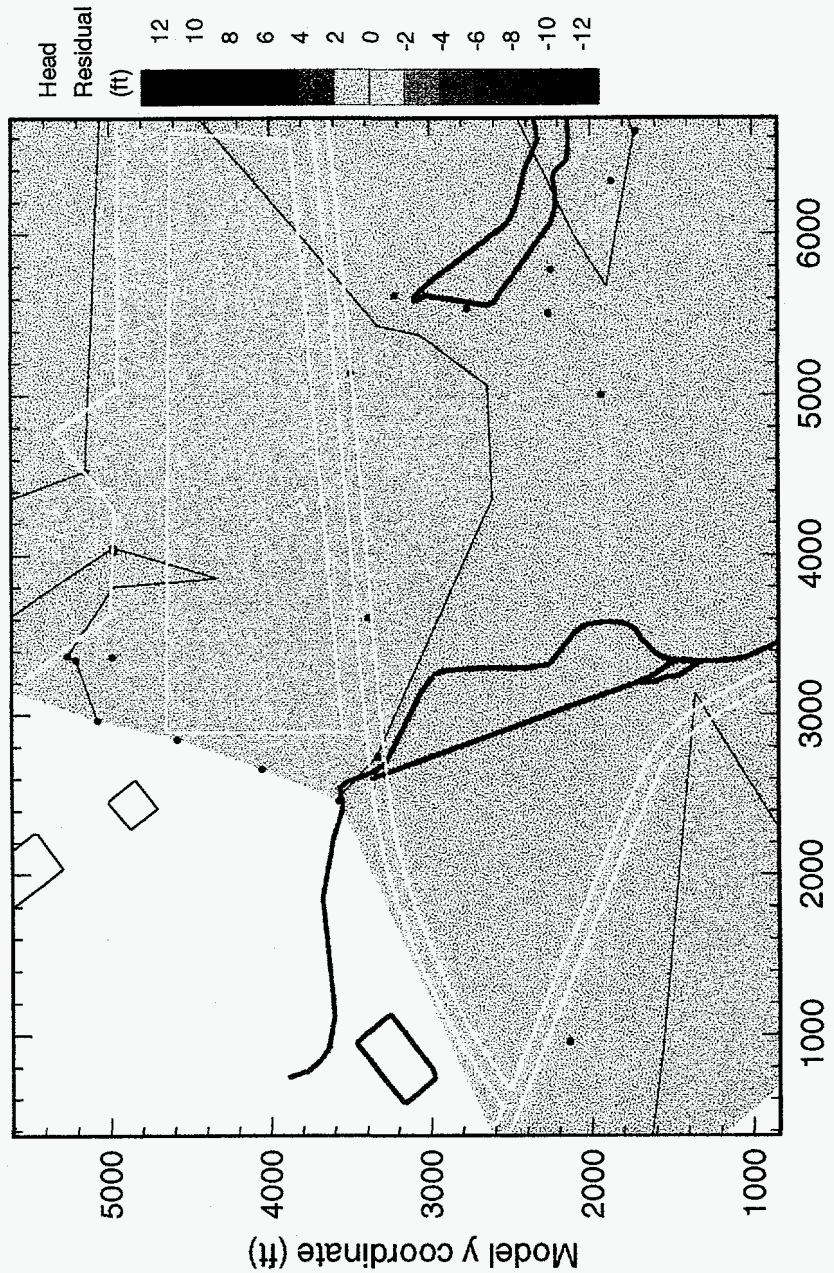

Figure 32. Contour map of Gordon aquifer head residuals.

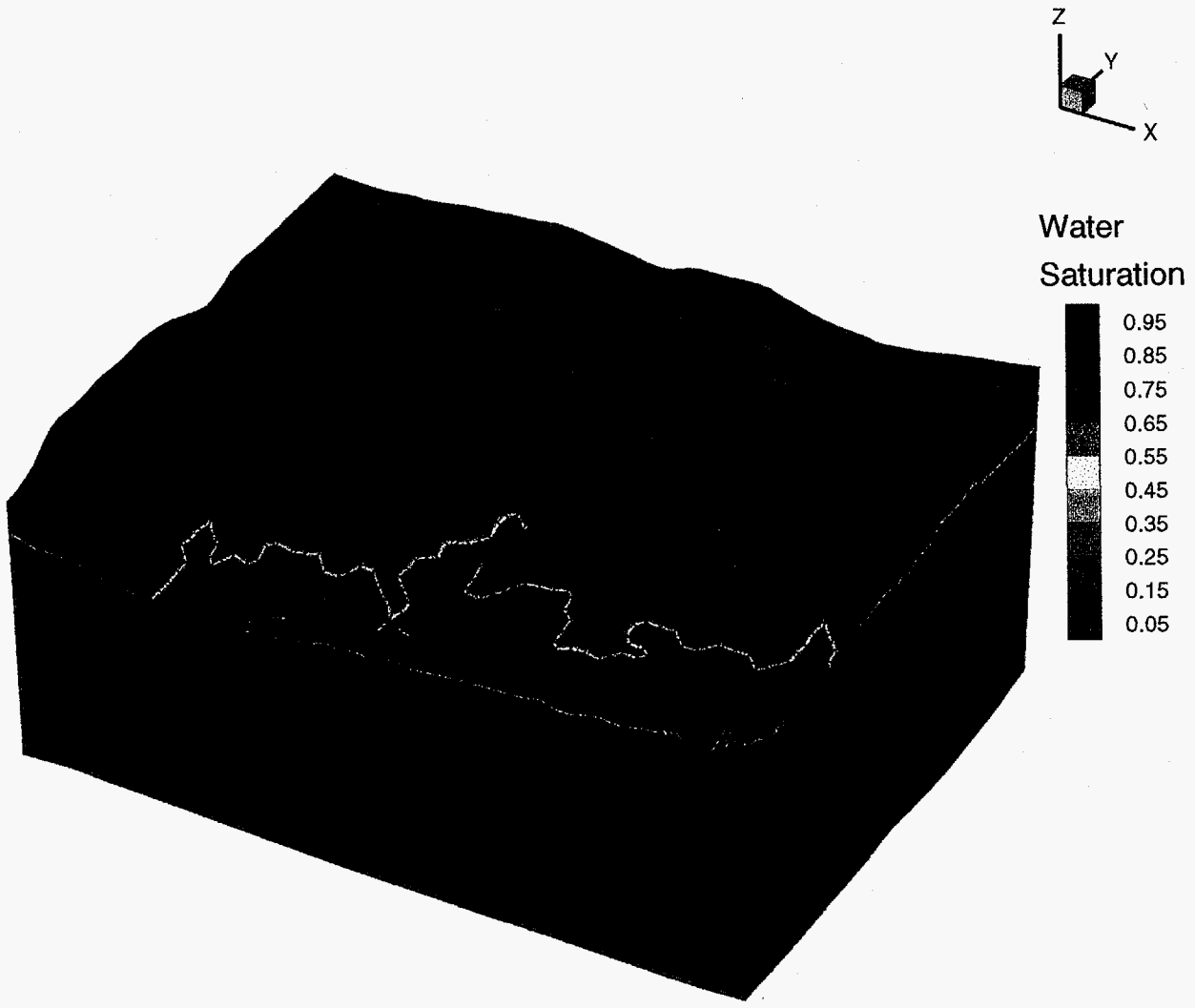

Figure 33. Simulated three-dimensional saturation distribution.

Figure 34. Simulated recharge distribution.

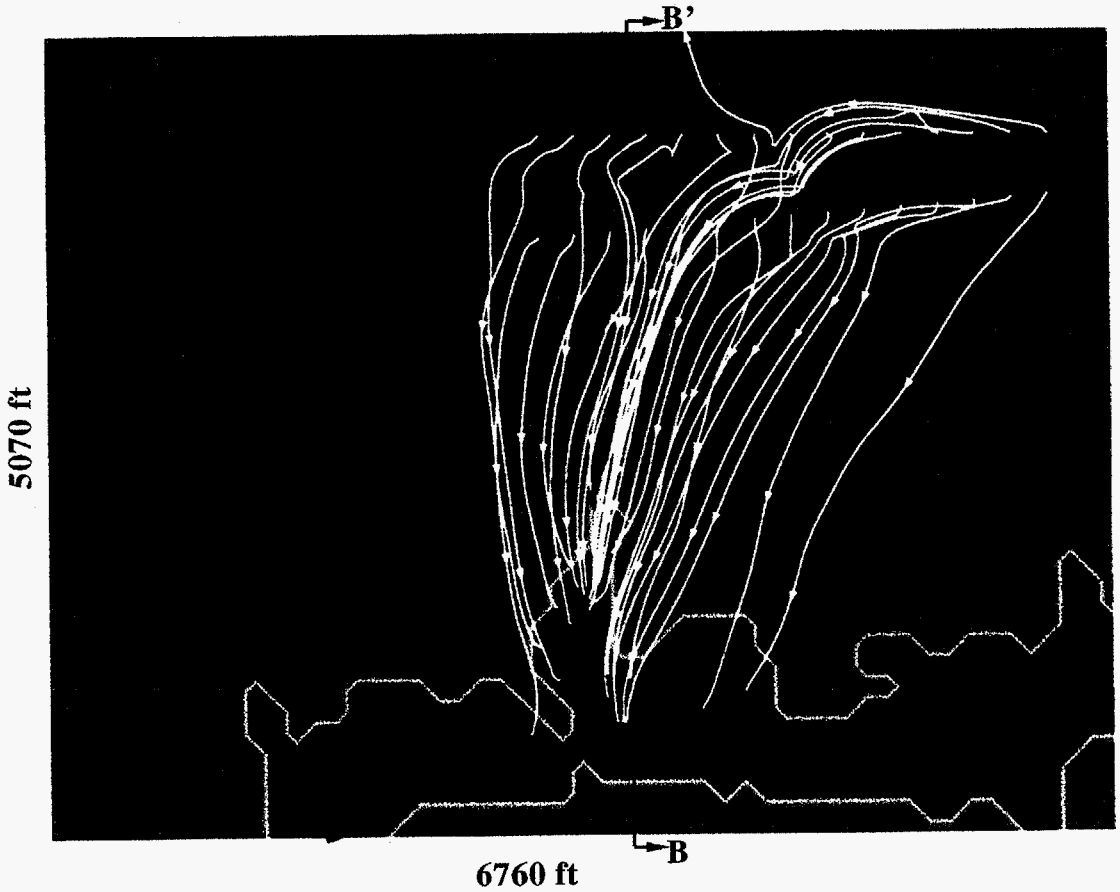

Figure 35. Three-dimensional pathlines originating from the Old Burial Ground projected onto a two-dimensional plane overlaying water saturation.

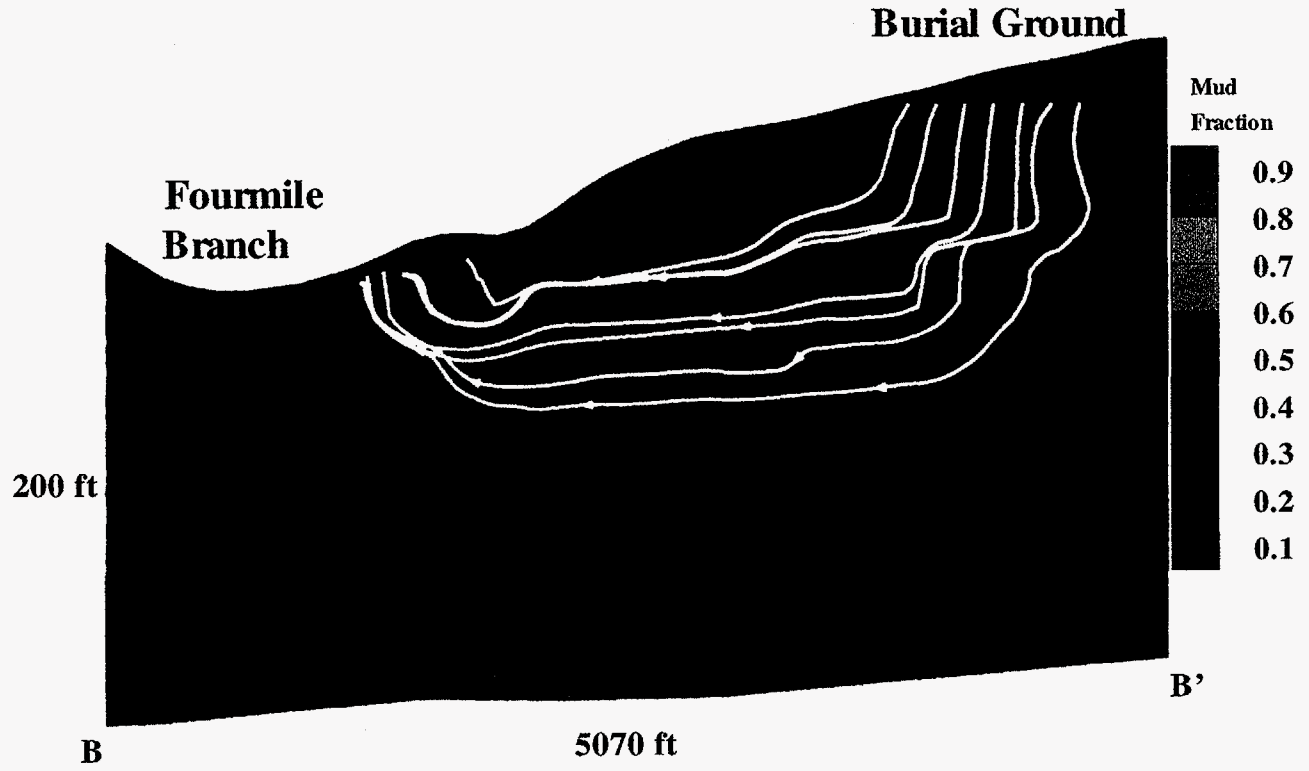

Figure 36. Three-dimensional pathlines projected onto cross-section B-B' in Figure 35 with mud fraction as the background.

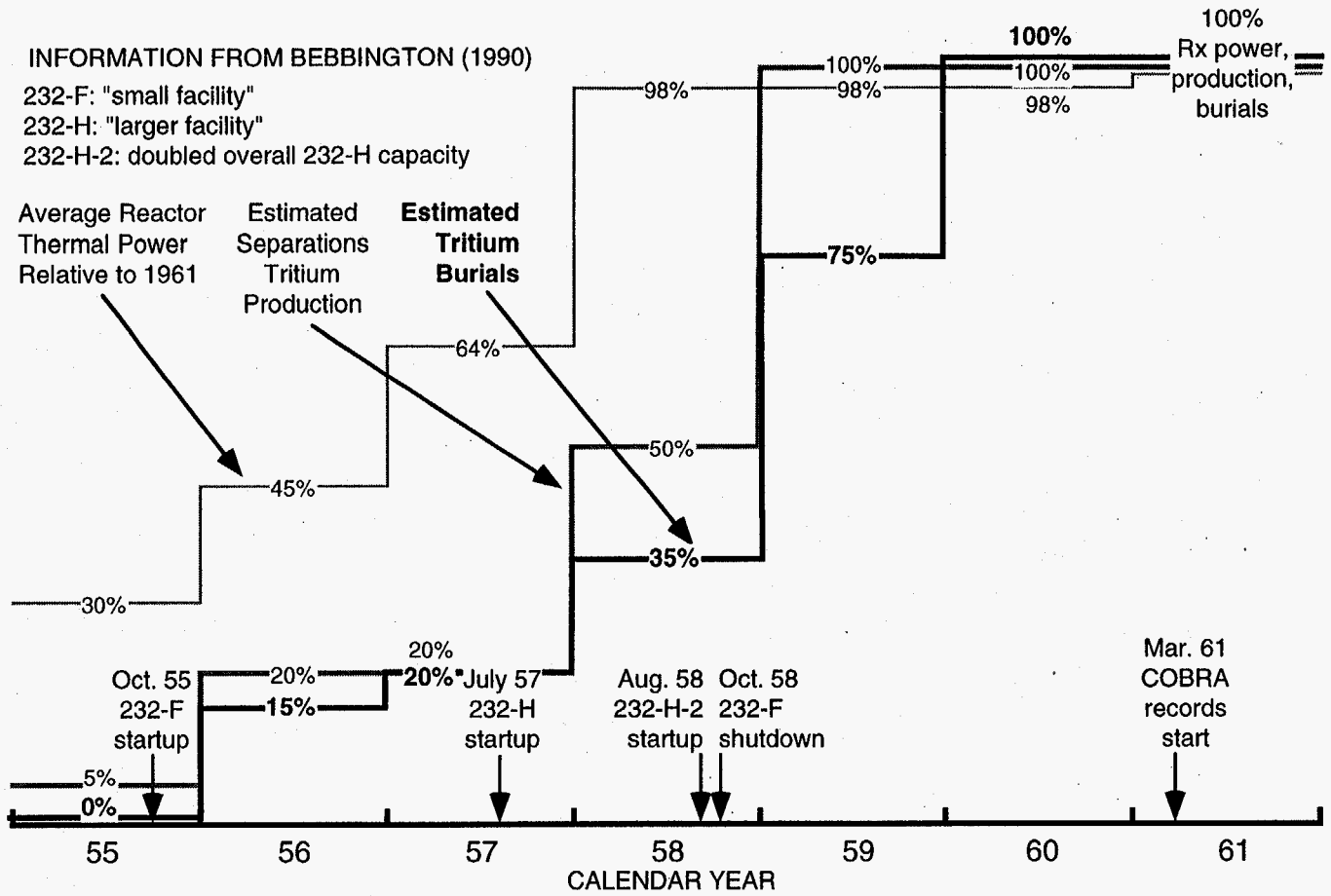

BASIS FOR TRITIUM PRODUCTION ESTIMATES:

- 100% value for 1959-60 based on assumption that full production was reached with 232-H-2 startup
- 50% value for 1958 based on assumption that 232-H-2 doubled burials in 1959
- 20% value for 1956-57 based on assumption that 232-H has 50% more capacity than 232-F
- 5% value for 1955 is 20% prorated over the 3 months from Oct. to Dec.
- estimates are also consistent with average reactor power assuming all five reactors are operating from 1955-61

BASIS FOR TRITIUM BURIAL ESTIMATES

- 6 month delay assumed between production at separations facility and burial
- consistent with Table 2 of Hyder (1993), namely, sum of 1955-1960 burials divided by 1961 burials is 2.45 compared to 2.2 in Table 2

Figure 37. Estimated pre-COBRA tritium burials relative to 1961.

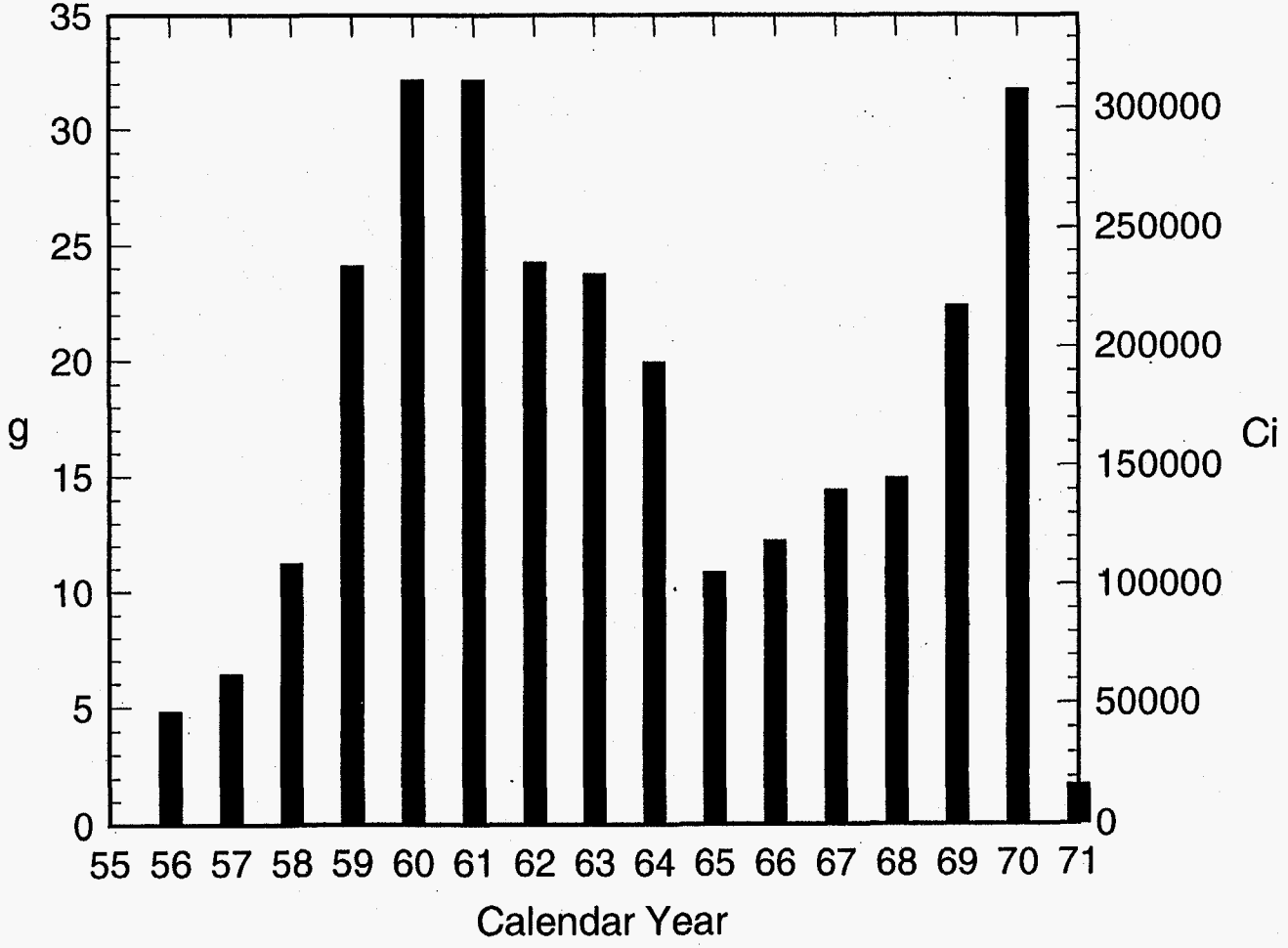

Figure 38. Estimated total annual tritium burials of all forms to the Old Burial Ground.

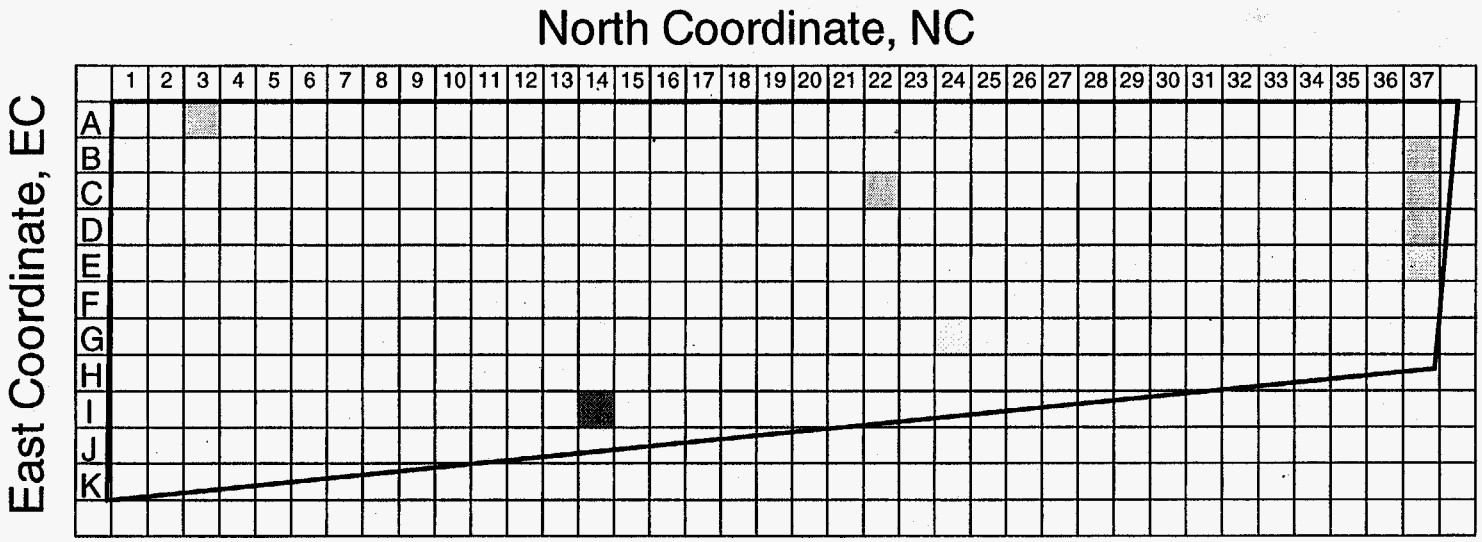

Figure 39a. Normalized spatial variation in tritium burials of all forms for the calendar year 1961.

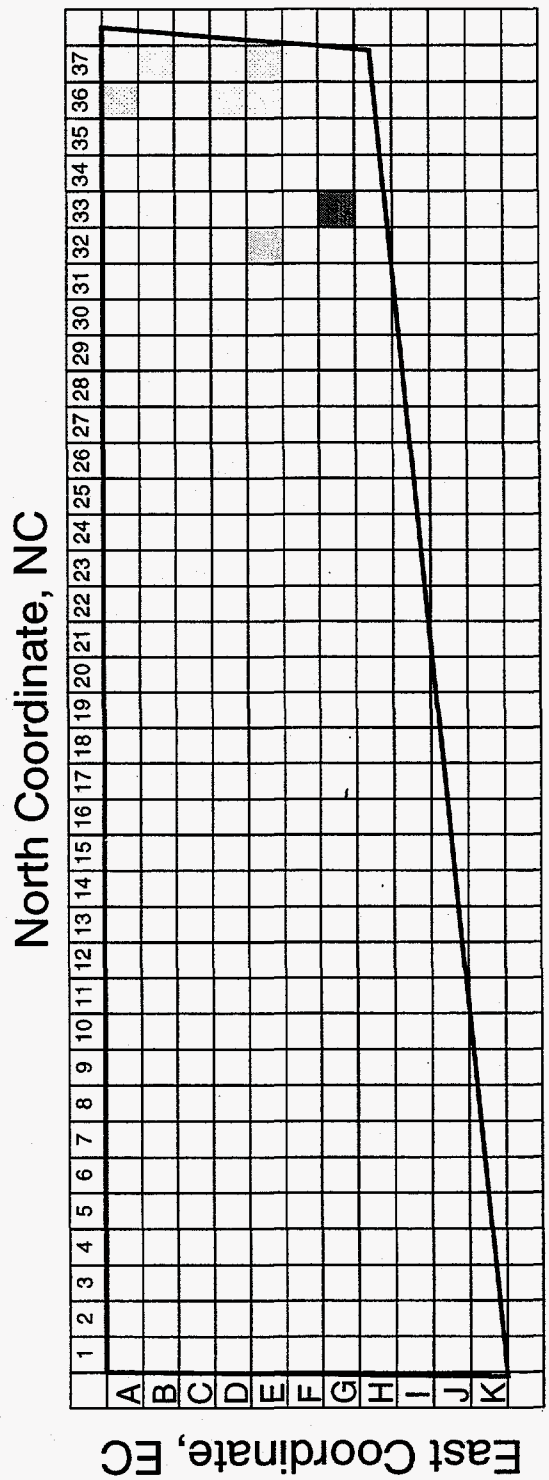

Figure 39b. Normalized spatial variation in tritium burials of all forms for the calendar year 1962.

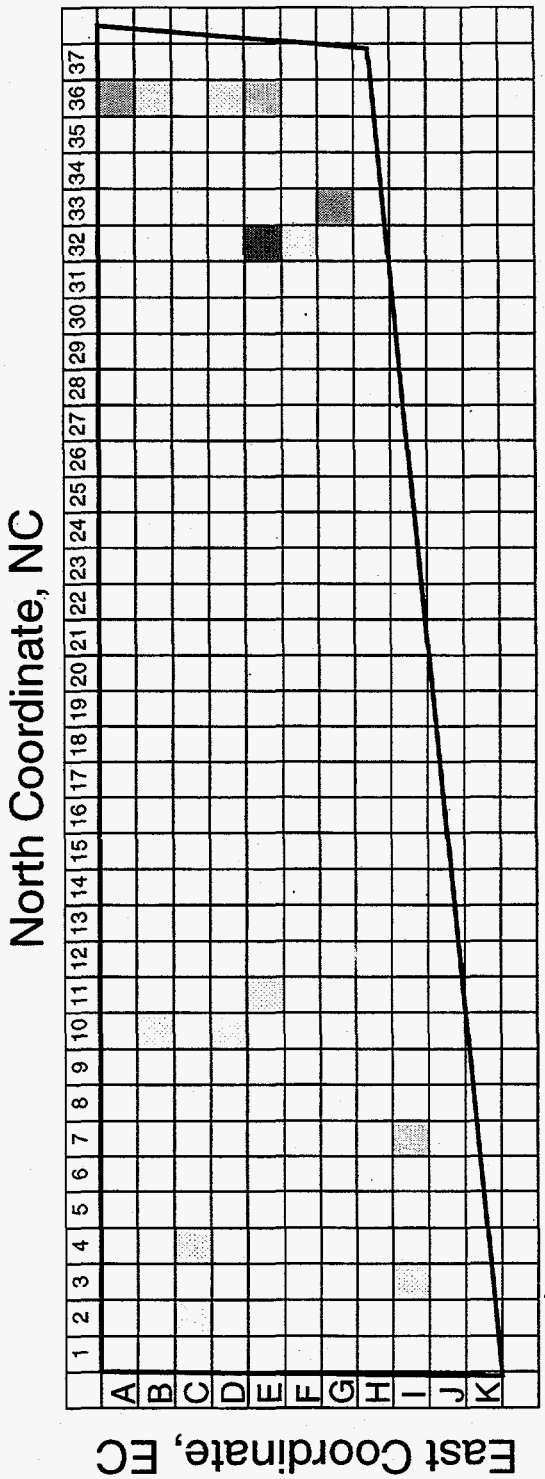

Figure 39c. Normalized spatial variation in tritium burials of all forms for the calendar year 1963.

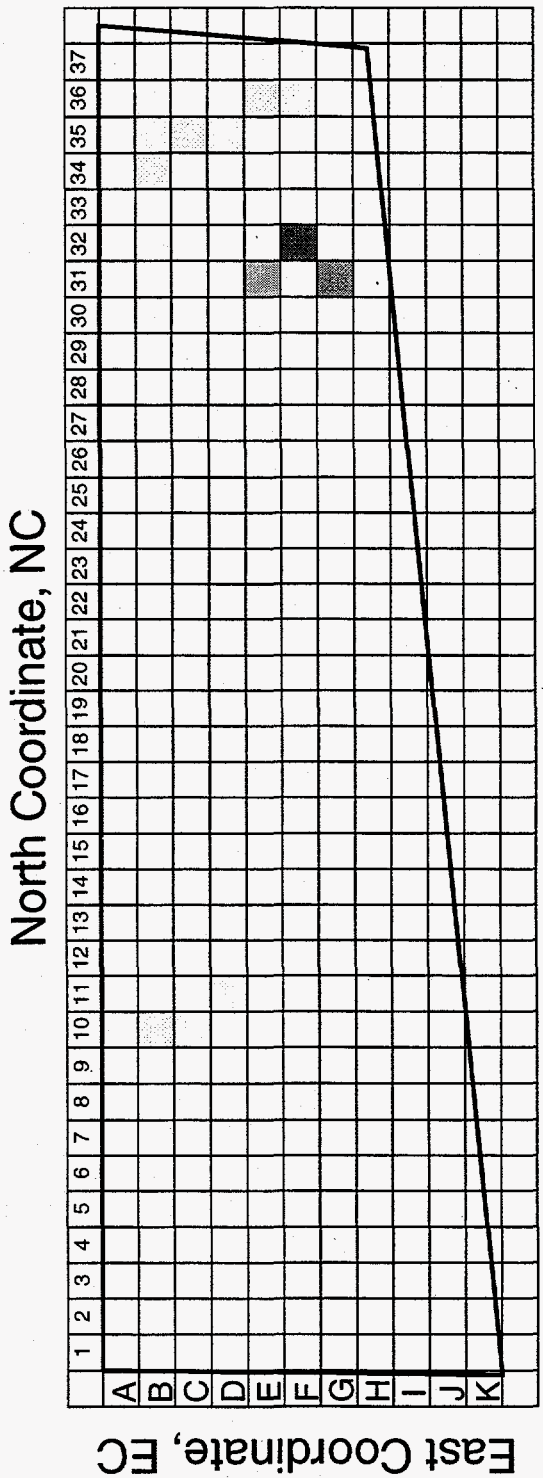

Figure 39d. Normalized spatial variation in tritium burials of all forms for the calendar year 1964.

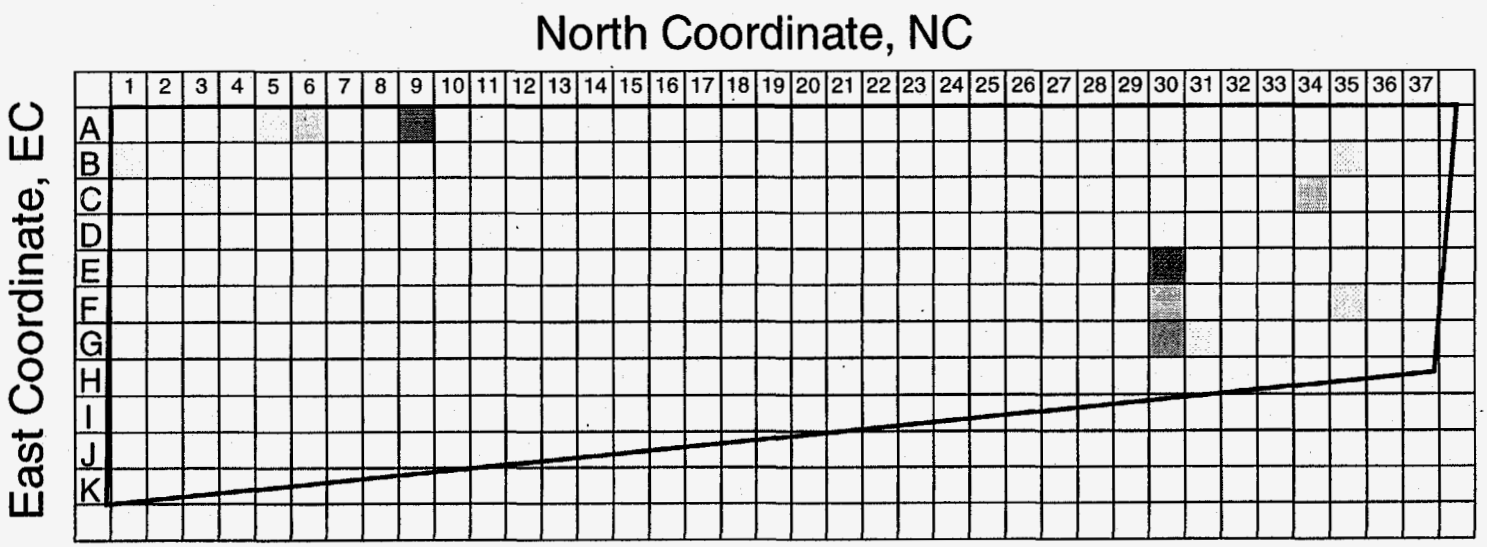

Figure 39e. Normalized spatial variation in tritium burials of all forms for the calendar year 1965.

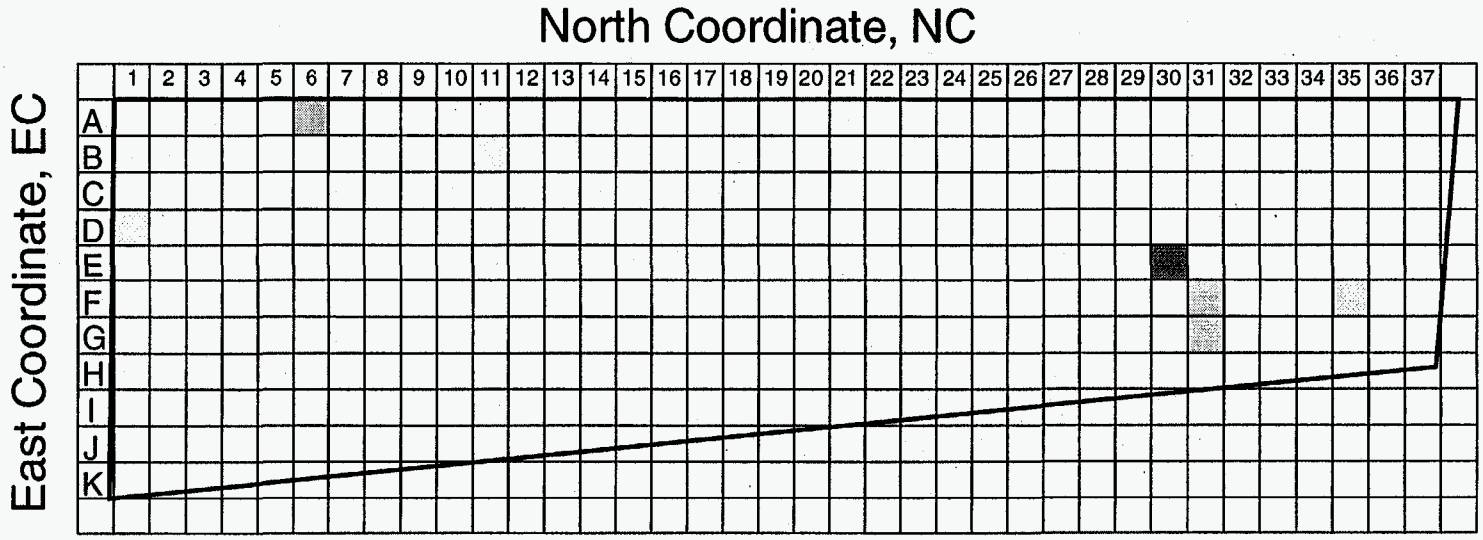

Figure 39f. Normalized spatial variation in tritium burials of all forms for the calendar year 1966.

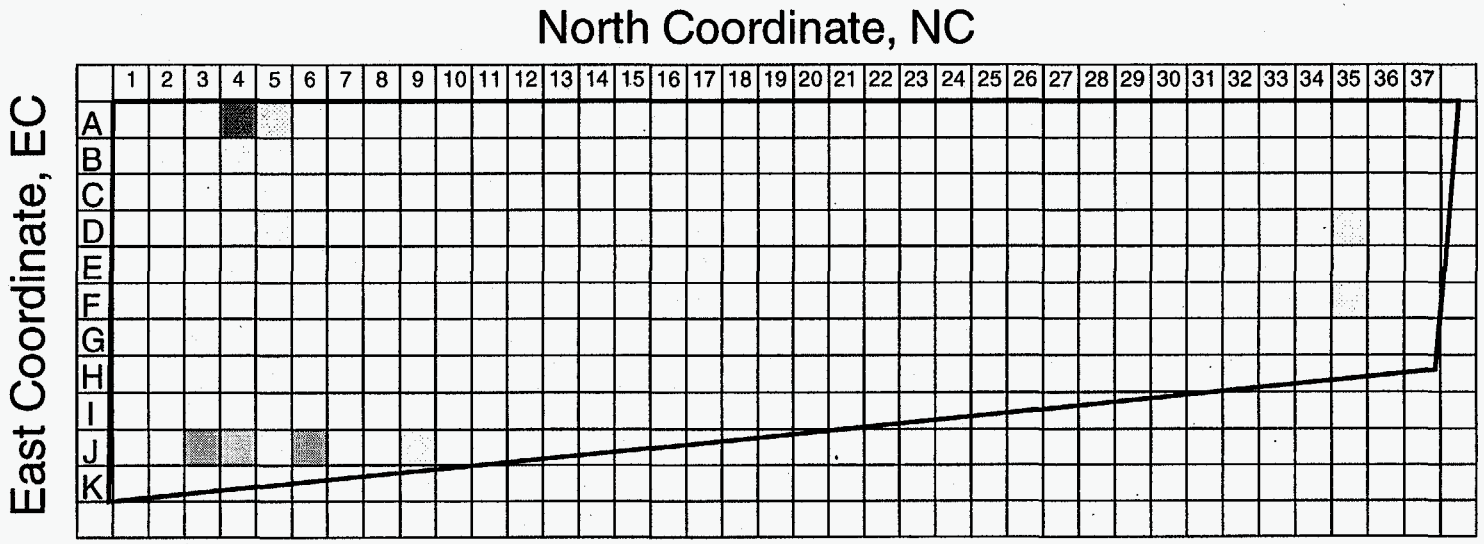

Figure 39g. Normalized spatial variation in tritium burials of all forms for the calendar year 1967.

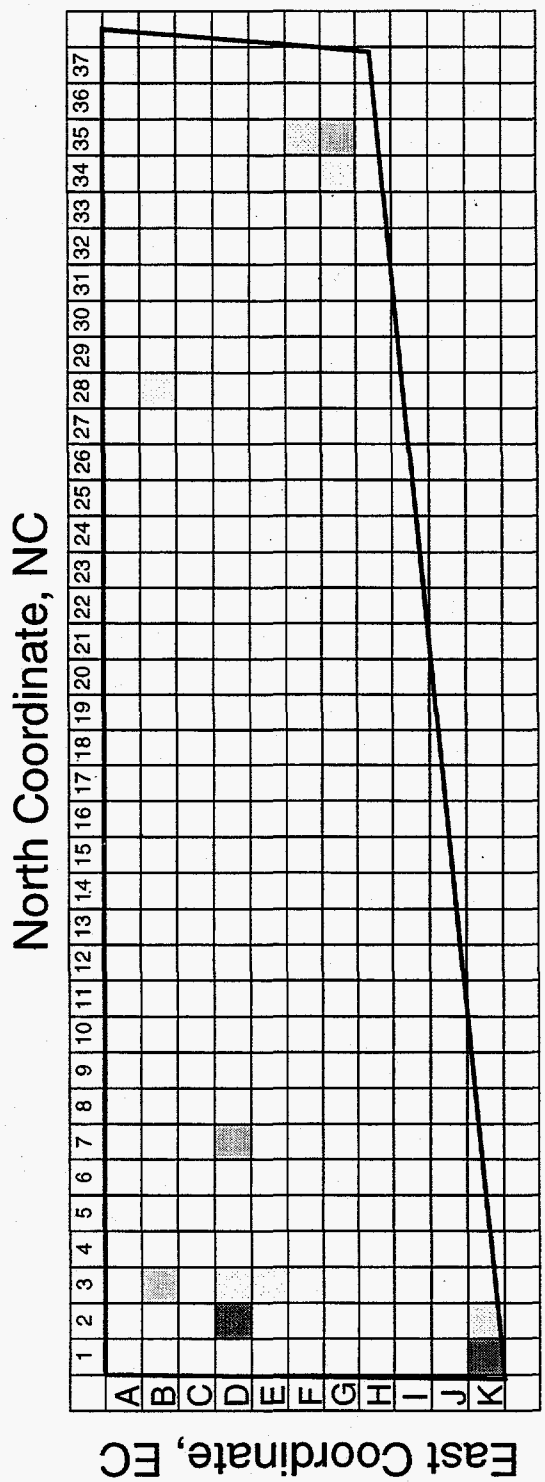

Figure 39h. Normalized spatial variation in tritium burials of all forms for the calendar year 1968.

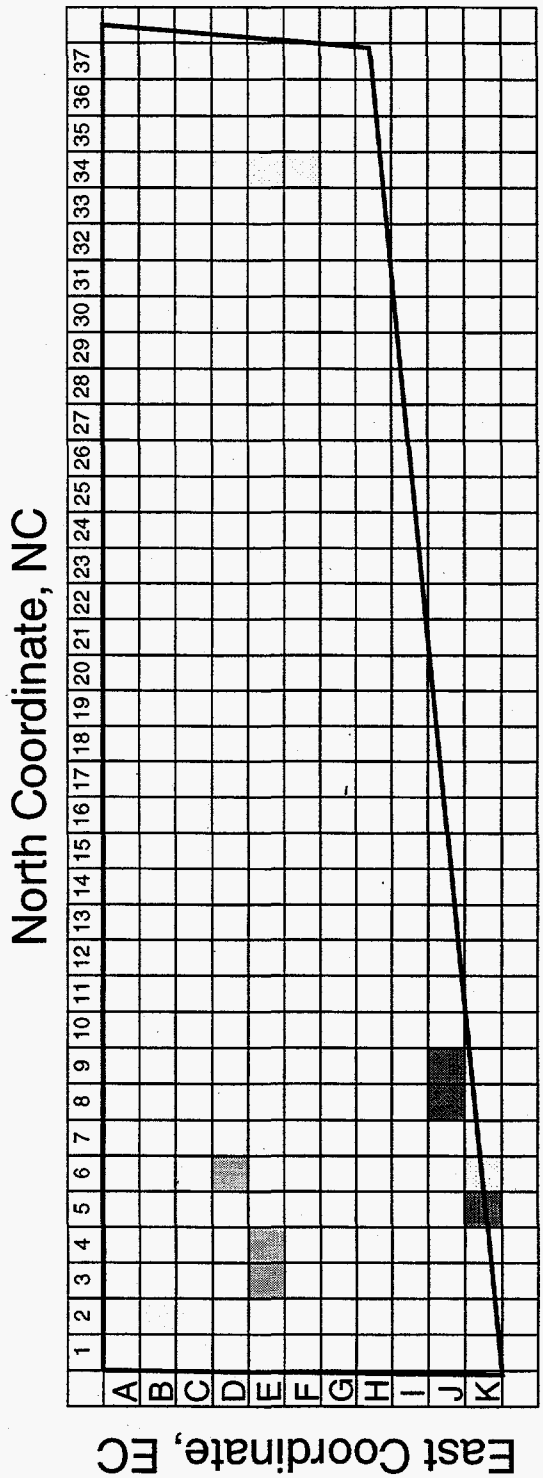

Figure 39i. Normalized spatial variation in tritium burials of all forms for the calendar year 1969.

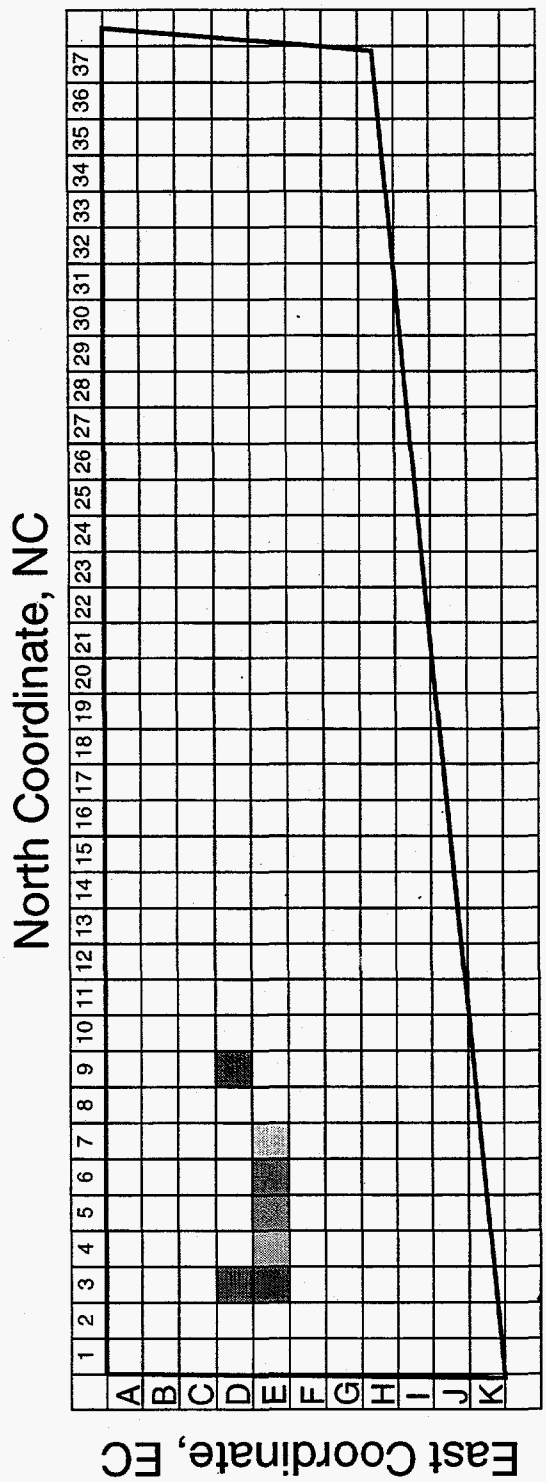

Figure 39j. Normalized spatial variation in tritium burials of all forms for the calendar year 1970.

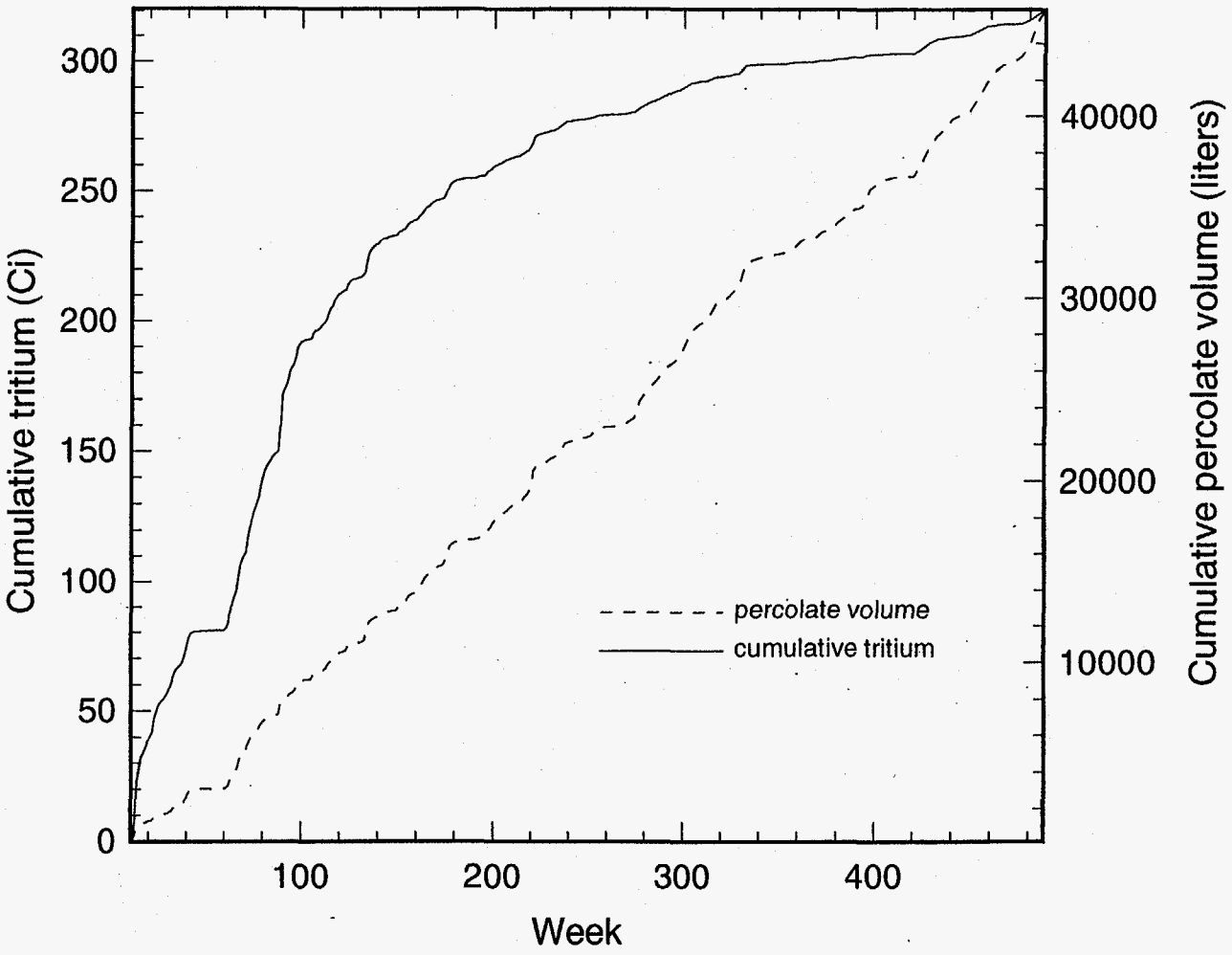

Figure 40. Cumulative Curie content and volume of percolate for tritium lysimeter.

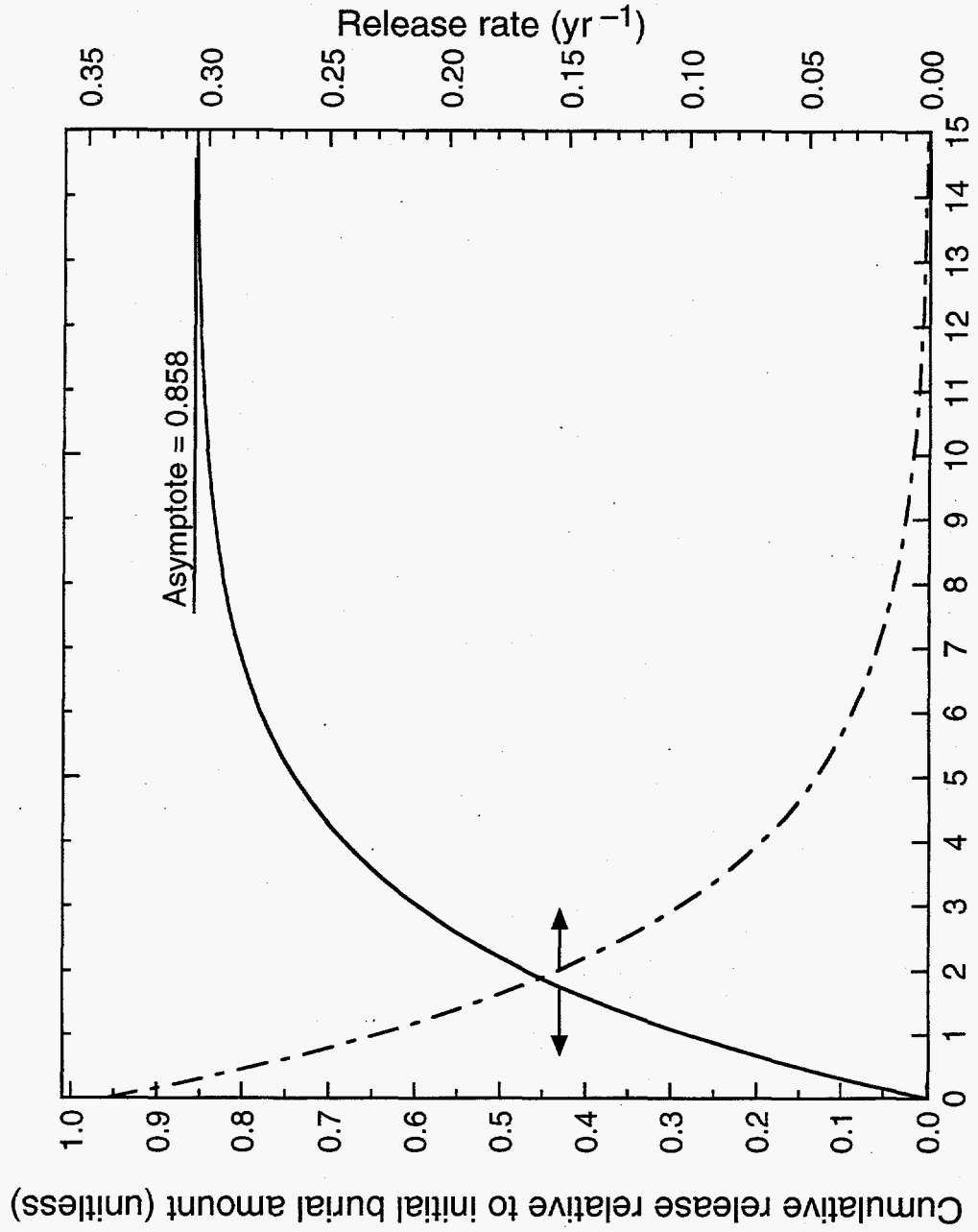

Figure 41. Relative tritium release rate and cumulative released amount for spent melt waste forms.

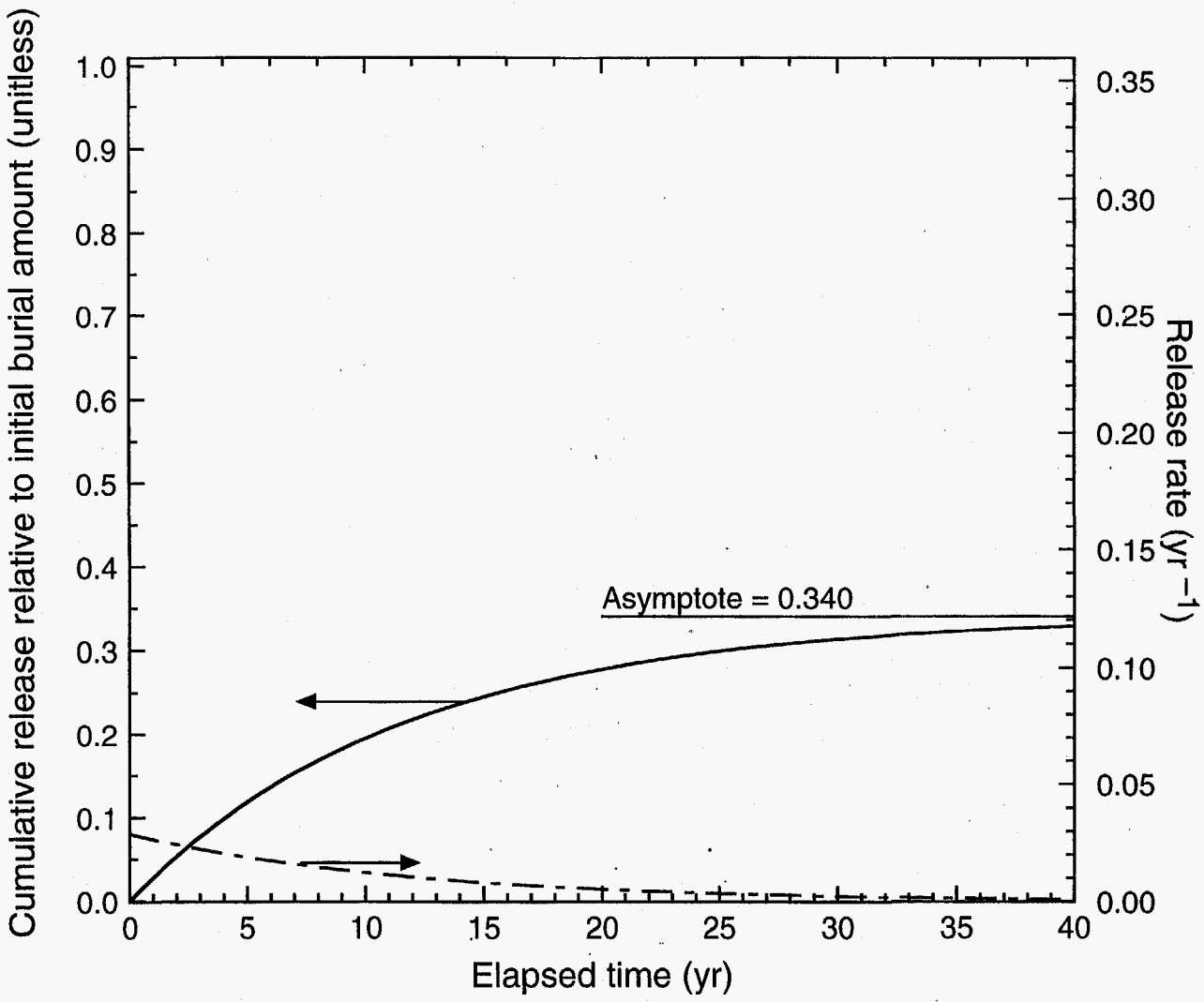

Figure 42. Relative tritium release rate and cumulative released amount for non-spent melt waste forms.

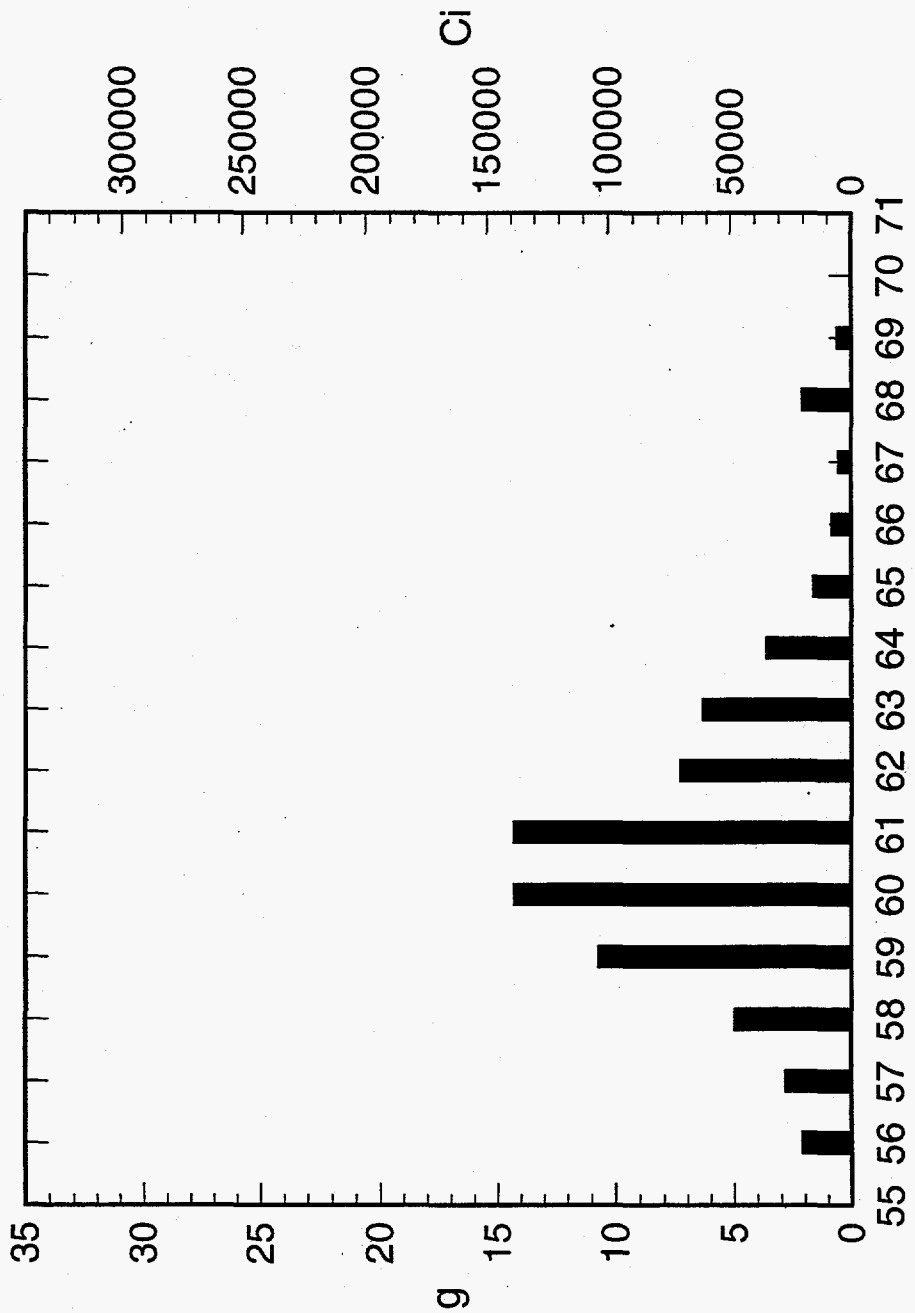

Figure 43. Estimated total annual tritium burials of spent melts to the Old Burial Ground.

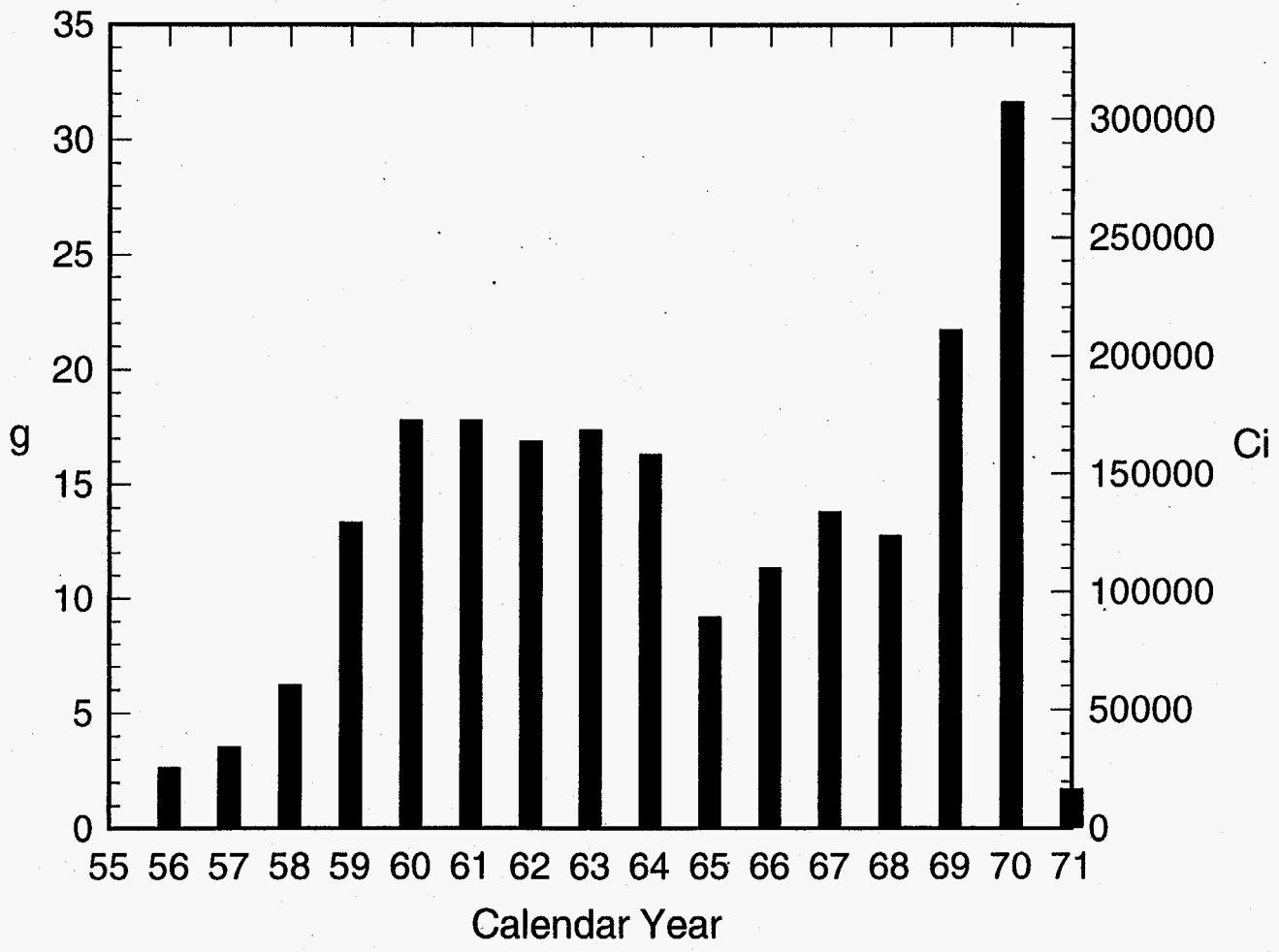

Figure 44. Estimated total annual tritium burials of non-spent melts to the Old Burial Ground.

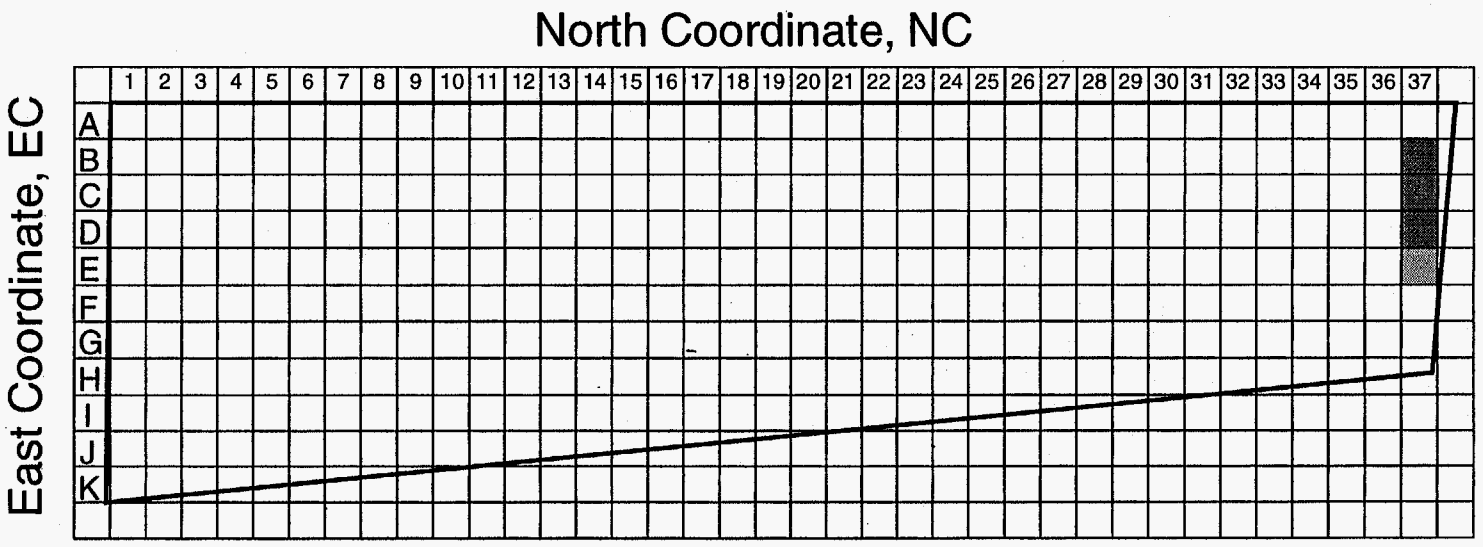

Figure 45a. Normalized spatial variation in tritium burials of spent melts for the calendar year 1961.

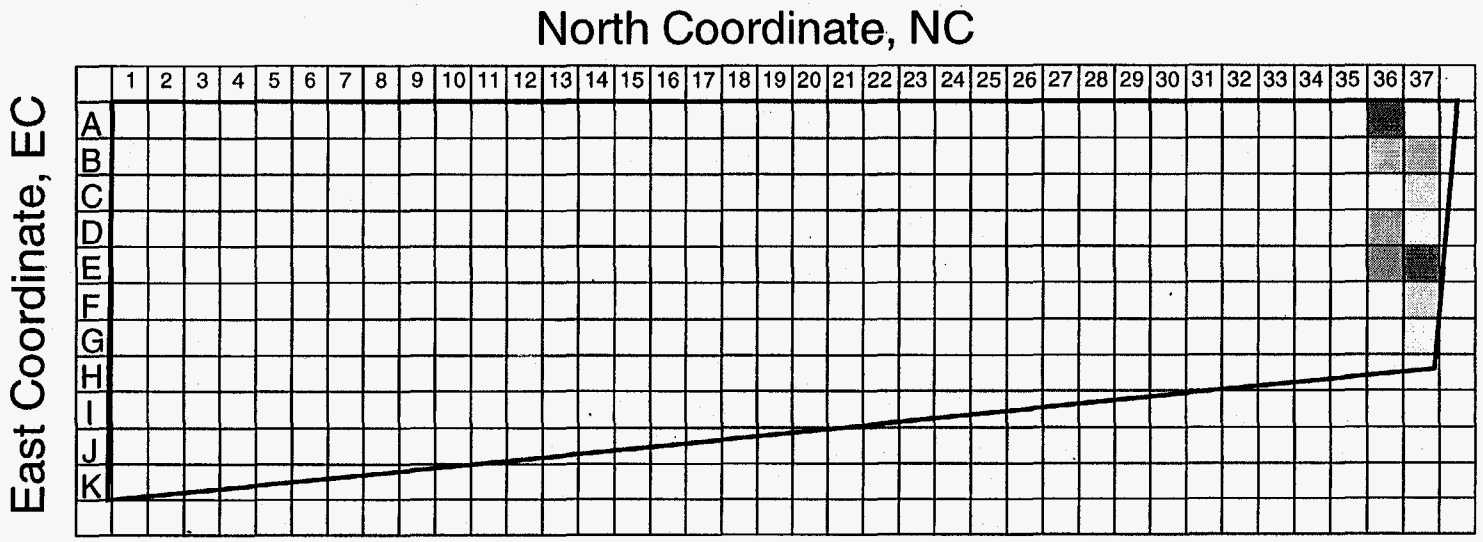

Figure 45b. Normalized spatial variation in tritium burials of spent melts for the calendar year 1962.

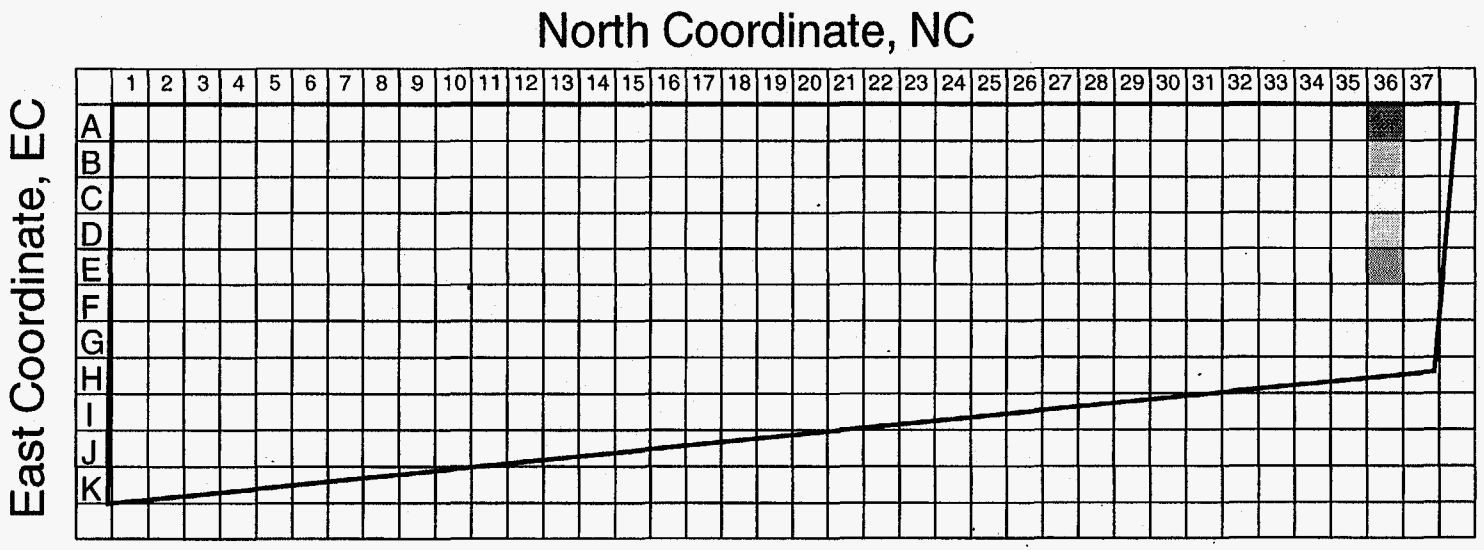

Figure 45c. Normalized spatial variation in tritium burials of spent melts for the calendar year 1963.

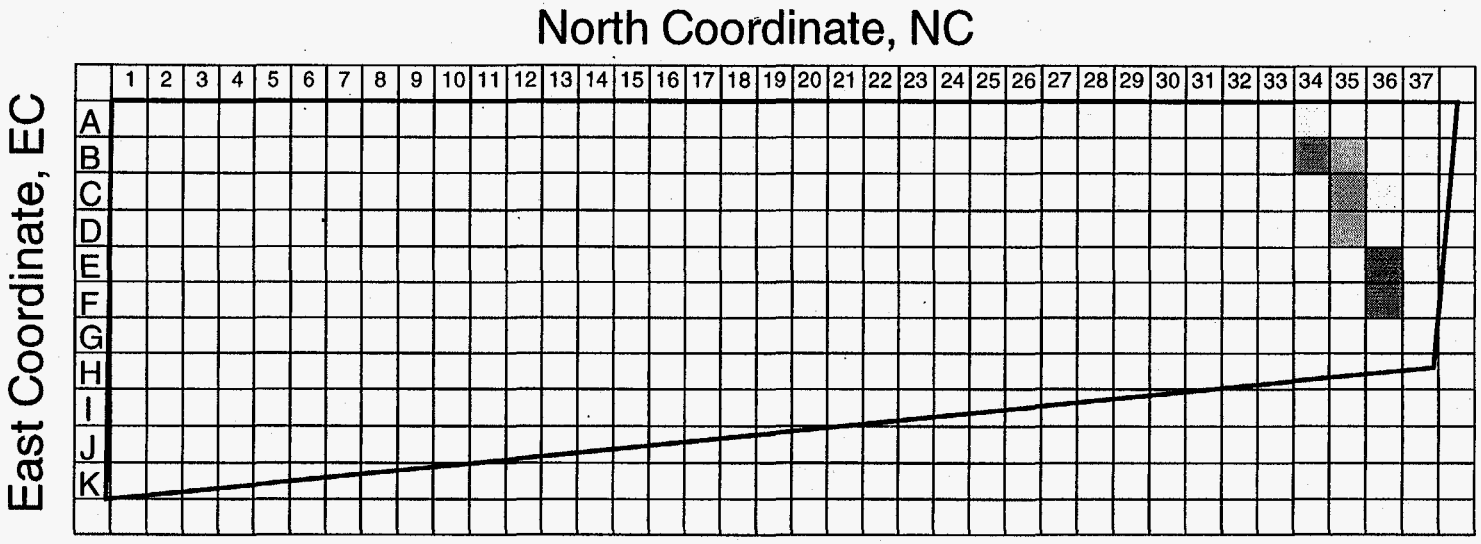

Figure 45d. Normalized spatial variation in tritium burials of spent melts for the calendar year 1964.

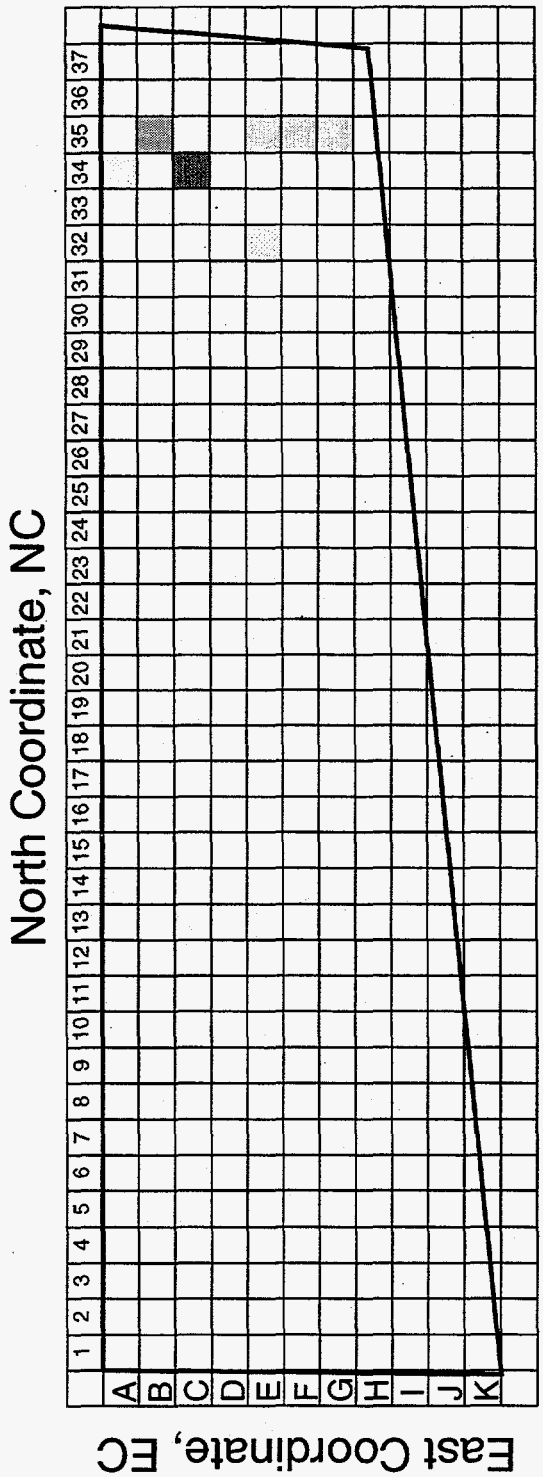

Figure 45e. Normalized spatial variation in tritium burials of spent melts for the calendar year 1965.

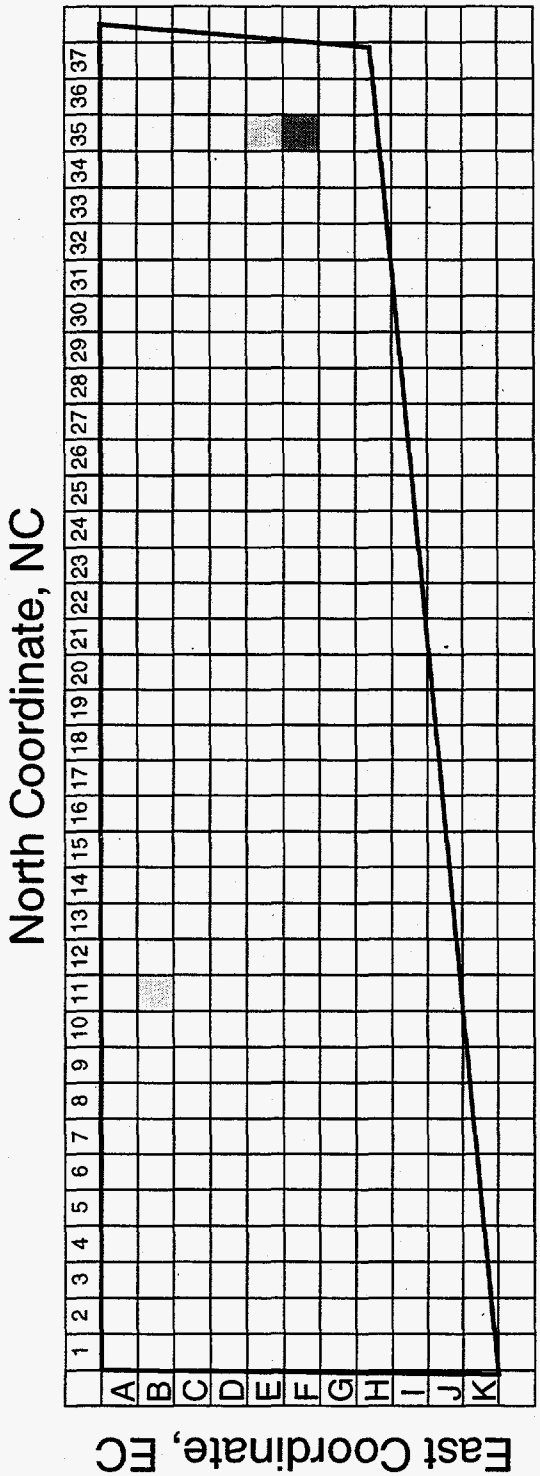

Figure 45f. Normalized spatial variation in tritium burials of spent melts for the calendar year 1966.

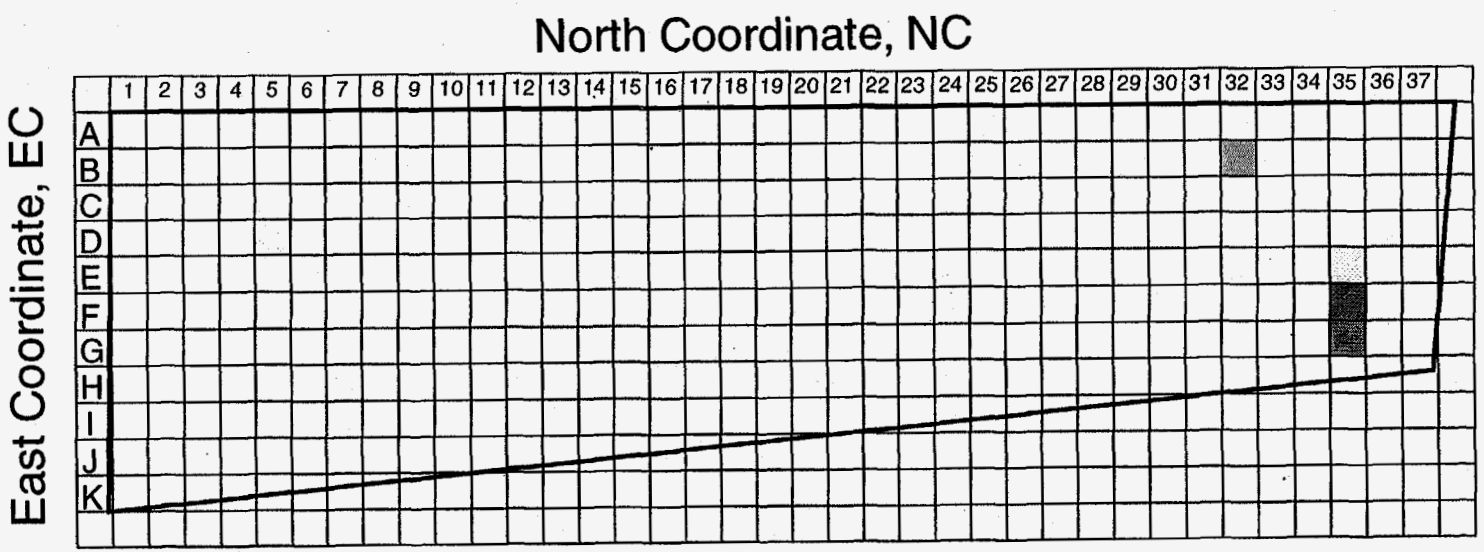

Figure 45g. Normalized spatial variation in tritium burials of spent melts for the calendar year 1967.

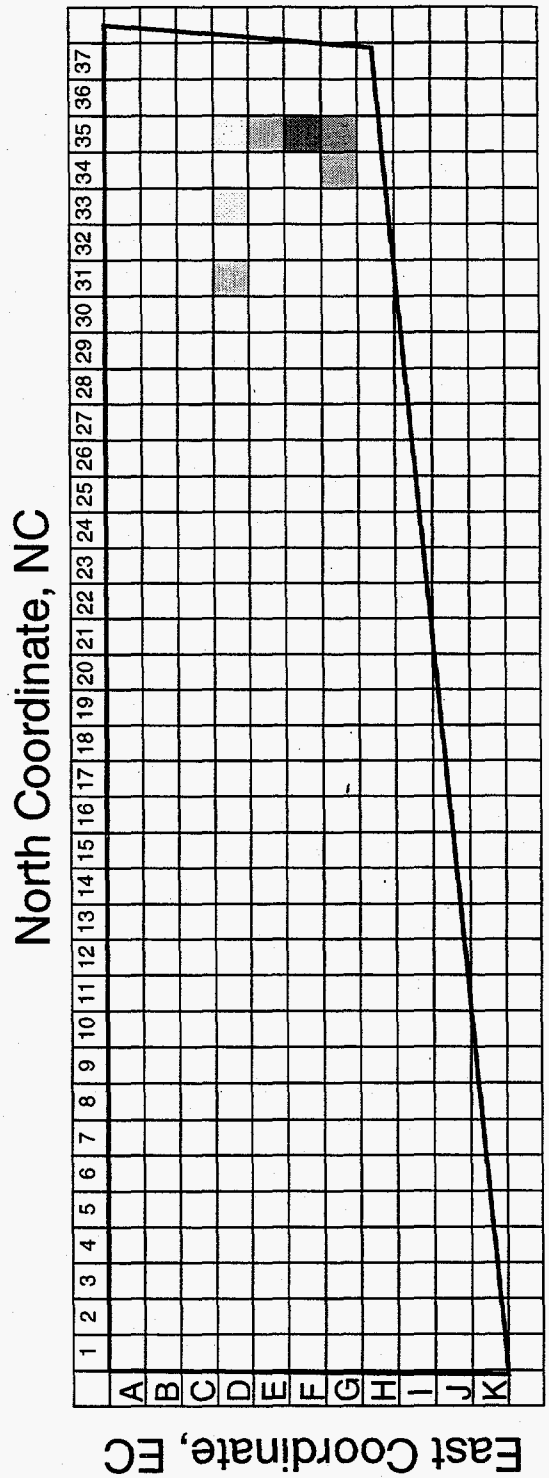

Figure 45h. Normalized spatial variation in tritium burials of spent melts for the calendar year 1968.

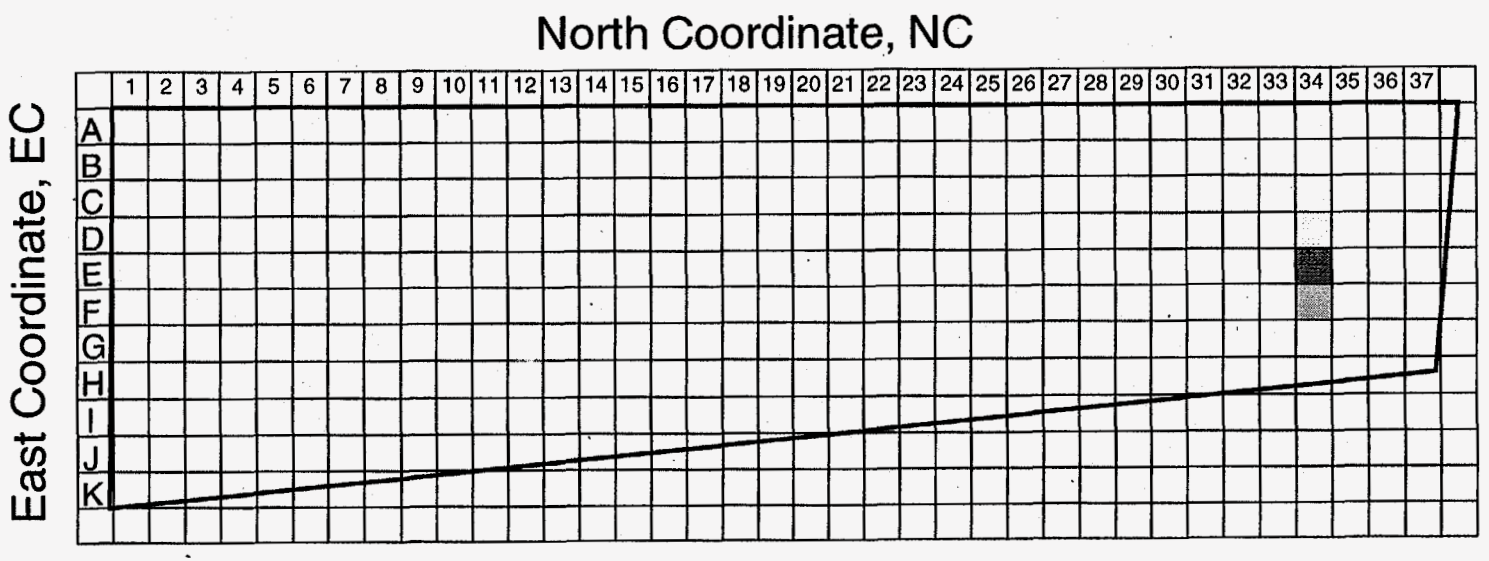

Figure 45i. Normalized spatial variation in tritium burials of spent melts for the calendar year 1969.

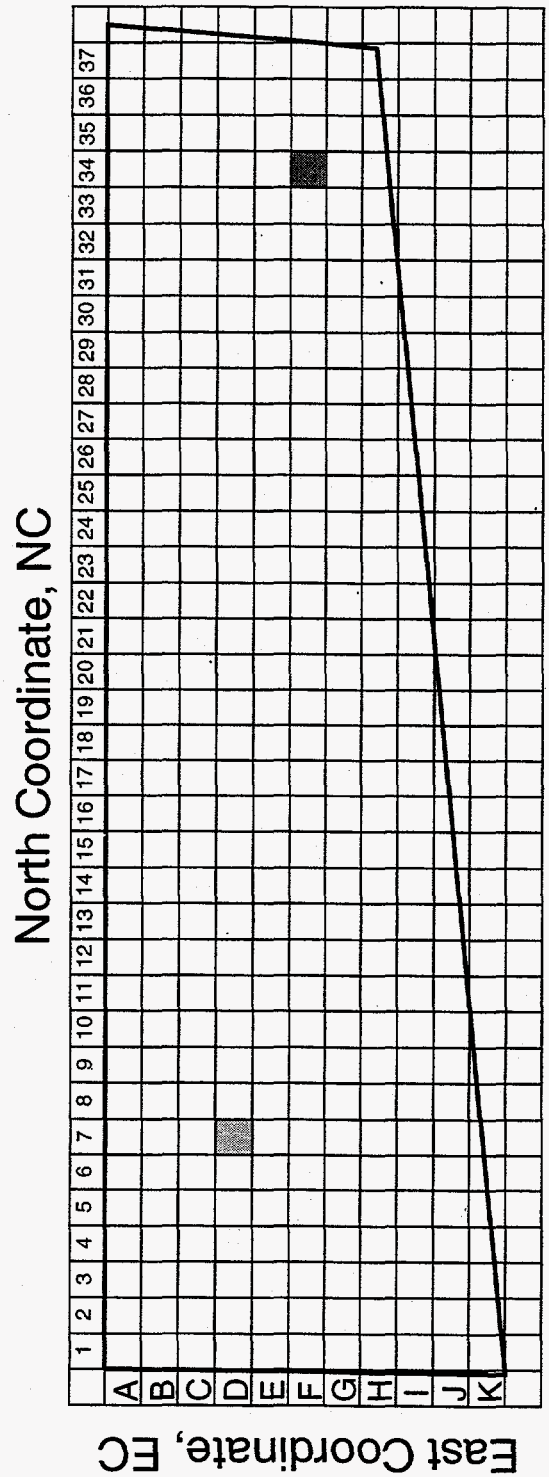

Figure 45j. Normalized spatial variation in tritium burials of spent melts for the calendar year 1970.

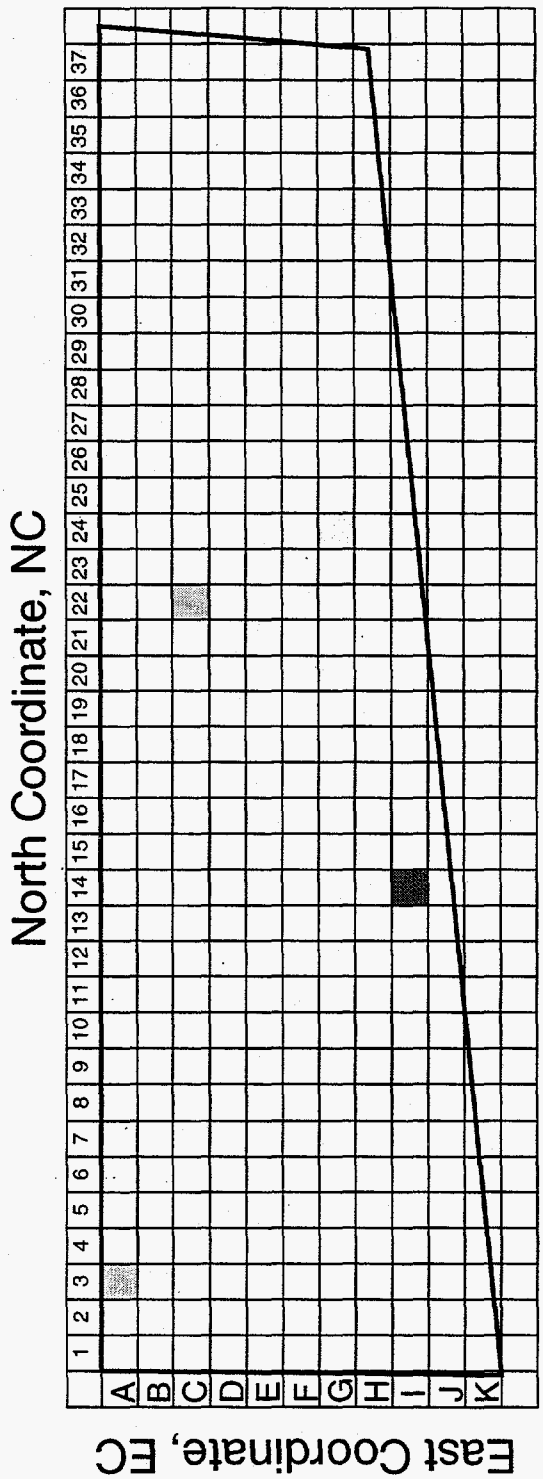

Figure 46a. Normalized spatial variation in tritium burials of non-spent melts for the calendar year 1961.

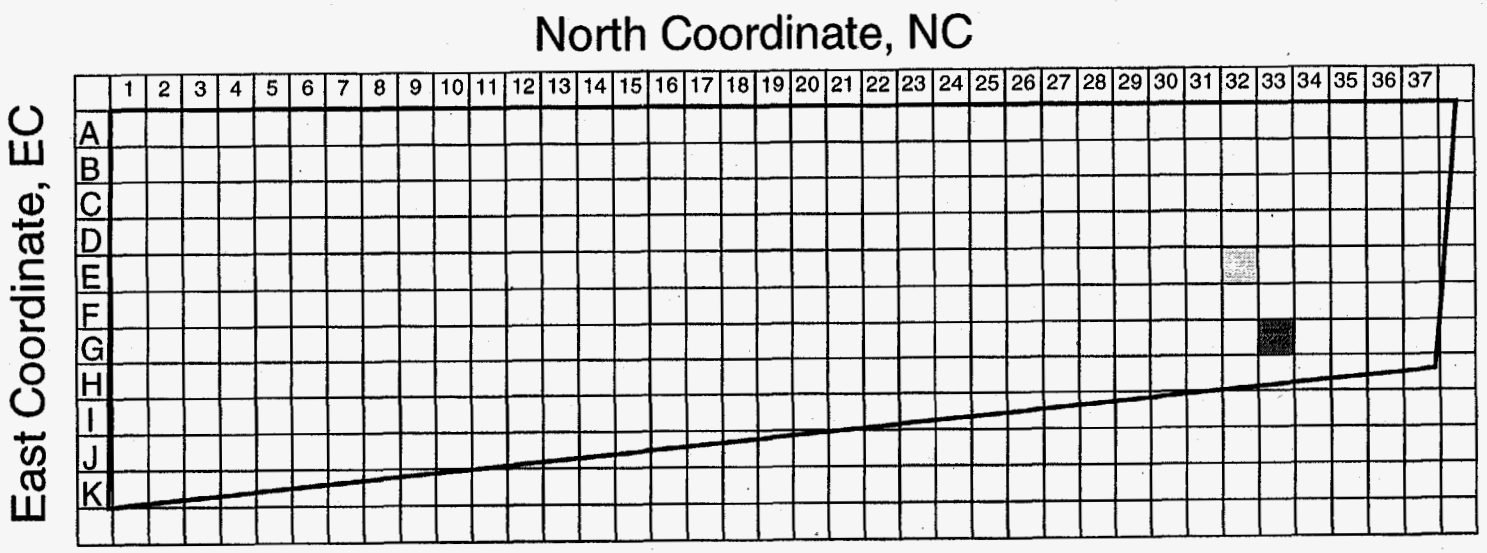

Figure 46b. Normalized spatial variation in tritium burials of non-spent melts for the calendar year 1962.

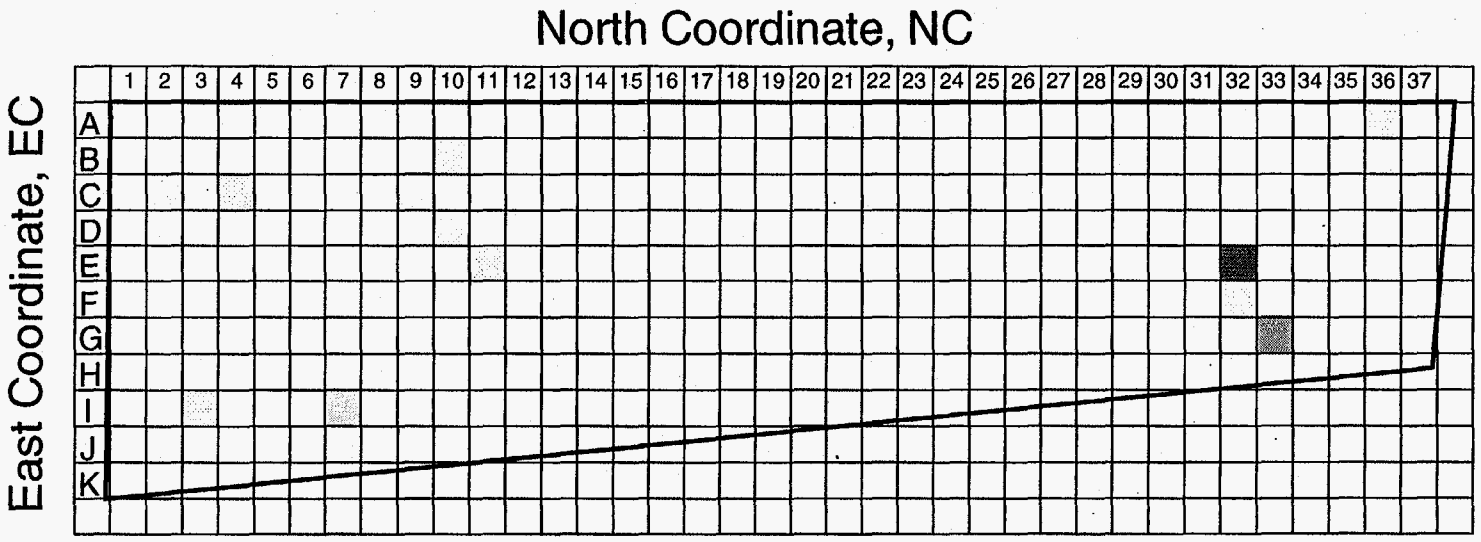

Figure 46c. Normalized spatial variation in tritium burials of non-spent melts for the calendar year 1963.

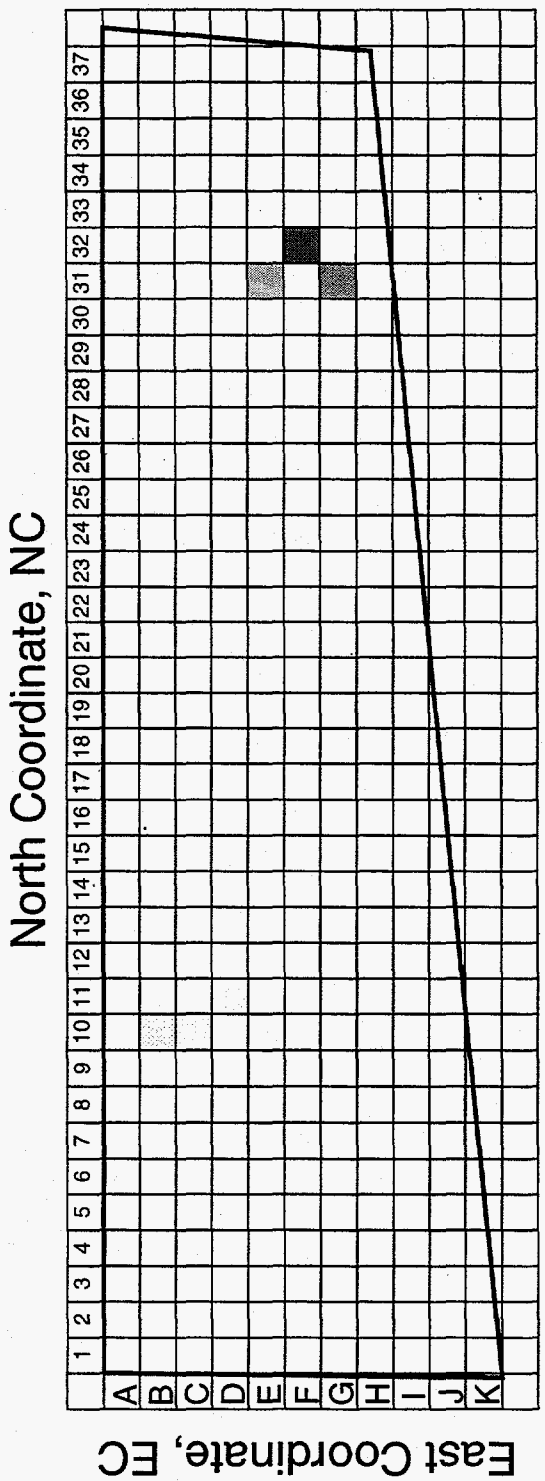

Figure 46d. Normalized spatial variation in tritium burials of non-spent melts for the calendar year 1964.

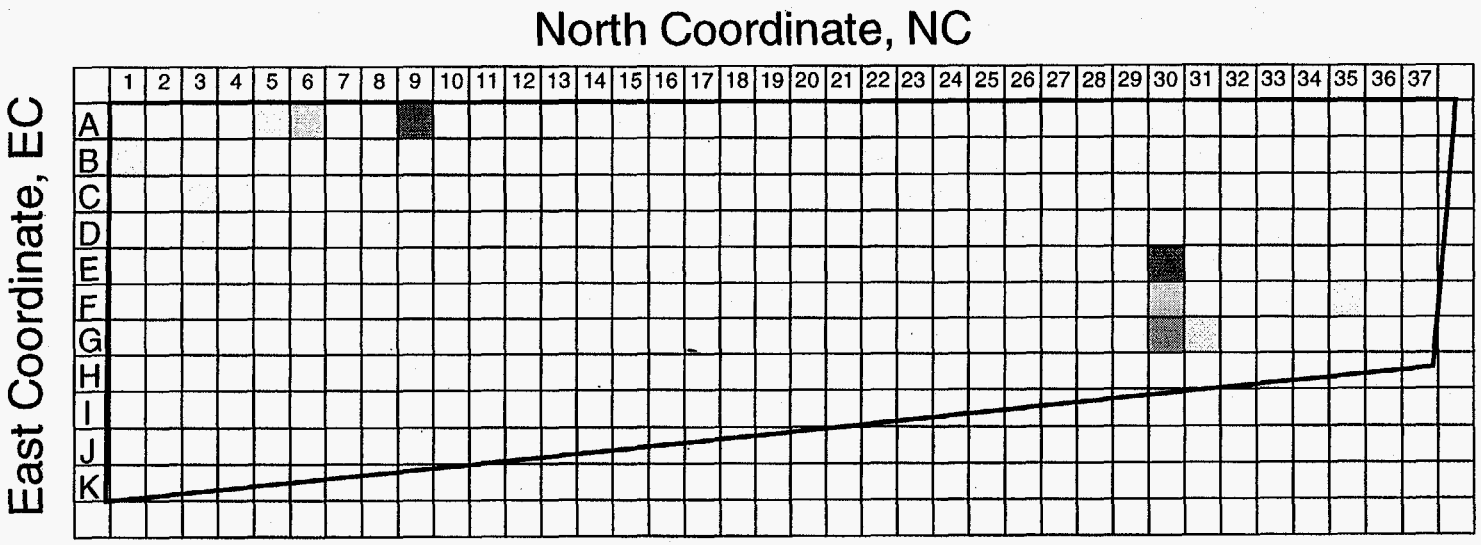

Figure 46e. Normalized spatial variation in tritium burials of non-spent melts for the calendar year 1965.

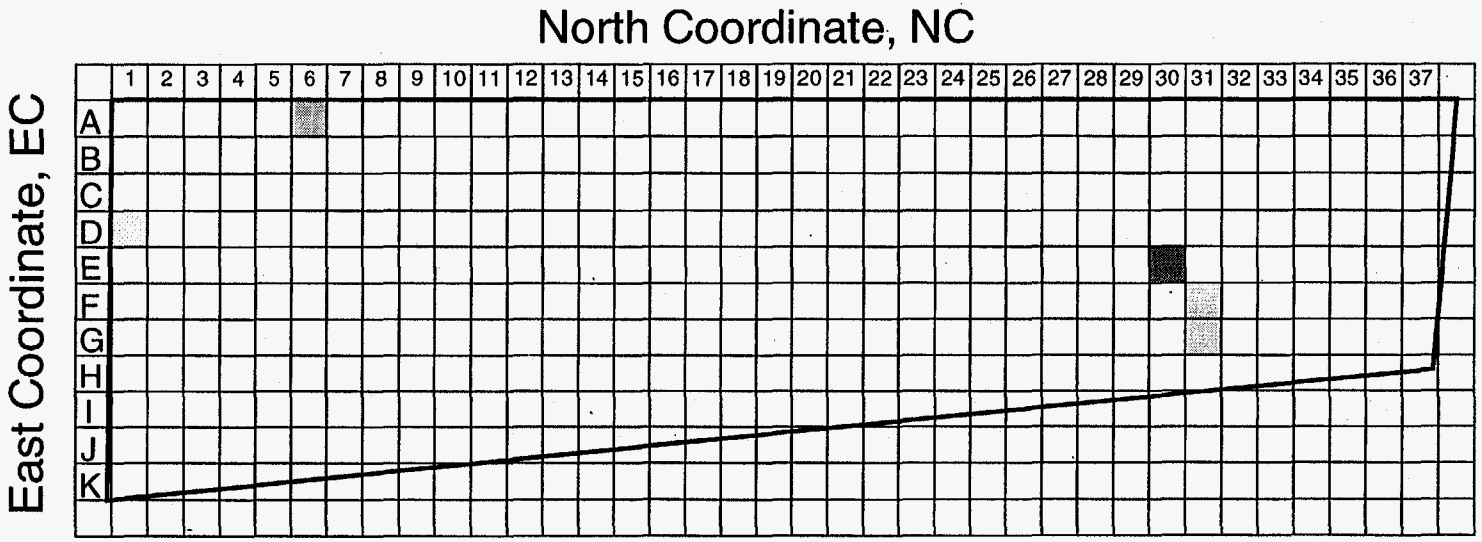

Figure 46f. Normalized spatial variation in tritium burials of non-spent melts for the calendar year 1966.

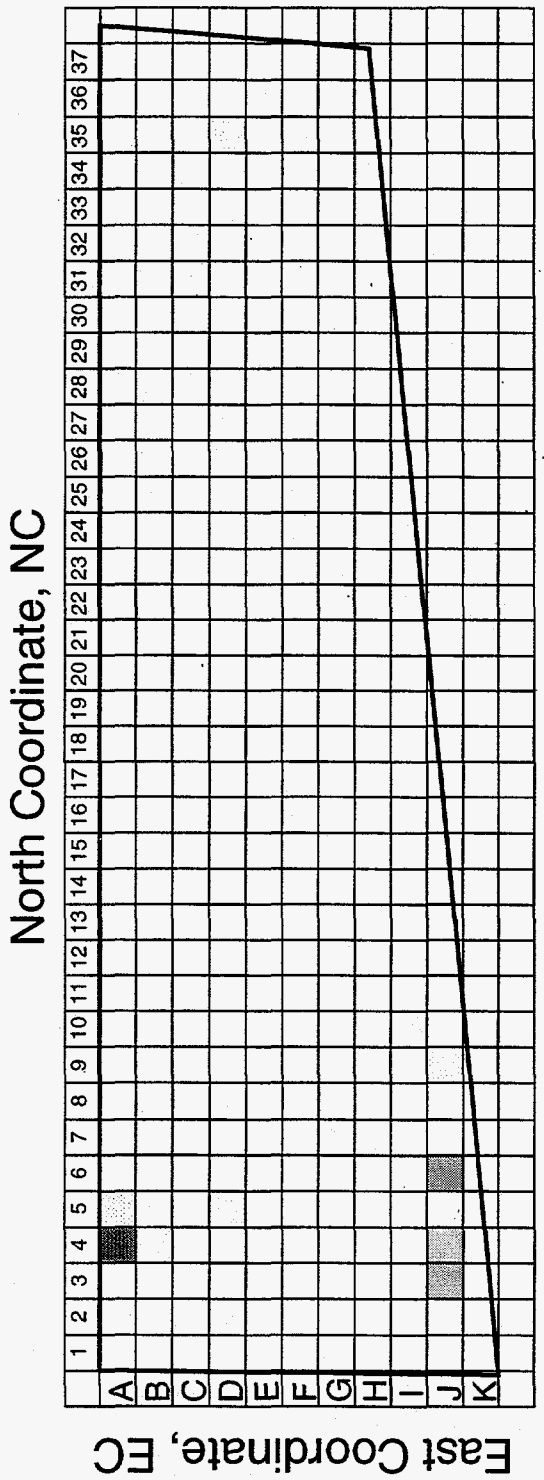

Figure 46g. Normalized spatial variation in tritium burials of non-spent melts for the calendar year 1967.

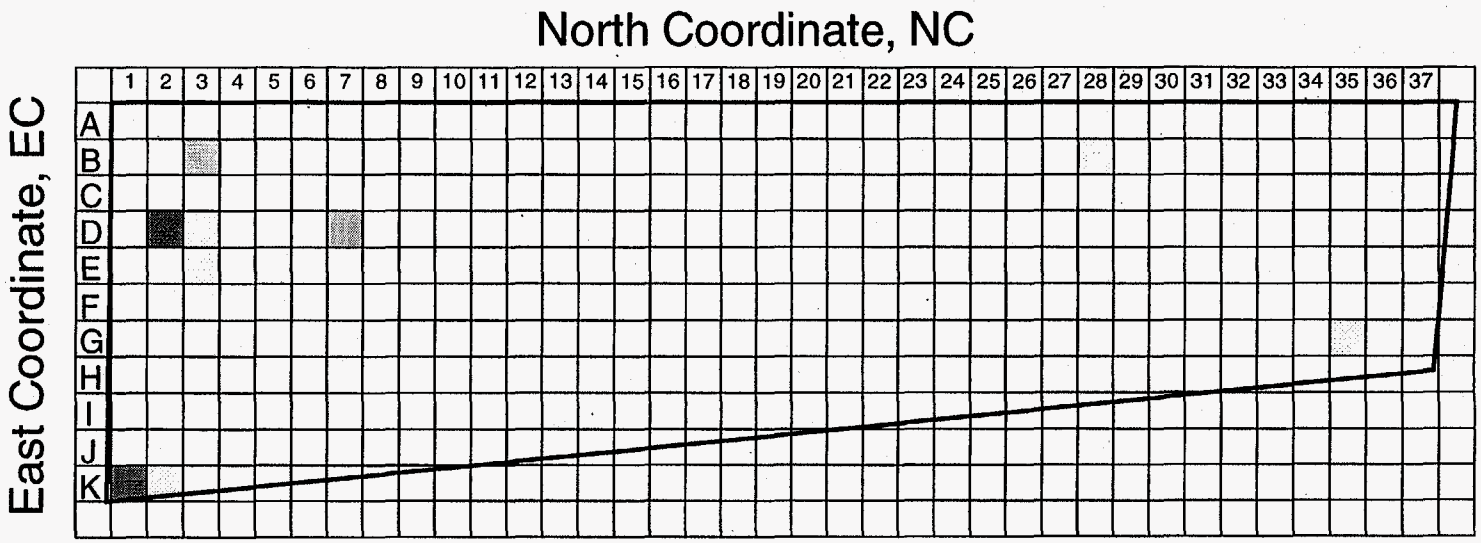

Figure 46h. Normalized spatial variation in tritium burials of non-spent melts for the calendar year 1968.

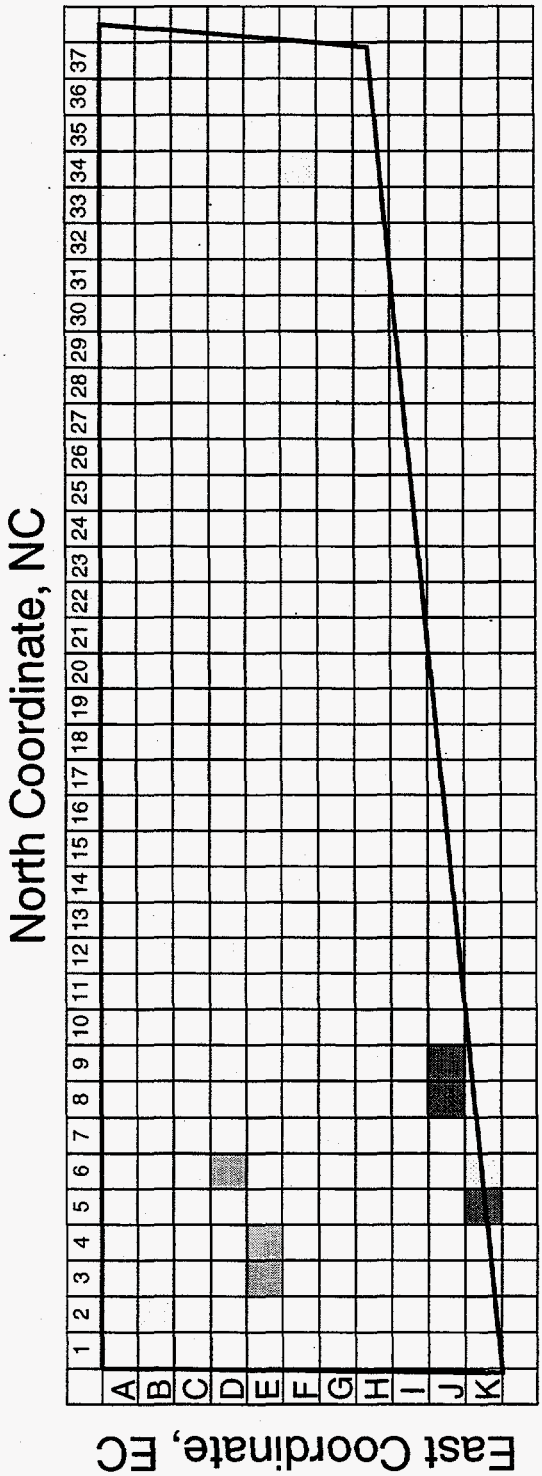

Figure 46i. Normalized spatial variation in tritium burials of non-spent melts for the calendar year 1969.

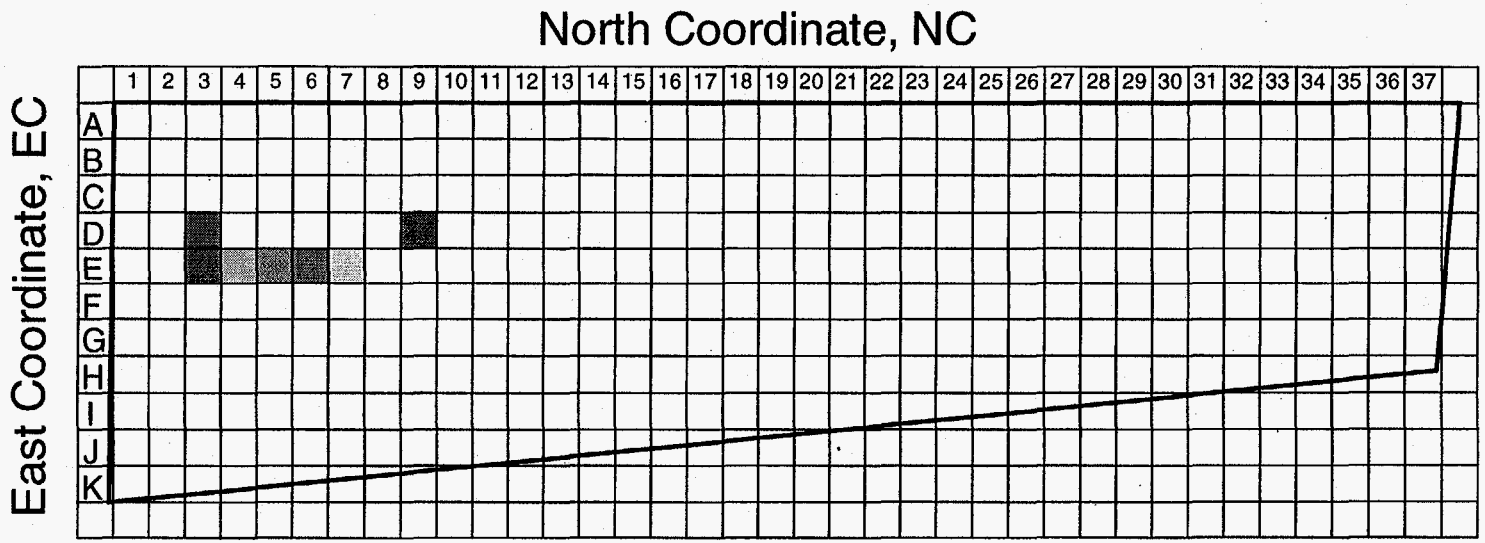

Figure 46j. Normalized spatial variation in tritium burials of non-spent melts for the calendar year 1970.

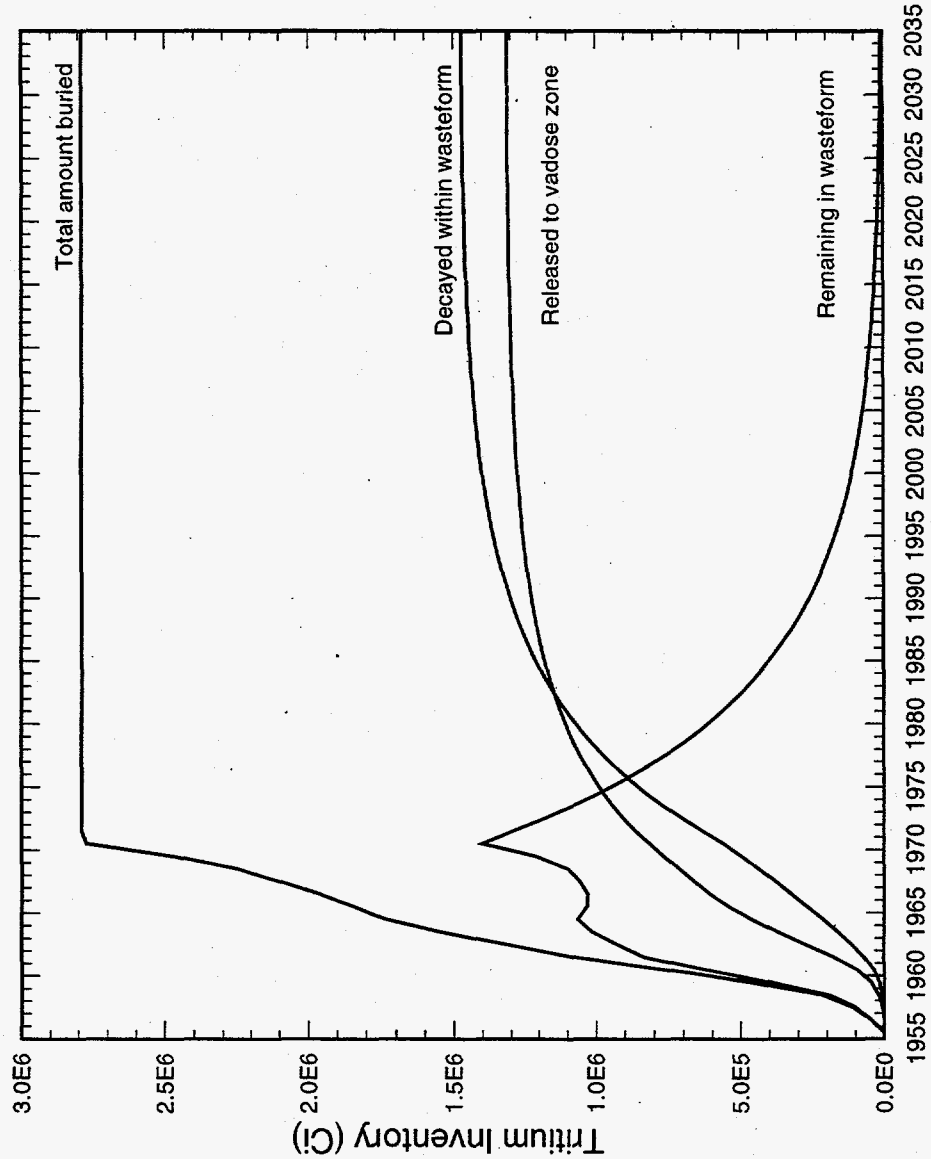

Figure 47. Tritium accounting through time with respect to buried waste forms with $k = 0.029\ yr^{-1}$ for non-spent melts.

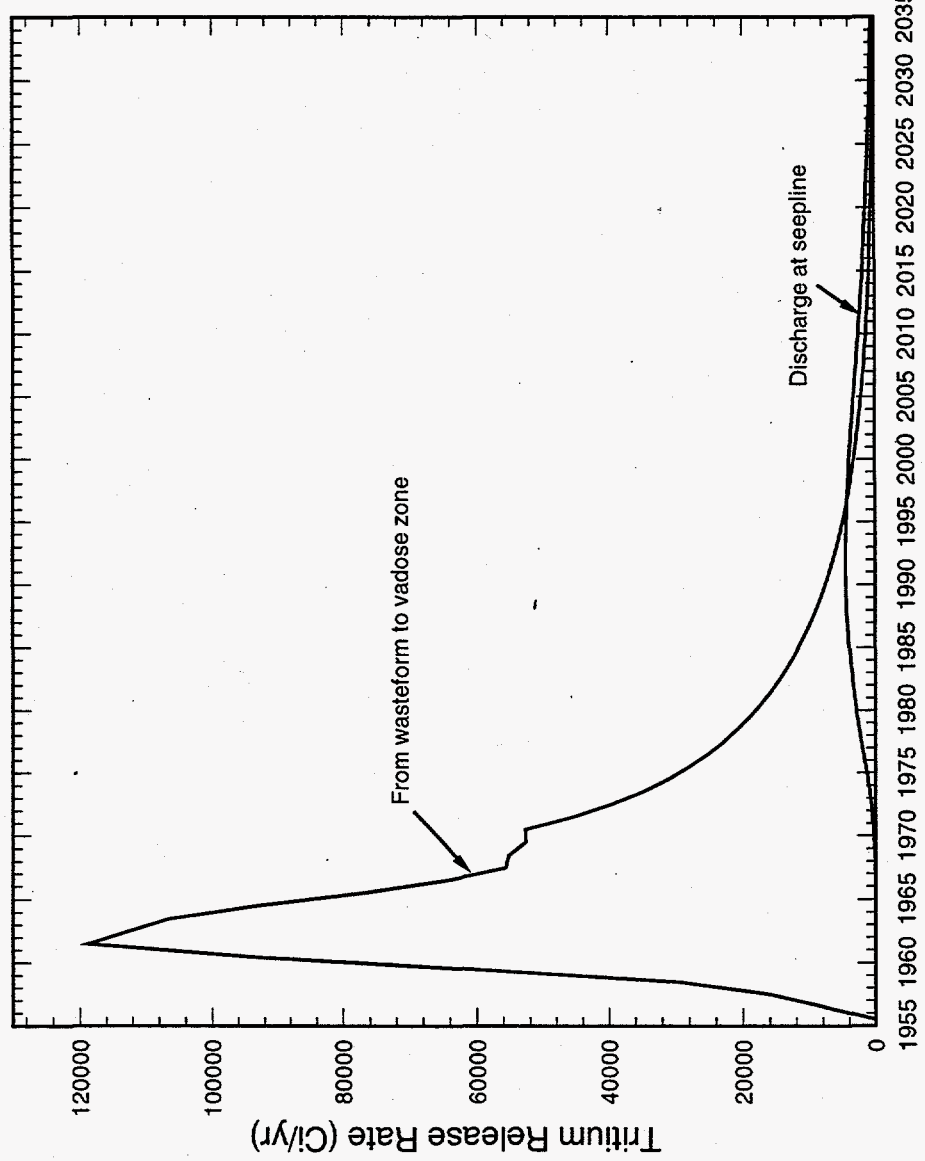

Figure 48. Tritium release rates with $k = 0.029\ yr^{-1}$ for non-spent melts.

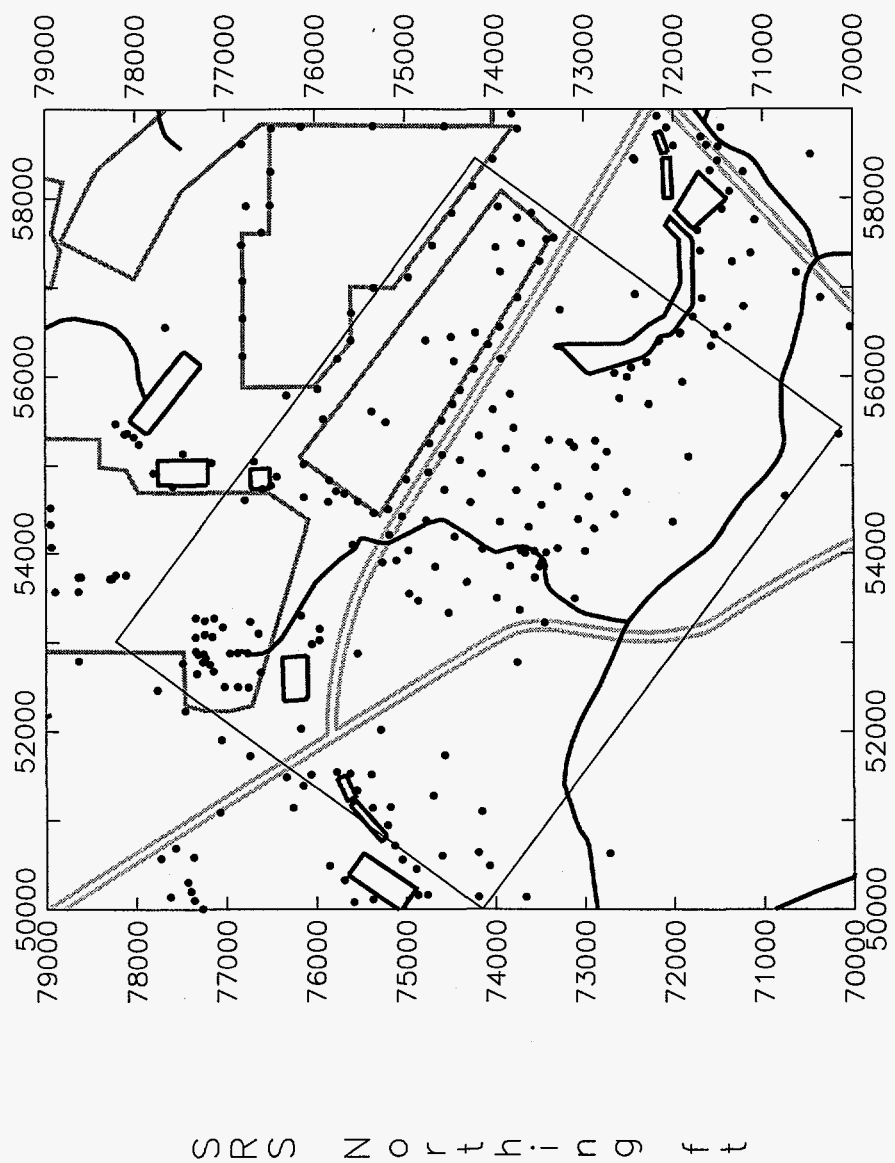

Figure 49. Locations of "upper" aquifer zone tritium concentration data for 1994.

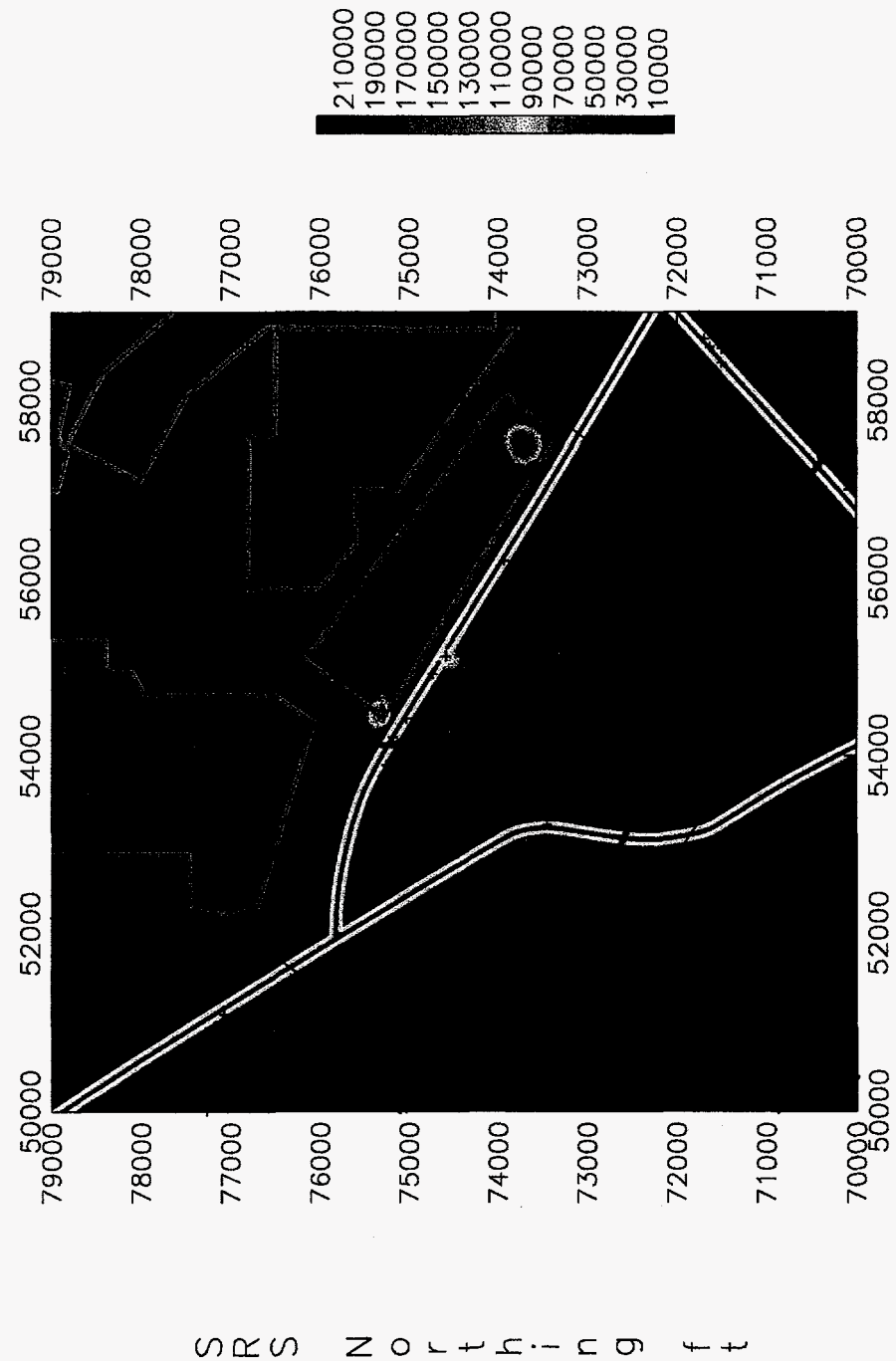

Figure 50. Two-dimensional contour plot of tritium concentration in the "upper" aquifer zone for 1994 based on monitoring data.

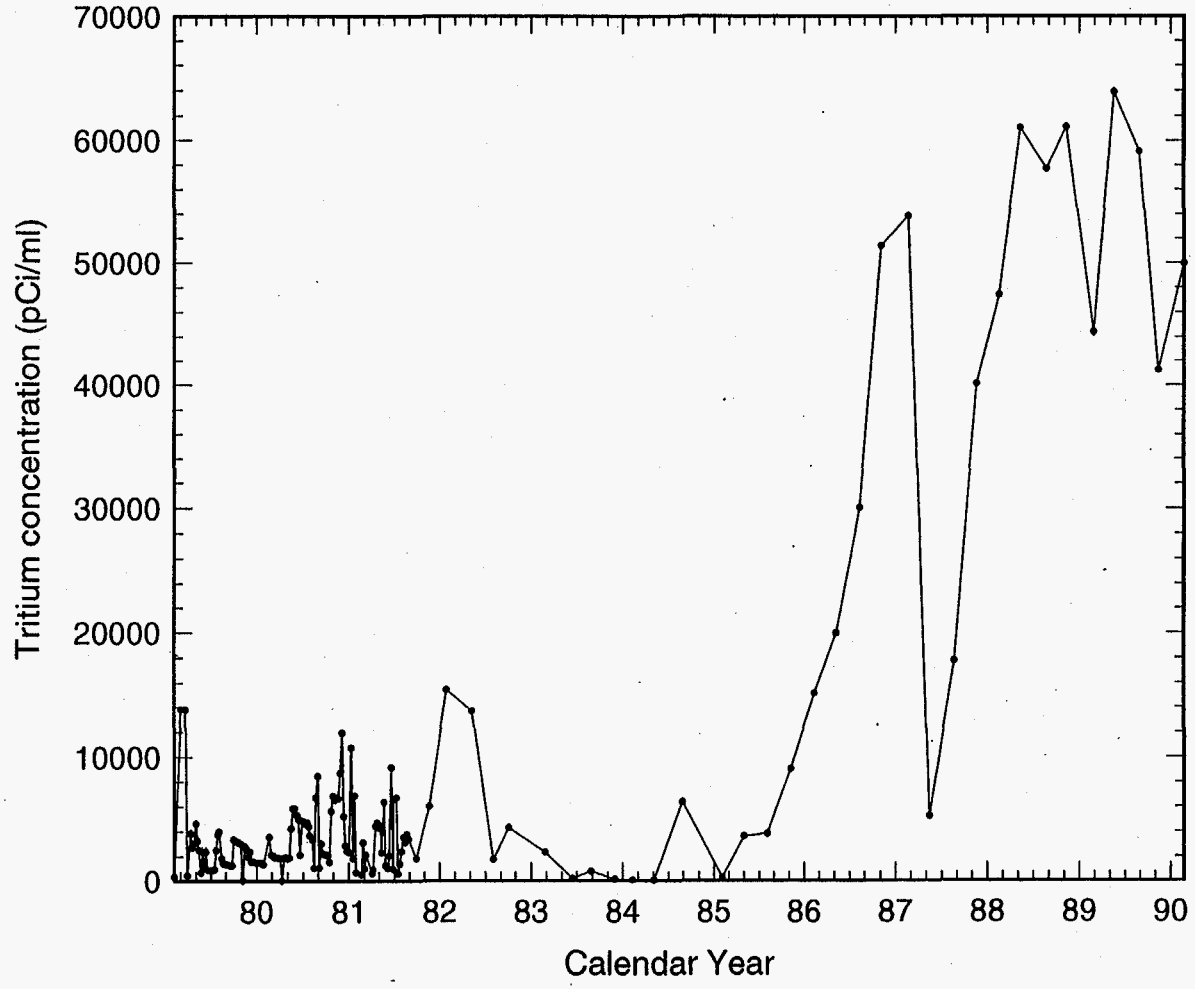

Figure 51. Transient tritium concentration data for well BG-56.

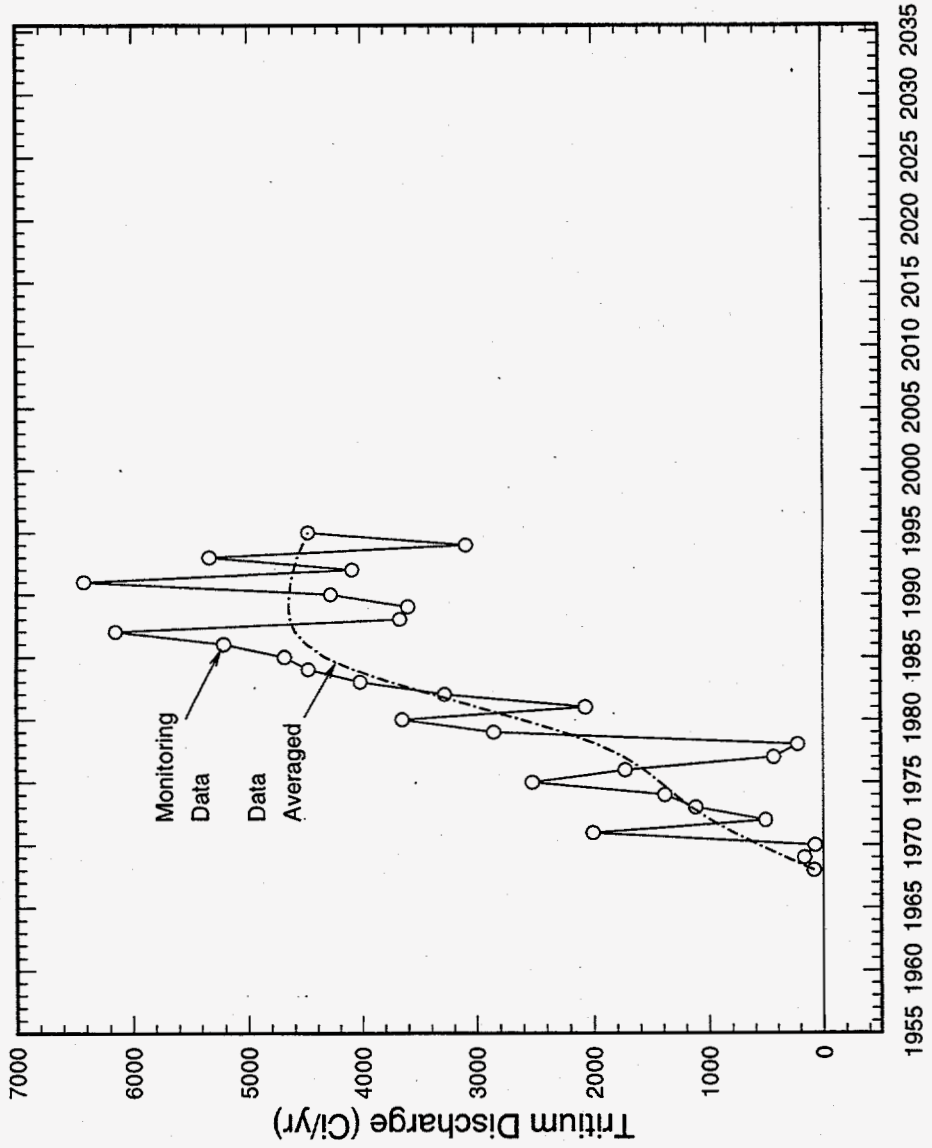

Figure 52. Annual tritium discharges to Fourmile Branch from the Old Burial Ground.

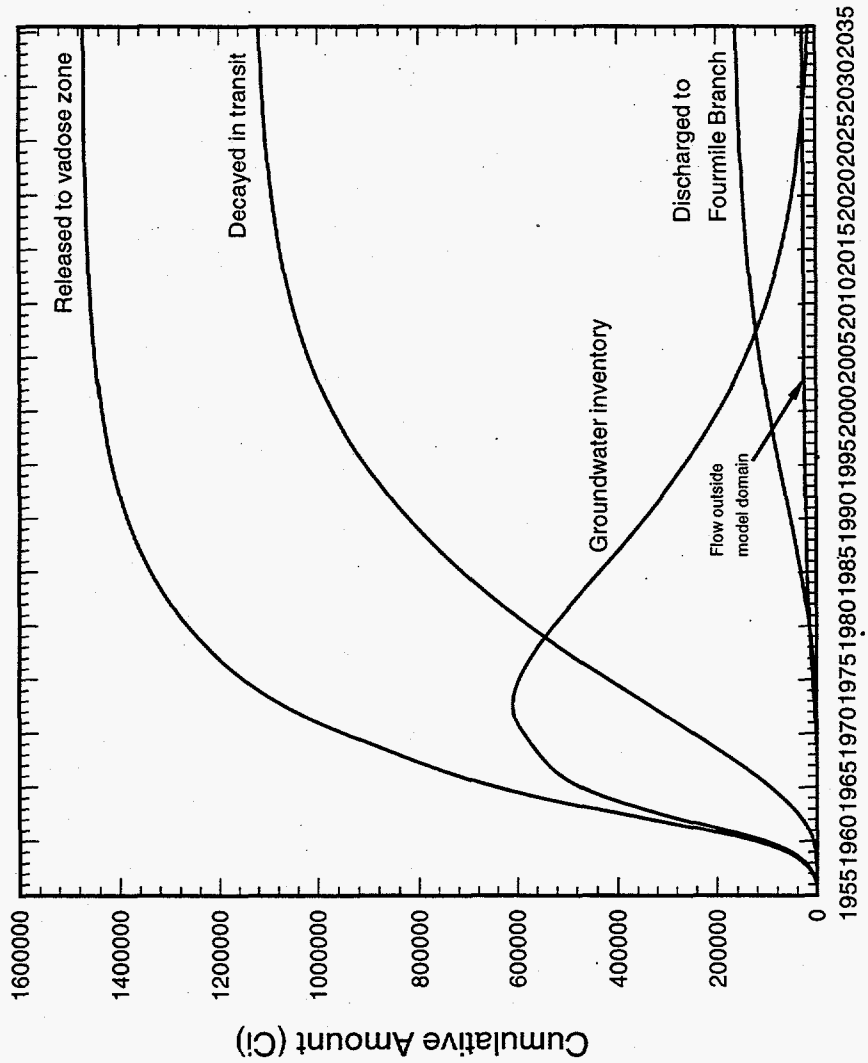

Figure 53. Tritium accounting through time with respect to the amount released to the vadose zone ($k = 0.029\ yr^{-1}$ for non-spent melts, 23% porosity, 65 ft dispersivity).

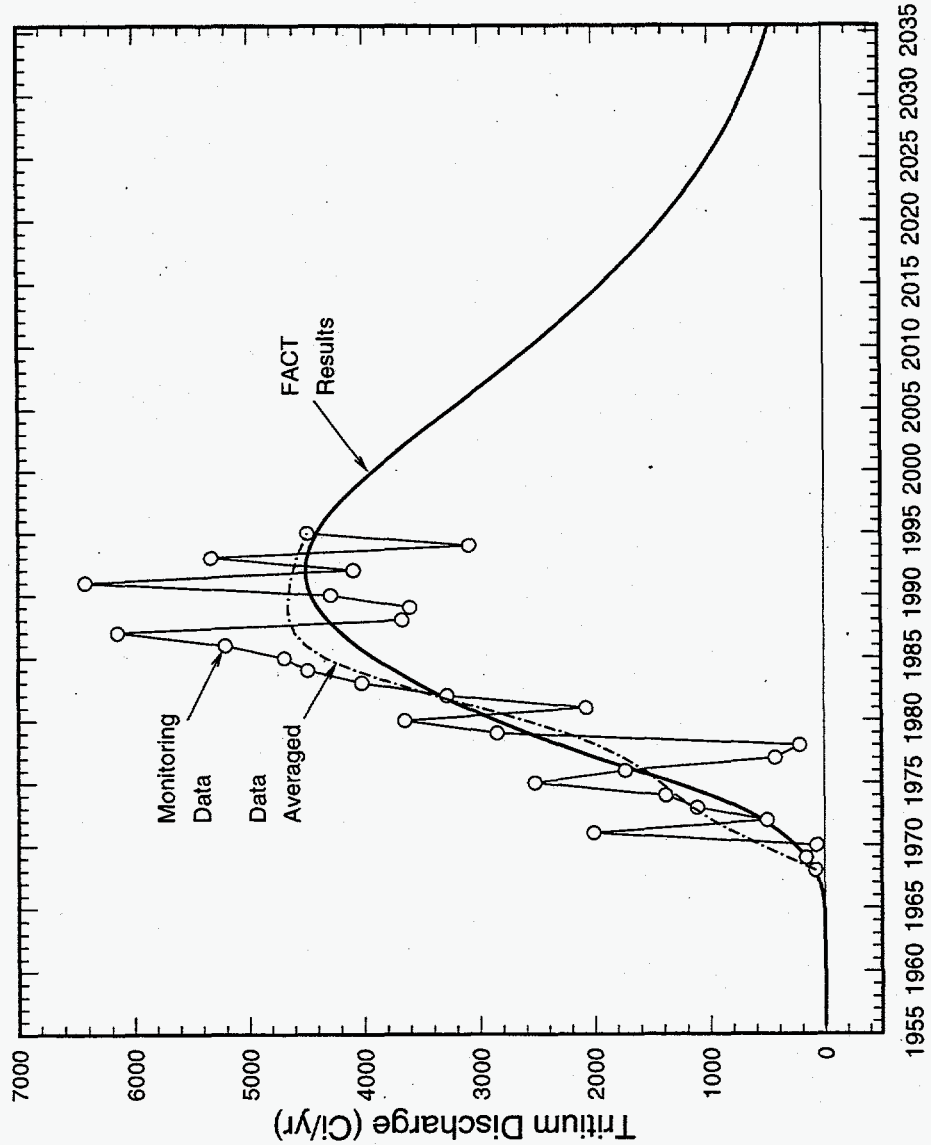

Figure 54. Comparison of predicted and measured tritium discharges to Fourmile Branch ($k = 0.029\ yr^{-1}$ for non-spent melts, 23% porosity, 65 ft dispersivity).

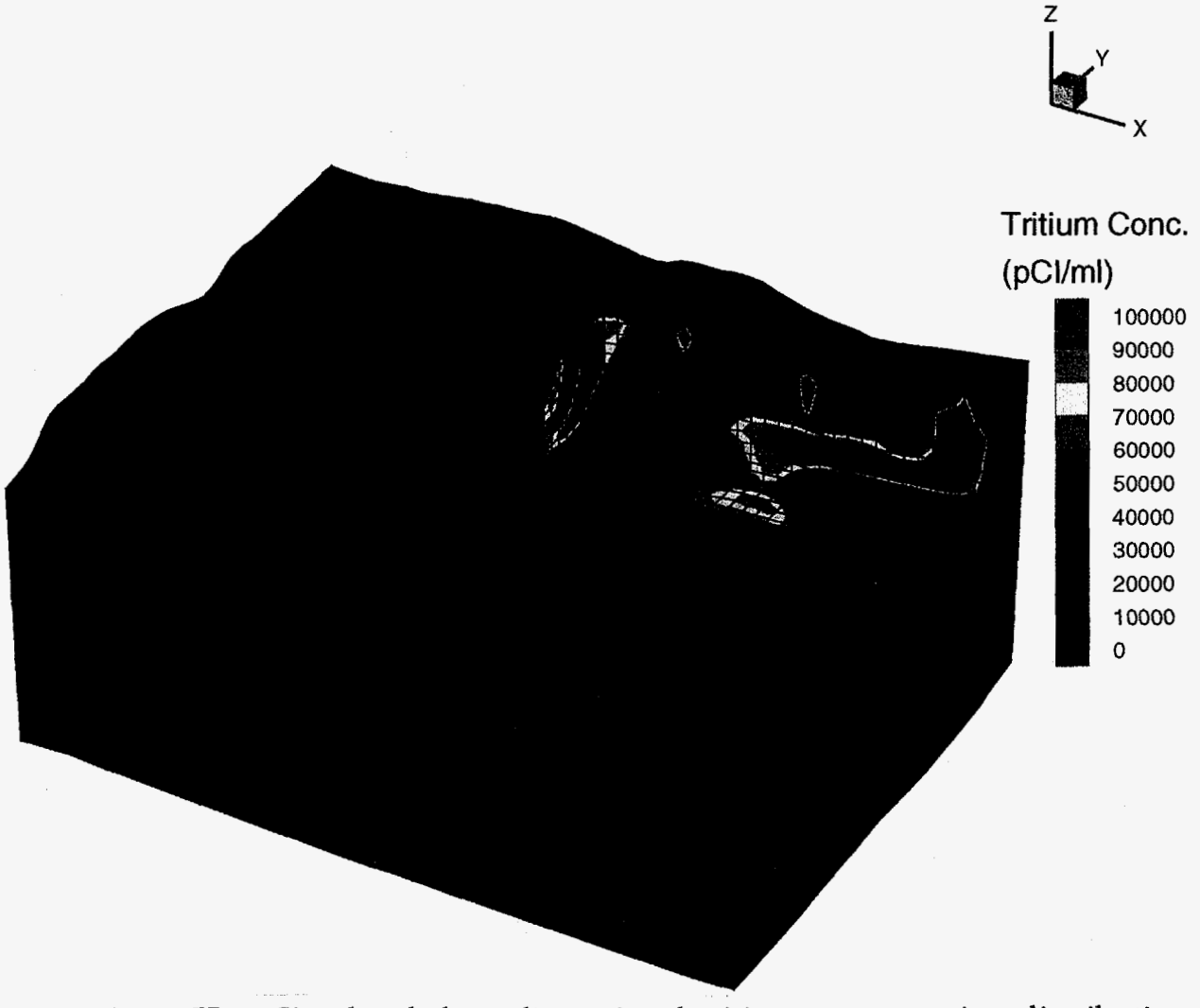

Figure 55. Simulated three-dimensional tritium concentration distribution for 1995.

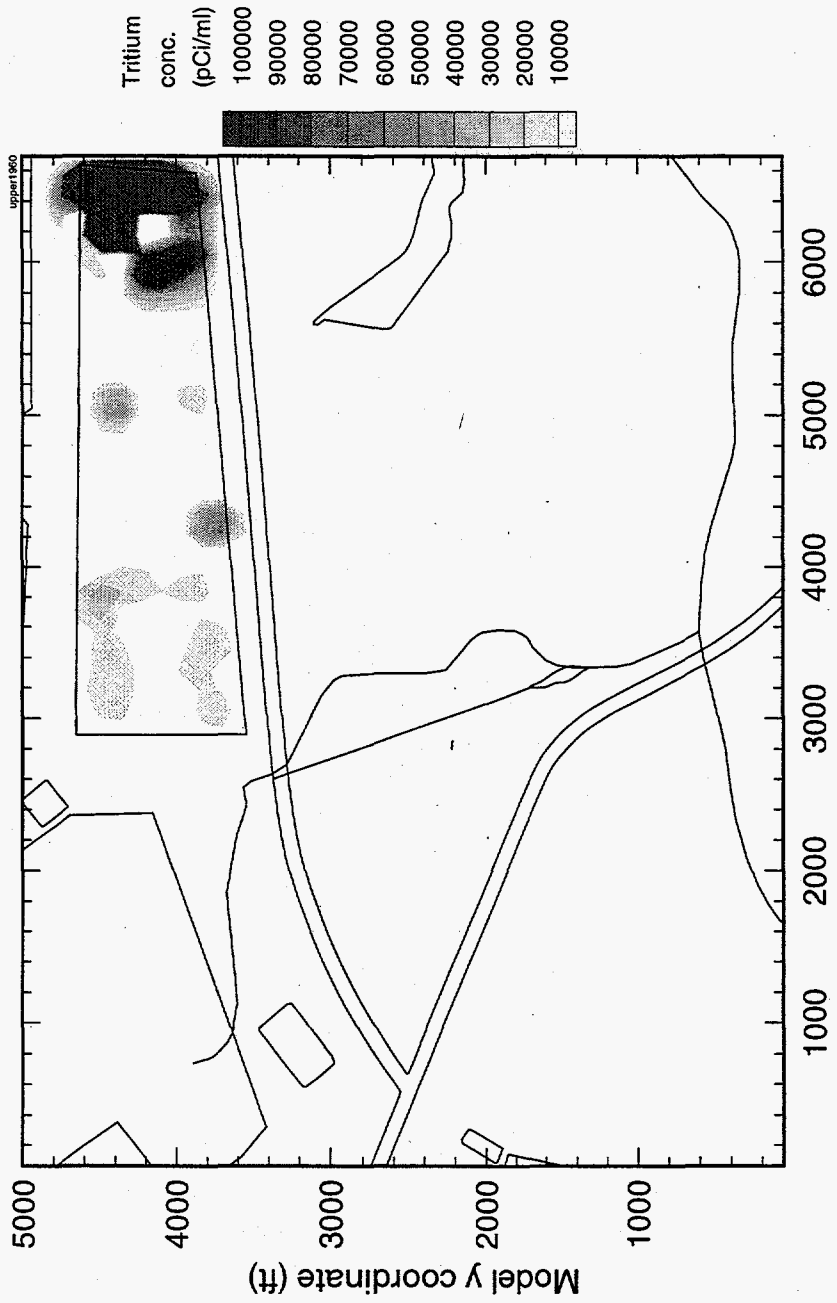

Figure 56a. Contour plot of predicted "upper" aquifer zone tritium concentration for 1960.

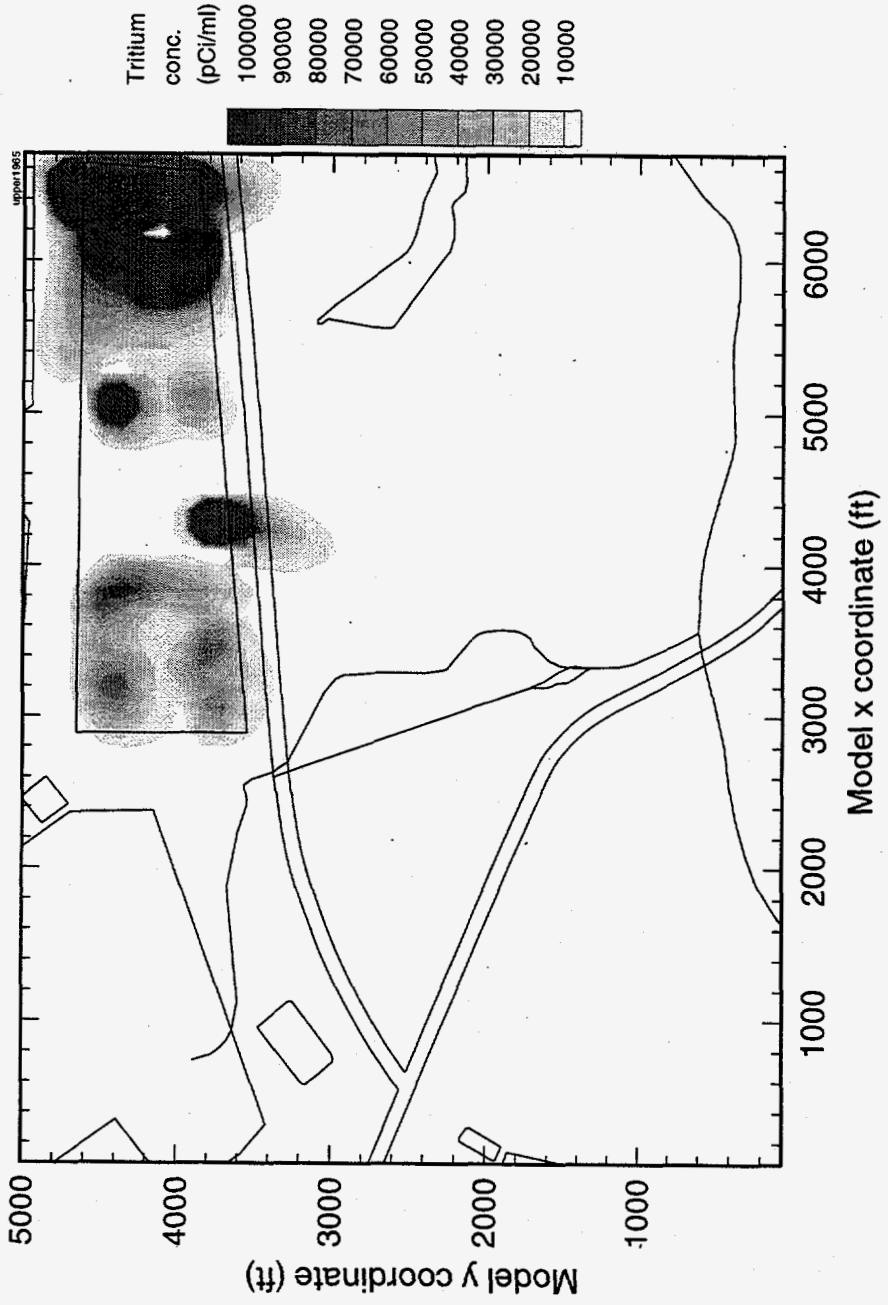

Figure 56b. Contour plot of predicted "upper" aquifer zone tritium concentration for 1965.

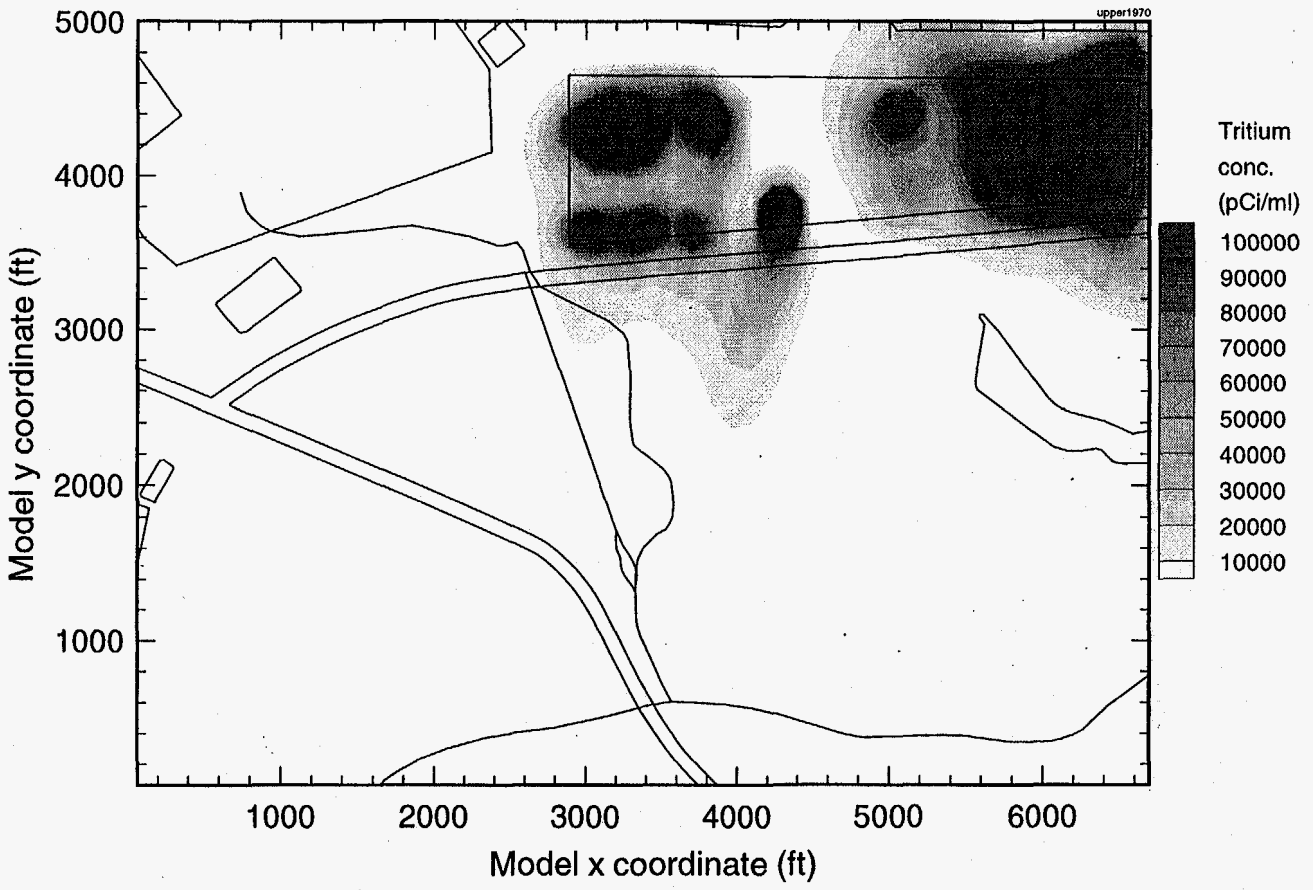

Figure 56c. Contour plot of predicted "upper" aquifer zone tritium concentration for 1970.

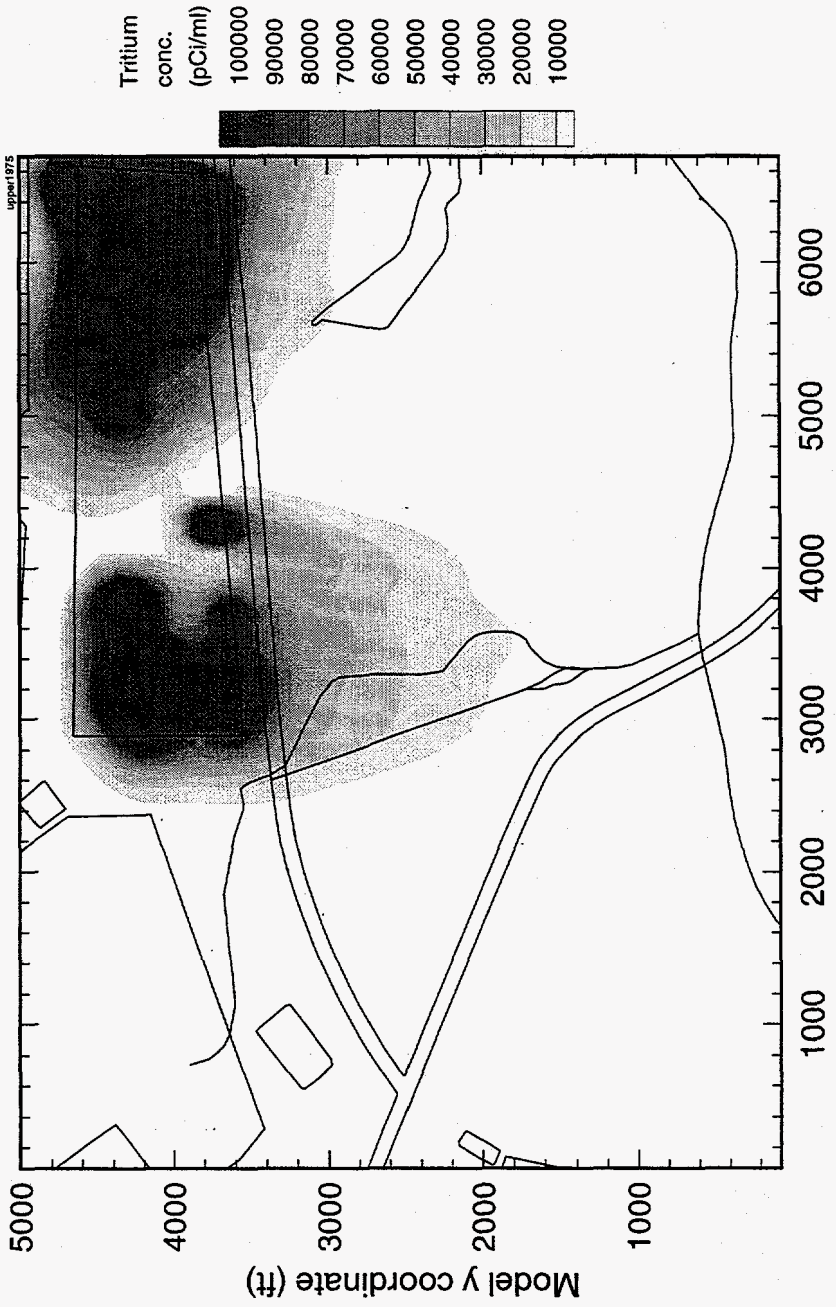

Figure 56d. Contour plot of predicted "upper" aquifer zone tritium concentration for 1975.

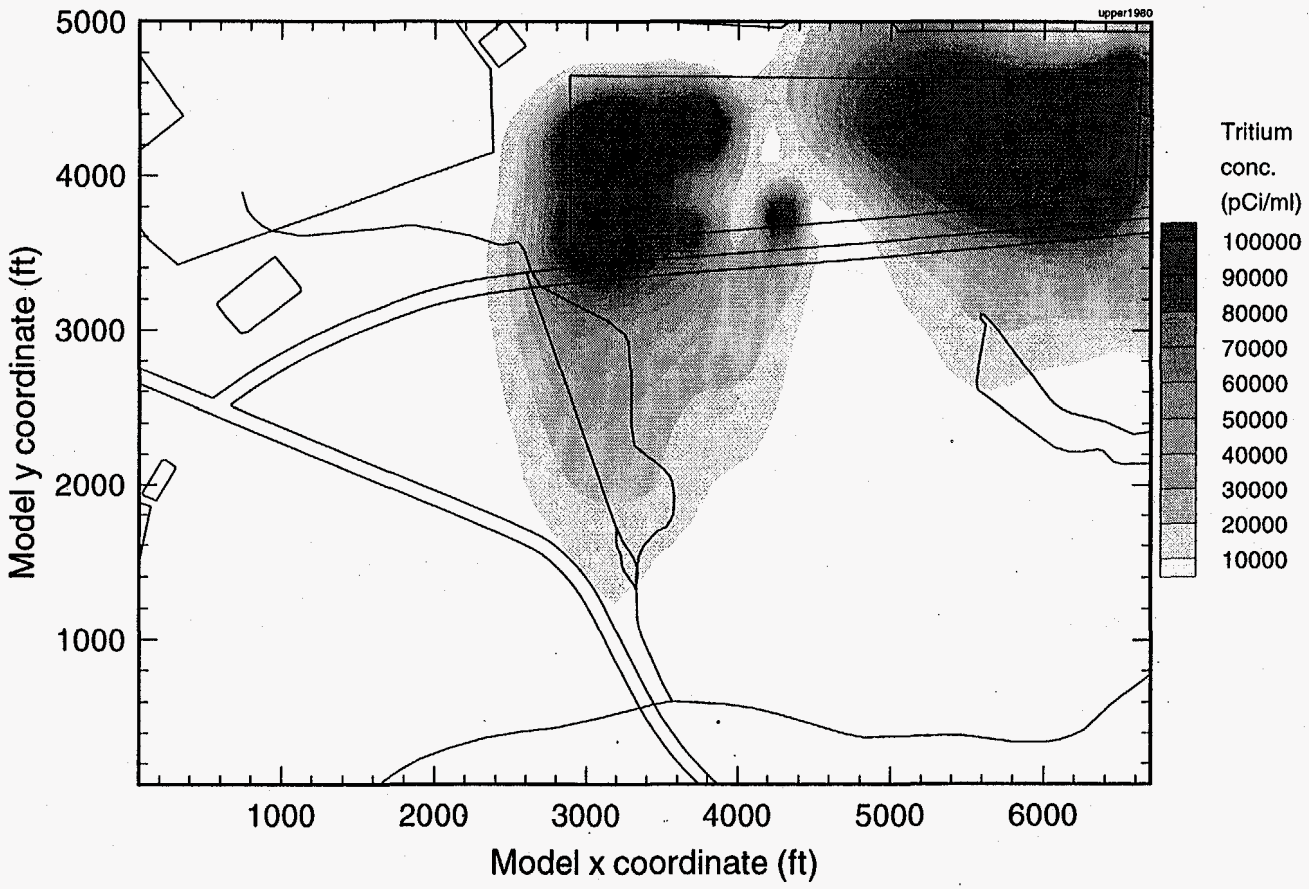

Figure 56e. Contour plot of predicted "upper" aquifer zone tritium concentration for 1980.

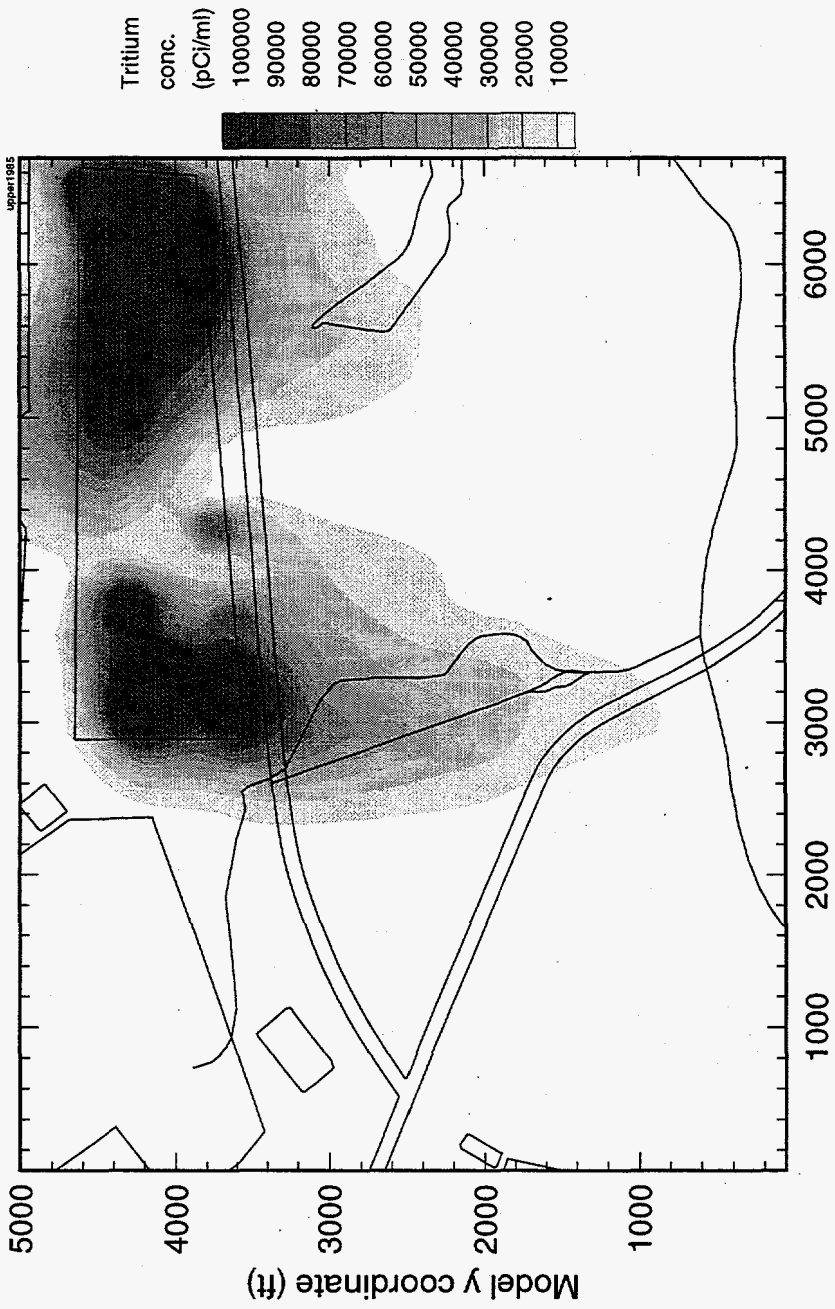

Figure 56f. Contour plot of predicted "upper" aquifer zone tritium concentration for 1985.

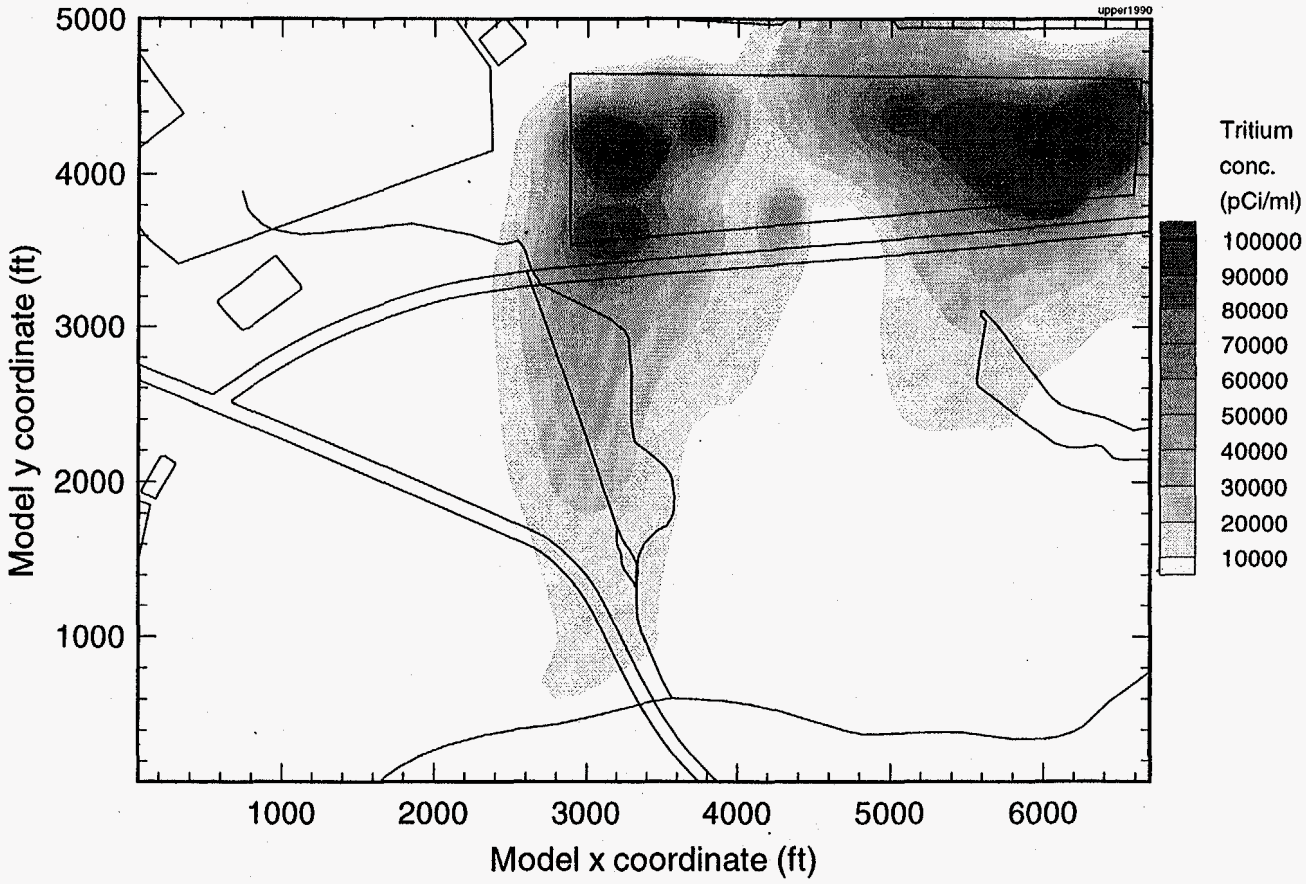

Figure 56g. Contour plot of predicted "upper" aquifer zone tritium concentration for 1990.

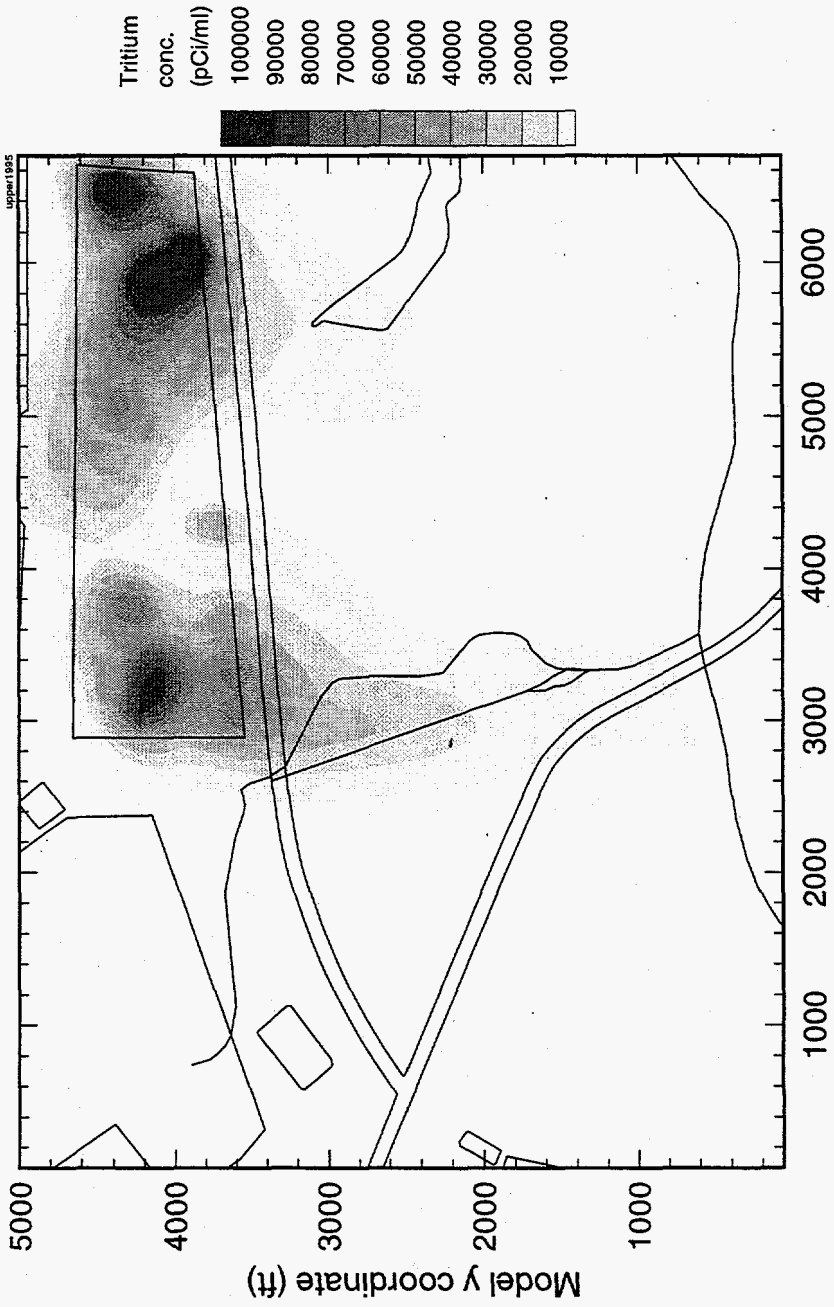

Figure 56h. Contour plot of predicted "upper" aquifer zone tritium concentration for 1995.

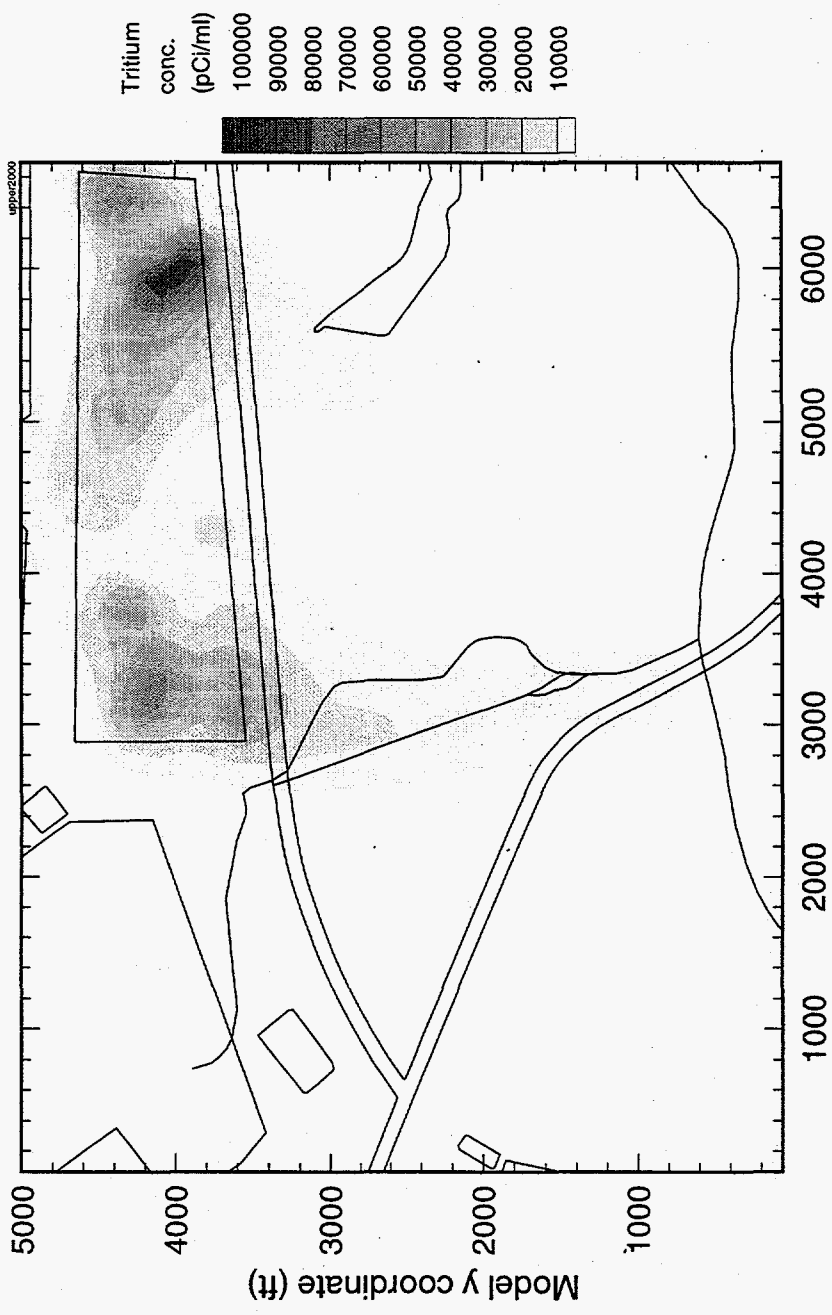

Figure 56i. Contour plot of predicted "upper" aquifer zone tritium concentration for 2000.

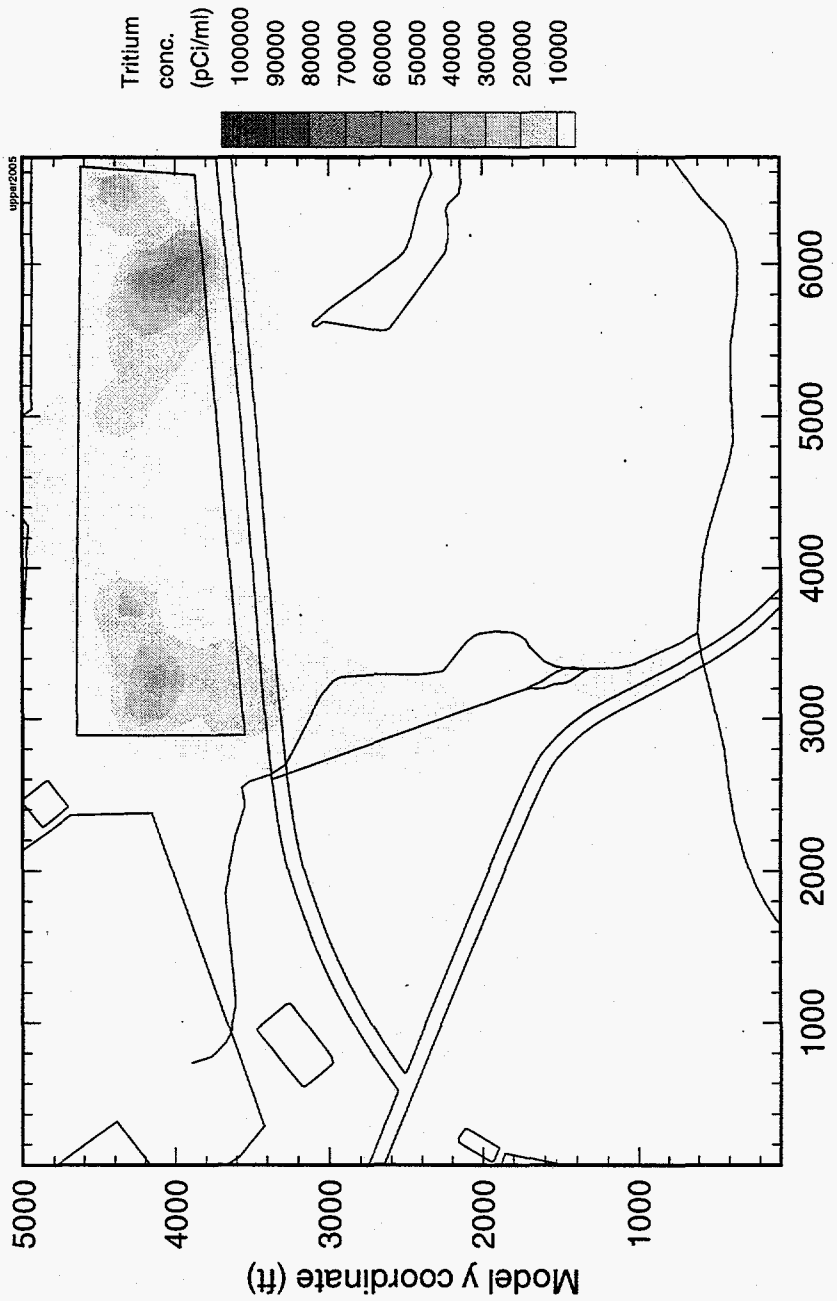

Figure 56j. Contour plot of predicted "upper" aquifer zone tritium concentration for 2005.

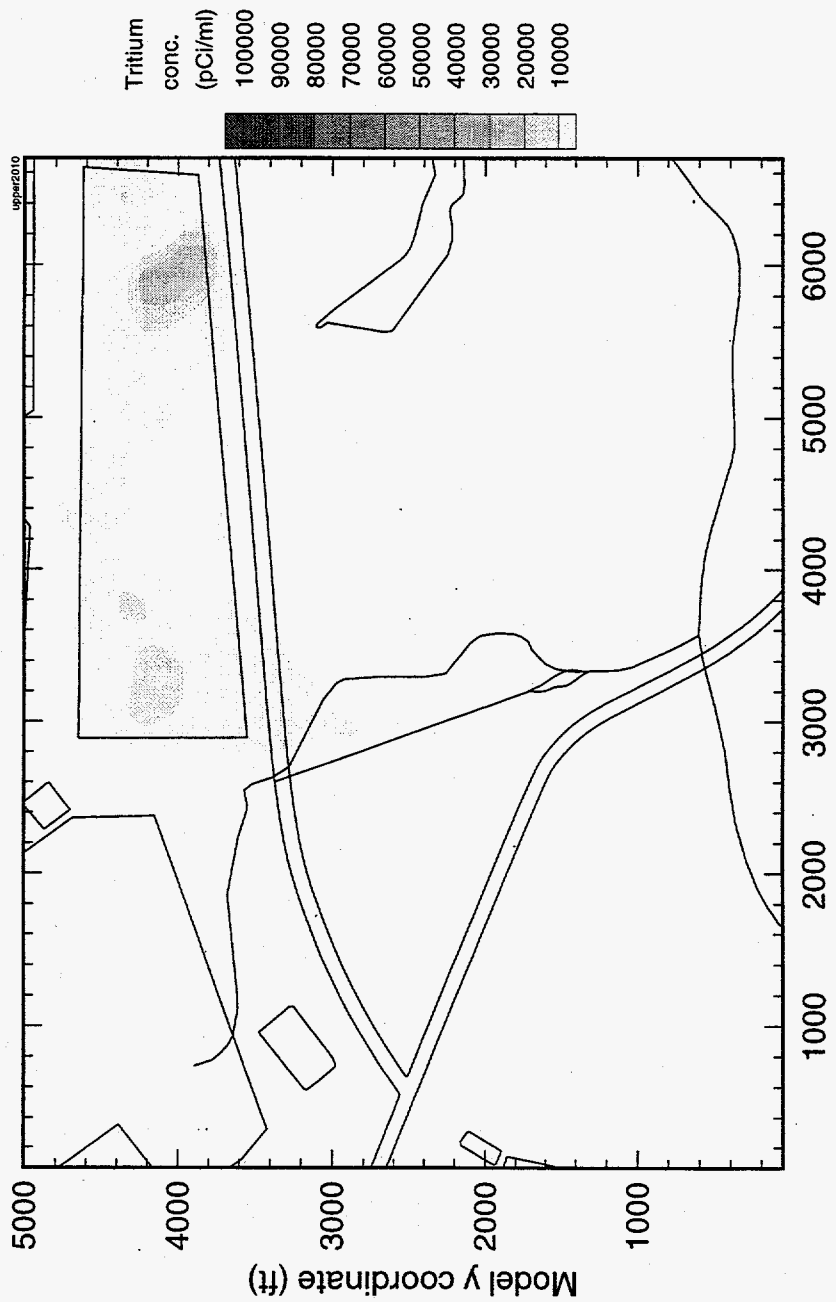

Figure 56k. Contour plot of predicted "upper" aquifer zone tritium concentration for 2010.

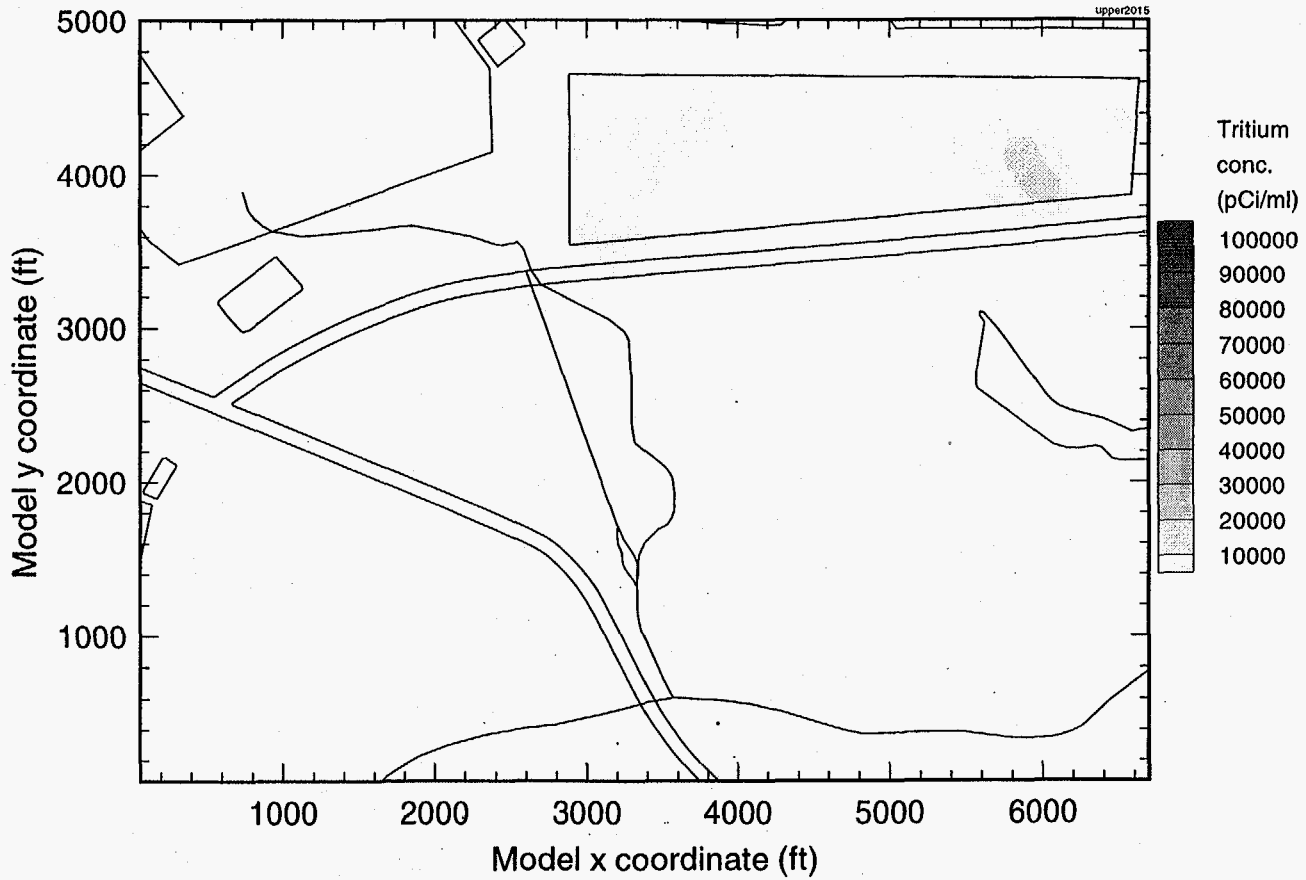

Figure 56l. Contour plot of predicted "upper" aquifer zone tritium concentration for 2015.

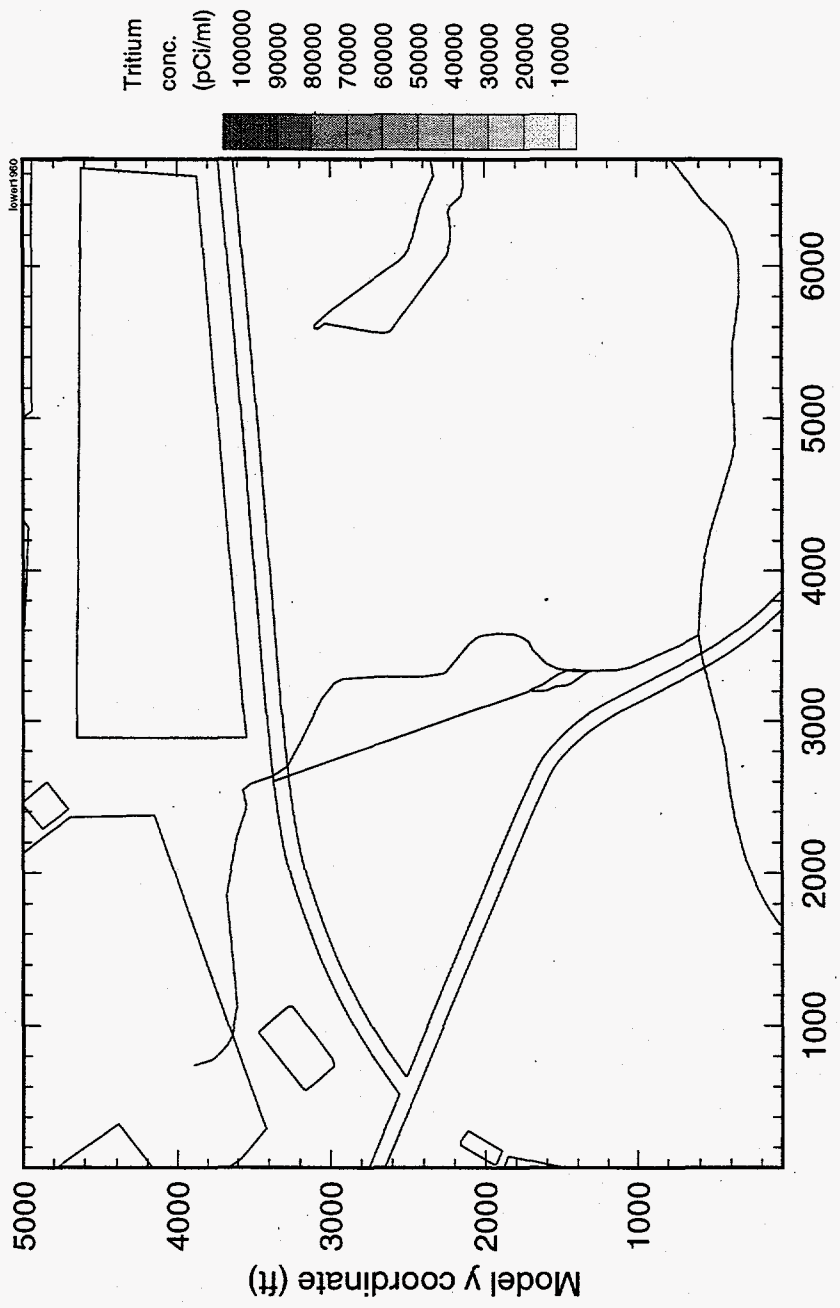

Figure 57a. Contour plot of predicted "lower" aquifer zone tritium concentration for 1960.

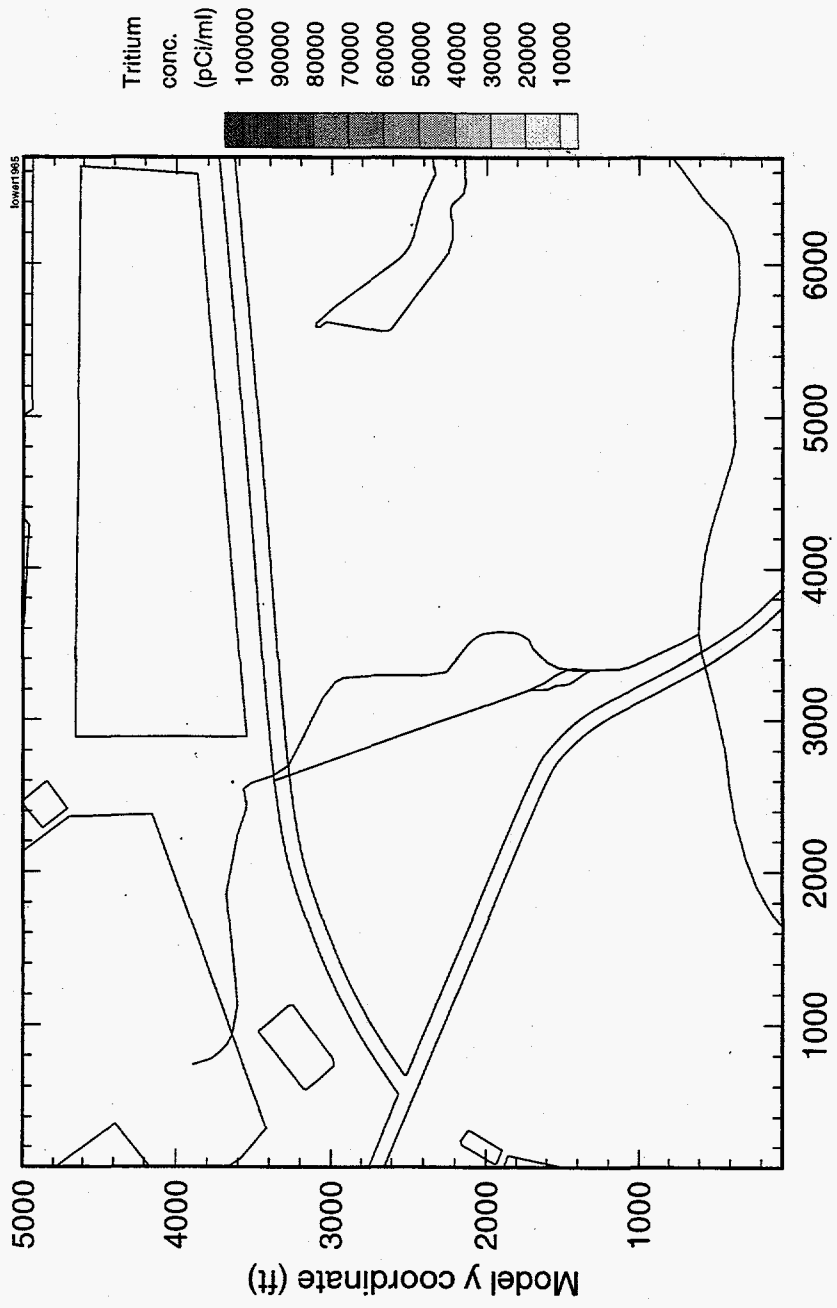

Figure 57b. Contour plot of predicted "lower" aquifer zone tritium concentration for 1965.

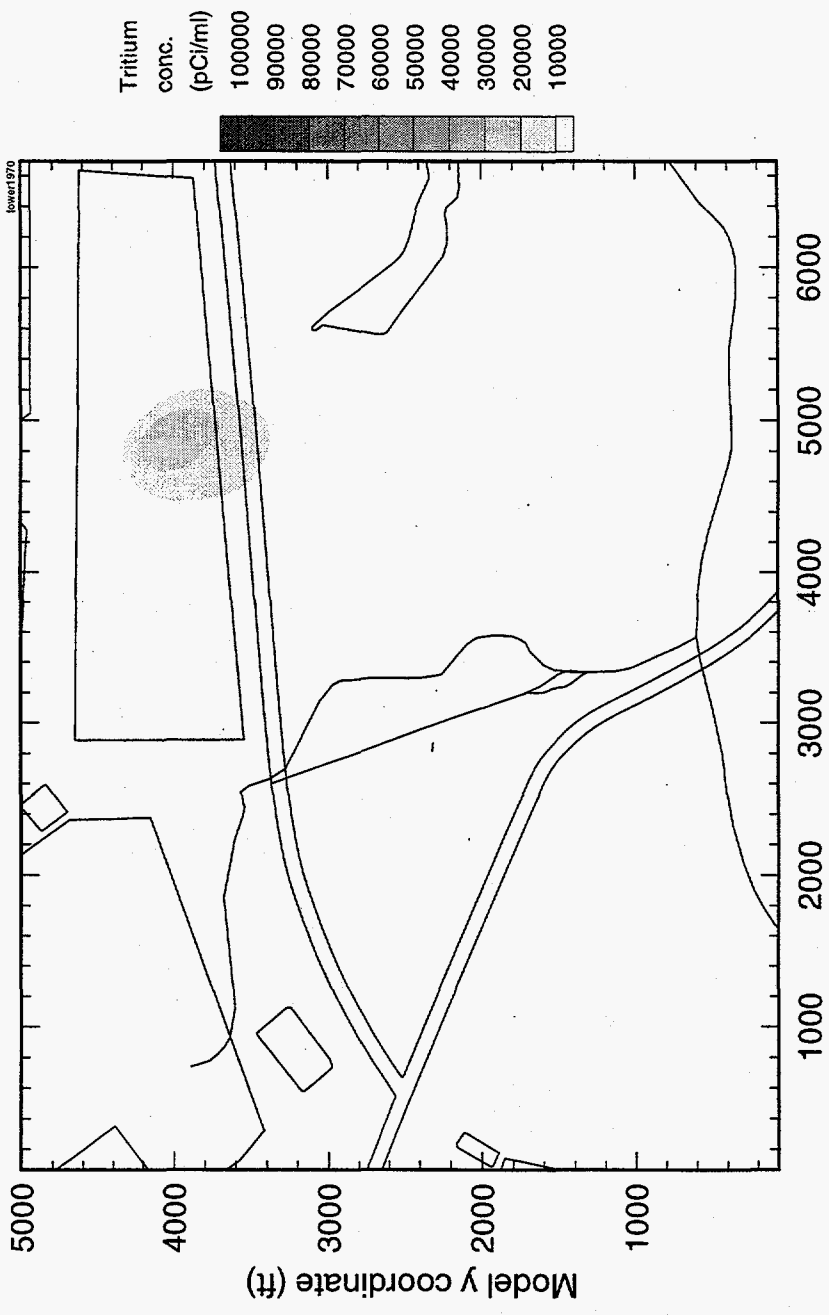

Figure 57c. Contour plot of predicted "lower" aquifer zone tritium concentration for 1970.

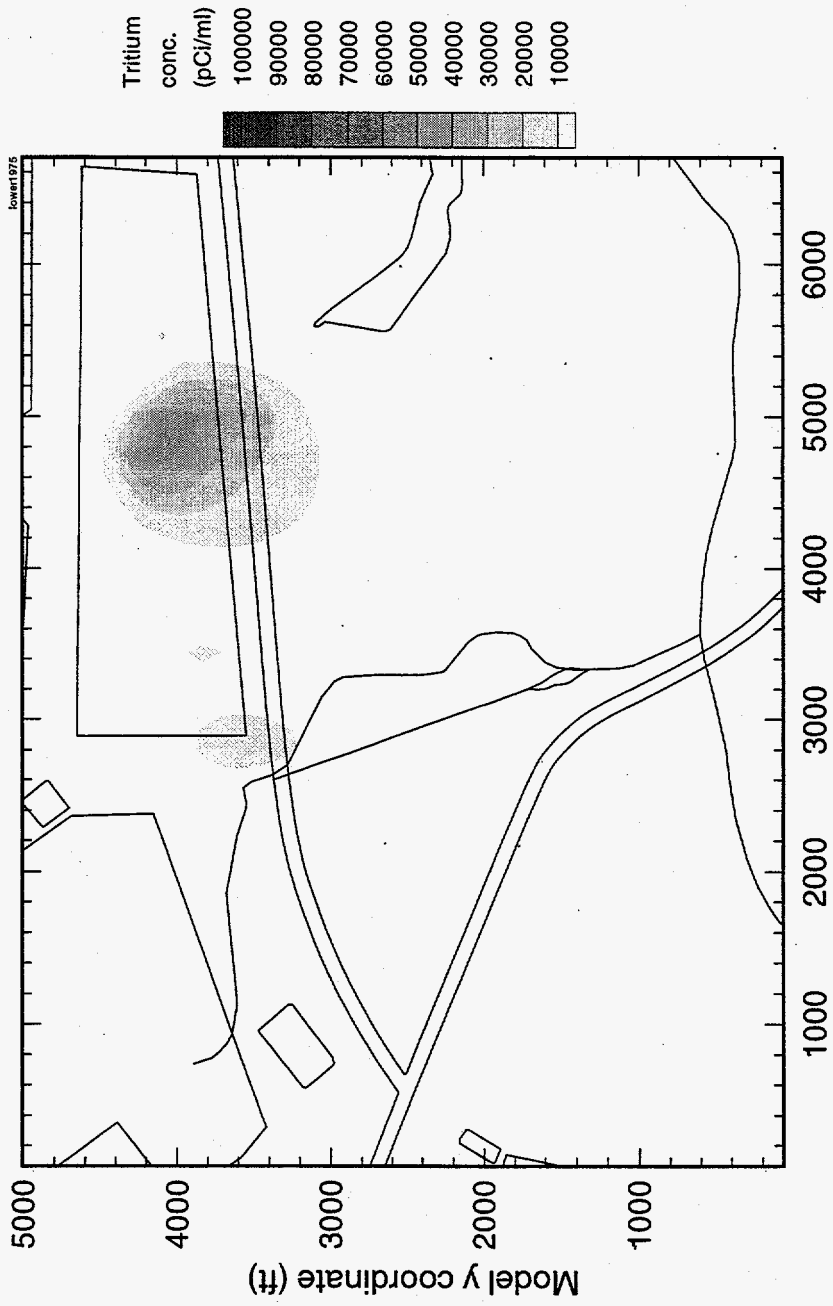

Figure 57d. Contour plot of predicted "lower" aquifer zone tritium concentration for 1975.

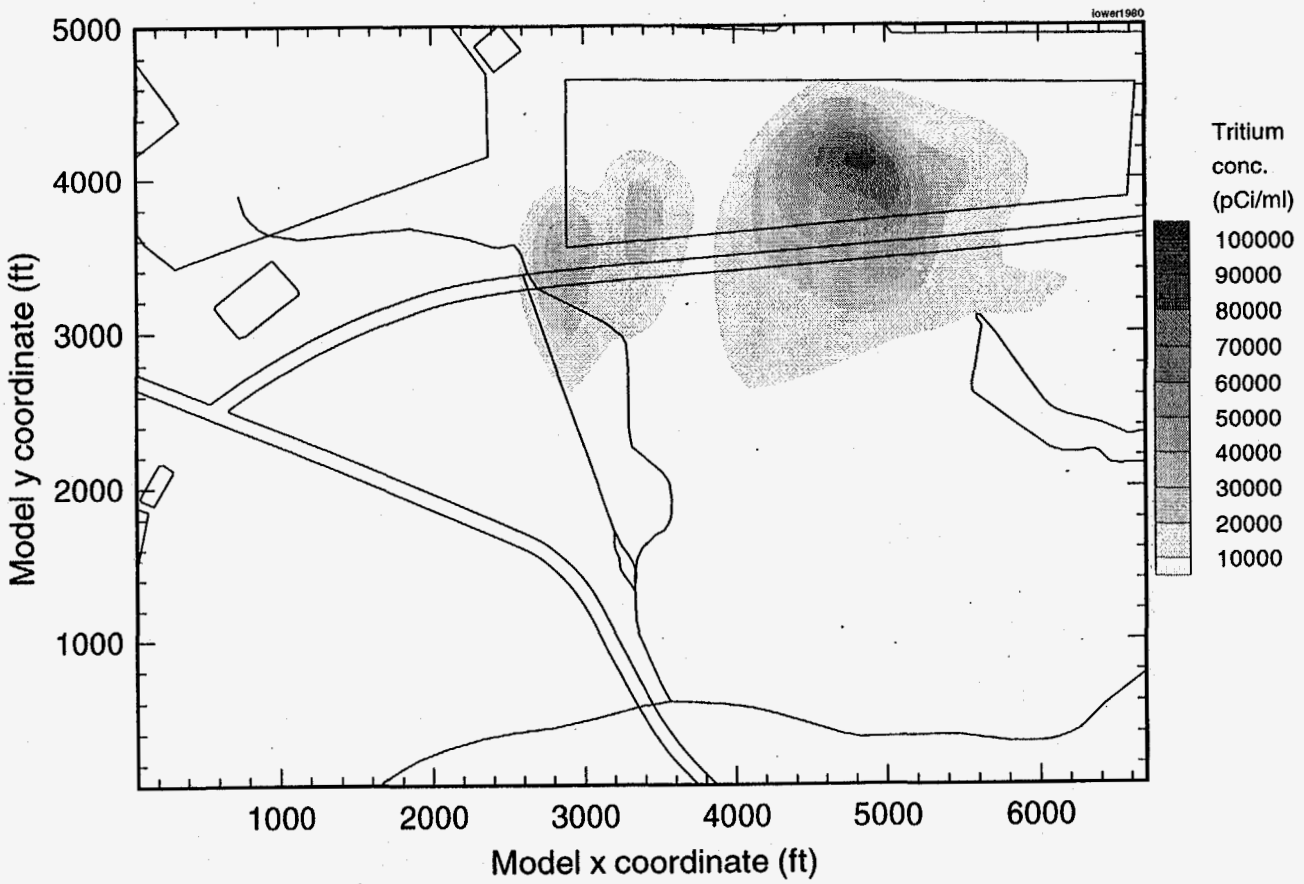

Figure 57e. Contour plot of predicted "lower" aquifer zone tritium concentration for 1980.

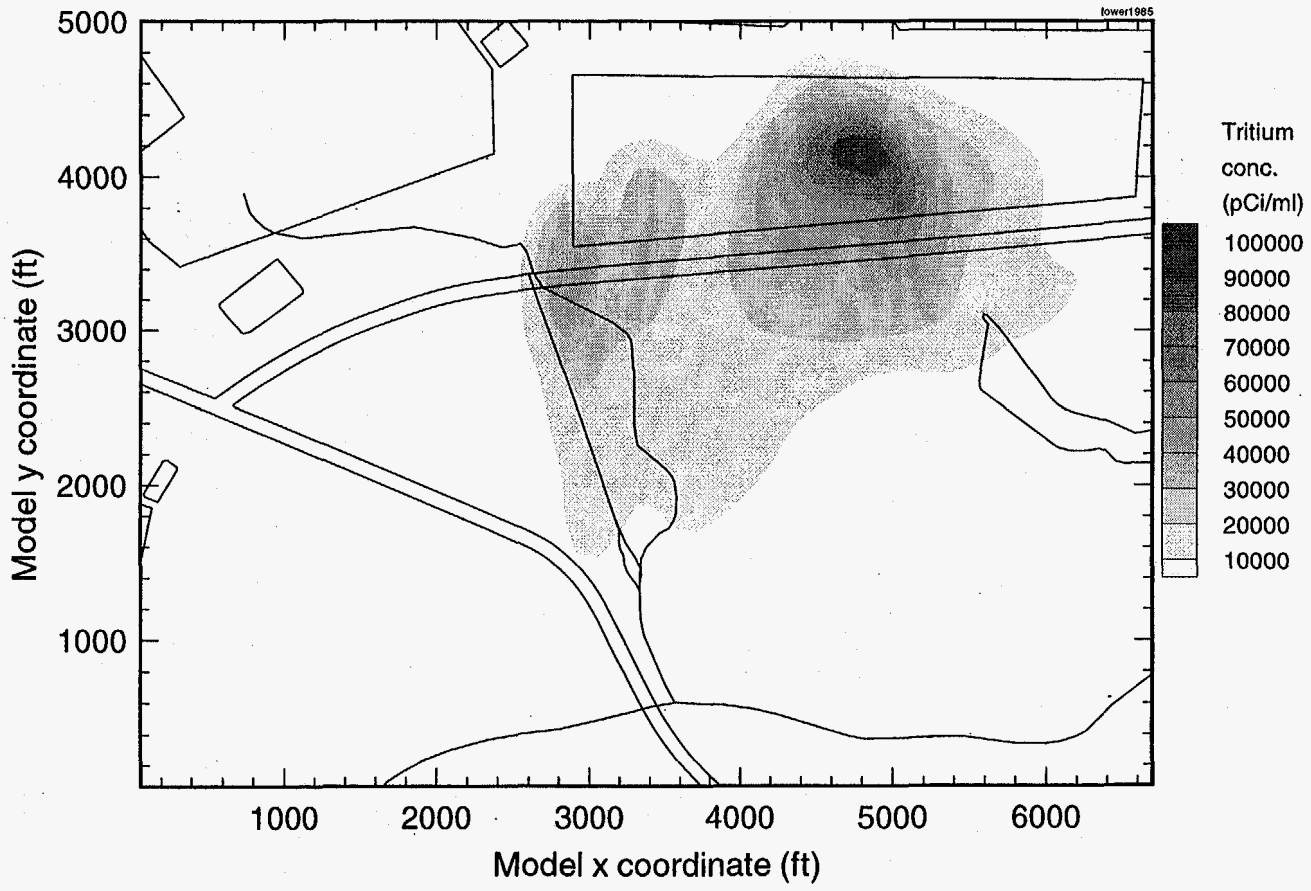

Figure 57f. Contour plot of predicted "lower" aquifer zone tritium concentration for 1985.

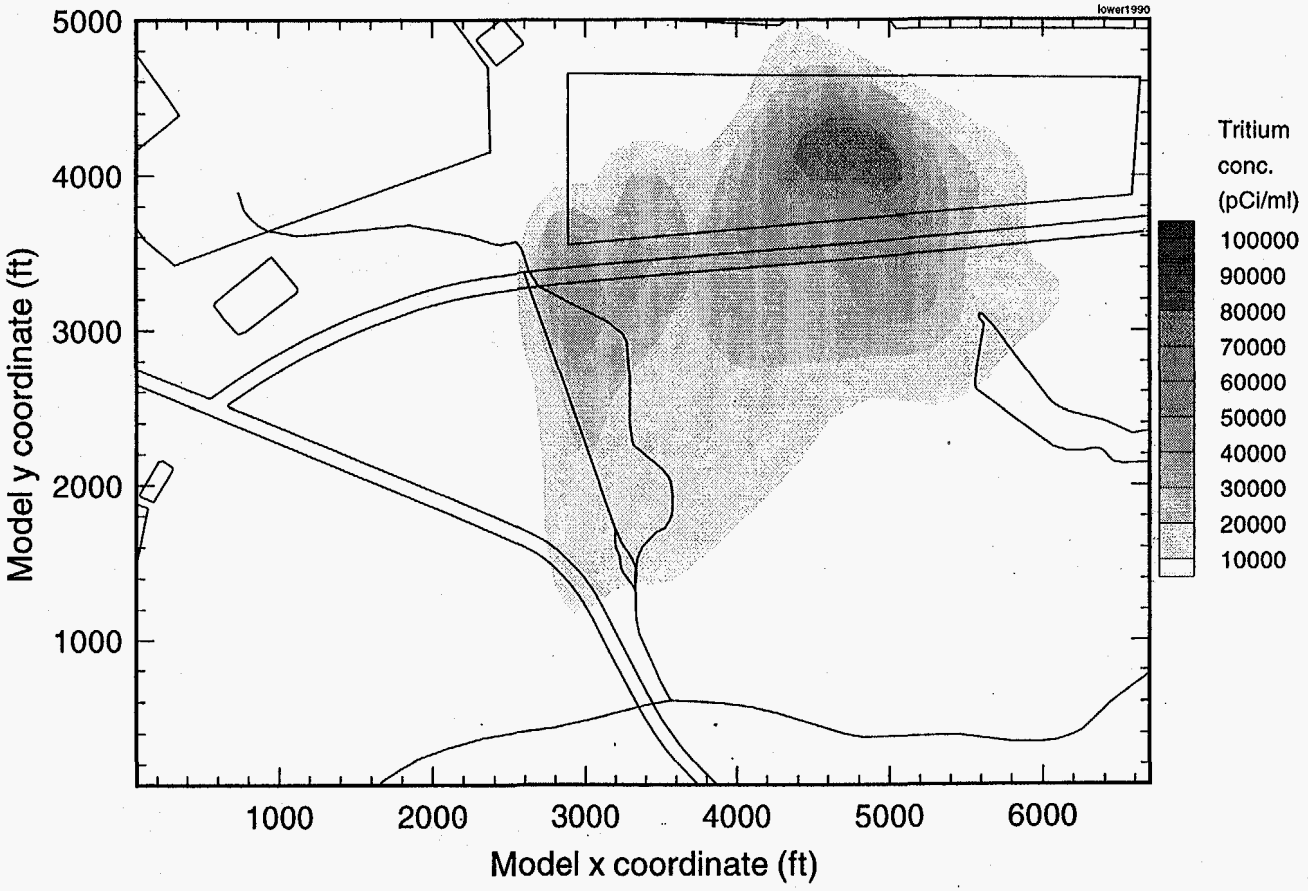

Figure 57g. Contour plot of predicted "lower" aquifer zone tritium concentration for 1990.

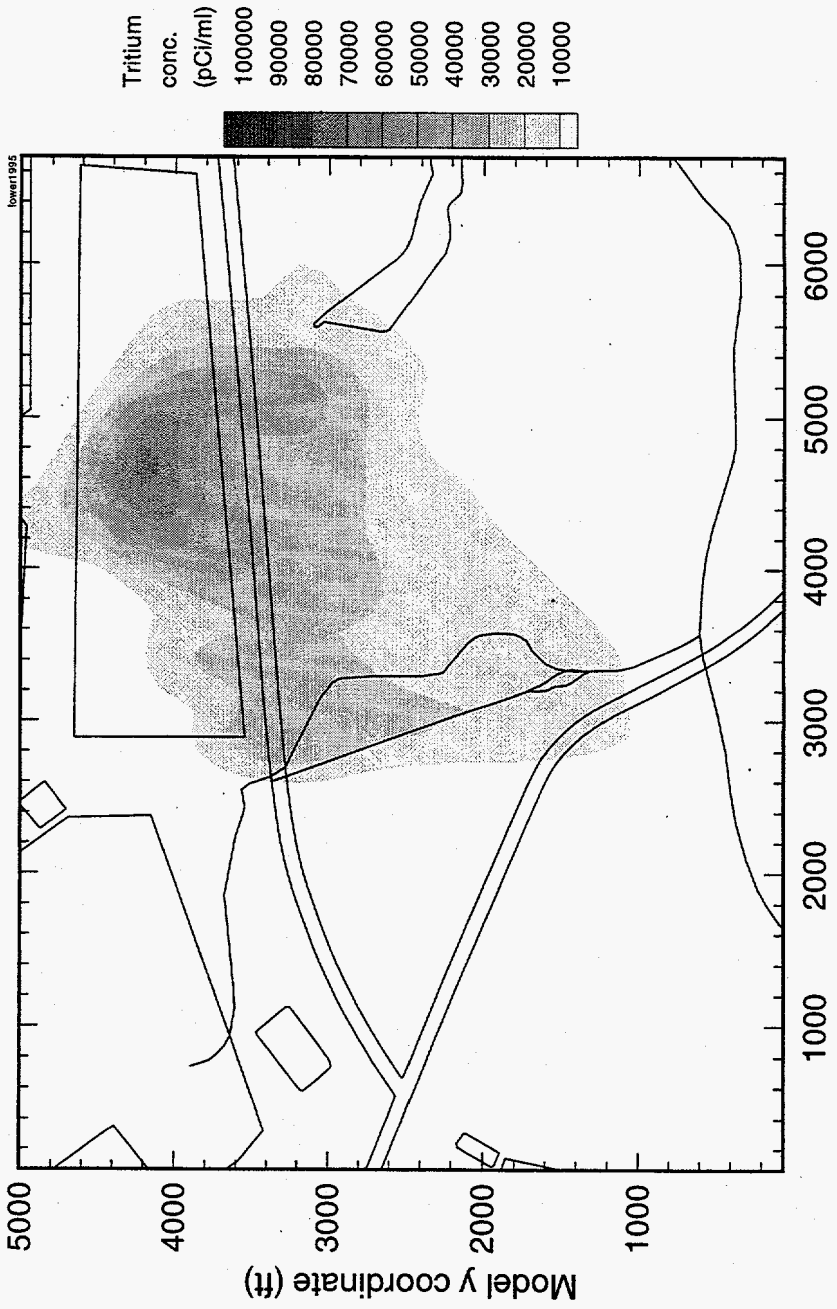

Figure 57h. Contour plot of predicted "lower" aquifer zone tritium concentration for 1995.

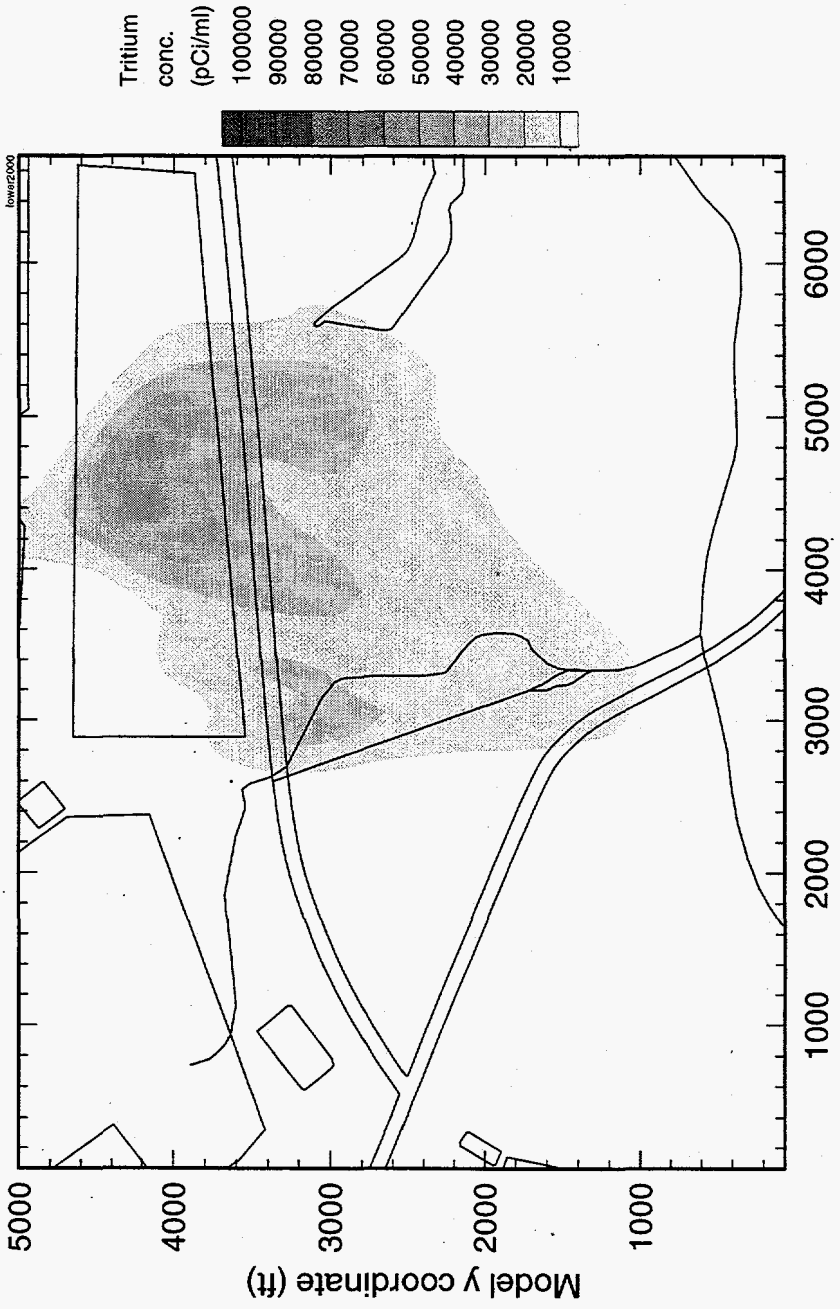

Figure 57i. Contour plot of predicted "lower" aquifer zone tritium concentration for 2000.

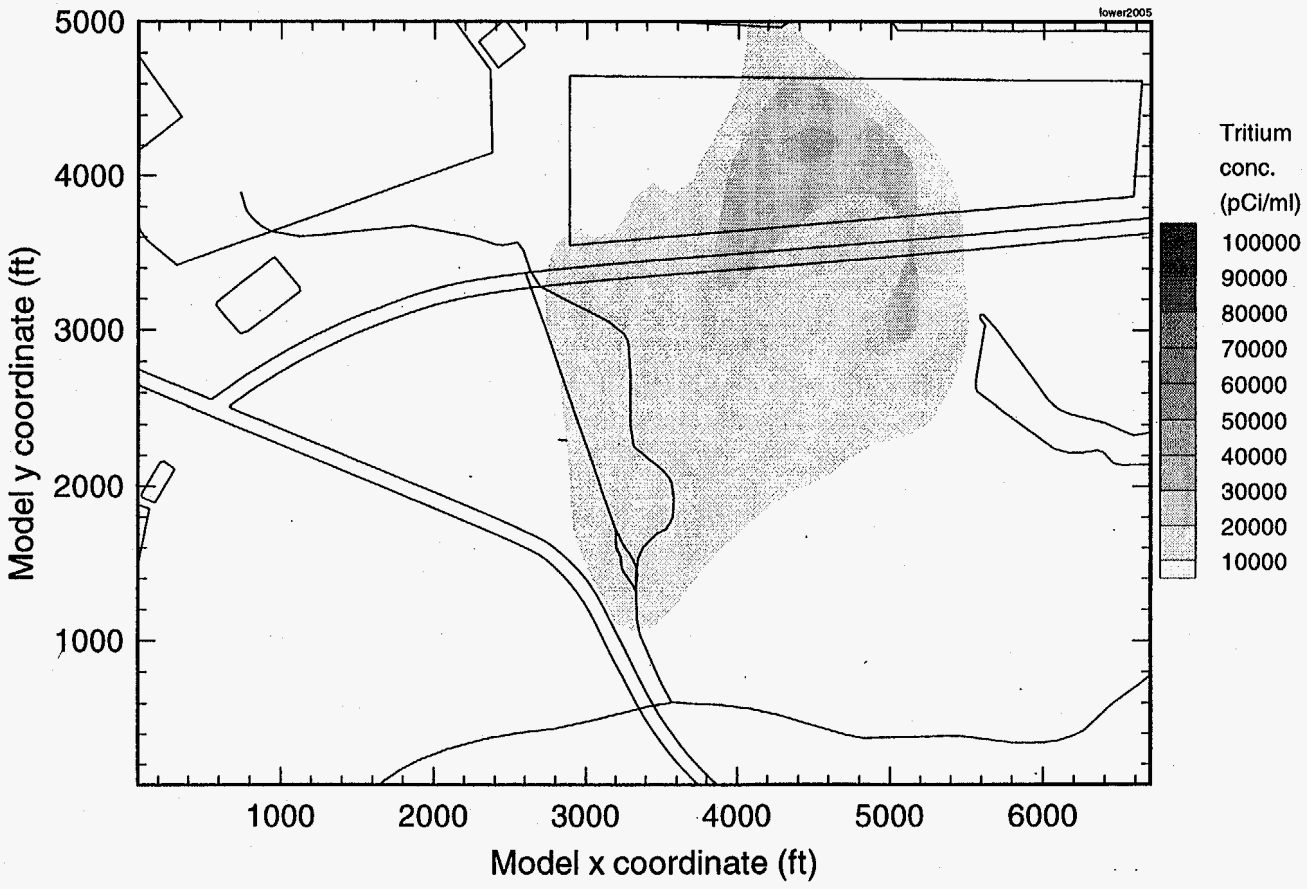

Figure 57j. Contour plot of predicted "lower" aquifer zone tritium concentration for 2005.

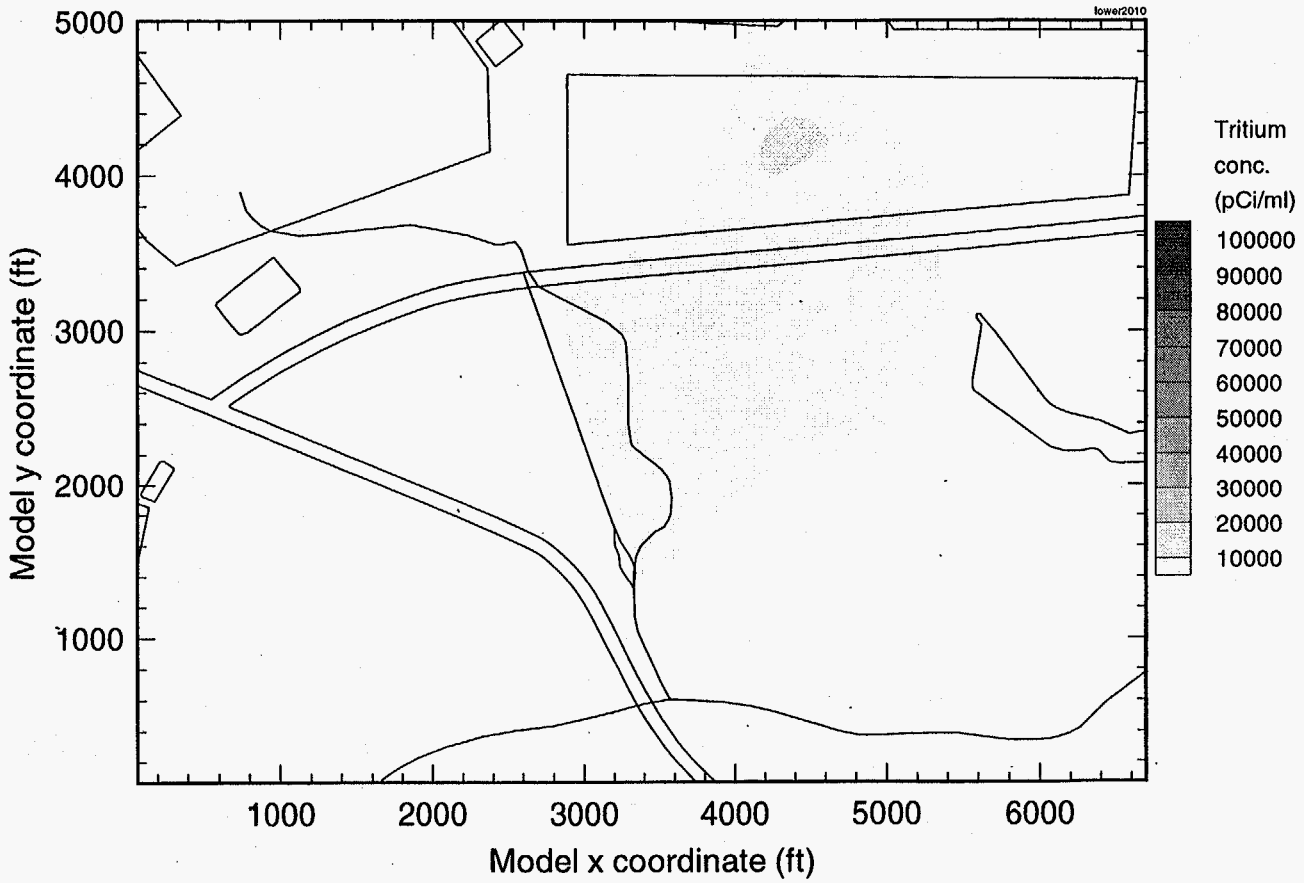

Figure 57k. Contour plot of predicted "lower" aquifer zone tritium concentration for 2010.

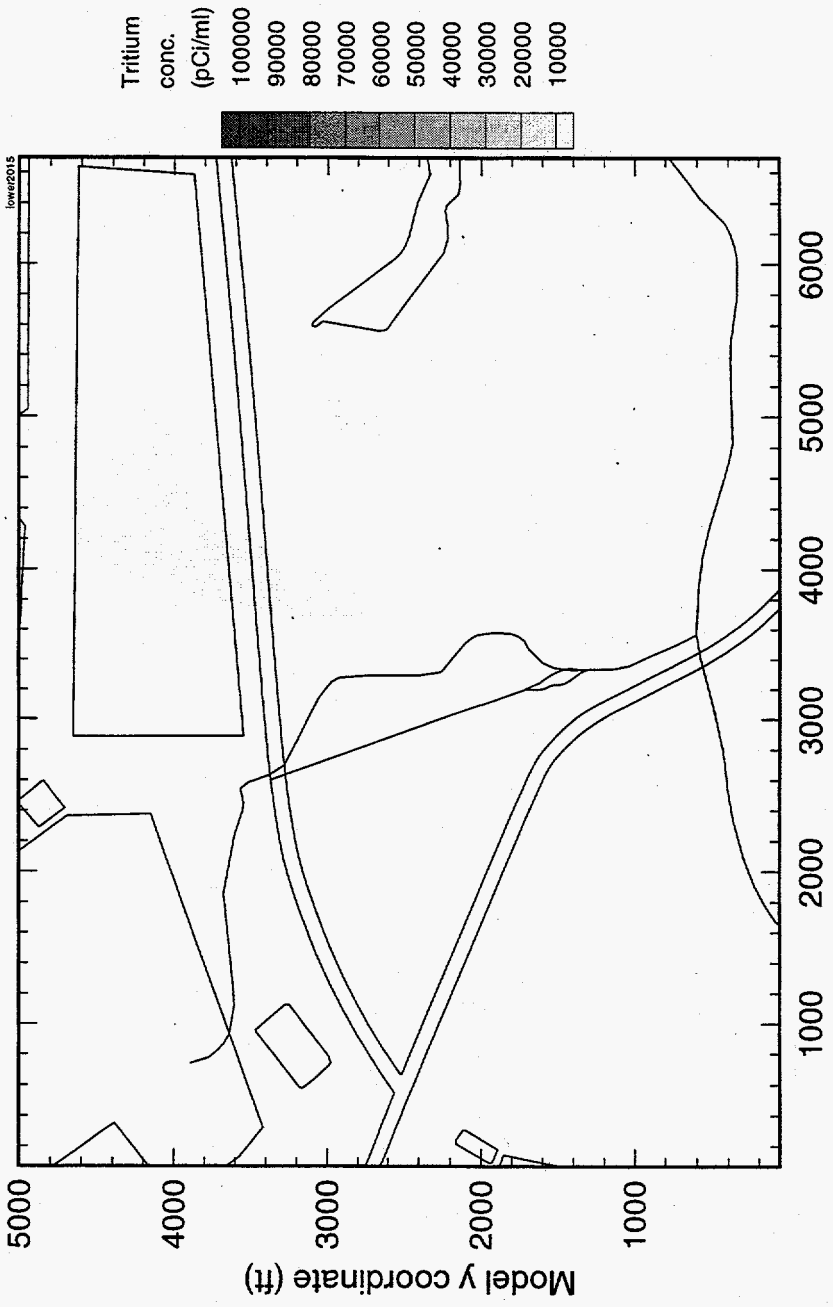

Figure 571. Contour plot of predicted "lower" aquifer zone tritium concentration for 2015.

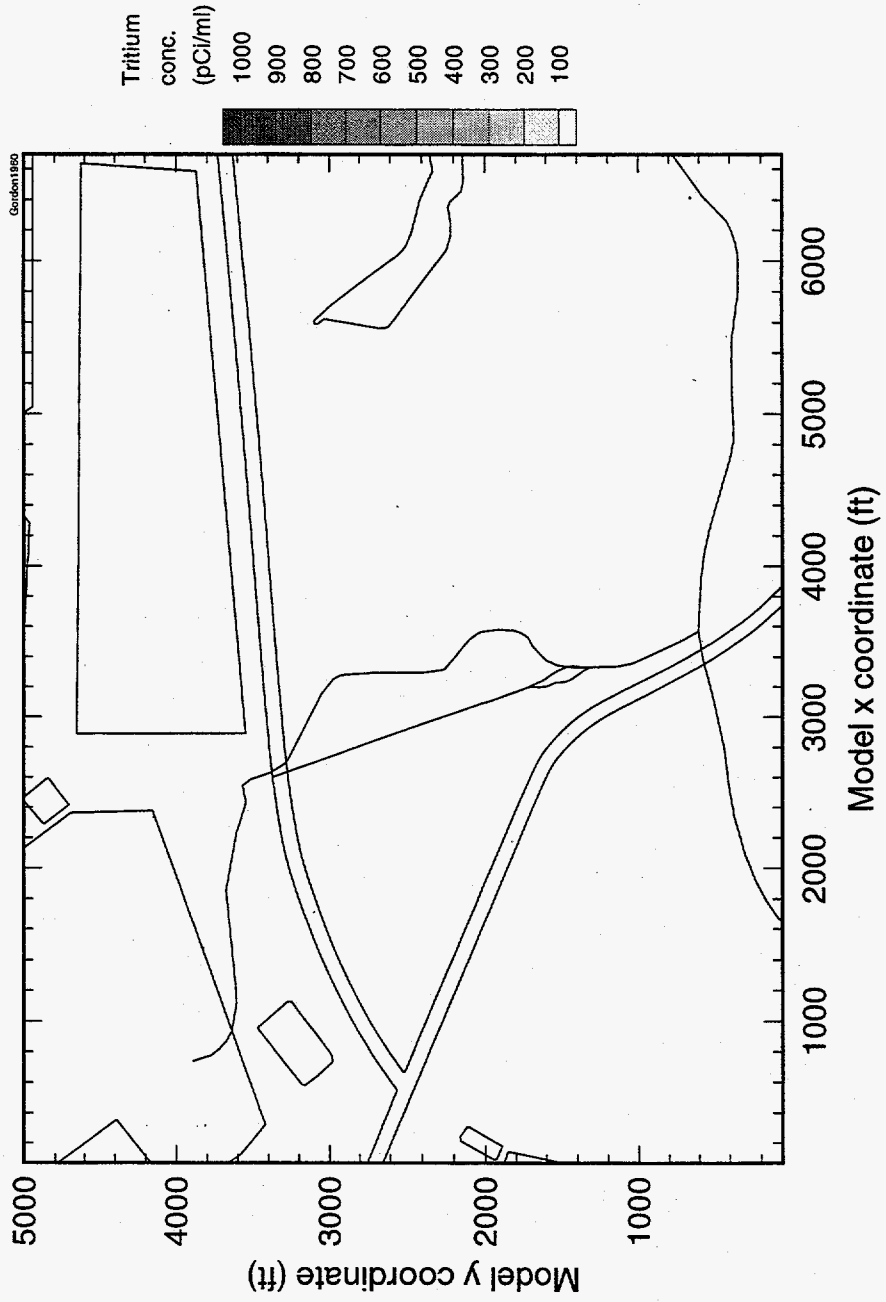

Figure 58a. Contour plot of predicted Gordon aquifer tritium concentration for 1960.

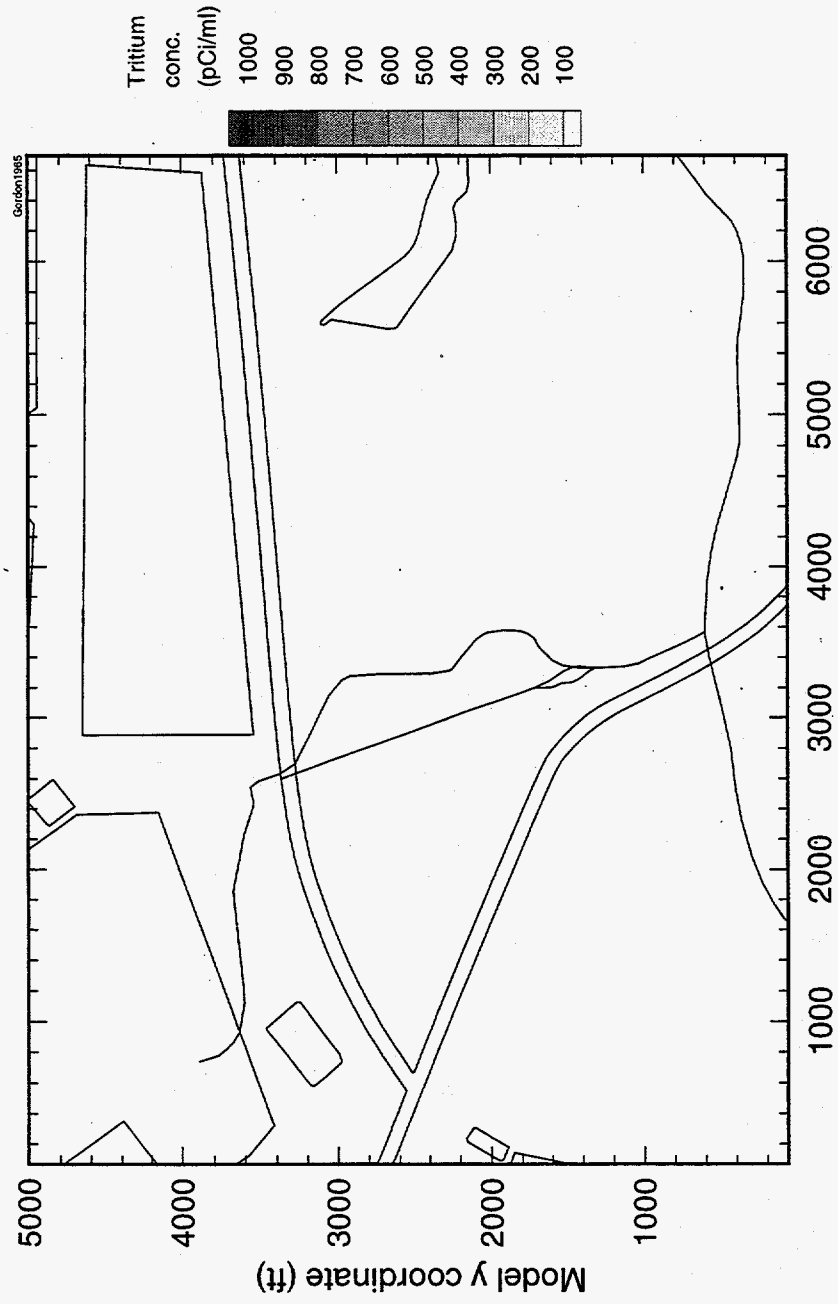

Figure 58b. Contour plot of predicted Gordon aquifer tritium concentration for 1965.

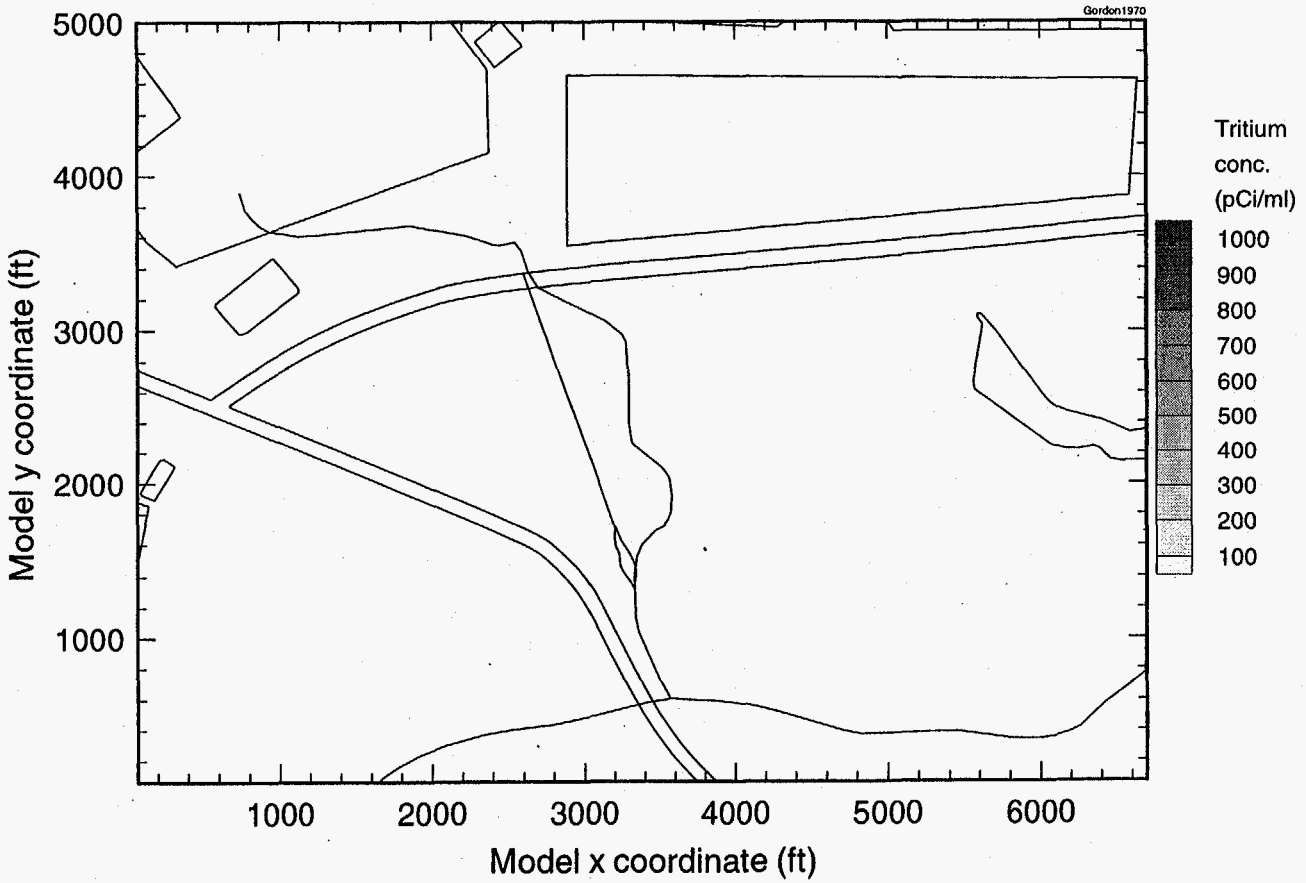

Figure 58c. Contour plot of predicted Gordon aquifer tritium concentration for 1970.

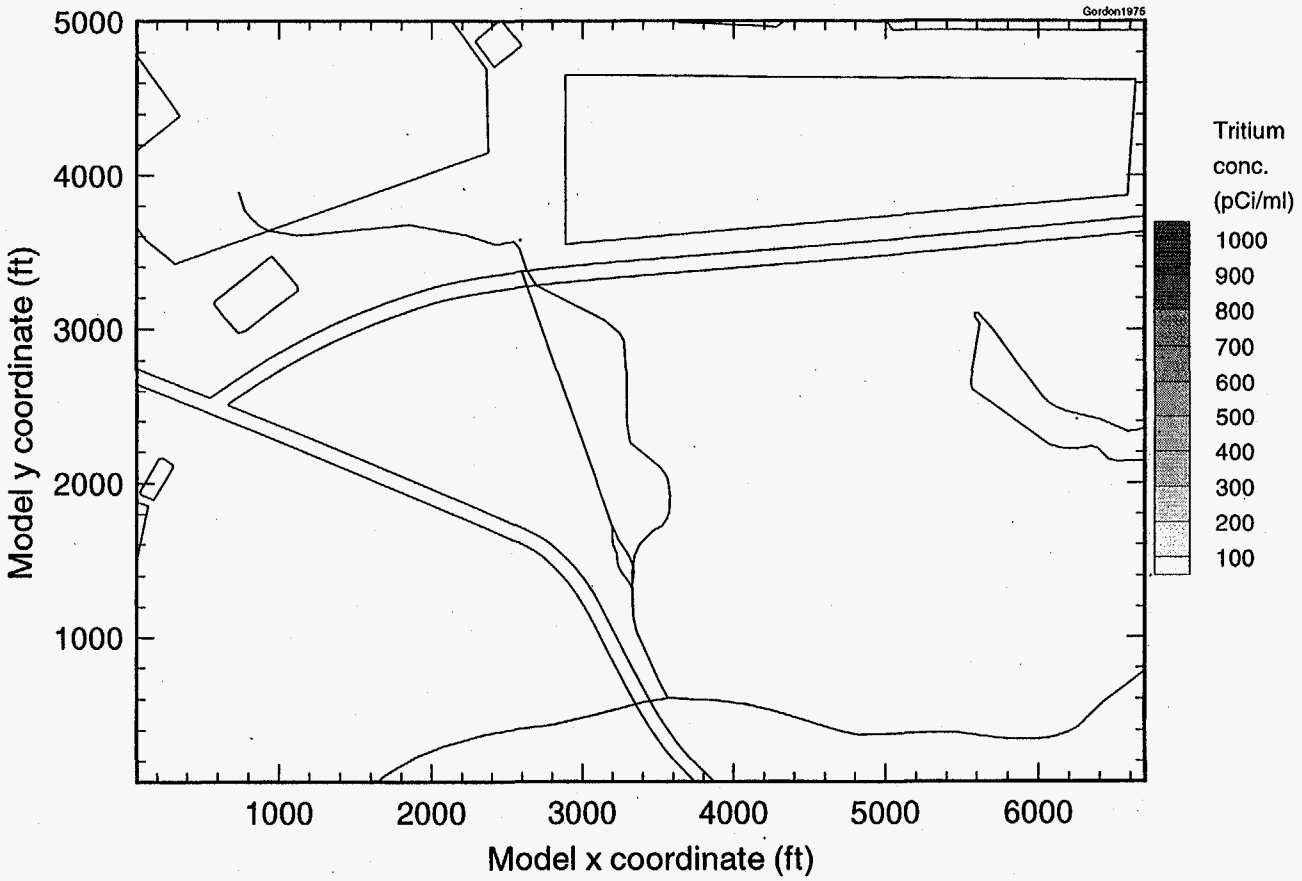

Figure 58d. Contour plot of predicted Gordon aquifer tritium concentration for 1975.

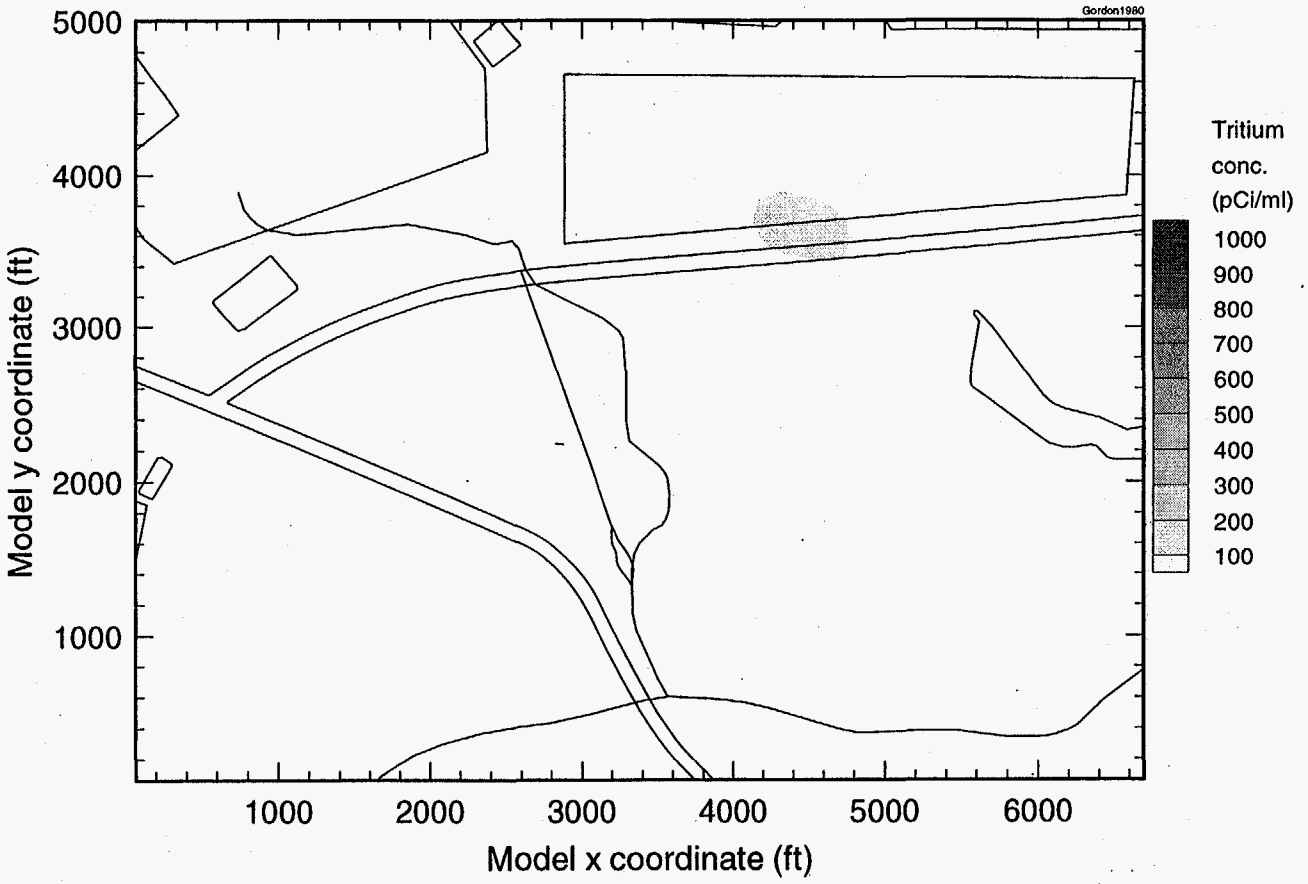

Figure 58e. Contour plot of predicted Gordon aquifer tritium concentration for 1980.

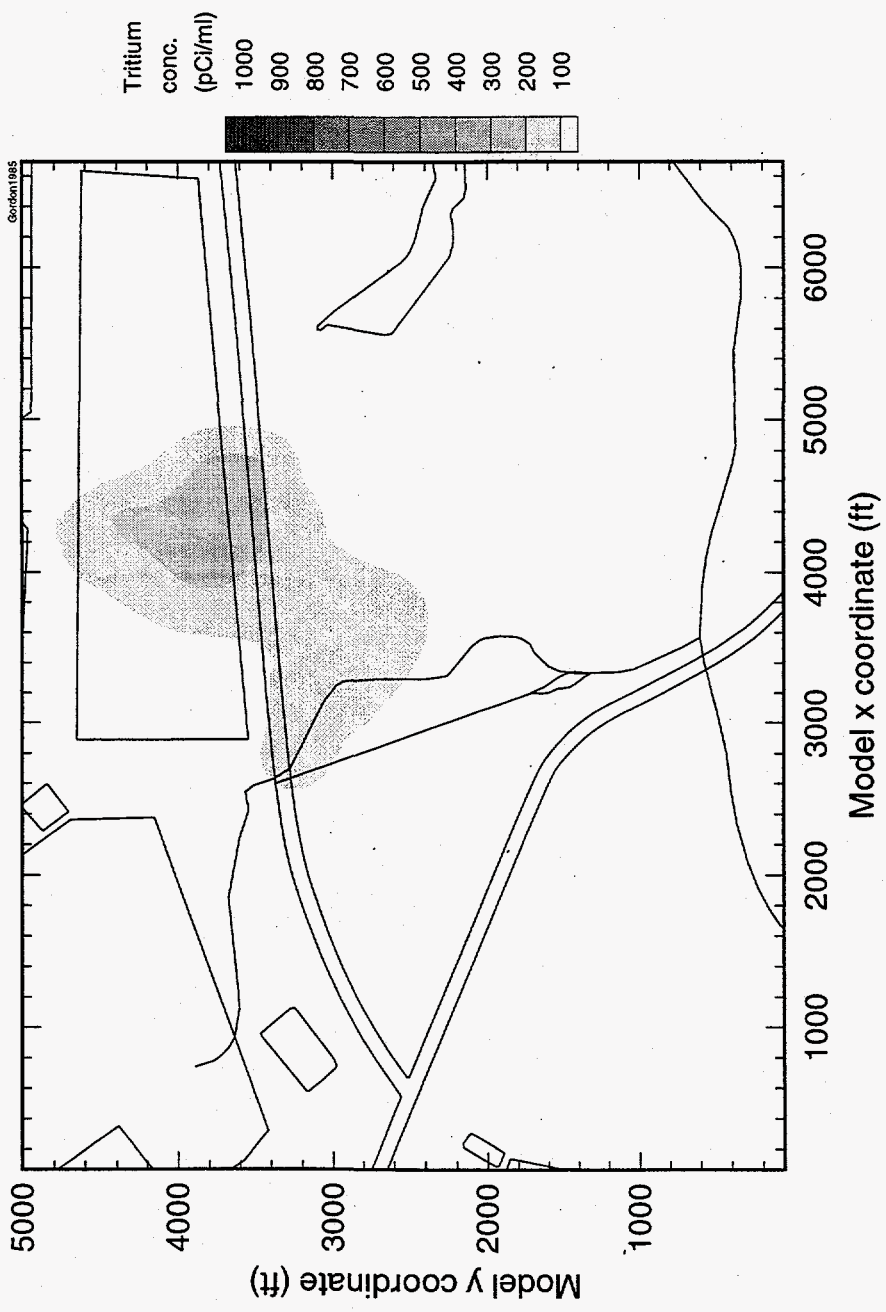

Figure 58f. Contour plot of predicted Gordon aquifer tritium concentration for 1985.

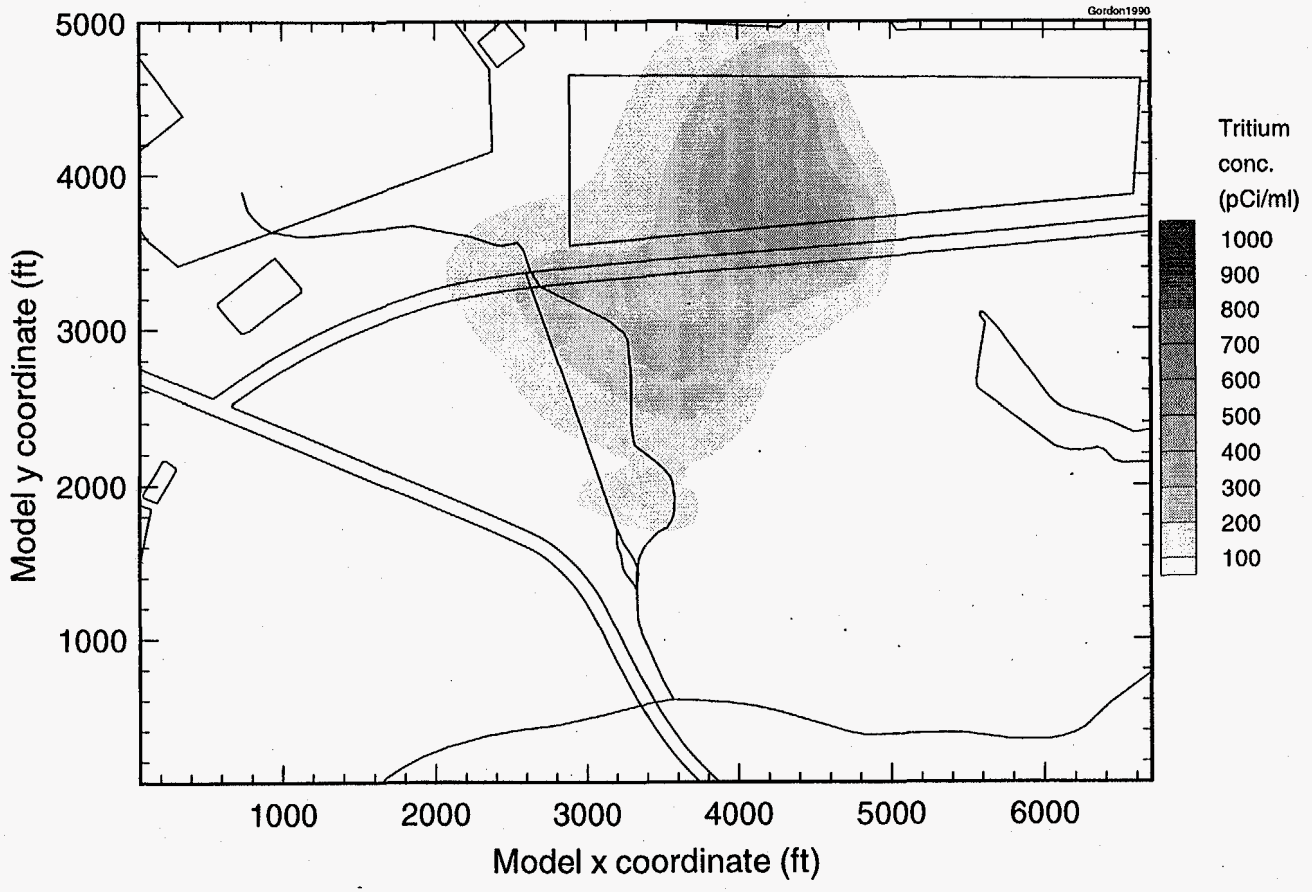

Figure 58g. Contour plot of predicted Gordon aquifer tritium concentration for 1990.

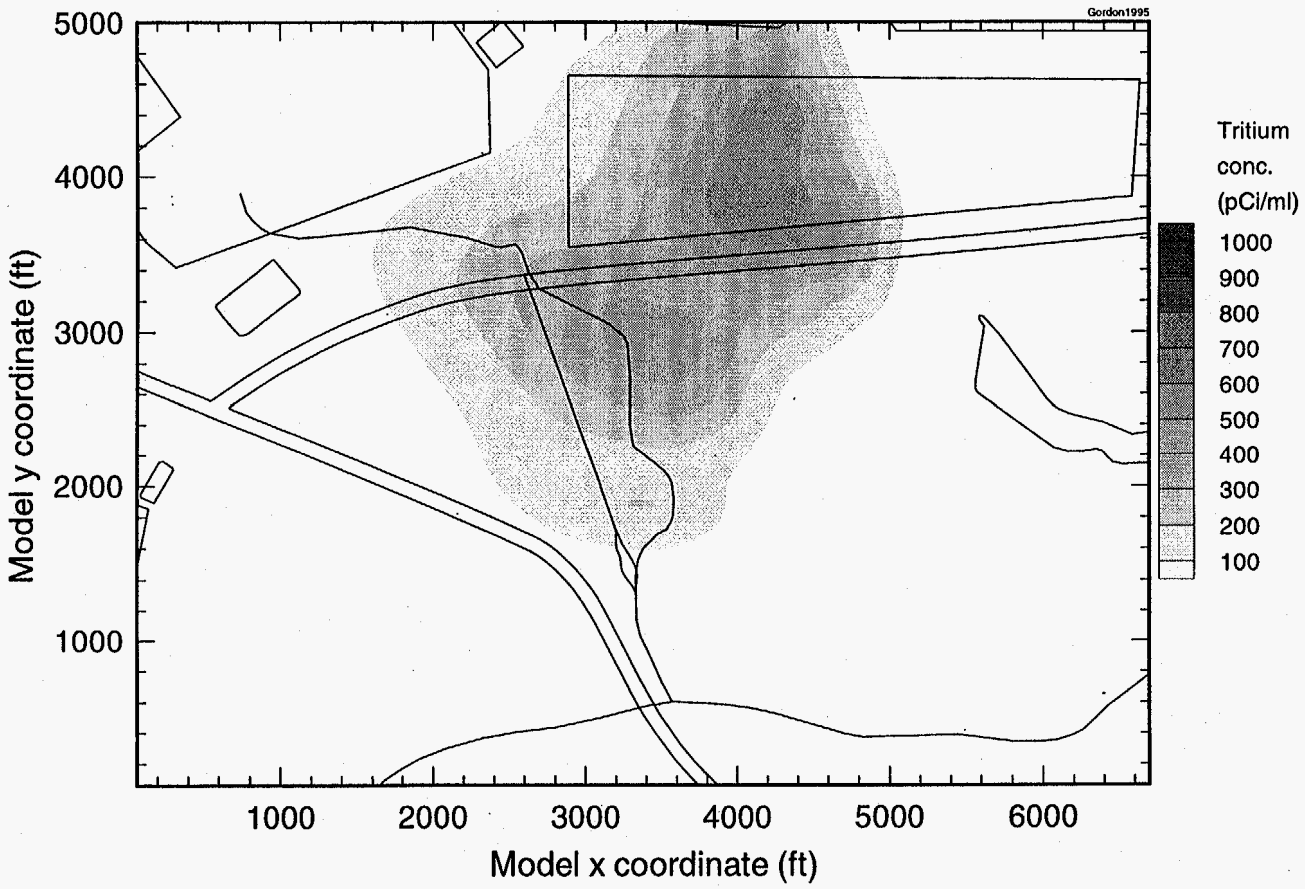

Figure 58h. Contour plot of predicted Gordon aquifer tritium concentration for 1995.

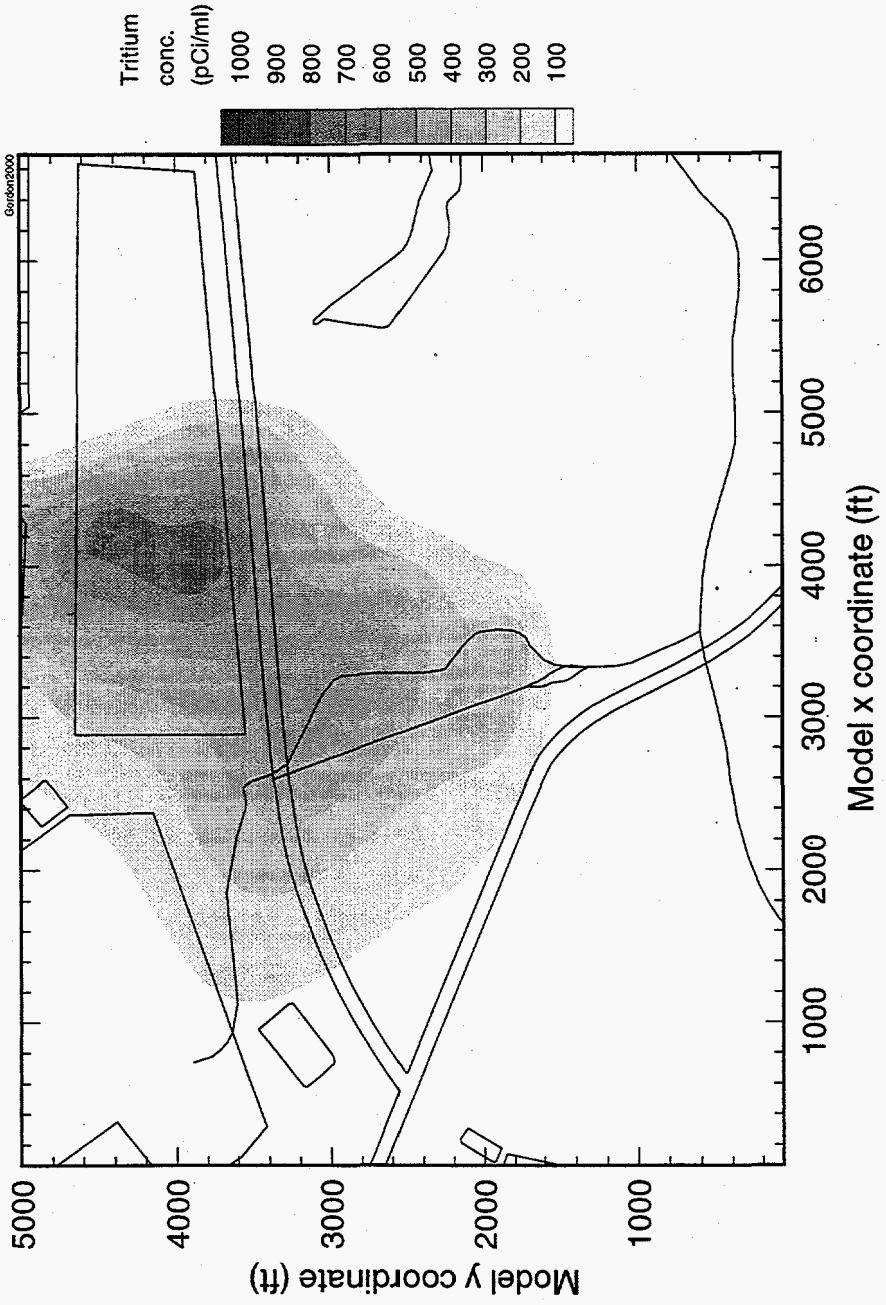

Figure 58i. Contour plot of predicted Gordon aquifer tritium concentration for 2000.

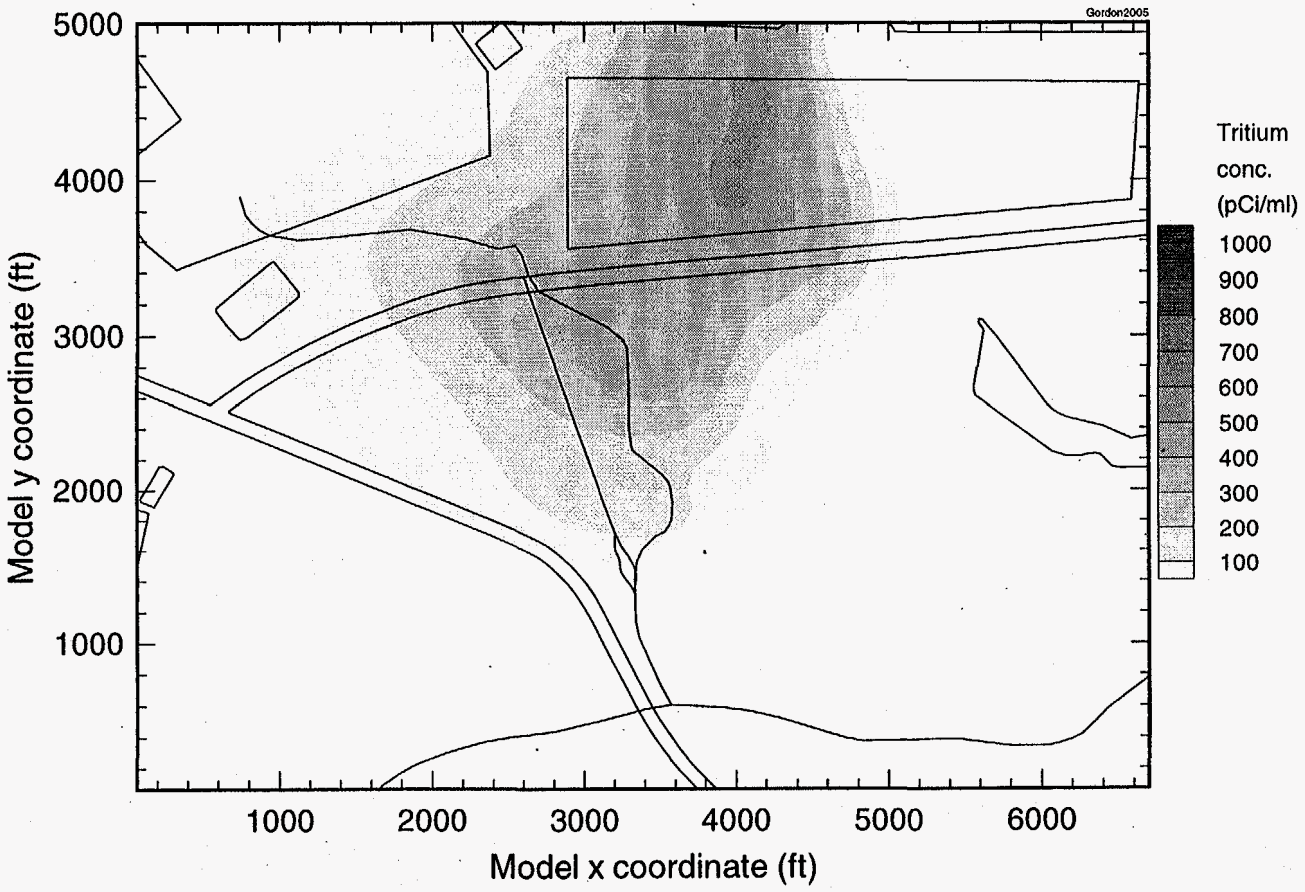

Figure 58j. Contour plot of predicted Gordon aquifer tritium concentration for 2005.

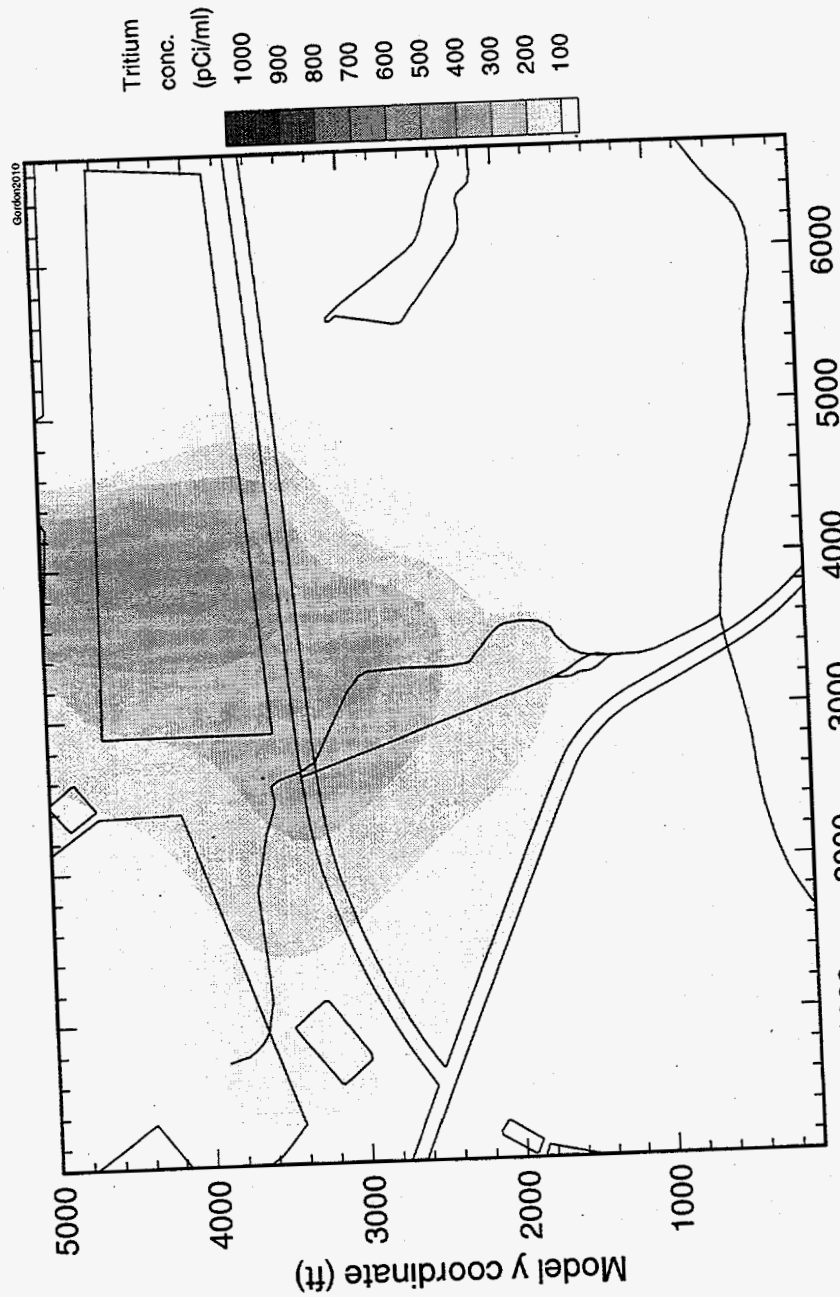

Figure 58k. Contour plot of predicted Gordon aquifer tritium concentration for 2010.

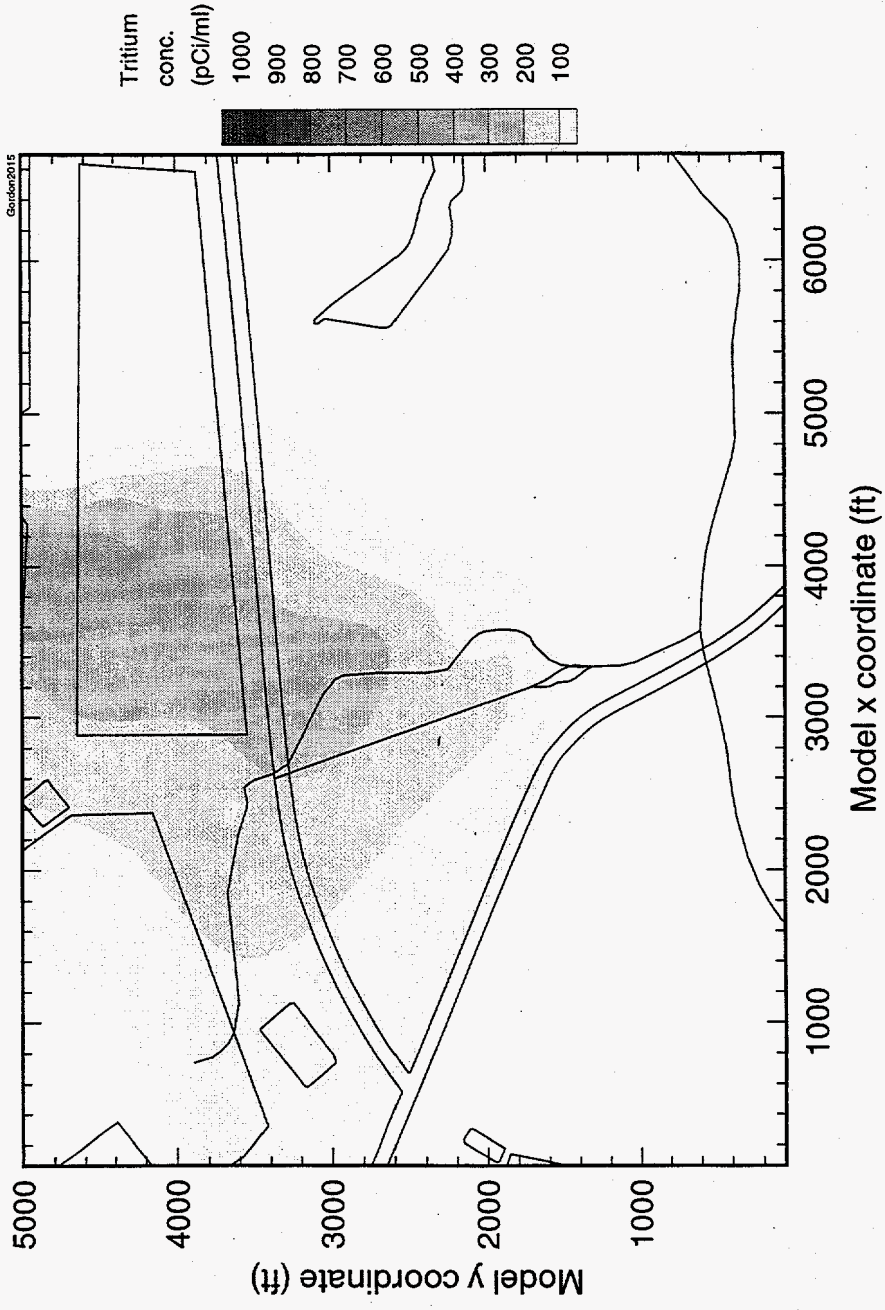

Figure 58l. Contour plot of predicted Gordon aquifer tritium concentration for 2015.

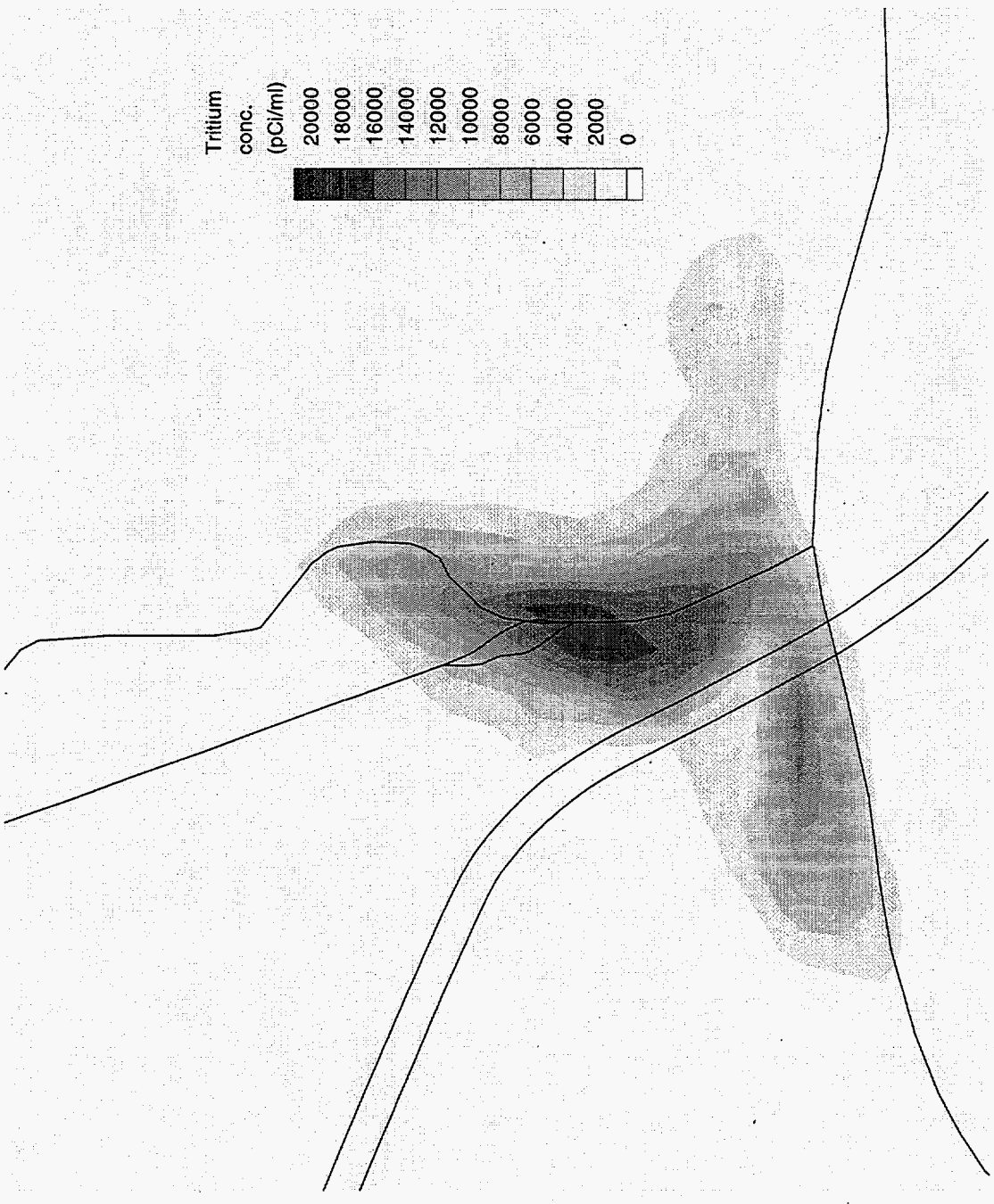

Figure 59. Simulated seepage face tritium concentrations for 1995.

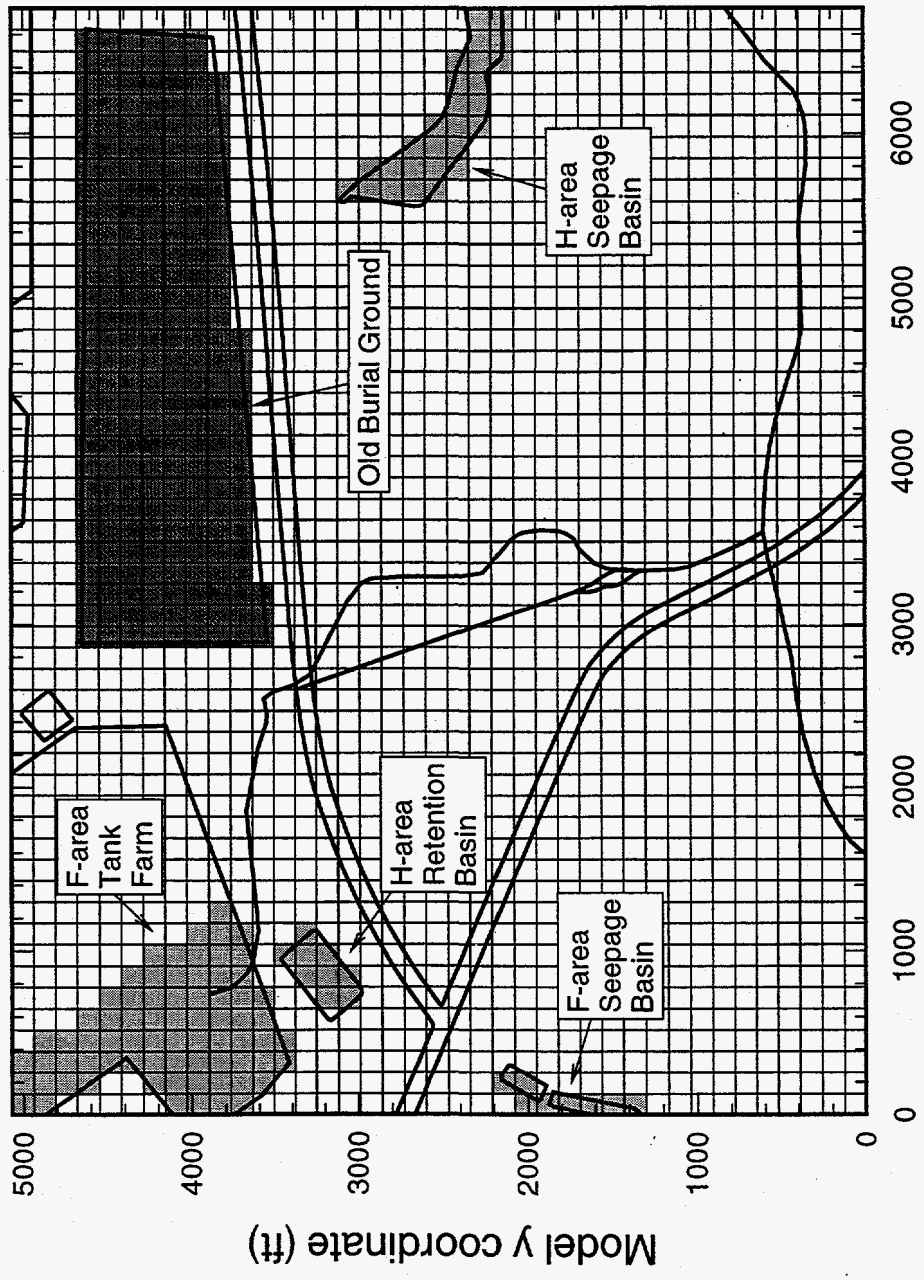

Figure 60 Map of low conductivity surface elements corresponding to engineered surfaces.

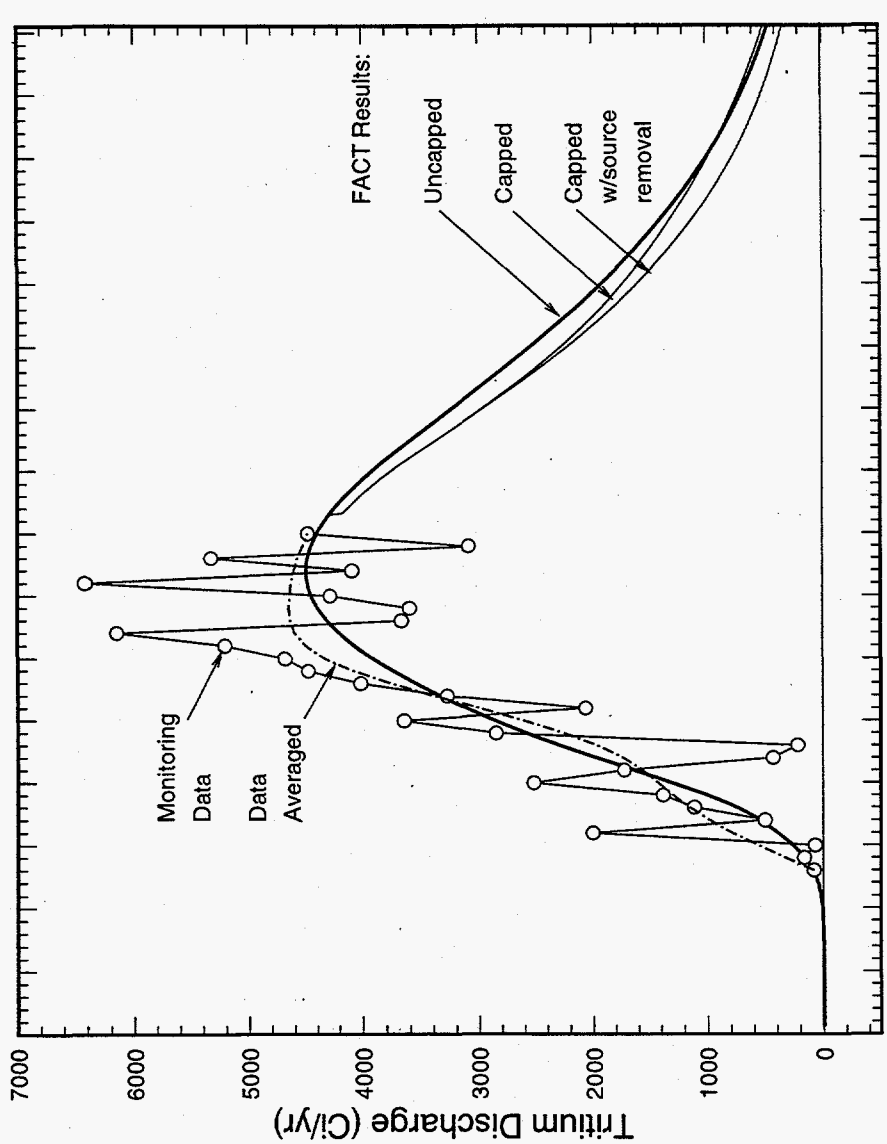

Figure 61. Estimated effect of capping on tritium discharges to Fourmile Branch ($k = 0.029\ yr^{-1}$ for non-spent melts, 23% porosity, 65 ft dispersivity).

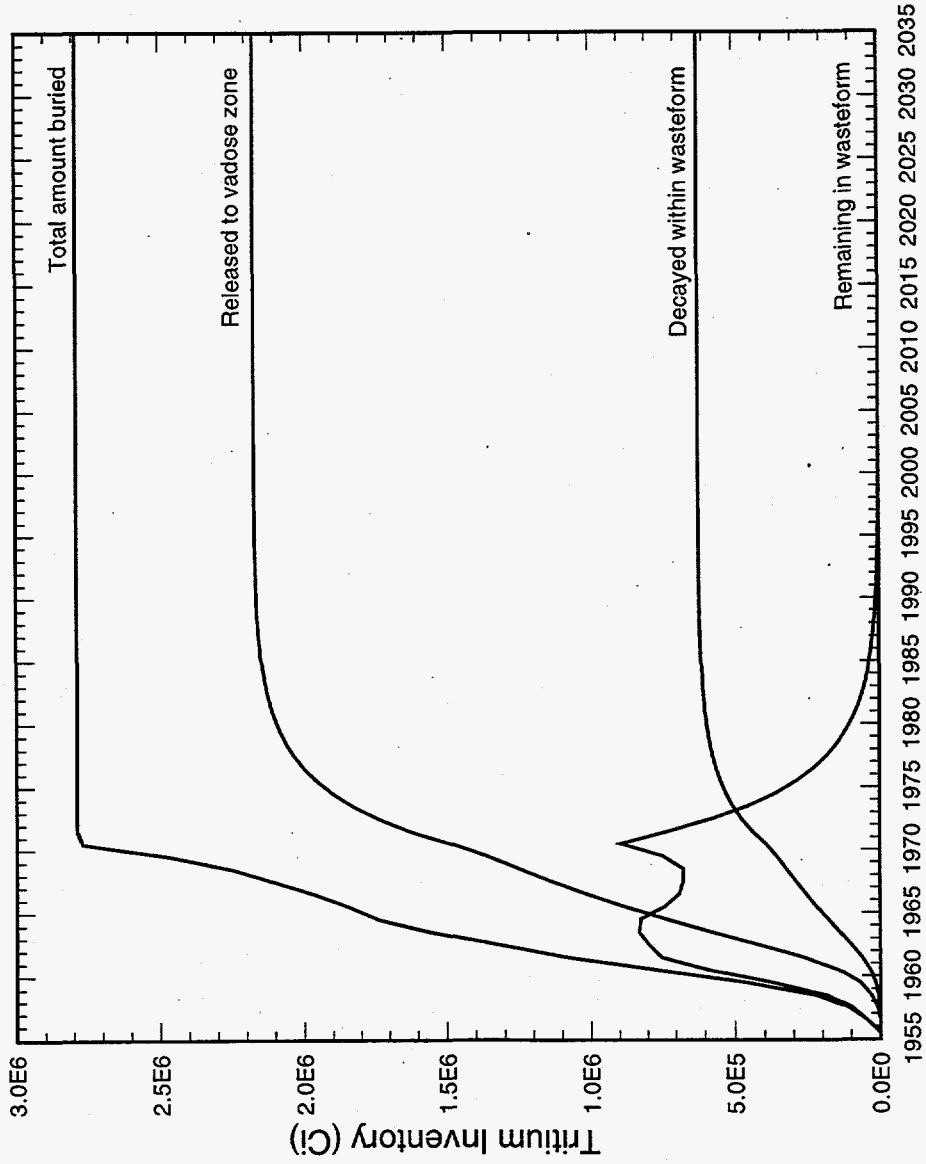

Figure 62. Tritium accounting through time with respect to buried waste form with $k = 0.17\ yr^{-1}$ for non-spent melts.

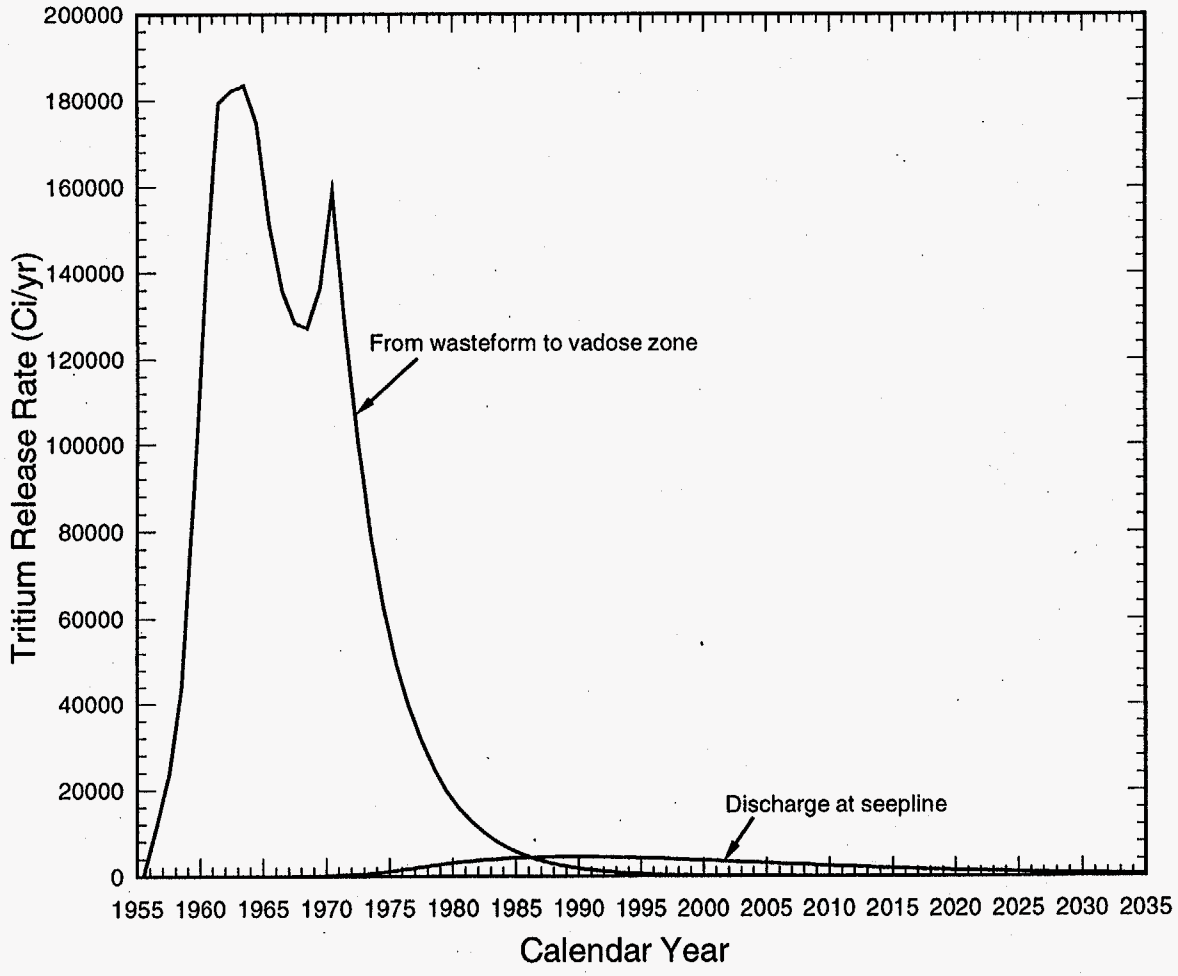

Figure 63. Tritium release rates with k = 0.17 yr^{-1} for non-spent melts.

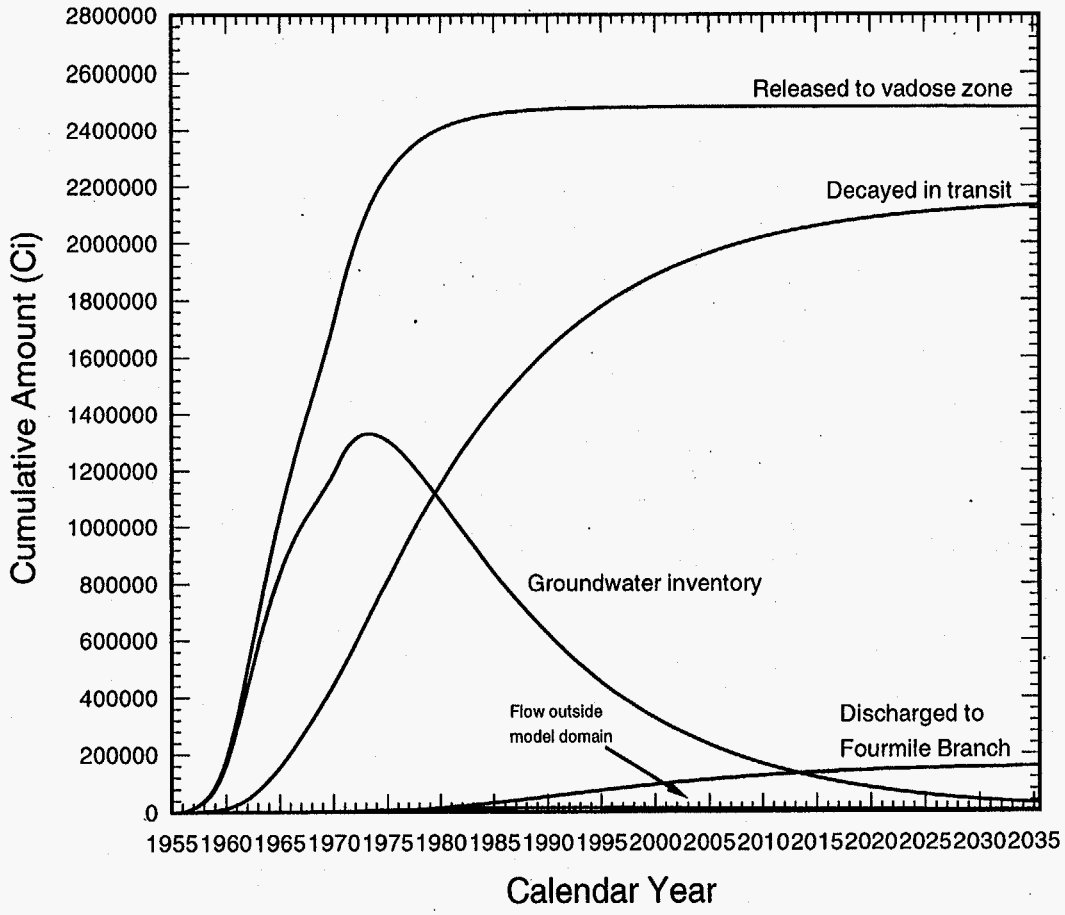

Figure 64. Tritium accounting through time with respect to the amount released to the vadose zone ($k = 0.17\ yr^{-1}$ for non-spent melts, 45% porosity, 300 ft dispersivity).

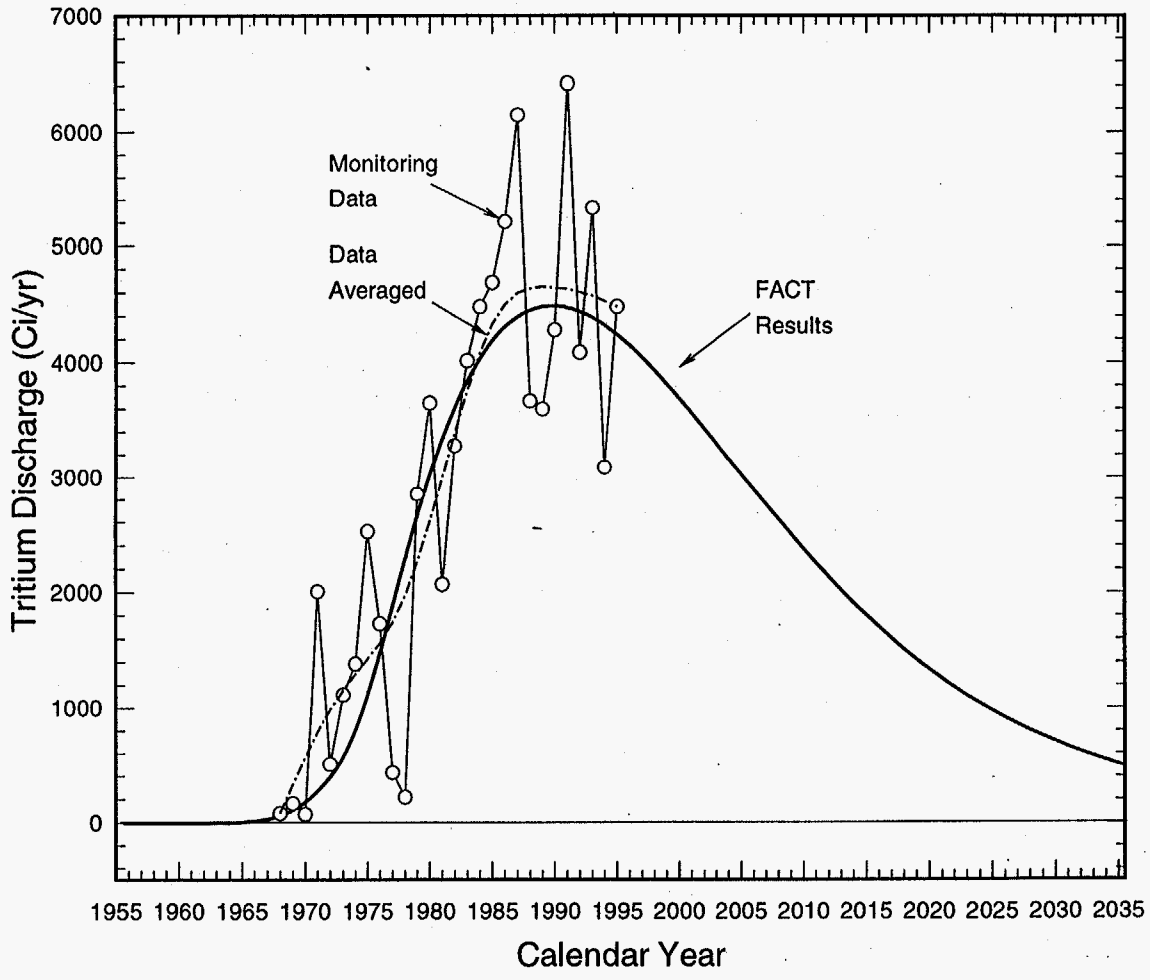

Figure 65. Comparison of predicted and measured tritium discharges to Fourmile Branch for no action and capping remedial alternatives (k = 0.17 yr^{-1} for non-spent melts, 45% porosity, 300 ft dispersivity).

Table 1. Listing of core descriptions considered for the present study.

BGO 3D
BGO 6A
BGO 8A
BGO 9AA
BGO 10AA
BGO 12A
BGO 14A
BGO 16A
BGO 18A
BGO 21D
BGO 25A
BGO 41A
BGO 42C
BGO 43AA
BGO 44AA
BGO 45A
BGO 46B
BGO 47A
BGO 48C
BGO 49A
BGO 50A
BGX 1A
BGX 2B
BGX 4A
BGX 7D
BGX 9D
BGX 11D
FAC 1SB
FCH 1
FCH 2
FCH 3
FCH 4
FCH 5
FCH 6
FSB 93C
FSB 95C
FSB112A *
FSB113A
FSB114A
FSB115C
FSB116C
FSB120A
FSB121C *
FSB122C *
FSB123C
FSB PD* (no E-file available)
FSB TA
HCH 1 *
HCH 2 *
HCH 3
HCH 4
HCH 5
HMD 1D
HMD 2D
HMD 3D
HMD 4D
HPC 1 *
HPT 1A *
HPT 2A *
HSB101C
HSB103C
HSB105C
HSB107C
HSB109C
HSB111C
HSB113C
HSB115C
HSB117A
HSB118A
HSB119A
HSB120A
HSB121A
HSB122A
HSB123A
HSB124A
HSB139A
HSB140A
HSB141A
HSB143C
HSB144A
HSB145C
HSB146AR
HSB148C
HSB151C
HSB152C
HSB PC
P 18TA*
P 27TA*
P 28TA
YSC 1A *
YSC 1C *
YSC 2A *
YSC 3SB*
YSC 4A *
YSC 5A *
BGO003A
BGO051AA
OFS002SB
OFS003SB
OFS004SB
OFS005SB

* == not used in gridding

Table 2. Cores used to define mud fraction probability distribution function.

BGO009AA	BGO010AA	BGO041A	BGO042C	BGO043AA	BGO044AA	BGO045A	BGO046B
BGO047A	BGO048C	BGO049A	BGO050A	BGX001A	BGX002B	BGX004A	BGX007D
BGX009D	BGX011D	FAC001SB	FCH001	FCH002	FCH003	FCH004	FCH005
FCH006	FSBTA	FSB115C	FSB116C	FSB120A	FSB121C	FSB122C	FSB123C
HCH001	HCH002	HCH003	HCH004	HCH005	HMD001D	HMD002D	HMD003D
HMD004D	HSB140A	HSB141A	HSB143C	HSB144A	HSB145C	HSB146A	HSB148C
HSB151C	HSB152C	P027TA	P028TA	BGO003A	BGO051AA	OFS002SB	OFS003SB
OFS004SB	OFS005SB						

Table 3. Average mud fractions for sand, clayey sand, sandy clay, and clay.

Soil Label	id	# Data Points	Average Mud Fraction
SD	1	7284	0.116
CLSD	2	938	0.352
SDCL	3	448	0.632
CL	4	598	0.910

Table 4. Hydrostratigraphic unit boundaries from Thayer et al. (1993).

No	Core ID	SRS Northing (ft)	SRS Easting (ft)	"upper" aquif. (ft)	"tan clay" (ft)	"lower" aquif. (ft)	Gordon c.u. (ft)	Gordon aquif. (ft)	Meyers Branch (ft)
1	BGO 1D	73737.9	58779.3	293	NP	NP	NP	NP	NP
2	BGO 3D	75351.3	58809.2	290.8	NP	NP	NP	NP	NP
3	BGO 5C	76476.9	58794.5	294.2	218.2	201.2	NP	NP	NP
4	BGO 6A	76487.2	58316.8	283.8	209.8	194.8	120.8	119.8	NP
5	BGO 8A	76569	57618.3	281.3	213.3	199.3	130.3	120.3	NP
6	BGO 9AA	76975.69	57371.94	282.8	223.8	210.8	134.8	124.8	NP
7	BGO 10A	76805.18	57050.92	299.1	209.1	207.1	131.1	124.1	NP
8	BGO 10AA	76997.88	56990.54	298.8	218.8	206.8	129.8	125.8	NP
9	BGO 12A	76804.63	56250.68	311.4	199.4	186.4	137.4	132.4	NP
10	BGO 14A	76377.54	55838.32	300.2	220.2	212.2	133.2	127.2	NP
11	BGO 16A	75756.95	56194.15	302.8	195.8	182.8	130.8	125.8	NP
12	BGO 18A	75599.89	56699.67	292.9	204.9	198.9	130.9	125.9	NP
13	BGO 21D	74688.53	57470.66	283	NP	NP	NP	NP	NP
14	BGO 23D	74238.09	58132.96	287	NP	NP	NP	NP	NP
15	BGO 25A	76158.5	55668.08	294.7	211.7	200.7	137.7	127.7	NP
16	BGO 26A	76144.6	55014.2	285.1	219.1	205.1	133.1	129.1	NP
17	BGO 27C	75666.3	54671.4	273.9	198.9	191.9	NP	NP	NP
18	BGO 29A	75560	54103.5	262.1	196.1	185.1	124.1	113.1	NP
19	BGO 31C	74978	54816.2	271.1	198.1	188.1	NP	NP	NP
20	BGO 33C	74479.7	55681.4	277.4	200.4	191.4	NP	NP	NP
21	BGO 35C	73953.9	56545.7	271.4	204.4	197.4	NP	NP	NP
22	BGO 37C	73498.2	57279.2	284.3	199.3	191.3	NP	NP	NP
23	BGO 41A	76469.52	55403.69	298.3	217.3	208.3	138.3	131.3	NP
24	BGO 42C	76404.71	55522.27	295.9	215.9	208.9	NP	NP	NP
25	BGO 43AA	77066.01	56268.64	312.2	195.2	187.2	135.2	127.2	NP
26	BGO 44AA	76757.02	57880.51	283.3	222.3	199.3	131.3	120.3	NP
27	BGO 45A	75830.03	54550.14	276.9	206.9	200.9	133.9	129.9	NP
28	BGO 46B	75012.1	54444.65	263.4	199.4	193.4	128.4	126.4	NP
29	BGO 47A	74728.83	54914.04	264.8	197.8	189.8	130.8	124.8	NP
30	BGO 48C	74599.64	55124.38	274.7	197.7	191.7	NP	NP	NP
31	BGO 49A	73902.78	56205.08	269.1	201.1	192.1	119.1	115.1	NP
32	BGO 50A	75201.16	54179.77	253.5	193.5	183.5	132.5	128.5	NP
33	BGX 1A	76831.89	58590.35	288.9	210.9	197.9	131.9	126.9	NP
34	BGX 2B	77203.4	58256.5	289.2	216.2	198.2	140.2	127.2	NP
35	BGX 4A	77879.2	57215.6	288.8	224.8	212.8	129.8	123.8	NP
36	BGX 7D	78349.3	58312.8	276.9	224.9	219.9	156.9	143.9	NP
37	BGX 9D	76936	59522.1	277.4	207.4	202.4	139.4	131.4	NP
38	BGX 11D	75300.7	59581.4	273.6	192.6	176.6	125.6	116.6	NP
39	FAC 1SB	78138	55243	312.2	224.2	217.2	149.2	NP	NP
40	FCH 1	79488.82	52843.11	317	214	202	142	126	67
41	FCH 2	78500	52599.59	288.6	212.6	196.6	141.6	129.6	57.6
42	FCH 3	78059.22	52087.22	307.4	207.4	196.4	140.4	131.4	59.4
43	FCH 4	77514.56	52021.03	297.6	196.6	186.6	127.6	120.6	41.6
44	FCH 5	76992.12	51667.65	284.2	196.2	191.2	129.2	128.2	36.2
45	FCH 6	76410.33	51245.7	290.8	187.8	180.8	122.8	119.8	23.8
46	FSB 76A	76131.9	51391.6	291.5	ND	ND	120.5	116.5	NP
47	FSB 78A	74757.7	50172.8	270.5	162.5	146.5	104.5	99.5	NP
48	FSB 79A	73664.5	50149.6	216.1	173.1	164.1	103.1	100.1	18.1
49	FSB 87A	75601.7	50115.8	285.6	175.6	172.6	114.6	108.6	NP
50	FSB 89C	75553.2	51345.2	279.1	186.1	180.1	NP	NP	NP

Table 4. (cont'd)

No	Core ID	SRS Northing (ft)	SRS Easting (ft)	"upper" aquif. (ft)	"tan clay" (ft)	"lower" aquif. (ft)	Gordon c.u. (ft)	Gordon aquif. (ft)	Meyers Branch (ft)
51	FSB 91C	75213.3	50953.5	277	168	161	NP	NP	NP
52	FSB 93C	74897.3	50458.3	274	166	151	NP	NP	NP
53	FSB 95C	74971.7	50016.7	281.8	173.8	157.8	NP	NP	NP
54	FSB 96A	74882.2	49778.7	277.7	166.7	153.7	108.7	100.7	NP
55	FSB 97A	75171.2	49965.7	283.8	162.8	151.8	110.8	106.8	NP
56	FSB 98A	75389.8	50121.6	280.7	171.7	159.7	108.7	106.7	NP
57	FSB 99A	75675.6	50314.8	285.3	178.3	173.3	115.3	112.3	NP
58	FSB100A	75534.4	50958.4	283.8	184.8	182.8	117.8	113.8	NP
59	FSB101A	75719	51191.3	282.9	190.9	182.9	118.9	115.9	NP
60	FSB112A	74231.4	48809.1	227	164	144	103	98	NP
61	FSB113A	74167.5	51068.1	221.3	178.3	171.3	109.3	104.3	22.3
62	FSB114A	75297.4	52046.6	250	178	173	114	110	NP
63	FSB115C	72515.5	49736	205.8	180.8	164.8	100.8	85.8	5.8
64	FSB116C	72725.5	50645.9	200.5	175.5	170.5	NP	NP	NP
65	FSB120A	75538.9	49175.7	278	181	165	112	110	NP
66	FSB121C	75155.7	48413.1	254.4	173.4	162.4	NP	NP	NP
67	FSB122C	73881.8	48195	216	164	148	104	NP	NP
68	FSB123C	74566.7	51750.5	236.3	183.3	172.3	NP	NP	NP
69	FSB PD	74549.2	49849.81	252.6	ND	ND	NP	NP	NP
70	FSB TA	75649.1	51658.3	275.4	191.4	187.4	117.4	115.4	24.4
71	HC 12	73187	59504	287.3	195.3	190.3	NP	NP	NP
72	HCH 1	72796.39	60923.42	284.2	202.2	187.2	135.2	126.2	18.2
73	HCH 2	72519.61	60091.79	270.9	195.9	179.9	130.9	122.9	-0.1
74	HCH 3	71998.82	59917.33	263.8	196.8	178.8	129.8	122.8	NP
75	HCH 4	72449.59	59139.93	269.9	192.9	182.9	122.9	113.9	NP
76	HCH 5	71810.36	59331.53	255	192	180	123	119	-10
77	HMD 1D	78731.7	56973.9	262.7	228.7	225.7	138.7	126.7	NP
78	HMD 2D	79665.8	57269.7	259.3	222.3	216.3	143.3	138.3	NP
79	HMD 3D	79578.7	57745.2	257.5	223.5	218.5	154.5	149.5	NP
80	HMD 4D	79160.4	58188.5	248.5	223.5	219.5	152.5	140.5	NP
81	HPC 1	70395.4	62493.6	293.5	194.5	187.5	115.5	109.5	27.5
82	HPT 1A	74847.1	60587	232.9	ND	ND	118.9	114.9	52.9
83	HPT 2A	75061.8	60200.5	257.7	ND	ND	120.7	117.7	56.7
84	HSB 65A	72436.2	58436	270.7	203.7	198.7	118.7	112.7	NP
85	HSB 68A	71526.9	56892.1	247.4	198.4	193.4	116.4	110.4	NP
86	HSB 69A	71549.4	56465.1	234.1	187.1	181.1	115.1	112.1	NP
87	HSB 83A	71648.6	58606.1	234.9	194.9	187.9	113.9	103.9	11.9
88	HSB 84A	71586.2	56359.1	226.4	204.4	180.4	118.4	110.4	NP
89	HSB 85A	73791.9	58943.4	292.1	204.1	200.1	126.1	119.1	NP
90	HSB 86A	72520.2	55985.9	260	185	178	112	109	NP
91	HSB101C	72001.9	58604.4	256.3	195.3	189.3	NP	NP	NP
92	HSB103C	71593.9	58323.6	245.2	195.2	181.2	NP	NP	NP
93	HSB105C	71447.3	57883.8	247.2	190.2	183.2	NP	NP	NP
94	HSB107C	71698.5	57432	258.3	198.3	190.3	NP	NP	NP
95	HSB109C	71684.8	56895.6	259.4	203.4	189.4	NP	NP	NP
96	HSB111C	71919.4	56501.9	253.7	187.7	170.7	NP	NP	NP
97	HSB113C	72312.3	56160.4	258.7	187.7	173.7	NP	NP	NP
98	HSB115C	72653.2	56043.2	266.8	208.8	196.8	NP	NP	NP
99	HSB117A	72733.6	55170.1	234.1	215.1	191.1	122.1	116.1	NP
100	HSB118A	72696.4	55775.6	245	183	173	119	114	NP

Table 4. (cont'd)

No	Core ID	SRS Northing (ft)	SRS Easting (ft)	"upper" aquif. (ft)	"tan clay" (ft)	"lower" aquif. (ft)	Gordon c.u. (ft)	Gordon aquif. (ft)	Meyers Branch (ft)
101	HSB119A	73082.5	56100.2	254.8	212.8	194.8	114.8	110.8	NP
102	HSB120A	73395.1	56431.9	266	203	196	112	110	NP
103	HSB121A	72024.8	57389.6	272.3	197.3	184.3	113.3	109.3	NP
104	HSB122A	72195.9	57747.4	269.4	188.4	177.4	110.4	108.4	NP
105	HSB123A	72189.8	58124.8	262.3	194.3	184.3	112.3	106.3	NP
106	HSB124A	72199.6	58514.6	263.9	ND	ND	121.9	115.9	NP
107	HSB139A	71127.4	57365.4	231.5	189.5	178.5	118.5	114.5	NP
108	HSB140A	70050.3	56535.4	234	194	181	111	105	NP
109	HSB141A	71213.6	59168.7	252.6	180.6	166.6	118.6	112.6	NP
110	HSB143C	73738.2	52773.2	220.1	198.1	179.1	NP	NP	NP
111	HSB144A	71892.1	56200.5	233.6	185.6	178.6	108.6	103.6	NP
112	HSB145C	71098.9	57769	233.7	183.7	174.7	NP	NP	NP
113	HSB146AR	70478.9	58454	249.6	185.6	162.6	121.6	111.6	NP
114	HSB148C	70151.5	55344.2	248.9	186.9	174.9	NP	NP	NP
115	HSB151C	72997.9	54014.9	211.6	192.6	182.6	NP	NP	NP
116	HSB152C	72012	54346.7	212.1	198.1	186.1	NP	NP	NP
117	HSB TB	72394	58696.1	267.1	207.1	199.1	110.1	106.1	9.1
118	HSB PC	72119.31	55650.03	227.8	187.8	177.8	NP	NP	NP
119	P 18TA	67576.5	47652.8	296.7	174.7	166.7	90.7	85.7	-17.3
120	P 27TA	70382	64022.9	274.1	180.1	169.1	129.1	127.1	49.1
121	P 28TA	79284.3	55441.1	285.2	214.2	210.2	140.2	132.2	63.2
122	YSC 1A	78039.9	65438.93	268.9	209.9	198.9	158.9	153.9	68.9
123	YSC 1C	78186.24	65855.46	272.5	214.5	212.5	163.5	156.5	NP
124	YSC 2A	78311.53	66100.08	281.7	219.7	214.7	161.7	150.7	NP
125	YSC 3SB	77680	65920	277	211	205	149	140	NP
126	YSC 4A	77050.08	65883.5	287.5	222.5	213.5	159.5	144.5	86.5
127	YSC 5A	74295.93	67134.86	273	221	209	136	128	NP

Table 5. Fourmile Branch flow rates for date of minimum station 3 flow rate by water year.

Water Year (Oct.-Sep.)	Date	Station 3 Flowrate (cfs)	Station 4 Flowrate (cfs)	Station 5B Flowrate (cfs)	Station 6 minus Station 4 Flowrate (cfs)	Station 6 Flowrate (cfs)	Station 7 Flowrate (cfs)
93	9/16	1.0	–	–	–	–	–
92	7/15	2.6	2.1	1.7	1.1	3.2	6.1
91	10/5	1.5	2.4	2.4	2.4	4.8	7.8
90	8/11	1.2	4.7	4.7	2.9	7.6	20.
89	9/19	1.4	3.4	3.4	2.3	5.7	6.1
88	8/10	1.6	3.2	3.2	4.4	7.6	8.8
87	8/23	2.2	3.5	3.5	2.2	5.7	5.8
86	10/20	1.6	2.7	2.7	5.2	7.9	8.8
85	5/20	1.5	2.1	2.1	3.6	5.7	6.3
84							
83							
82							
81							
80	7/14	1.4	1.9	–		5.0	6.9
averages		**1.67**	**2.89**	**2.93**	**3.01**	**5.91**	

cfs - cubic feet per second

Table 6. Hydrologic parameters used in Old Burial Ground groundwater flow model.

Property	**0 ≤ mf ≤ 0.1**	**0.1 ≤ mf ≤ 0.25**	**0.25 ≤ mf ≤ 0.5**	**0.5 ≤ mf ≤ 1**	**Gordon confining unit**	**Gordon aquifer**
Horizontal conductivity, K_h	40 ft/d	5 ft/d	$K_v \times R$ (0.15)	$K_v \times R$ (0.0003)	3×10^{-5} ft/d	40 ft/d
Vertical conductivity, K_v	K_h/R (13.3 ft/d)	K_h/R (1.7 ft/d)	0.05 ft/d	0.0001 ft/d	K_h/R (1×10^{-5} ft/d)	K_h/R (13.3 ft/d)
Conductivity ratio, R	3	3	3	3	3	3
Effective porosity, η	0.23	0.23	0.23	0.23	0.23	0.23
Specific storage, S_s	3×10^{-5}	1×10^{-4}	2×10^{-4}	3×10^{-4}	assigned by mud fraction	assigned by mud fraction

mf ≡ mud fraction

Table 7. Summary of hydraulic head residuals between model and data (ft).

Overall rms head (or conc) difference:	3.38
Upper Three Runs aquifer, "upper" zone	
rms of (FACT-data) differences:	3.426
avg of (FACT-data) differences:	-1.389
avg of |FACT-data| differences:	2.534
max of {FACT-data} differences:	-11.632
Upper Three Runs aquifer, "lower" zone	
rms of (FACT-data) differences:	3.865
avg of (FACT-data) differences:	-1.561
avg of |FACT-data| differences:	3.095
max of {FACT-data} differences:	-9.083
Gordon aquifer	
rms of (FACT-data) differences:	0.659
avg of (FACT-data) differences:	-0.081
avg of |FACT-data| differences:	0.539
max of {FACT-data} differences:	-1.375

Table 8. Documents relevant to tritium transport from the Old Burial Ground to Fourmile Branch.

Doc No.	Author(s)	Title	Comments
GENERAL:			
Health Physics, v10, 229-236, 1964	J. W. Fenimore	Land burial of solid radioactive waste during a 10-year period	Good information about first 10 years of operation. Scrap metals have radionuclides dispersed throughout the metal leaving little for leaching. Process equipment decontaminated before burial. Results of a tracer study.
DPST-70-460	J. C. Corey and J. H. Horton	Savannah River Plant burial ground practices	Good general discussion of operations.
DP-1366	J. H. Horton and J. C. Corey	Storing solid radioactive wastes at the Savannah River Plant	1975 grid well tritium concentration data.
DPST-77-300	J. W. Fenimore and R. L. Hooker	The assessment of solid low-level waste management at the Savannah River Plant	Average and maximum tritium concentration data for BG well series, 1956 to 1974, which indicate more or less background? Source of tritium is said to be the spent melts.
DPST-82-725	J. W. Fenimore	The burial ground as a containment system: 25 years of subsurface monitoring at the Savannah River Plant facility	Results of 1957-1970 tracer study in southwest corner (p. 20, Figure 10). Between burial ground and F-effluent highest concentration is 64000 pCi/ml and is 6000 pCi/ml at outcrop (THESE ARE PROBABLY ~1980 MEASUREMENTS!) (p. 49). 850 Ci/yr. discharge to F-effluent.

Table 8. (cont'd)

DPST-83-829	J. A. Stone and E. J. Christensen eds.	Technical summary of groundwater quality protection program at the Savannah River Plant, vol. II - radioactive waste	200? 850? Ci/yr. discharge to F-effluent. Results of soil coring done between burial ground and F-effluent. Tritium concentration in BG wells for 1980 and 1981. BGC wells for 1980-1982.
DPST-85-694	W. J. Jaegge, N. L. Kolb, B. B. Looney, I. W. Marine, O. A. Towler and J. R. Cook	Radiactive waste burial grounds	2m/yr flow rate in unsaturated zone (p. 27). Results of 57-70 tracer study in southwest corner (p. 35).
WSRC-RP-90-1140	WSRC	RFI/RI workplan for the old radioactive burial ground, bldg. number 643-G (U)	Tritium plume shown in Figure 2-21.
duPont, 1990	W. P. Bebbington	History of duPont at the Savannah River Site	Early operations described.
BURIAL GROUND INVENTORY:			
WSRC-TR-93-316	M. L. Hyder	Tritium in the burial ground of the Savannah River Site (U)	Summary including hypotheses for spent melt release mechanism.
WSRC-RP-91-709	J. R. Cook	Radionuclide inventory of E area (U)	Total tritium estimated at 172g. This estimate does not include burials past 1970; including these gives 205g.
DISCHARGE TO FOUR MILE BRANCH:			
WSRC-RP-93-459	B. B. Looney, J. S. Haselow, C. M. Lewis, M. K. Harris, D. E. Wyatt and C. S. Hetrick	Projected tritium releases from F & H area seepage basins and the Solid Waste Disposal Facilities to Fourmile Branch (U)	Discharge to FMB data (Table 2). Projected discharge.
see below		Annual monitoring reports, 1968 to present	

Table 8. (cont'd)

CONCENTRATION AT OUTCROP:			
WSRC-TR-93-526, Rev. 0	K. L. Dixon and V. A. Rogers	Results of the fourth quarter tritium survey of the F- and H-area seeplines: March 1993 (U)	Dec. 92 and Mar. 93
WSRC-TR-94-286, Rev. 1	K. L. Dixon, V. A. Rogers and B. B. Looney	Results of the quarterly tritium survey of Fourmile Branch and its seeplines in the F- and H-areas of SRS: September 1993 (U)	March, June, Sept. 93
WSRC-TR-94-365, Rev. 1	K. L. Dixon and C. L. Cummins	Quarterly sampling of the wetlands along the old F-area effluent ditch: May 1994 (U)	May 94
OBG GRID WELLS:			
none	J. W. Fenimore	Radionuclides in 643G ground water - 1973-76	OBG grid well data and interpretation; 452000gal pumped from G21. 300pCi/ml peak background. 60/40 split between west and east. Hypothesis that waste forms in west end leach tritium
DPST-77-495	J. W. Fenimore	Radioactivity trends in Burial Grounds wells - 1975-1976	OBG grid well data and interpretation. >3 year percolation time?
DPST-78-426	J. W. Fenimore	Annual summary of burial ground grid well assays - 1977	OBG grid well data and interpretation.
DPST-79-452	J. W. Fenimore	Annual summary of burial ground grid well assays - 1978	OBG grid well data and interpretation. "considerable stratification" of tritium. Tritium was discovered to be outcropping in eroded F-effluent in fall 1978.
DPST-80-266	J. W. Fenimore	Annual summary of burial ground grid well assays - 1979	OBG grid well data and interpretation. F-effluent under repair.

Table 8. (cont'd)

DPST-81-643	J. W. Fenimore	Annual summary of burial ground grid well assays - 1980	OBG grid well data and interpretation. F-effluent repair completed Nov. 1980. Detailed description of repair.
DPST-83-1033	R. H. Emslie, P. M. Weimorts and J. A. Stone	Subsurface monitoring of groundwater at the SRP burial grounds: 1981-1982 summary of grid well assays	OBG grid well data and interpretation. Second coring of tritium plume at repair site.
DPST-84-605	R. H. Emslie and P. M. Weimorts	Subsurface monitoring of groundwater at the SRP burial grounds: 1983 summary of grid well assays	OBG grid well data and interpretation. G-34 now dominant.
DPST-85-353	J. A. Stone and P. M. Weimorts	Subsurface monitoring of groundwater at the SRP burial ground: 1984 summary of grid well assays	OBG grid well data and interpretation. References soil coring done by G21 (G21A,B,P?).
OBG GROUNDWATER FLOW:			
DPST-76-265	J. W. Fenimore	643-G ground water flow path	Grid wells southwest of OBG indicate discharge to eroded F-effluent drainage instead of Fourmile Branch. Repairs recommended.
DPST-79-265	E. L. Albenesius and J. W. Fenimore	Tritium migration from the burial ground to Four Mile Creek - Reappraisal of flow paths and travel times	Summary of logic leading to stream repair. ~1000 Ci/yr discharge around 1979. Repair predicted to practically eliminate discharges. Without repair maximum discharge predicted to be 4000 Ci/yr. Tracer tests are described.
OFFSITE PAPERS:			
DP-MS-68-23	J. W. Fenimore	Tracing soil moisture and groundwater flow at the Savannah River Plant	Tracer tests at OBG and other locations are described.

Table 8. (cont'd)

DP-MS-75-25	R. H. Hawkins	Migration of tritum from a nuclear waste burial site	Early discussion of spent melt immersion and lysimeter experiments.
DP-MS-82-61	J. A. Stone, J. W. Fenimore, R. H. Hawkins, S. B. Oblath and J. P. Ryan Jr.	Shallow land burial of solid low-level radioactive wastes -- 30 years of experience at the Savannah River Plant	Summary document. Kd's.
DP-MS-83-89	J. A. Stone, S. B. Oblath, R. H. Hawkins, R. H. Emslie, J. P. Ryan Jr. and C. M. King	Migration studies at the Savannah River Plant shallow land burial site	Overview of subsurface monitoring, lysimeters, soil-water chemistry.
DP-MS-84-82	J. A. Stone, S. B. Oblath, R. H. Hawkins, R. H. Emslie, S. L. Hoeffner and C. M. King	Radionuclide migration studies at the Savannah River Plant humid shallow land burial site for low-level waste	Soil cores around G-21 indicate that most tritium does NOT arise near G-21 but from more distant and easterly sources (G-34 area?). Spent melts have released most of tritium and plume has moved far from source. Kd's.
DP-MS-85-86	J. A. Stone, S. B. Oblath, R. H. Hawkins, M. W. Grant, S. L. Hoeffner and C. M. King	Waste migration studies at the Savannah River Plant burial ground	Mainly discusses the various lysimeter studies.
TRITIUM LYSIMETERS:			
DPST-81-548	R. H. Hawkins	Tritium released from spent melts by water immersion	Immersion test results. References basis for Ci content of spent melts.
DPST-85-384	M. W. Grant and R. H. Hawkins	Results of the spent melt lysimeter experiment	Results, hypotheses and conclusions at experiment completion.
DPSTN-4363	M. W. Grant	duPont Lab Notebook issued 19Apr85	Contains raw data from spent melt lysimeter experiment.

Table 8. (cont'd)

WSRC-TR-91-597	A. D. Yu and J. R. Cook	An estimation of tritium inventory limits for the E-area vaults (U)	Contains a fit to the tritium lysimeter data using a leaching model. See Figure 4 and Appendix B.
SS DIFFUSIVITY:			
J. Nucl. Mat., v43, 119-125, 1972	J. H. Austin and T. S. Elleman	Tritium diffusion in 304- and 316-stainless steels in the temperature range 25 to 222C	See Figure 4.
J. Nucl. Mat., v211, 156-167, 1994	A. Roustila, N. Kuromoto, A. M. Brass and J. Chene	Quantitative analysis of tritium distribution in austenitic stainless steels welds	See page 160.
Nucl. Tech., v26, 192-200, 1975	M. R. Louthan Jr., J. A. Donovan and G. R. Caskey Jr.	Tritium absorption in Type 304L stainless steel	SRL data and correlation for SS.
J. Nucl. Mat., v73, 77-88, 1978	P. M. Abraham, T. S. Elleman and K. Verghese	Diffusion and trapping of tritium in grainboundaries of 304L stainless steel	Not useful.
J. Nucl. Mat., v85&86, 335-339, 1979	J. A. Swansiger and R. Bastasz	Tritium and deuterium permeation in stainless steels: influence of thin oxide films	Not useful.
J. Nucl. Mat., v85&86, 257-269, 1979	V. A. Maroni and E. H. Van Deventer	Materials considerations in tritium handling systems	Not useful.
AL/LI DIFFUSIVITY:			
J. Nucl. Mat., v116, 141-146, 1983	M. Nakashima, M. Saeki, Y. Aratono and E. Tachikawa	Diffusivity of tritium in Li-Al alloys	See Figure 4.
J. Nucl. Mat., v120, 267-271, 1984	M. Saeki, M. Nakashima, Y. Aratono and E. Tachikawa	Effects of lithium concentration on chemical behavior of tritium in Li-Al alloys	

Table 8. (cont'd)

UNSATURATED ZONE:			
Soil Sci., v100, n6, 377-383, 1965	J. H. Horton and R. H. Hawkins	Flow path of rain from the soil surface to the water table	Referenced in DPST-75-218.
Soil Sci. Soc. Proc., v28, 725-728, 1964	C. C. Haskell and R. H. Hawkins	D2O-Na24 method for tracing soil moisture movement in the field	Referenced in DPST-75-218.
DPST-75-218	J. H. Horton	Soil moisture flow as related to the burial of solid radioactive waste	"water flows in the unsaturated soil column at a rate of about 7 feet per year (3,4)".
ANNOTATED BIBLIOGRAPHY:			
Q-ESR-E-00001	J. P. Kanzleiter and T. E. Rehder	Mixed Waste Management Facility (MWMF) Old Burial Ground (OBG) source control technology & inventory study (U)	
HISTORICAL INFORMATION:			
14Oct80 memo	anonymous	"a condensed history of SRP from 1950 to 1975"	1954: 76 acres designated as a solid waste burial ground. Bldg. 232-H (tritium) started in July 1957
duPont, 1990	W. P. Bebbington	History of duPont at the Savannah River Plant	First tritium facility, 232-F, opened Oct. 1955. 232-H online July 1957. 232-H capacity doubled in 1958.
WSRC-RP-92-349	H. P. Holcomb	Transcription of a presentation by Dr. E. L. Albenesius, "SRS burial ground operation from a historical perspective" (U)	Implies spent melt crucibles in east end are THE tritium source. Unsaturated conditions are just as effective for getting activity moving as saturated. Equipment was decontaminated prior to burial. An extensive bibliography by J. A. Stone for work through about 1984.

Table 8. (cont'd)

WSRC-RP-89-1229	E. G. Orebaugh and R. M. Wallace	Quantification of hazards associated with the decay storage/disposal of tritium crucibles	Talks about the decision to plug crucibles with epoxy.
ANNUAL MONITORING REPORTS:			
DPSP-61-25-4 (deleted version)	Works Technical Department	Health physics regional monitoring semiannual report, July through December 1960	
DPSP-62-25-2 (deleted version)	Works Technical Department	Health physics regional monitoring semiannual report, January through June 1961	
DPSP-62-25-9 (deleted version)	Works Technical Department	Health physics regional monitoring semiannual report, July through December 1961	
DPSP-63-25-3 (deleted version)	Works Technical Department	Health physics environmental monitoring semiannual report, January through June 1962	
DPSP-63-25-10 (deleted version)	Works Technical Department	Health physics environmental monitoring semiannual report, July through December 1962	
DPSPU-64-11-12	Works Technical Department	Health physics regional monitoring annual report, 1963	
DPST-66-302	C. Ashley	Environmental monitoring at the Savannah River Plant annual report - 1965	
DPST-67-302	C. Ashley	Environmental monitoring at the Savannah River Plant annual report - 1966	
DPST-69-302	C. Ashley	Environmental monitoring at the Savannah River Plant annual report - 1968	

Table 8. (cont'd)

DPST-70-302	C. Ashley	Environmental monitoring at the Savannah River Plant annual report - 1969
DPST-71-302	C. Ashley	Environmental monitoring at the Savannah River Plant annual report - 1970
DPSPU-72-302	C. Ashley	Environmental monitoring at the Savannah River Plant annual report - 1971
DPSPU-73-302	C. Ashley and C. C. Zeigler	Environmental monitoring at the Savannah River Plant annual report - 1972
DPSPU-74-302	C. Ashley and C. C. Zeigler	Environmental monitoring at the Savannah River Plant annual report - 1973
DPSPU-75-302	C. Ashley and C. C. Zeigler	Environmental monitoring at the Savannah River Plant annual report - 1974
DPSPU-76-302	C. Ashley and C. C. Zeigler	Environmental monitoring at the Savannah River Plant annual report - 1975
DPSPU-77-302	C. Ashley and C. C. Zeigler	Environmental monitoring at the Savannah River Plant annual report - 1976
DPSPU-78-302	C. Ashley and C. C. Zeigler	Environmental monitoring at the Savannah River Plant annual report - 1977
DPSPU-79-302	C. Ashley and C. C. Zeigler	Environmental monitoring at the Savannah River Plant annual report - 1978
DPSPU-80-302	C. Ashley, C. C. Zeigler, P. A. Culp and D. L. Smith	Environmental monitoring at the Savannah River Plant annual report - 1979
DPSPU-81-302	C. C. Zeigler, P. A. Culp and D. L. Smith	Environmental monitoring at the Savannah River Plant annual report - 1980

Table 8. (cont'd)

DPSPU-82-302	C. Ashley and C. C. Zeigler	Environmental monitoring at the Savannah River Plant annual report - 1981
DPSPU-83-302	C. Ashley, P. C. Padezanin and C. C. Zeigler	Environmental monitoring at the Savannah River Plant annual report - 1982
DPSPU-84-302	C. Ashley, P. C. Padezanin and C. C. Zeigler	Environmental monitoring at the Savannah River Plant annual report - 1983
DPSPU-85-302	C. C. Zeigler, I. B. Lawrimore and W. E. O'Rear	Environmental monitoring at the Savannah River Plant annual report - 1984
DPSPU-86-30-1	C. C. Zeigler, I. B. Lawrimore, E. M. Heath and J. E. Till	U.S. Department of Energy Savannah River Plant environmental report, annual report for 1985
DPSPU-87-30-1	C. C. Zeigler, E. M. Heath, L. B. Taus and J. L. Todd	U.S. Department of Energy Savannah River Plant environmental repor, annual report for 1986
DPSPU-88-30-1	S. C. Mikol, L. T. Burckhalter, J. L. Todd and D. K. Martin	U.S. Department of Energy Savannah River Plant environmental report, annual report for 1987
WSRC-RP-89-59-1	H. A. Davis, D. K. Martin and J. L. Todd	Savannah River Site environmental report for 1988 (U)
WSRC-IM-90-60	C. L. Cummins, D. K. Martin and J. L. Todd	Savannah River Site environmental report for 1989 (U)
WSRC-IM-91-28	C. L. Cummins, D. K. Martin and J. L. Todd	1990 Savannah River Site environmental report (U)

Table 8. (cont'd)

WSRC-TR-92-186	M. W. Arnett, L. K. Karapatakis, A. R. Mamatey and J. L. Todd	Savannah River Site environmental report for 1991 (U)	
WSRC-TR-93-75	M. W. Arnett, L. K. Karapatakis and A. R. Mamatey	Savannah River Site environmental report for 1992	
WSRC-TR-94-77	M. W. Arnett	Savannah River Site environmental data for 1993	
ESH-EMS-95-251, Rev. 1	C. W. Worley	Fourth quarter 1994 tritium inventory in Savannah River Site streams and the Savannah River (U)	
DRAWINGS:			
S5-6-308		Burial ground trench layout, sheet no. 1	Western portion.
S5-6-309		Burial ground trench layout, sheet no. 2	Central portion.
S5-6-310		Burial ground trench layout	Eastern portion.

Table 9. Outline of literature information relevant to tritium transport from the Old Burial Ground to Fourmile Branch.

-Operations
  -"burial ground used continuously since 1953" (DPST-70-460)
  -Designated 1954 (14Oct08 memo)
  -Pre-COBRA operation (Fenimore Health Physics paper)
  -Trenches are 20 feet deep with minimum of 4 feet of soil cover (DPST-70-460)
  -F-effluent repair (DPST-81-643)
  -452k gallons pumped from G21 (Fenimore report)
-Inventory
  -Total amounts
  -Spatial and temporal distribution
  -SWC tracer study implications (DPST-82-725)
  BEBBINGTON CHRONOLOGY:
  -"Initial construction included a small facility (232-F) in F Area and a larger facility (232-H) in H Area..." (p. 38)
  -"In October of 1955, the facility for extracting tritium from irradiated targets started up." (p. 53)
  -"By 1955, however, defense needs required greater production of tritium..." (p. 66)
  -see reactor power figures, pp. 69-70. Roughly linear increase between 1954 and 1958.
  -"The first small facility for the recovery of tritium from irradiated lithium-aluminum control-rod slugs started up in 232-F building in October 1955. In July 1957 a larger tritium facility began operation in 232-H. In 1958 the capacity of 232-H was doubled." (p. 72)
  -"In 1956, construction resumed in H Area of a tritium separations facility (232-H)... By the end of the year the second tritium production line in 232-H was operating." (p. 112) CONFLICT!
  -"Tritium continued to be separated and purified in both 232-F and 232-H until August of 1958 when a new, higher-capacity separations line, 232-H-2, went into service. In October the F-Area tritium facility was shut down permanently. Later it was found possible to operate with 232-H-2 alone." (p. 113)
  -Drawings
-Release mechanism(s)
  -Tritium lysimeter data
  -Diffusion models and parameters
  -Hyder's hypothesis - sources in west and east (WSRC-TR-93-316)
  -Fenimore's hypothesis - sources in west and east (Fenimore doc.)
  -Albenesius' hypothesis - spent melts are source (WSRC-RP-92-349)
-Groundwater concentrations
  -Grid wells
  -BG, BGO, etc. (EMS database)
  -Cone penetrometer and HydroPunch
  -Seepline
  -Max 64000 pCi/ml, 6000 at seepline in ~1980 (DPST-82-725)
  -Estimated 1980 and 1981 plume boundaries (DPST-83-829 & WSRC-RP-90-1140)
  -Considerable stratification, higher concentrations deeper, 90% below well screen (DPST-79-452, DPST-85-353, DP-MS-84-82)
-Discharge to F-effluent ditch
  -Stream monitoring data (Annual monitoring reports,1968-93)
  -850 Ci/yr. estimate around 1980? (DPST-82-725)
  -Projected discharges (WSRC-RP-93-459)

Table 10 Comparison of groundwater tritium inventories estimated from monitoring data and predicted from transport modeling (base and sensitivity cases).

Calendar year	Monitoring data (10^3 Ci)	Transport model base case (10^3 Ci)	Transport model sensitivity case (10^3 Ci)
1973	4	608	1329
1974	21	602	1317
1975	25	592	1291
1976	82	580	1255
1977	77	566	1213
1978	256	551	1166
1979	73	535	1117
1980	111	517	1066
1981	92	500	1014
1982	50	481	963
1983	42	463	912
1984	95	444	863
1985	149	426	815
1986	204	408	769
1987	424	389	725
1988	233	371	682
1989	99	354	642
1990	187	336	604
1991	177	320	567
1992	35	303	533
1993	39	287	500
1994	52	272	469

Appendix

List of Tables

Table A1. Lithologic description of OFS-3SB core.

Column headings are defined as follows:

Heading	Top elevation	
UAT	"upper" aquifer zone	("upper" aquifer top)
UAB	"tan clay" confining zone	("upper" aquifer bottom)
LAT	"lower" aquifer zone	("lower" aquifer top)
LAB	Gordon confining unit	("lower" aquifer bottom)
GAT	Gordon aquifer	(Gordon aquifer top)
GAB	Meyers Branch confining system	(Gordon aquifer bottom)

Environmental Sciences Section Operating Procedure 2-15, Rev. 2 provides a detailed explanation of each heading.

WELL	DEEP	R	I	COLOR	STRUCTUR	GR	SD	MD	MX	MD	R	CG	CS	CM	CT	CB	NAME	S	PR	PT	MU	GL	LI	SU	H	FOSSILS
OFS003SB	1	0																								DRILLEDOUT
OFS003SB	2	0																								DRILLEDOUT
OFS003SB	3	0																								DRILLEDOUT
OFS003SB	4	0																								DRILLEDOUT
OFS003SB	5	0																								DRILLEDOUT
OFS003SB	6	0																								DRILLEDOUT
OFS003SB	7	0																								DRILLEDOUT
OFS003SB	8	0																								DRILLEDOUT
OFS003SB	9	0																								DRILLEDOUT
OFS003SB	10	0																								DRILLEDOUT
OFS003SB	11		2	DBRYE	MTDPU	2	90	8	LP	M	4					0	SD	P	M	BP	.1	0	0	0	C	
OFS003SB	12		2	DBRYE	WSPWH	1	92	7	GR	M	3					0	SD	P	M	BP	.1	0	0	0	C	
OFS003SB	13		2	DYEOR	WSPWH	1	92	7	LP	F	3					0	SD	P	M	BP	.1	0	0	0	C	
OFS003SB	14		2	DYEOR	WSPWH	1	93	6	LP	F	3					0	SD	M	M	BP	.1	0	0	0	C	
OFS003SB	15		2	DYEOR	WSPWH	.1	94	6	GR	F	3					0	SD	M	M	BP	.1	0	0	0	C	
OFS003SB	16		2	DYEOR	WSPWH	.1	95	5	GR	M	3					0	SD	M	M	BP	.1	0	0	0	C	
OFS003SB	17		2	DORYE	BUWSPWH	1	94	5	GR	M	4					0	SD	M	M	BP	.1	0	0	0	C	
OFS003SB	18		2	DORYE	WSPWH	2	93	5	LP	M	4					0	SD	M	M	BP	.1	0	0	0	C	
OFS003SB	19		2	DORYE	WSPWH	2	93	5	LP	M	4					0	SD	M	M	BP	.1	0	0	0	C	
OFS003SB	20		2	MBROR		1	94	5	GR	M	3					0	SD	M	M	BP	.1	0	0	0	C	
OFS003SB	21		2	DORYE		.1	94	6	GR	M	3					0	SD	M	M	BP	.1	0	0	0	C	
OFS003SB	22		2	DORYE	WSPWH	.1	94	6	GR	M	3					0	SD	M	M	BP	.1	0	0	0	C	
OFS003SB	23		2	DORYE	WSPWH	.1	95	5	GR	M	3					0	SD	M	M	BP	.1	0	0	0	C	
OFS003SB	24		2	DORYE	WSPWH	.1	94	6	GR	M	3					0	SD	M	M	BP	.1	0	0	0	C	
OFS003SB	25		1	DORYE		0	94	6	VC	M	3					0	SD	M	M	BP	.1	0	0	0	C	
OFS003SB	26		2	DYEOR	WSPWH	0	94	6	VC	F	3					0	SD	M	G	BP	.1	0	0	0	A	
OFS003SB	27		2	DYEOR	WSPWH	0	94	6	VC	F	3					0	SD	M	G	BP	.1	0	0	0	A	
OFS003SB	28		2	DYEOR	WSPWH	0	96	4	VC	F	3					0	SD	M	G	BP	.1	0	0	0	A	

Table A1. (cont'd)

OFS003SB	29		2	DYEOR	WSPWH	0	96	4	VC	F	3					0	SD		M	G	BP	.1	0	0	0	C					
OFS003SB	30		2	MBRRE	WSPWH	.1	96	4	GR	M	3					0	SD		M	G	BP	.1	0	0	0	C					
OFS003SB	31		2	MBRRE	WSPWHCL	.1	96	4	GR	M	3					0	SD		M	G	BP	.1	0	0	0	C					
OFS003SB	32		2	DYEBR		.1	96	4	GR	M	3					0	SD		M	G	BP	.1	0	0	0	A					
OFS003SB	33		2	DYEBR	WSPWHCL	.1	94	6	GR	M	3					0	SD		P	M	BP	.1	0	0	0	C					
OFS003SB	34		2	DYEBR	WSPWHCL	.1	94	6	GR	M	3					0	SD		P	M	BP	.1	0	0	0	C					
OFS003SB	35		2	DYEBR	WSPWHCL	.1	93	7	GR	M	3					0	SD		P	M	BP	.1	0	0	0	C					
OFS003SB	36		2	DYEBR	IFE	1	84	15	LP	F	2				2	0	SD		P	P	BP	.1	0	0	0	R					
OFS003SB	37		2	WYEBR	WSPWHCL	.1	90	10	GR	F	2					0	SD		P	M	BP	.1	0	0	0	C					
OFS003SB	38		2	MYEBR	IWHCL	.1	85	15	GR	M	3					0	SD		P	M	BP	1	0	0	0	R					
OFS003SB	39		2	DYEOR	WSPWHCL	.1	85	15	GR	M	3					0	SD		P	M	BP	1	0	0	0	C					
OFS003SB	40		2	DYEOR	IWHCL	2	68	30	GR	M	3					0	CLSD		P	P	BP	1	0	0	0	C					
OFS003SB	41		2	DYEOR	WSPWHICL	2	75	23	GR	M	3					0	SD		V	M	BP	1	0	0	0	C					
OFS003SB	42		2	DYEOR	WSPWH	1	92	7	GR	M	3					0	SD		M	M	BP	1	0	0	0	A					
OFS003SB	43		1	DYEOR	WSPWH	1	92	7	GR	M	3					0	SD		M	G	BP	1	0	0	0	C					
OFS003SB	44	2	1	DYEOR	WSPWH	1	92	7	GR	M	3					0	SD		M	G	BP	1	0	0	0	R					
OFS003SB	45	0															SD														
OFS003SB	46		1	DORBR	IWHCLB	1	94	5	LP	M	4					0	SD		P	E	BP	.1	0	0	0	C					
OFS003SB	47		2	DORBR	IWHCLB	4	89	7	LP	M	3					0	SD		P	G	BP	.1	0	0	0	R					
OFS003SB	48		1	LBRYE		3	91	6	LP	C	4					0	SD		P	G	BP	.1	0	0	0	R					
OFS003SB	49	7	2	MYEBR		5	75	20	GR	ST	4					0	SD		P	P	BP	.1	0	0	0	R					
OFS003SB	50	0															CLSD														
OFS003SB	51		3	DORYE	IDORSD	0	27	73	M	ST	2					0	SDCL		V	P	MI	.1	0	0	0	R					
OFS003SB	52		3		IDORSD	0	28	72	C	ST	2					0	SDCL		V	P	MI	.1	0	0	0	R					
OFS003SB	53		2	DORYE	ILTAYECL	.1	85	15	GR	M	3					0	SD		P	G	BP	.1	0	0	0	R					
OFS003SB	54	6	1	LTAYE		1	94	5	GR	M	3					0	SD		M	E	BP	1	0	0	0	R					
OFS003SB	55	0															SD														
OFS003SB	56	0															SD														
OFS003SB	57	0															SD														
OFS003SB	58	0															SD														
OFS003SB	59	4	2	LTAYE		0	60	40	C	ST	3					0	CLSD		V	P	BP	.1	0	0	0	R					
OFS003SB	60	0															SD														
OFS003SB	61		1	DBROR		1	94	5	GR	M	3					0	SD		M	G	BP	.1	0	0	0	C					
OFS003SB	62		1	DYEOR	ILTACL	.1	90	10	UP	M	3					0	SD		M	G	BP	1	0	0	0	C					
OFS003SB	63	3	2	DYE	ILTACL	.1	60	40	GR	M	3					0	CLSD		P	M	BP	.1	0	0	0	C					
OFS003SB	64	0															CLSD														SHELBYTUBE
OFS003SB	65	0															SD														SHELBYTUBE
OFS003SB	66	6	2	DYEOR	IDTACL	1	79	20	GR	M	3					0	SD		M	M	BP	1	0	0	0	C					
OFS003SB	67	0															SD														
OFS003SB	68		2	DBROR		2	88	10	GR	C	4					0	SD		P	G	BP	1	0	0	0	C					
OFS003SB	69		2	DTA	IDORSD	0	45	55	C	ST	3					0	SDCL		V	P	BP	.1	0	0	0	C					
OFS003SB	70		3	DTA	IMYEORSD	0	15	85	C	ST	3					0	CL		V	P	MI	.1	0	0	0	R					
OFS003SB	71		3	DYETA	FS	0	10	90	M	CL	3					0	CL		V	P	MI	.1	0	0	0	R					
OFS003SB	72		3	DYETA	IDYEORSD	0	15	85	M	CL	3					0	CL		V	P	MI	.1	0	0	0	R					
OFS003SB	73		2	DBRYE	IFSTACL	2	68	30	GR	C	4					0	CLSD		P	P	BP	.1	0	0	0	C					

Table A1. (cont'd)

OFS003SB	74	5	2	MBRGN	WSPBKGN	.1	80	20	GR	M	3	0	99	0	0	.1	SD	P	M	BP	.1	0	0	0	C		
OFS003SB	75	0															SD										
OFS003SB	76		2	MBRGN	IPBCL	.1	95	5	GR	M	3	10	65	25	0	15	MCCASD	P	M	BP	.1	.1	0	0	C	YEPL	
OFS003SB	77		2	LGNWH	IBRGNCL	.1	95	5	GR	M	3	20	70	10	0	25	CASD	P	M	BP	.1	.1	0	0	C	GIPLYE	
OFS003SB	78		2	LGN	ISDSLMC	.1	93	2	GR	M	3	20	75	15	0	55	SDSL	P	P	MI	.1	.1	0	0	C	GIPLYE	
OFS003SB	79		2	LGN	ISDBL	2	88	10	GR	M	4	15	80	5	0	30	SLCASD	P	M	BP	.1	1	0	0	C	GIPLYE	
OFS003SB	80		2	LGN	LGNCLB	25	50	25	LP	ST	4	50	50	0	0	5	SLCLPBSD	V	P	BP	.1	.1	0	0	R	PL	
OFS003SB	81		2	LGN		3	92	5	GR	M	3	5	55	40	0	30	MCCASD	P	M	BP	.1	.1	0	0	C	PL	
OFS003SB	82		2	LGN		2	91	7	GR	M	3	5	55	40	0	30	MCCASD	P	M	BP	.1	0	0	0	R	PL	
OFS003SB	83		2	LGN		7	88	5	LP	C	4	20	20	60	0	30	MCSD	P	M	BP	.1	.1	0	0	R	PL	
OFS003SB	84		3	LWHGN		10	85	5	LP	C	4	30	20	50	0	40	SLMCSD	P	M	BP	.1	.1	0	0	R	PL	
OFS003SB	85		3	LWHGN	ISL	15	78	7	LP	C	4	40	20	40	.1	55	SDMCSL	P	M	MO	.1	1	0	0	R	PLGI	
OFS003SB	86		3	LWHGN	IWHSPBL	10	85	5	LP	M	3	10	40	50	1	55	SDBLMC	P	M	MI	.1	1	0	0	C	PLYE	
OFS003SB	87		3	LWHGN	ILPIGNBL	3	92	5	GR	M	3	10	50	40	2	45	MCCASD	P	M	BP	.1	1	0	0	C	PLYE	
OFS003SB	88		3	LWHGN		.1	95	5	GR	M	3	10	50	40	1	35	MCCASD	P	M	BP	.1	1	0	0	C	PLYE	
OFS003SB	89		2	LBRGN	IWHSDBL	.1	70	30	GR	M	3	15	25	60	.1	25	BLMCCLSD	P	M	BP	.1	.1	0	0	C	YEPL	
OFS003SB	90		2	DYEOR	IFSLGNCL	.1	55	45	GR	M	3					0	CLSD	P	M	BP	.1	0	0	0	C		
OFS003SB	91		2	DYEOR		0	88	12	VC	M	3	99	0	0	0	.1	SD	M	M	BP	.1	0	0	0	C	PL	
OFS003SB	92		2	DYEOR	LGNCLB	0	92	8	VC	M	3					0	SD	M	G	BP	.1	0	0	0	C		
OFS003SB	93		2	DYEOR	WSPBK	0	93	7	VC	M	3					0	SD	M	G	BP	.1	0	0	0	C		
OFS003SB	94		3	LGN	FSWSPBK	0	7	93	M	CL	2	0	99	0	0	.1	CL	V	P	MI	.1	0	0	0	R		
OFS003SB	95		3	LGN	FSWSPBK	0	15	85	C	ST	2	0	99	0	0	.1	CL	V	P	MI	.1	.1	0	0	R	PL	
OFS003SB	96		3	LGN	ICLTSTCL	0	25	75	M	CL	2	15	80	5	0	2	CASDCL	V	P	MI	.1	.1	0	0	R	YEPL	
OFS003SB	97		3	LGN	FSWSPBK	.1	25	75	GR	ST	2	0	0	9	0	.1	SDCL	V	P	MI	.1	.1	.0	0	R		
OFS003SB	98		2	LWHGN	IPBIWHSL	10	85	5	LP	M	4	10	5	85	0	20	MCSD	V	P	MI	1	.1	0	0	R	GAPL	
OFS003SB	99		2	LBRGN	IGNPBCL	5	88	7	LP	M	3					0	SD	V	M	BP	1	0	0	0	R		
OFS003SB	100		2	LGN	IFSLTACL	1	74	25	GR	M	3				1	0	CLSD	P	M	BP	1	0	0	0	R		
OFS003SB	101		2	LBRGN	ILGNCL	2	88	10	LP	M	3					0	SD	M	M	BP	1	0	0	0	C		
OFS003SB	102		2	LBRGN	IWHMCSD	5	80	15	LP	M	3	0	0	99	0	.1	SD	P	M	BP	.1	0	0	0	C		
OFS003SB	103		2	LBRGN	IPBCLSD	10	65	25	LP	M	4	0	0	99	0	.1	CLSD	V	P	BP	1	0	0	0	C		
OFS003SB	104		2	LGN	MTWHCASD	2	73	25	GR	F	3	5	65	30		25	CACLSD	P	P	BP	.1	1	0	0	C	PLYE	
OFS003SB	105		2	LBRGN	IWHMCSD	.1	94	6	GR	F	3	3	7	90	.1	15	MCSD	P	M	BP	.1	1	0	0	C	PLYE	
OFS003SB	106		2	MBRGN	IWHMCSD	.1	94	6	GR	F	3	5	5	90	.1	.1	SD	P	M	BP	1	.1	0	0	C	PL	
OFS003SB	107	9	2	MBRGN	WSPLGN	.1	85	15	GR	F	3					0	SD	P	M	BP	.1	0	0	0	C		
OFS003SB	108		2	MBRGN	ICLSDISD	.1	85	15	GR	F	3					0	SD	P	M	BP	.1	0	0	0	C		
OFS003SB	109		2	DBRGN	ICTSD	.1	90	10	GR	F	3	95	5	0	1	.1	SD	P	M	BP	.1	0	0	0	C		
OFS003SB	110		2	MGNBR	ISLMTLGN	1	91	8	GR	M	3	60	40	0	0	.1	SD	P	M	BP	.1	0	0	0	C	PLYE	
OFS003SB	111		2	MGNBR	WSPLBRGN	.1	90	10	GR	F	3					0	SD	M	M	BP	1	0	0	0	C		
OFS003SB	112		2	MBROR	WSPLBRGN	0	94	6	VC	F	3					0	SD	M	G	BP	.1	0	0	0	C		
OFS003SB	113		1	MBROR	WSPLBRCL	.1	92	8	GR	F	3					0	SD	W	G	BP	1	0	0	0	C		
OFS003SB	114		1	LTAOR		0	99	.1	VC	F	3					0	SD	W	E	BP	.1	0	0	0	C		
OFS003SB	115	8	1	MGNOR	MTLGN	.1	95	5	GR	F	3					0	SD	W	G	BP	1	0	0	0	C		
OFS003SB	116		1	DBROR		1	95	4	GR	M	4					0	SD	W	G	BP	.1	0	0	0	C	YE	
OFS003SB	117		2	MBROR	ICTSD	.1	95	5	GR	F	3				1	0	SD	W	G	BP	1	0	0	0	A		
OFS003SB	118		2	MBROR		.1	92	8	GR	F	3					0	SD	M	G	BP	1	0	0	0			

Table A1. (cont'd)

OFS003SB	119		2	MBROR	WSPGNGY	.1	94	6	GR	F	3					0	SD		M	G	BP	1	0	0	0	C					
OFS003SB	120	0															SD														
OFS003SB	121		2	DBROR	WSPWHCL	.1	90	10	GR	M	4					0	SD		M	M	BP	1	0	0	0	C					
OFS003SB	122		2	VAROR	IGNORSD	.1	92	8	GR	F	3					0	SD		M	M	BP	1	0	0	0	A					
OFS003SB	123		2	DBROR	WSPMTA	0	94	6	C	F	4					0	SD		M	G	BP	1	0	0	0	A					
OFS003SB	124	0															SD														
OFS003SB	125	0															SD														
OFS003SB	126		2	DGNOR	BUBDBROR	0	94	6	C	F	3					0	SD		W	G	BP	1	0	0	0	A					
OFS003SB	127	9	2	DGNOR		0	94	6	C	F	3					0	SD		W	G	BP	1	0	0	0	C					
OFS003SB	128		2	DGNOR		0	96	4	C	F	3					0	SD		W	G	BP	1	.1	0	0	A					
OFS003SB	129	4	3	DGNOR	ICTSD	0	90	10	C	F	3				1	0	SD		W	M	BP	1	.1	0	0	A					
OFS003SB	130	0															SD														
OFS003SB	131		1	MBROR		1	95	4	GR	C	4					0	SD		M	G	BP	.1	0	0	0	R					
OFS003SB	132		2	MBROR		1	95	4	GR	C	4					0	SD		M	G	BP	.1	0	0	0	R					
OFS003SB	133		2	MBROR		1	93	6	GR	C	4					0	SD		M	G	BP	.1	0	0	0	R					
OFS003SB	134		2	DGNBR	WSPWHICT	1	74	25	GR	F	3				10	0	CLSD		P	P	BP	.1	1	0	0	C					
OFS003SB	135	3	2	DBROR	MTLBRGN	1	59	40	GR	F	2				3	0	CLSD		P	P	BP	.1	2	0	0	C					
OFS003SB	136	0															CLSD														SHELBYTUBE
OFS003SB	137	0															CLSD														SHELBYTUBE
OFS003SB	138		2	MGYGN		2	68	40	GR	ST	3					0	CLSD		P	P	BP	1	2	0	0	C					
OFS003SB	139	9	2	DBROR	WSPLGNST	.1	98	2	GR	F	3					0	SD		W	G	BP	.1	0	0	0	C					
OFS003SB	140	0															SD														
OFS003SB	141	0															SD														
OFS003SB	142	0															SD														
OFS003SB	143		1	DBROR	BDORBR	1	95	4	GR	M	3					0	SD		P	G	BP	.1	0	0	0	C					
OFS003SB	144		1	MYEOR		0	99	1	C	F	3					0	SD		M	G	BP	3	0	0	0	C					
OFS003SB	145		1	LORTA	ILGNGYSD	1	99	.1	GR	M	4					0	SD		W	E	BP	.1	0	0	0	C					
OFS003SB	146		1	MGNOR	WSPLGNST	0	98	2	C	F	3					0	SD		W	G	BP	3	0	0	0	C					
OFS003SB	147		2	DORYE	BMORBLBR	0	99	1	C	F	3					0	SD		M	G	BP	.1	0	0	0	C					
OFS003SB	148		2	DORYE	BMOR	0	99	1	C	F	3					0	SD		M	G	BP	.1	0	0	0	C					
OFS003SB	149		2	MBRYE		0	99	1	C	F	3					0	SD		M	G	BP	.1	0	0	0	C					
OFS003SB	150		2	MBRYE		0	99	1	C	F	3					0	SD		M	G	BP	.1	0	0	0	C					
OFS003SB	151		2	MBRYE		.1	97	3	GR	F	2					0	SD		M	G	BP	.1	0	0	0	C					
OFS003SB	152		2	MBRYE		.1	97	3	GR	F	2					0	SD		M	G	BP	.1	0	0	0	C					
OFS003SB	153		2	DORYE	BLGY	.1	99	1	GR	F	2					0	SD		M	G	BP	.1	0	0	0	C					
OFS003SB	154		2	DBKGN		2	96	2	GR	F	2					0	SD		P	E	BP	1	0	0	0	R					
OFS003SB	155		2	DBKGN		2	96	2	GR	F	2					0	SD		P	E	BP	1	0	0	0	R					
OFS003SB	156		2	DBROR	BDBKGN	3	92	5	LP	F	2					0	SD		P	E	BP	1	0	0	0	C					
OFS003SB	157		2	MBROR	MTMBR	3	94	3	LP	M	3					0	SD		P	E	BP	.1	0	0	0	C					
OFS003SB	158		2	MBROR	MTMBR	2	95	3	GR	M	3					0	SD		P	E	BP	1	0	0	0	C					
OFS003SB	159		2	DYEOR	WSPLGNST	1	97	2	GR	M	3					0	SD		M	E	BP	1	0	0	0	C					
OFS003SB	160		1	MTAOR		1	98	1	GR	M	3					0	SD		W	E	BP	1	0	0	0	R					
OFS003SB	161		1	MTAOR		.1	98	2	GR	M	3					0	SD		W	E	BP	.1	0	0	0	R					
OFS003SB	162		1	MTAOR		0	99	1	VC	M	3					0	SD		W	E	BP	.1	0	0	0	R					
OFS003SB	163		1	MTAOR		0	99	1	VC	M	3					0	SD		W	E	BP	1	0	0	0	R					

Table A1. (cont'd)

OFS003SB	164		1	MTAOR		.1	99	1	GR	M	3					0	SD		W	E	BP	1	0	0	0	R			
OFS003SB	165	0															SD													
OFS003SB	166	2	1	MBROR		.1	93	7	GR	M	3					0	SD		W	E	BP	1	0	0	0	C			
OFS003SB	167	0															SD													
OFS003SB	168		1	DTAOR		0	99	1	VC	M	3					0	SD		W	E	BP	1	0	0	0	R			
OFS003SB	169		1	DTAOR		0	99	1	C	M	3					0	SD		W	E	BP	1	0	0	0	R			
OFS003SB	170		1	DTAOR		.1	98	2	GR	M	3					0	SD		W	E	BP	1	0	0	0	R			
OFS003SB	171		1	DYEOR		0	99	1	VC	M	3					0	SD		W	E	BP	.1	0	0	0	R			
OFS003SB	172		1	DYEOR		0	99	1	VC	M	3					0	SD		W	E	BP	.1	0	0	0	R			
OFS003SB	173		1	DYEOR		0	99	1	VC	M	3					0	SD		W	E	BP	.1	0	0	0	C			
OFS003SB	174		1	DYEOR		0	98	2	VC	F	3					0	SD		W	E	BP	.1	0	0	0	R			
OFS003SB	175	0															SD													
OFS003SB	176		1	DYEOR	DORCLB	0	99	1	VC	F	3					0	SD		W	E	BP	.1	0	0	0	R			
OFS003SB	177		1	DYEOR		.1	98	2	GR	F	3					0	SD		W	E	BP	.1	0	0	0	R			
OFS003SB	178	8	1	DYEOR	ILTAORSD	.1	97	3	GR	M	3					0	SD		W	E	BP	.1	0	0	0	R			
OFS003SB	179	0															SD													
OFS003SB	180	0															SD													
OFS003SB	181		1	MORYE		1	97	2	GR	M	3					0	SD		M	E	BP	1	0	0	0	R			
OFS003SB	182		1	MORYE		1	97	2	GR	M	3					0	SD		M	E	BP	2	0	0	0	R			
OFS003SB	183		1	MORYE		1	97	2	GR	M	3					0	SD		M	E	BP	.1	0	0	0	R			
OFS003SB	184		2	MORYE		1	94	5	LP	M	3					0	SD		M	G	BP	.1	0	0	0	C			
OFS003SB	185	6	2	MTAYE	IFSLGNST	2	81	15	LP	M	3					0	SD		M	M	BP	.1	.1	.1	.1	C			
OFS003SB	186	0															SD													
OFS003SB	187	0															SD													
OFS003SB	188		2	DGYGW	IFSDGNST	2	81	17	GR	M	2					0	SD		P	M	BP	1	.1	.1	.1	C			
OFS003SB	189		2	DGYGW	DGYCLB	1	94	5	LP	M	2					0	SD		M	M	BP	1	.1	.1	.1	C			
OFS003SB	190		2	DGYGW	IFSDGNCL	2	86	12	LP	M	2					0	SD		M	M	BP	1	1	1	.1	C			
OFS003SB	191	0															SD													
OFS003SB	192	0															SD													TDHOLE

Table A2. Stream coordinate and elevation data for Fourmile Branch and F-area outfalls.

Stream Label	SRS East (ft)	SRS North (ft)	Elevation (ft)
4Mile_Br	49884.0	72820.2	180.0
4Mile_Br	49963.2	72807.8	180.1
4Mile_Br	50029.3	72800.3	180.3
4Mile_Br	50094.4	72804.4	180.4
4Mile_Br	50156.5	72814.8	180.5
4Mile_Br	50213.9	72829.3	180.6
4Mile_Br	50266.4	72845.2	180.7
4Mile_Br	50312.7	72847.3	180.8
4Mile_Br	50359.3	72852.2	180.9
4Mile_Br	50404.7	72852.2	181.0
4Mile_Br	50481.1	72869.6	181.1
4Mile_Br	50570.8	72884.1	181.3
4Mile_Br	50615.8	72896.9	181.4
4Mile_Br	50670.4	72916.1	181.5
4Mile_Br	50729.8	72931.6	181.6
4Mile_Br	50781.0	72948.4	181.7
4Mile_Br	50847.4	72971.2	181.8
4Mile_Br	50896.9	72994.3	181.9
4Mile_Br	50926.4	73005.5	182.0
4Mile_Br	50974.7	73032.5	182.1
4Mile_Br	51021.0	73058.6	182.2
4Mile_Br	51076.3	73086.1	182.3
4Mile_Br	51118.2	73101.0	182.4
4Mile_Br	51156.1	73111.9	182.4
4Mile_Br	51209.5	73113.9	182.5
4Mile_Br	51254.2	73116.1	182.6
4Mile_Br	51301.0	73117.6	182.7
4Mile_Br	51341.6	73101.1	182.8
4Mile_Br	51373.5	73094.0	182.8
4Mile_Br	51403.9	73091.6	182.9
4Mile_Br	51442.9	73074.4	183.0
4Mile_Br	51488.1	73063.5	183.1
4Mile_Br	51559.4	73057.5	183.2
4Mile_Br	51616.1	73055.1	183.3
4Mile_Br	51653.2	73057.8	183.4
4Mile_Br	51685.0	73062.6	183.4
4Mile_Br	51747.9	73052.1	183.6
4Mile_Br	51788.8	73046.8	183.6
4Mile_Br	51843.4	73032.0	183.7
4Mile_Br	51895.0	73023.1	183.8
4Mile_Br	51944.1	73011.2	183.9
4Mile_Br	51982.2	73008.6	184.0
4Mile_Br	52022.8	73008.2	184.1
4Mile_Br	52085.0	72993.5	184.2
4Mile_Br	52149.6	72979.0	184.3
4Mile_Br	52225.0	72969.6	184.4
4Mile_Br	52263.9	72959.8	184.5
4Mile_Br	52296.2	72960.0	184.6
4Mile_Br	52329.5	72945.9	184.6
4Mile_Br	52365.2	72944.7	184.7
4Mile_Br	52398.7	72934.2	184.7
4Mile_Br	52439.4	72932.9	184.8

Table A2. (cont'd)

Stream Label	SRS East (ft)	SRS North (ft)	Elevation (ft)
4Mile_Br	52472.9	72918.5	184.9
4Mile_Br	52537.9	72904.4	185.0
4Mile_Br	52584.6	72891.5	185.1
4Mile_Br	52619.1	72874.2	185.1
4Mile_Br	52679.8	72832.6	185.3
4Mile_Br	52747.9	72774.8	185.4
4Mile_Br	52776.4	72737.6	185.5
4Mile_Br	52819.9	72699.6	185.6
4Mile_Br	52847.2	72675.8	185.7
4Mile_Br	52890.9	72658.5	185.7
4Mile_Br	52936.6	72630.3	185.8
4Mile_Br	52995.8	72593.8	186.0
4Mile_Br	53019.6	72583.0	186.0
4Mile_Br	53045.9	72575.7	186.2
4Mile_Br	53084.2	72564.0	186.6
4Mile_Br	53122.8	72540.2	187.0
4Mile_Br	53163.8	72527.4	187.4
4Mile_Br	53198.7	72513.9	187.7
4Mile_Br	53230.4	72500.8	188.0
4Mile_Br	53270.5	72484.4	189.1
4Mile_Br	53300.4	72471.1	190.0
4Mile_Br	53365.3	72423.0	190.2
4Mile_Br	53422.6	72372.8	190.3
4Mile_Br	53442.4	72354.9	190.4
4Mile_Br	53480.7	72340.3	190.4
4Mile_Br	53529.7	72301.9	190.6
4Mile_Br	53585.3	72258.2	190.7
4Mile_Br	53652.3	72204.3	190.9
4Mile_Br	53697.4	72172.5	191.0
4Mile_Br	53741.1	72133.4	191.1
4Mile_Br	53780.8	72088.7	191.2
4Mile_Br	53796.6	72069.9	191.3
4Mile_Br	53803.6	72040.7	191.3
4Mile_Br	53832.5	71977.4	191.4
4Mile_Br	53841.1	71943.6	191.5
4Mile_Br	53860.6	71911.3	191.6
4Mile_Br	53863.9	71899.7	191.6
4Mile_Br	53884.0	71886.7	191.7
4Mile_Br	53900.2	71857.0	191.7
4Mile_Br	53942.3	71808.9	191.8
4Mile_Br	53976.6	71778.1	191.9
4Mile_Br	54002.5	71758.8	192.0
4Mile_Br	54043.1	71735.9	192.1
4Mile_Br	54060.4	71721.0	192.2
4Mile_Br	54099.0	71701.8	192.3
4Mile_Br	54156.8	71663.4	192.5
4Mile_Br	54213.0	71634.9	192.7
4Mile_Br	54272.0	71591.5	192.9
4Mile_Br	54343.1	71563.3	193.1
4Mile_Br	54409.3	71534.9	193.3
4Mile_Br	54479.6	71493.9	193.5
4Mile_Br	54555.6	71446.2	193.7
4Mile_Br	54605.3	71415.0	193.9

Table A2. (cont'd)

Stream Label	SRS East (ft)	SRS North (ft)	Elevation (ft)
4Mile_Br	54633.1	71395.7	194.0
4Mile_Br	54705.9	71347.9	194.3
4Mile_Br	54762.3	71307.2	194.6
4Mile_Br	54793.7	71285.1	194.7
4Mile_Br	54855.2	71193.5	195.1
4Mile_Br	54889.4	71144.6	195.3
4Mile_Br	54935.9	71089.0	195.6
4Mile_Br	54989.8	71037.5	195.9
4Mile_Br	55013.0	71014.5	196.0
4Mile_Br	55061.7	70959.2	196.2
4Mile_Br	55126.7	70934.2	196.5
4Mile_Br	55159.8	70917.8	196.7
4Mile_Br	55215.6	70874.7	196.9
4Mile_Br	55280.0	70848.4	197.2
4Mile_Br	55372.3	70857.5	197.5
4Mile_Br	55450.6	70862.4	197.8
4Mile_Br	55498.7	70863.0	198.0
4Mile_Br	55557.6	70871.5	198.1
4Mile_Br	55603.8	70880.6	198.2
4Mile_Br	55659.9	70875.0	198.3
4Mile_Br	55713.8	70852.4	198.4
4Mile_Br	55782.9	70848.1	198.5
4Mile_Br	55859.7	70814.2	198.6
4Mile_Br	55912.6	70790.3	198.7
4Mile_Br	56015.1	70771.7	198.9
4Mile_Br	56090.8	70749.1	199.0
4Mile_Br	56143.7	70735.9	199.1
4Mile_Br	56177.0	70737.8	199.2
4Mile_Br	56234.0	70721.8	199.3
4Mile_Br	56330.0	70688.2	199.4
4Mile_Br	56400.8	70660.8	199.6
4Mile_Br	56463.6	70629.9	199.7
4Mile_Br	56555.9	70592.3	199.9
4Mile_Br	56634.3	70562.1	200.0
4Mile_Br	56712.4	70542.6	200.2
4Mile_Br	56793.6	70519.6	200.5
4Mile_Br	56865.3	70507.2	200.6
4Mile_Br	56906.4	70491.2	200.8
4Mile_Br	56954.6	70484.6	200.9
4Mile_Br	56993.1	70458.7	201.0
4Mile_Br	57092.5	70386.0	201.4
4Mile_Br	57149.5	70338.1	201.6
4Mile_Br	57171.6	70317.5	201.6
4Mile_Br	57205.8	70287.9	201.8
4Mile_Br	57249.5	70271.1	201.9
4Mile_Br	57287.6	70266.0	202.0
4Mile_Br	57309.4	70257.2	202.1
4Mile_Br	57322.4	70242.9	202.2
4Mile_Br	57353.6	70227.2	202.3
4Mile_Br	57361.0	70205.9	202.5
4Mile_Br	57370.3	70178.8	202.7
4Mile_Br	57366.4	70141.3	203.0
4Mile_Br	57359.6	70127.9	203.1

Table A2. (cont'd)

Stream Label	SRS East (ft)	SRS North (ft)	Elevation (ft)
4Mile_Br	57341.9	70107.2	203.2
4Mile_Br	57330.0	70070.4	203.5
4Mile_Br	57325.5	70039.9	203.7
4Mile_Br	57317.1	69997.5	204.0
4Mile_Br	57314.1	69982.7	204.1
4Mile_Br	57305.0	69951.2	204.2
4Mile_Br	57309.5	69899.4	204.4
4Mile_Br	57318.6	69840.3	204.7
4Mile_Br	57329.0	69773.8	205.0
4Mile_Br	57339.4	69739.5	205.1
4Mile_Br	57361.8	69707.9	205.3
4Mile_Br	57376.4	69663.2	205.5
4Mile_Br	57390.7	69643.3	205.6
4Mile_Br	57408.3	69624.4	205.7
4Mile_Br	57422.9	69599.6	205.8
4Mile_Br	57447.1	69577.4	205.9
4Mile_Br	57456.1	69563.2	206.0
4Mile_Br	57471.1	69544.1	206.0
4Mile_Br	57516.6	69519.2	206.2
4Mile_Br	57551.2	69490.2	206.3
4Mile_Br	57603.3	69477.5	206.4
4Mile_Br	57668.6	69451.4	206.5
4Mile_Br	57729.7	69426.7	206.7
4Mile_Br	57765.0	69415.5	206.7
4Mile_Br	57805.5	69410.8	206.8
4Mile_Br	57843.9	69392.5	206.9
4Mile_Br	57939.8	69374.1	207.1
4Mile_Br	57992.1	69368.5	207.2
4Mile_Br	58043.2	69353.3	207.3
4Mile_Br	58097.9	69345.3	207.4
4Mile_Br	58145.1	69312.3	207.6
4Mile_Br	58174.9	69265.3	207.7
4Mile_Br	58201.5	69217.7	207.8
4Mile_Br	58230.9	69163.8	207.9
4Mile_Br	58260.3	69114.8	208.0
4Mile_Br	58301.1	69033.0	208.2
4Mile_Br	58328.3	68965.3	208.4
4Mile_Br	58364.6	68892.5	208.6
4Mile_Br	58392.6	68824.5	208.7
4Mile_Br	58416.4	68737.0	208.9
4Mile_Br	58438.7	68695.9	209.1
4Mile_Br	58472.3	68657.1	209.2
4Mile_Br	58492.1	68611.0	209.3
4Mile_Br	58531.2	68551.2	209.4
4Mile_Br	58567.9	68490.5	209.6
4Mile_Br	58597.2	68415.0	209.8
4Mile_Br	58622.8	68330.8	210.0
4Mile_Br	58626.5	68244.6	210.2
4Mile_Br	58626.3	68151.2	210.5
4Mile_Br	58624.3	68075.4	210.7
4Mile_Br	58632.7	68006.0	210.9
4Mile_Br	58643.2	67964.6	211.0
4Mile_Br	58681.6	67926.2	211.2

Table A2. (cont'd)

Stream Label	SRS East (ft)	SRS North (ft)	Elevation (ft)
4Mile_Br	58705.2	67886.7	211.3
4Mile_Br	58760.0	67817.2	211.6
4Mile_Br	58799.1	67776.5	211.7
4Mile_Br	58863.3	67747.2	211.9
4Mile_Br	58911.9	67733.9	212.0
Old_Eff	53093.4	72547.3	189.9
Old_Eff	53115.3	72575.5	190.0
Old_Eff	53122.5	72604.9	190.0
Old_Eff	53135.1	72630.4	190.0
Old_Eff	53156.6	72658.3	190.2
Old_Eff	53189.8	72679.7	190.4
Old_Eff	53221.2	72700.6	190.5
Old_Eff	53261.6	72723.4	190.8
Old_Eff	53283.4	72739.2	190.9
Old_Eff	53286.7	72764.2	191.0
Old_Eff	53278.6	72839.3	192.0
Old_Eff	53289.0	72907.8	193.0
Old_Eff	53299.9	72970.1	194.0
Old_Eff	53327.3	73072.9	195.0
Old_Eff	53346.3	73112.7	196.0
Old_Eff	53399.8	73172.6	197.0
Old_Eff	53427.1	73199.9	198.0
Old_Eff	53451.5	73223.8	199.0
Old_Eff	53463.3	73234.7	200.0
Old_Eff	53494.1	73266.7	201.0
Old_Eff	53535.4	73299.6	202.0
Old_Eff	53553.9	73310.0	203.0
Old_Eff	53568.1	73317.5	204.0
Old_Eff	53582.5	73325.9	205.0
Old_Eff	53645.6	73353.1	206.0
Old_Eff	53783.5	73384.2	207.0
Old_Eff	53876.6	73425.9	208.0
Old_Eff	53967.2	73477.9	208.8
Old_Eff	53981.3	73505.4	209.0
Old_Eff	53997.3	73560.0	209.5
Old_Eff	53998.1	73622.6	210.0
Old_Eff	54006.0	73647.6	211.0
Old_Eff	54017.8	73687.4	212.0
Old_Eff	54017.9	73716.3	213.0
Old_Eff	54015.3	73740.4	214.0
Old_Eff	54018.4	73756.6	215.0
NewRock1	53463.3	73234.7	200.0
NewRock1	53470.1	73271.3	201.0
NewRock1	53469.4	73317.2	202.0
NewRock1	53468.9	73358.5	203.0
NewRock1	53473.5	73393.1	204.0
NewRock1	53481.6	73413.7	205.0
NewRock1	53514.1	73467.5	208.0
NewRock1	53527.0	73527.9	210.0
NewRock1	53549.6	73567.7	215.0
NewRock1	53592.2	73621.4	220.0
NewRock2	53493.5	73266.9	201.0
NewRock2	53532.7	73308.3	202.0

Table A2. (cont'd)

Stream Label	SRS East (ft)	SRS North (ft)	Elevation (ft)
NewRock2	53554.3	73349.1	203.0
NewRock2	53564.6	73394.2	204.0
NewRock2	53568.4	73424.3	205.0
NewRock2	53570.1	73450.3	210.0
NewRock2	53571.7	73527.3	215.0
NewRock2	53591.9	73621.9	220.0

Table A3. Laboratory hydraulic conductivity as a function of mud fraction for SRS Tertiary-aged sediments.

Bledsoe et al. (1990)

ID	Kv(ft/d)	Kh(ft/d)	%Sand
2	4.82e-4	8.79e-2	47.0
13	3.40e-2	1.84e-2	87.5
14	1.50e-3	4.73e-2	88.5
28	1.28e-5	1.02e-4	2.0
35	3.40e-5	7.94e-3	78.0
36	9.64e-3	9.92e-2	78.5
43	3.40e-1	1.45e+0	84.0
54	9.64e-5	1.13e-4	23.5
59	9.64e-2		88.5
60	1.73e-2		16.5
67	5.16e-5	3.23e-1	12.0
77	1.79e-4		14.5
88	9.58e-4	8.70e-4	48.0
1	1.59e-1	1.50e-1	86.0
8	1.28e-1	6.80e-4	74.5
31	7.65e-5	5.67e-5	65.0
41	2.58e-3	3.12e-3	54.5
42	1.90e-3	1.64e-2	27.5
81	5.70e-4	5.24e-4	68.5
3		1.45e-3	62.0
4	7.51e-6		72.5
9	7.37e-4	2.32e-4	58.5
15	1.13e-3	7.65e-2	74.0
16	1.05e-5	4.25e-5	12.5
17	3.40e-6		10.0
32	3.97e-2	8.79e-2	90.5
33	9.07e-5	1.05e-4	12.5
37	3.97e-5	5.95e-5	44.5
44	5.39e-2	6.80e-1	58.0
50	1.42e-4	1.22e-4	3.0
51	1.02e-3		
55	4.25e-5	3.69e-5	4.5
56	3.40e-5	1.13e-1	38.0
61	6.07e-5	1.02e-4	12.0
68	1.17e-1	1.07e-1	87.5
71	7.85e-3		18.0
72	7.03e-5	7.46e-5	14.0
78	9.75e-5	1.11e-4	13.5
82	2.86e-4	1.11e-4	66.0
89	1.71e-4	1.75e-4	49.0
90	8.28e-5	9.89e-5	0.0
7	5.67e-1	4.82e-1	82.0
12	1.16e-3	4.82e-3	75.0
40	9.64e-5	3.12e-4	68.0
48	4.82e-4	9.64e-4	80.5
49	3.69e-4	1.87e-4	75.5
53	3.69e-4		25.5
65	1.19e-1	2.48e+0	76.5
66	2.24e-4	3.15e-1	80.0
76	9.75e-5	1.11e-4	27.5

Table A3. (cont'd)

Riha (1993)

Sample	%Sand	Kv(cm/s)	Kh(cm/s)
IDS_2	36.3	3.5e-8	4.2e-8
IDS_3	78.3	3.3e-4	7.8e-5
IDS_4	91.4	1.5e-3	
IDS_5	90.4	5.5e-4	
IDS_6	30.1	4.0e-4	
IDS_7	93.8	1.1e-3	
IDS_8	44.	4.0e-7	3.7e-7
IDS_9	80.3	5.6e-4	
IDS_10	72.6	4.0e-5	1.9e-5
IDS_11	92.2	1.4e-3	
IDS_12	48.1	6.2e-9	1.2e-8
IDS_13	80.8	3.4e-7	3.4e-7
IDS_14	68.2	4.0e-7	5.5e-7
IDS_15	93.3	4.3e-5	4.5e-5
IDS_16	50.8	1.9e-7	5.6e-6
IDS_17	93.1	2.5e-4	8.5e-5
IDS_18	95.6	3.8e-4	1.2e-4
MWMF_1	89.	1.2e-3	
MWMF_2	90.	2.9e-3	
MWMF_3	61.	1.9e-4	
MWMF_4	77.5	1.1e-4	
MWMF_5	58.	5.0e-5	
MWMF_6	76.	1.7e-4	
MWMF_7	70.	1.0e-4	
MWMF_8	79.5	1.3e-3	

RUST (1995)

Boring	Unit	%mud	Kv(cm/s)	Kh(cm/s)
BGO003A	Ellenton	50	5.e-8	8.1e-8
BGO003A	GreenClay	78	4.e-9	7.4e-9
BGO003C	TanClay	50	2.4e-8	3.1e-6
BGO051AA	Ellenton	60	8.e-9	3.9e-9
BGO051B	GreenClay	51	5.8e-9	8.e-9
BGO051B	TanClay	97	3.9e-9	6.1e-9
BGO052A	Ellenton	98	3.8e-9	4.e-9
BGO052A	GreenClay	58	8.9e-9	1.5e-8
BGO052A	TanClay	99	4.3e-9	1.2e-8
OFS001SB	TanClay	-	1.2e-8	-
OFS003SB	TanClay	54	2.4e-8	6.e-5
OFS003SB	GreenClay	89	1.7e-9	2.8e-9
OFS004SB	TanClay	32	2.2e-7	1.9e-6
OFS004SB	GreenClay	60	4.e-9	2.3e-8
OFS005SB	TanClay	10	5.e-4	5.e-4
OFS005SB	GreenClay	62	1.6e-9	6.3e-9

Table A3. (cont'd)

digitized from Figure 11 of Kegley et al. (1994)

%mud	log(k) darcies
4.674759058	1.698125851
5.65930354	1.658659466
8.862774003	1.684501716
18.78373136	1.382032227
15.77881307	1.258819403
18.8417009	1.204433022
21.012126	1.273166274
20.97072662	1.14595995
13.78897847	1.1268706
16.55570991	.8915389717
14.83636606	.8201563247
20.84346602	.5244271638
17.85548828	.3858428508
24.65772523	-.316444546
39.69740062	.3183999647
39.75746069	-.490148937
42.78322025	-1.04655538
23.67113382	1.241910987
25.71132684	1.040018877
27.80015997	.8321407587
35.80498415	.8194793268
22.97504271	1.011524089
19.91373392	.7406169558
17.84082114	.6556427027
23.63869347	.6536574258
22.84151608	.5052538977
26.76651215	.5898667058
27.78619092	.4966048237
29.87766971	.2400602768
25.76372937	0.0760821
30.92533672	-.368041196
31.94942492	-.542413793
33.94650026	-.543657322
37.88110424	-.635780493
46.67925523	-1.02170208
52.82804992	-.665164904
64.01272306	-1.40245908

Other

Boring	%Fines	Kv(cm/s)	Kh(cm/s)	Reference
HIW2A	86	3.60E-09	4.00E-07	WSRC-RP-93-1575
HIW2A	26	1.00E-07	1.20E-07	WSRC-RP-93-1575
FIW1MC	85	1.50E-08	5.30E-07	WSRC-RP-92-896
FIW2MA	87	1.38E-08	8.00E-06	WSRC-RP-92-896
FIW2MA	48	7.40E-09	1.50E-08	WSRC-RP-92-896
HIW1MC	18	1.90E-07	5.00E-06	WSRC-RP-92-896
HCH2	64	5.17E-08	6.20E-08	ATEC (1992)
HCH2	76	1.10E-07	1.63E-07	ATEC (1992)
HCH3	87	5.43E-07	7.36E-07	ATEC (1992)
HCH3	22	3.89E-07	4.10E-07	ATEC (1992)
HCH1	8	8.03E-05	9.07E-05	ATEC (1992)
HCH1	13	1.52E-05	3.54E-05	ATEC (1992)
HCH1	83	1.60E-08	1.91E-08	ATEC (1992)
FCH2	58	8.39E-09	7.59E-09	ATEC (1992)
FCH2	35	6.84E-09	8.99E-09	ATEC (1992)
FCH2	20	3.33E-08	7.94E-08	ATEC (1992)
HCH2	12	4.84E-05	6.31E-05	ATEC (1992)
HCH3	37	1.69E-06	3.88E-06	ATEC (1992)

Table A3. (cont'd)

Other (cont'd)

Boring	%Fines	Kv(cm/s)	Kh(cm/s)	Reference
FCH4	48	5.71E-09	7.42E-09	ATEC (1992)
FCH4	57	3.24E-08	7.90E-08	ATEC (1992)
HCH4	73	2.50E-08	3.10E-08	ATEC (1992)
HCH4	41	8.86E-08	1.22E-07	ATEC (1992)
FCH5	97	9.71E-09	1.14E-08	ATEC (1992)
FCH5	6	3.87E-04	5.36E-04	ATEC (1992)
FCH1	99	7.29E-09	7.24E-09	ATEC (1992)
FCH1	54	3.09E-07	4.12E-07	ATEC (1992)
FCH1	26	1.30E-05	3.84E-05	ATEC (1992)
FCH3	97	2.24E-08	2.43E-08	ATEC (1992)
FCH3	11	5.36E-07	5.62E-07	ATEC (1992)
FCH3	43	5.14E-08	1.02E-07	ATEC (1992)
FCH5	8	4.33E-05	5.58E-05	ATEC (1992)
FCH5	42	9.68E-08	1.14E-07	ATEC (1992)
HMD-1C	86	4.8E-10	2.1E-09	AT&E (1991)
HMD-2C	83	3.4E-10	1.9E-09	AT&E (1991)
HMD-3C	20	6.7E-07	1.3E-06	AT&E (1991)
HMD-4C	27	3.2E-06	2.7E-05	AT&E (1991)
BGX001A	96	1.2E-09	8.3E-09	AT&E (1991)
BGX002B	94	1.5E-09	7.0E-09	AT&E (1991)
BGX002B	39	6.5E-09	1.4E-08	AT&E (1991)
BGX004A	90	2.9E-09	6.0E-09	AT&E (1991)
BGX004C	27	2.1E-08	4.7E-08	AT&E (1991)
BGX007D	74	2.3E-08		AT&E (1991)
BGX009D	50	3.4E-08	1.2E-07	AT&E (1991)
BGX009D	44	4.4E-08	1.6E-07	AT&E (1991)
BGX011D	40	6.6E-09	3.2E-08	AT&E (1991)
BGX011D	48	4.0E-07		AT&E (1991)
BGX-1A	96	1.2E-09	8.3E-09	AT&E (1991)
BGX-2B	94	1.5E-09	7.0E-09	AT&E (1991)
BGX-2B	39	6.5E-09	1.4E-08	AT&E (1991)
BGX-4A	90	2.9E-09	6.0E-09	AT&E (1991)
BGO009AA	85	2.0E-08	7.3E-08	AT&E (1991)
BGO009AA	40	2.7E-08	6.2E-07	AT&E (1991)
BGO010A	65	1.1E-09	2.1E-08	AT&E (1991)
BGO041A	18	3.4E-05	3.0E-07	AT&E (1991)
BGO041A	40	1.0E-08	1.3E-07	AT&E (1991)
BGO043AA	73	3.1E-09	8.6E-09	AT&E (1991)
BGO044AA	18	1.2E-05	8.3E-05	AT&E (1991)
BGO045A	97	1.9E-08	2.5E-08	AT&E (1991)
BGO045A	44	7.2E-08	4.5E-08	AT&E (1991)
BGO047A	23	1.2E-06	2.0E-06	AT&E (1991)
BGO049A	50	3.7E-08	5.2E-05	AT&E (1991)

Table A4. Time-averaged well hydraulic head data for the "upper" aquifer zone within the Upper Three Runs aquifer.

Well Label	SRS East (ft)	SRS North (ft)	Elevation (ft)
BG 52	55524.0	75910.0	229.5
BG 53	55073.0	76157.0	229.3
BG 54	54830.0	75837.0	228.5
BG 55	54590.0	75525.0	227.1
BG 56	54481.0	75206.0	227.6
BG 57	54820.0	75000.0	225.9
BG 58	55162.0	74790.0	227.3
BG 59	55508.0	74593.0	230.0
BG 60	55850.0	74386.0	231.0
BG 61	56360.0	74075.0	233.1
BG 62	56530.0	73971.0	234.3
BG 63	56870.0	73754.0	236.6
BG 64	57212.0	73547.0	239.4
BG 65	57552.0	73340.0	237.4
BG 66	57805.0	73585.0	236.5
BG 67	57902.0	73954.0	236.7
BG 104	59888.0	77038.0	224.6
BG 107	60120.0	74803.0	235.8
BG 108	59827.0	74383.0	238.8
BG 109	59626.0	73926.0	240.4
BG 110	59277.0	73354.0	241.4
BGO 1D	58779.0	73737.0	238.6
BGO 2D	58809.0	74552.0	238.6
BGO 3D	58809.0	75351.0	235.8
BGO 4D	58803.0	76150.0	232.4
BGO 5D	58784.0	76477.0	231.3
BGO 6D	58297.0	76487.0	231.5
BGO 7D	57917.0	76494.0	234.2
BGO 8D	57617.0	76588.0	234.4
BGO 9D	57478.0	76811.0	231.8
BGO 10D	57030.0	76805.0	231.9
BGO 10DR	57073.0	76804.0	232.5
BGO 11D	56651.0	76805.0	231.0
BGO 12D	56231.0	76805.0	230.8
BGO 13D	55840.0	76805.0	230.0
BGO 14DR	55789.0	76322.0	231.7
BGO 15D	55859.0	75973.0	229.6
BGO 16D	56202.0	75751.0	230.7
BGO 17D	56399.0	75599.0	230.7
BGO 17DR	56407.0	75604.0	232.9
BGO 18D	56711.0	75600.0	231.9
BGO 19D	56997.0	75350.0	232.1
BGO 20D	57113.0	74962.0	234.1
BGO 21D	57470.0	74688.0	234.7
BGO 22D	57817.0	74482.0	232.4
BGO 22DR	57831.0	74471.0	237.9
BGO 23D	58133.0	74238.0	235.9
BGO 24D	58438.0	74012.0	236.7
BGO 26D	55015.0	76128.0	227.7
BGO 27D	54680.0	75677.0	227.4
BGO 28D	54457.0	75348.0	226.1
BGO 29D	54099.0	75592.0	227.5

Table A4. (cont'd)

Well Label	SRS East (ft)	SRS North (ft)	Elevation (ft)
BGO 30D	54499.0	75187.0	225.7
BGO 31D	54841.0	74985.0	226.6
BGO 32D	55250.0	74727.0	227.5
BGO 33D	55695.0	74468.0	230.2
BGO 34D	56082.0	74228.0	232.8
BGO 35D	56556.0	73946.0	234.3
BGO 36D	56888.0	73743.0	236.4
BGO 37D	57292.0	73490.0	237.7
BGO 38D	57557.0	73329.0	235.3
BGO 39D	57831.0	73583.0	235.0
BGO 40D	54638.0	76125.0	223.6
BGO 44D	57910.0	76759.0	232.7
BGO 45D	54585.0	75854.0	228.8
BGO 46D	54420.0	75033.0	226.4
BGO 47D	54922.0	74739.0	227.4
BGO 48D	55121.0	74586.0	227.8
BGO 49D	56198.0	73931.0	235.8
BGO 50D	54209.0	75181.0	226.2
BGX 1D	58608.0	76809.0	230.0
BGX 9D	59522.0	76936.0	227.3
BGX 10D	59765.0	76183.0	226.6
BGX 11D	59581.0	75300.0	236.8
BGX 12D	59674.0	74410.0	240.4
BRR 1D	50588.0	77365.0	216.6
BRR 2D	50306.0	77431.0	215.4
BRR 3D	50203.0	77398.0	215.1
BRR 4D	50104.0	77360.0	214.8
BRR 5D	50009.0	77266.0	215.1
FAC 3	55322.0	78018.0	230.5
FAC 4	55472.0	78223.0	228.9
FAC 5	55241.0	77960.0	224.3
FAC 5P	55314.0	78175.0	230.6
FAC 7	55356.0	78123.0	221.8
FAC 8	55366.0	78090.0	226.5
FAL 1	53756.0	78115.0	218.7
FAL 2	53757.0	78231.0	217.1
FCA 1N	53675.0	79037.0	299.2
FCA 2C	53712.0	78296.0	298.0
FCA 2D	53715.0	78295.0	225.4
FCA 9D	53733.0	78600.0	225.6
FCA 10A	53571.0	78640.0	225.3
FCA 10C	53717.0	78642.0	302.3
FCA 10D	53732.0	78640.0	226.5
FCA 16A	53568.0	78899.0	225.2
FCA 16D	53719.0	78898.0	225.2
FCA 16T	53579.0	78898.0	297.6
FCA 19D	53719.0	78271.0	217.0
FCB 2	55046.0	76679.0	231.0
FCB 3	54874.0	76427.0	223.2
FCB 5	54773.0	76492.0	228.5
FCB 6	54733.0	76582.0	228.9
FET 1D	53299.0	76165.0	223.4
FET 2D	52981.0	76045.0	222.0

Table A4. (cont'd)

Well Label	SRS East (ft)	SRS North (ft)	Elevation (ft)
FET 3D	53025.0	75961.0	222.0
FET 4D	53149.0	75959.0	222.6
FSB 76	51388.0	76141.0	218.3
FSB 77	50713.0	75129.0	212.7
FSB 78	50164.0	74764.0	209.2
FSB 79	50139.0	73663.0	202.0
FSB 87D	50081.0	75586.0	213.5
FSB 88D	51527.0	75621.0	215.5
FSB 89D	51335.0	75548.0	214.9
FSB 90D	51140.0	75376.0	214.5
FSB 91D	50946.0	75207.0	212.9
FSB 92D	50557.0	75045.0	211.5
FSB 93D	50452.0	74888.0	210.8
FSB 94DR	50162.0	74869.0	210.6
FSB 95D	50008.0	74977.0	209.7
FSB 95DR	49996.0	74991.0	210.6
FSB 97D	49975.0	75188.0	210.5
FSB 98D	50111.0	75371.0	212.9
FSB 99D	50326.0	75691.0	211.8
FSB104D	49255.0	73865.0	203.7
FSB105D	49833.0	75244.0	208.5
FSB105DR	49841.0	75258.0	211.4
FSB106D	50636.0	74193.0	206.9
FSB107D	51149.0	75177.0	213.2
FSB108D	51142.0	76260.0	217.2
FSB109D	50488.0	75855.0	213.1
FSB110D	50141.0	74193.0	205.1
FSB111D	51515.0	75382.0	214.5
FSB112D	48780.0	74223.0	206.7
FSB113D	51098.0	74154.0	208.0
FSB114D	52018.0	75278.0	217.4
FSB115D	49728.0	72504.0	191.8
FSB116D	50629.0	72727.0	192.2
FSB117D	50486.0	74070.0	205.5
FSB118D	51276.0	74697.0	211.5
FSB119D	50600.0	74599.0	208.9
FSB120D	49163.0	75568.0	210.4
FSB121DR	48429.0	75151.0	208.5
FSB122D	48201.0	73865.0	204.3
FSB123D	51734.0	74562.0	212.7
FSL 1D	52992.0	79063.0	225.2
FSL 2D	52790.0	78636.0	226.7
FSL 3D	52465.0	77765.0	224.2
FSL 4D	52230.0	77452.0	218.9
FSL 5D	51903.0	77047.0	222.4
FSL 6D	51727.0	76733.0	221.2
FSL 7D	51485.0	76327.0	220.5
FSL 8D	51513.0	76054.0	219.7
FSL 9D	51543.0	75768.0	218.6
FSS 1D	53897.0	75257.0	223.5
FSS 2D	53918.0	75103.0	223.0
FSS 3D	53548.0	74960.0	220.7
FSS 4D	52876.0	75537.0	218.3

Table A4. (cont'd)

Well Label	SRS East (ft)	SRS North (ft)	Elevation (ft)
FTF 1	53179.0	77413.0	229.4
FTF 2	53275.0	77336.0	225.3
FTF 3	53244.0	77235.0	224.1
FTF 4	53268.0	77132.0	224.4
FTF 5	53168.0	77035.0	225.1
FTF 6	53062.0	77151.0	224.1
FTF 8	53059.0	77336.0	227.5
FTF 9	52769.0	77482.0	223.6
FTF 10	52905.0	77336.0	223.8
FTF 11	52748.0	77180.0	225.2
FTF 12	52648.0	77321.0	226.8
FTF 13	53098.0	76637.0	224.7
FTF 15	53230.0	76732.0	226.1
FTF 16	52879.0	76758.0	223.1
FTF 17	52884.0	76872.0	223.0
FTF 18	52879.0	76955.0	222.8
FTF 19	52670.0	77139.0	222.2
FTF 20	52500.0	77015.0	221.8
FTF 21	52498.0	76866.0	222.8
FTF 22	52494.0	76751.0	221.6
FTF 23	52660.0	76611.0	222.0
FTF 25A	52868.0	77308.0	223.3
FTF 26	52875.0	77250.0	223.3
FTF 27	52823.0	77227.0	223.4
HAC 1	61415.0	72171.0	269.1
HAC 2	61366.0	72220.0	268.6
HAC 3	61313.0	72183.0	268.9
HAC 4	61372.0	72120.0	269.2
HAP 1	63398.0	71209.0	270.7
HAP 2	63519.0	71122.0	270.1
HC 1E	61864.0	71746.0	275.0
HC 2E	61861.0	71784.0	270.5
HC 2F	61861.0	71780.0	274.3
HC 4B	63408.0	71596.0	268.0
HC 5B	61705.0	73266.0	256.1
HC 6B	62070.0	72150.0	268.9
HC 11C	62131.0	74496.0	236.6
HCA 1	63109.0	72521.0	268.9
HCA 3	63108.0	72651.0	268.7
HCA 4	62942.0	72523.0	268.6
HCB 1	63921.0	71426.0	262.9
HCB 2	63797.0	71289.0	267.8
HCB 3	63919.0	71098.0	266.1
HET 1D	60546.0	71948.0	267.4
HET 2D	60094.0	72006.0	258.2
HET 3D	60110.0	72093.0	258.6
HET 4D	60166.0	72178.0	259.0
HR3 11	60146.0	71402.0	259.3
HR3 13	60065.0	71649.0	258.1
HR8 11	59559.0	71945.0	245.8
HR8 12	59330.0	71780.0	239.3
HR8 13	59300.0	71559.0	237.8
HR8 14	59612.0	71431.0	244.0

Table A4. (cont'd)

Well Label	SRS East (ft)	SRS North (ft)	Elevation (ft)
HSB 65	58432.0	72425.0	234.3
HSB 65C	58447.0	72439.0	233.2
HSB 66	56928.0	72429.0	226.9
HSB 67	58424.0	71505.0	225.2
HSB 68	56901.0	71528.0	224.4
HSB 69	56475.0	71546.0	220.7
HSB 70	55758.0	72606.0	227.5
HSB 71	55279.0	72875.0	225.1
HSB 83D	58601.0	71628.0	225.8
HSB 84D	56349.0	71583.0	219.8
HSB 85C	58947.0	73802.0	239.0
HSB 86D	55996.0	72522.0	225.9
HSB100D	58796.0	72073.0	233.3
HSB101D	58594.0	71997.0	230.8
HSB102D	58393.0	71952.0	228.0
HSB103D	58315.0	71588.0	226.0
HSB104D	58075.0	71370.0	225.4
HSB105D	57877.0	71454.0	225.8
HSB106D	57644.0	71727.0	226.3
HSB107D	57412.0	71696.0	225.1
HSB108D	57145.0	71688.0	223.9
HSB109D	56885.0	71685.0	223.4
HSB110D	56672.0	71785.0	222.8
HSB111D	56494.0	71926.0	222.6
HSB111E	56487.0	71932.0	222.7
HSB112D	56408.0	72161.0	223.7
HSB112E	56399.0	72166.0	223.6
HSB113D	56164.0	72302.0	223.6
HSB114D	56104.0	72474.0	224.6
HSB115D	56039.0	72662.0	225.5
HSB116D	55988.0	72898.0	226.4
HSB117D	55155.0	72747.0	224.8
HSB125D	58584.0	71498.0	221.6
HSB126D	57169.0	70633.0	204.9
HSB127D	56788.0	71218.0	218.5
HSB129D	55103.0	71837.0	208.5
HSB130D	54651.0	70757.0	200.1
HSB131D	56891.0	70365.0	205.2
HSB132D	58799.0	71469.0	221.7
HSB133D	59102.0	71943.0	234.8
HSB134D	58296.0	71217.0	222.5
HSB135D	56552.0	71396.0	218.6
HSB136D	55941.0	71906.0	221.5
HSB137D	55696.0	72278.0	223.0
HSB138D	55260.0	73160.0	224.0
HSB139D	57384.0	71133.0	223.3
HSB140D	56560.0	70036.0	215.4
HSB141D	59170.0	71184.0	243.5
HSB142D	53493.0	73113.0	198.3
HSB143D	52774.0	73754.0	213.9
HSB145D	57753.0	71088.0	221.7
HSB146D	58493.0	70469.0	223.0
HSB147D	55804.0	73827.0	234.0

Table A4. (cont'd)

Well Label	SRS East (ft)	SRS North (ft)	Elevation (ft)
HSB148D	55355.0	70160.0	214.9
HSB149D	57286.0	71338.0	224.5
HSB150D	58692.0	71692.0	228.1
HSB151D	54026.0	72997.0	208.0
HSB152D	54362.0	72011.0	206.4
HSL 1D	58925.0	72179.0	235.6
HSL 2D	59423.0	72190.0	242.1
HSL 3D	59770.0	72251.0	250.0
HSL 4D	60171.0	72453.0	261.5
HSL 5D	60339.0	72562.0	263.8
HSL 6D	60531.0	72659.0	260.6
HSL 7D	60723.0	72674.0	260.3
HSL 8D	61117.0	72688.0	261.5
HSS 1D	64675.0	67610.0	268.6
HSS 2D	64785.0	67355.0	267.2
HSS 3D	64709.0	68257.0	281.5
HTF 1	62067.0	71745.0	271.8
HTF 2	62175.0	71610.0	273.0
HTF 4	61942.0	71630.0	272.5
HTF 5	62110.0	71390.0	277.6
HTF 6	62228.0	71259.0	276.4
HTF 7	62112.0	71130.0	275.6
HTF 8	61965.0	71270.0	274.5
HTF 9	61698.0	71652.0	271.5
HTF 10	61838.0	71520.0	270.8
HTF 11	61722.0	71398.0	271.6
HTF 12	61593.0	71520.0	270.7
HTF 13	61586.0	71856.0	273.4
HTF 14	61462.0	71858.0	273.2
HTF 15	61353.0	71700.0	272.8
HTF 16	61950.0	72150.0	269.0
HTF 17	61188.0	72600.0	262 8
HTF 18	61223.0	71771.0	270.5
HTF 19	61079.0	71902.0	268.5
HTF 20	61086.0	72073.0	267.3
HTF 21	61261.0	71998.0	268.5
HTF 22	62553.0	71363.0	273.9
HTF 23	62670.0	71363.0	274.1
HTF 24	62775.0	71362.0	273.9
HTF 25	62902.0	71224.0	273.9
HTF 26	62815.0	71090.0	274.0
HTF 27	62660.0	71057.0	274.2
HTF 28	62515.0	71080.0	275.7
HTF 29	62414.0	71229.0	274.2
HTF 31	62662.0	70747.0	274.6
HTF 32	62807.0	70880.0	273.9
HTF 34	61978.0	71144.0	272.6
MGA 36	57891.0	73904.0	238.4
MGC 9	55610.0	75372.0	229.6
MGC 11	55770.0	75252.0	232.2
MGC 23	56726.0	74528.0	236.4
MGC 32	57448.0	73982.0	245.7
MGE 9	55489.0	75215.0	229.7

Table A4. (cont'd)

Well Label	SRS East (ft)	SRS North (ft)	Elevation (ft)
MGE 21	56446.0	74487.0	235.1
MGG 15	55851.0	74699.0	233.1
MGG 19	56174.0	74456.0	232.9
MGG 23	56491.0	74214.0	235.8
MGG 28	56895.0	73905.0	237.2
MGG 36	57541.0	73413.0	238.8
NBG 1	53879.0	79300.0	224.1
NBG 2	53958.0	79099.0	224.8
NBG 3	54068.0	78939.0	218.1
NBG 4	54329.0	78942.0	217.1
NBG 5	54515.0	78943.0	217.6
P 27D	64008.0	70376.0	266.9
SBG 1	63749.0	74619.0	237.8
SBG 2	64939.0	74570.0	237.6
SBG 3	65265.0	73699.0	236.9
SBG 4	65010.0	72399.0	240.6
SBG 5	64499.0	72208.0	249.1
SBG 6	63860.0	73599.0	244.2
SCA 2	64697.0	73850.0	242.2
SCA 3	64571.0	73959.0	241.3
SCA 3A	64571.0	73965.0	270.9
SCA 4	64563.0	73856.0	241.7
SCA 4A	64567.0	73855.0	269.1
SCA 5	64630.0	74092.0	242.0
SCA 6	64637.0	73706.0	242.2
SLP 1	64449.0	72958.0	244.8
SLP 2	64529.0	72863.0	244.4
YSC 1C	65855.0	78186.0	217.5
YSC 2D	66130.0	78320.0	217.1
Z 2	53181.0	74785.0	218.1
Z 3	51328.0	75086.0	212.2
Z 8	51584.0	76640.0	218.0
Z 9	50570.0	77732.0	214.8
Z 11	61750.0	72539.0	296.4
Z 12	61400.0	71198.0	274.4
Z 13	62203.0	70785.0	274.6
Z 15	63419.0	72802.0	263.7
ZBG 1	65584.0	76584.0	234.1
ZBG 1A	65598.0	76588.0	279.7
ZBG 2	67472.0	76170.0	221.5
ZDT 1	65114.0	71644.0	239.5
ZDT 2	65059.0	71696.0	241.1
ZW 4	56556.0	77667.0	232.6
ZW 5	54708.0	75767.0	227.5
ZW 7	60300.0	72399.0	265.8
ZW 8	63801.0	70800.0	270.8
ZW 9	61400.0	73198.0	251.9
ZW 10	63401.0	73212.0	249.7
CC-9	54065.0	73295.0	214.9
CC-13	54390.0	73060.0	216.4
CC-17	54710.0	72820.0	220.0
GG-17	54470.0	72495.0	207.8
GG-21	54793.0	72260.0	211.8

Table A4. (cont'd)

Well Label	SRS East (ft)	SRS North (ft)	Elevation (ft)
M-5	54690.0	74820.0	228.6
M-9	55020.0	74590.0	228.0
M-17	55650.0	74100.0	235.0
M-21	55985.0	73870.0	237.9
Q-5	54470.0	74500.0	226.0
Q-9	54775.0	74260.0	226.9
Q-13	55100.0	74020.0	227.4
Q-17	55425.0	73780.0	241.6
Q-21	55745.0	73540.0	233.1
S-3	54070.0	74492.0	224.0
S-4	53678.0	74319.0	222.1
S-5	53370.0	73913.0	221.0
S-6	53222.0	73440.0	204.6
S-9	53785.0	74919.0	226.1
S-15	53930.0	75381.0	231.5
S-16	53491.0	75223.0	226.2
U-5	54219.0	74176.0	223.0
U-9	54540.0	73945.0	223.8
U-13	54863.0	73700.0	232.4
U-17	55185.0	73470.0	226.2
U-21	55506.0	73225.0	227.3
Y-7	54140.0	73730.0	218.2
Y-9	54300.0	73615.0	220.8
Y-13	54625.0	73380.0	223.2
Y-17	54950.0	73140.0	224.7
Y-21	55270.0	72900.0	224.0

Table A5. Time-averaged well hydraulic head data for the "lower" aquifer zone within the Upper Three Runs aquifer.

Well Label	SRS East (ft)	SRS North (ft)	Elevation (ft)
BG 91	56649.0	78031.0	219.1
BG 92	56828.0	79019.0	209.0
BG 93	57160.0	79930.0	201.1
BG 94	57494.0	80867.0	191.4
BG 95	58407.0	80059.0	193.3
BG 96	58297.0	79396.0	198.5
BG 101	59277.0	78740.0	195.7
BG 103	59752.0	77883.0	200.4
BG 122	56789.0	78581.0	211.3
BGO 5C	58794.0	76476.0	216.6
BGO 6B	58346.0	76553.0	219.7
BGO 6C	58307.0	76487.0	220.1
BGO 8C	57618.0	76579.0	225.4
BGO 10B	56978.0	76982.0	220.9
BGO 10C	57041.0	76805.0	220.2
BGO 12C	56241.0	76805.0	220.0
BGO 12CR	56215.0	76806.0	222.4
BGO 13DR	55840.0	76824.0	232.2
BGO 14C	55839.0	76367.0	221.0
BGO 14CR	55789.0	76337.0	224.9
BGO 16B	56183.0	75767.0	220.3
BGO 27C	54671.0	75666.0	220.3
BGO 29C	54099.0	75577.0	223.9
BGO 30C	54512.0	75181.0	219.1
BGO 31C	54816.0	74978.0	225.5
BGO 33C	55681.0	74479.0	224.9
BGO 35C	56545.0	73953.0	228.3
BGO 37C	57279.0	73498.0	229.1
BGO 42C	55522.0	76404.0	224.4
BGO 43CR	56237.0	77035.0	226.6
BGO 43D	56238.0	77056.0	232.3
BGO 44B	57865.0	76756.0	221.9
BGO 44C	57894.0	76757.0	221.7
BGO 45B	54563.0	75840.0	220.6
BGO 45C	54577.0	75835.0	223.9
BGO 46B	54444.0	75012.0	218.9
BGO 46C	54433.0	75022.0	221.1
BGO 47C	54933.0	74752.0	223.7
BGO 48C	55124.0	74599.0	224.5
BGO 49C	56202.0	73917.0	229.0
BGO 50C	54197.0	75190.0	219.5
BGX 1C	58599.0	76820.0	216.9
BGX 2B	58256.0	77203.0	213.3
BGX 2D	58265.0	77192.0	216.3
BGX 3D	57780.0	77577.0	216.1
BGX 4C	57202.0	77886.0	215.9
BGX 4D	57186.0	77893.0	217.0
BGX 5D	57308.0	78402.0	210.6
BGX 6D	57524.0	78740.0	207.6
BGX 7D	58312.0	78349.0	207.7
BGX 8DR	58942.0	77589.0	206.5
BGX 12C	59675.0	74427.0	235.7

Table A5. (cont'd)

Well Label	SRS East (ft)	SRS North (ft)	Elevation (ft)
FAC 4	55472.0	78223.0	228.9
FBP 1A	51080.0	78893.0	206.8
FBP 4	51368.0	79320.0	211.6
FNB 1	54271.0	80151.0	210.8
FNB 2	54362.0	80442.0	207.0
FNB 3	54105.0	80553.0	209.2
FNB 4	53843.0	80409.0	213.1
FSB 76C	51396.0	76112.0	212.7
FSB 78C	50170.0	74772.0	207.7
FSB 79C	50171.0	73668.0	196.6
FSB 87C	50093.0	75591.0	208.4
FSB 88C	51518.0	75619.0	211.9
FSB 89C	51345.0	75553.0	211.4
FSB 90C	51148.0	75382.0	210.3
FSB 91C	50953.0	75213.0	210.3
FSB 93C	50458.0	74897.0	208.4
FSB 94C	50180.0	74869.0	207.7
FSB 95C	50016.0	74971.0	205.9
FSB 95CR	49987.0	75001.0	208.2
FSB 97C	49970.0	75179.0	207.7
FSB 98C	50116.0	75381.0	209.2
FSB 99C	50320.0	75683.0	209.2
FSB102C	50834.0	73582.0	195.1
FSB103C	49651.0	74210.0	202.3
FSB104C	49248.0	73872.0	200.5
FSB105C	49828.0	75234.0	207.2
FSB106C	50651.0	74190.0	201.1
FSB107C	51158.0	75184.0	209.7
FSB110C	50150.0	74190.0	201.6
FSB111C	51526.0	75383.0	211.1
FSB112C	48794.0	74227.0	202.6
FSB113C	51084.0	74160.0	203.1
FSB114C	52033.0	75288.0	213.8
FSB115C	49736.0	72515.0	184.2
FSB116C	50645.0	72725.0	189.6
FSB120C	49171.0	75549.0	206.8
FSB121C	48413.0	75155.0	205.0
FSB122C	48195.0	73881.0	200.5
FSB123C	51750.0	74566.0	210.8
HC 1B	61877.0	71745.0	254.9
HC 2C	61872.0	71784.0	254.2
HC 2D	61866.0	71784.0	256.3
HC 4A	63409.0	71606.0	244.7
HC 5A	61710.0	73265.0	213.8
HC 6A	62060.0	72150.0	252.2
HC 10B	61600.0	75801.0	208.4
HC 12B	59488.0	73186.0	241.6
HMD 1D	56973.0	78731.0	210.9
HMD 2D	57269.0	79665.0	202.3
HMD 3D	57745.0	79578.0	201.8
HMD 4D	58188.0	79160.0	201.9
HSB 65B	58439.0	72445.0	224.7
HSB 68B	56882.0	71525.0	217.8

Table A5. (cont'd)

Well Label	SRS East (ft)	SRS North (ft)	Elevation (ft)
HSB 68C	56872.0	71524.0	218.6
HSB 70C	55757.0	72597.0	223.9
HSB 71C	55281.0	72866.0	223.1
HSB 83B	58594.0	71639.0	223.2
HSB 83C	58614.0	71636.0	225.1
HSB 84B	56352.0	71603.0	211.2
HSB 84C	56360.0	71597.0	214.5
HSB 85B	58953.0	73789.0	233.9
HSB 86B	55976.0	72519.0	223.0
HSB 86C	55984.0	72529.0	225.8
HSB100C	58806.0	72077.0	226.3
HSB101C	58604.0	72001.0	225.3
HSB102C	58399.0	71960.0	224.6
HSB103C	58323.0	71593.0	223.6
HSB104C	58082.0	71376.0	220.6
HSB105C	57883.0	71447.0	219.7
HSB106C	57651.0	71720.0	221.8
HSB107C	57432.0	71698.0	219.5
HSB108C	57155.0	71688.0	218.9
HSB109C	56895.0	71684.0	219.0
HSB110C	56680.0	71779.0	219.4
HSB111C	56501.0	71919.0	220.7
HSB112C	56417.0	72156.0	222.1
HSB113C	56160.0	72312.0	222.6
HSB114C	56107.0	72464.0	224.4
HSB115C	56043.0	72653.0	225.2
HSB116C	55989.0	72888.0	225.8
HSB117C	55162.0	72740.0	222.6
HSB125C	58592.0	71503.0	223.4
HSB126C	57178.0	70627.0	203.6
HSB127C	56792.0	71210.0	210.1
HSB129C	55110.0	71830.0	205.4
HSB130C	54643.0	70762.0	199.7
HSB131C	56894.0	70374.0	203.4
HSB132C	58787.0	71472.0	222.1
HSB133C	59110.0	71949.0	230.4
HSB134C	58289.0	71210.0	220.8
HSB135C	56560.0	71390.0	206.5
HSB136C	55949.0	71900.0	217.8
HSB137C	55700.0	72269.0	220.9
HSB139C	57374.0	71129.0	214.5
HSB140C	56551.0	70049.0	206.2
HSB141C	59170.0	71196.0	229.6
HSB142C	53505.0	73119.0	198.9
HSB143C	52773.0	73738.0	210.0
HSB145C	57769.0	71098.0	214.0
HSB146C	58473.0	70471.0	210.2
HSB148C	55344.0	70151.0	202.0
HSB151C	54014.0	72997.0	208.7
HSB152C	54346.0	72012.0	199.2
P 27C	64004.0	70391.0	245.2
SBG 2	64939.0	74570.0	237.6
YSC 4C	65901.0	77059.0	227.5

Table A5. (cont'd)

Well Label	SRS East (ft)	SRS North (ft)	Elevation (ft)
ZW 2	54388.0	80701.0	207.1
ZW 3	57078.0	80746.0	201.1
S-6	53222.0	73440.0	204.6

Table A6. Time-averaged well hydraulic head data for the Gordon aquifer.

Well Label	SRS East (ft)	SRS North (ft)	Elevation (ft)
BGO 6A	58316.0	76487.0	159.0
BGO 8A	57618.0	76569.0	160.5
BGO 8AR	57617.0	76598.0	160.2
BGO 9AA	57371.0	76975.0	157.7
BGO 10A	57050.0	76805.0	169.0
BGO 10AA	56990.0	76997.0	157.9
BGO 10AR	57063.0	76806.0	158.6
BGO 12A	56250.0	76804.0	181.0
BGO 12AR	56259.0	76803.0	158.0
BGO 14A	55838.0	76377.0	157.7
BGO 14AR	55788.0	76351.0	159.7
BGO 16A	56194.0	75757.0	160.7
BGO 16AR	56217.0	75743.0	161.3
BGO 18A	56699.0	75599.0	160.8
BGO 25A	55668.0	76158.0	160.3
BGO 26A	55014.0	76144.0	159.5
BGO 29A	54103.0	75560.0	159.5
BGO 41A	55403.0	76469.0	158.6
BGO 43A	56253.0	77061.0	158.5
BGO 43AA	56268.0	77066.0	156.8
BGO 44A	57851.0	76755.0	158.6
BGO 44AA	57880.0	76757.0	158.7
BGO 45A	54550.0	75830.0	160.9
BGO 47A	54914.0	74728.0	162.7
BGO 49A	56205.0	73902.0	165.6
BGO 50A	54179.0	75201.0	160.1
BGX 1A	58590.0	76831.0	161.5
BGX 4A	57215.0	77879.0	155.4
FSB 76A	51391.0	76131.0	154.6
FSB 76B	51394.0	76122.0	151.1
FSB 78A	50172.0	74757.0	155.3
FSB 78B	50178.0	74765.0	153.7
FSB 79A	50149.0	73664.0	157.4
FSB 79B	50159.0	73666.0	157.2
FSB 87A	50115.0	75601.0	153.3
FSB 87B	50104.0	75597.0	150.4
FSB 96A	49778.0	74882.0	152.1
FSB 96AR	49746.0	74914.0	153.1
FSB 97A	49965.0	75171.0	151.6
FSB 98A	50121.0	75389.0	150.4
FSB 98AR	50105.0	75362.0	152.0
FSB 99A	50314.0	75675.0	150.2
FSB100A	50958.0	75534.0	150.9
FSB101A	51191.0	75719.0	151.0
FSB112A	48809.0	74231.0	153.6
FSB113A	51068.0	74167.0	158.6
FSB114A	52046.0	75297.0	155.5
FSB120A	49175.0	75538.0	148.3
HC 1A	61867.0	71755.0	175.8
HC 2A	61866.0	71794.0	176.3
HC 2B	61876.0	71785.0	176.0
HSB 65A	58436.0	72436.0	170.4
HSB 68A	56892.0	71526.0	171.0

Table A6. (cont'd)

Well Label	SRS East (ft)	SRS North (ft)	Elevation (ft)
HSB 69A	56465.0	71549.0	171.4
HSB 83A	58606.0	71648.0	172.5
HSB 84A	56359.0	71586.0	171.2
HSB 85A	58943.0	73791.0	168.3
HSB 86A	55985.0	72520.0	167.8
HSB117A	55170.0	72733.0	166.3
HSB118A	55775.0	72696.0	166.8
HSB119A	56100.0	73082.0	166.2
HSB120A	56431.0	73395.0	165.6
HSB121A	57389.0	72024.0	170.8
HSB122A	57747.0	72195.0	170.5
HSB123A	58124.0	72189.0	171.8
HSB124A	58514.0	72199.0	191.7
HSB124AR	58531.0	72202.0	172.4
HSB139A	57365.0	71127.0	172.8
HSB140A	56535.0	70050.0	175.8
HSB141A	59168.0	71213.0	175.0
HSB144A	56200.0	71892.0	170.9
HSB146A	58454.0	70478.0	176.1
P 27B	64000.0	70405.0	181.2
YSC 1A	65438.0	78039.0	161.3
YSC 2A	66100.0	78311.0	162.6
YSC 5A	67134.0	74295.0	180.5

Table A7. Hydraulic head data used to create a head contour map for the "upper" aquifer zone (Figure 14).

Well Label	SRS East (ft)	SRS North (ft)	Head (ft)
BG 52	55524.0	75910.0	229.5
BG 53	55073.0	76157.0	229.3
BG 54	54830.0	75837.0	228.5
BG 55	54590.0	75525.0	227.1
BG 56	54481.0	75206.0	227.6
BG 57	54820.0	75000.0	225.9
BG 58	55162.0	74790.0	227.3
BG 59	55508.0	74593.0	230.0
BG 60	55850.0	74386.0	231.0
BG 61	56360.0	74075.0	233.1
BG 62	56530.0	73971.0	234.3
BG 63	56870.0	73754.0	236.6
BG 64	57212.0	73547.0	239.4
BG 65	57552.0	73340.0	237.4
BG 66	57805.0	73585.0	236.5
BG 67	57902.0	73954.0	236.7
BG 104	59888.0	77038.0	224.6
BG 107	60120.0	74803.0	235.8
BG 108	59827.0	74383.0	238.8
BG 109	59626.0	73926.0	240.4
BG 110	59277.0	73354.0	241.4
BGO 1D	58779.0	73737.0	238.6
BGO 2D	58809.0	74552.0	238.6
BGO 3D	58809.0	75351.0	235.8
BGO 4D	58803.0	76150.0	232.4
BGO 5D	58784.0	76477.0	231.3
BGO 6D	58297.0	76487.0	231.5
BGO 7D	57917.0	76494.0	234.2
BGO 8D	57617.0	76588.0	234.4
BGO 9D	57478.0	76811.0	231.8
BGO 10D	57030.0	76805.0	231.9
BGO 10DR	57073.0	76804.0	232.5
BGO 11D	56651.0	76805.0	231.0
BGO 12D	56231.0	76805.0	230.8
BGO 13D	55840.0	76805.0	230.0
BGO 14DR	55789.0	76322.0	231.7
BGO 15D	55859.0	75973.0	229.6
BGO 16D	56202.0	75751.0	230.7
BGO 17D	56399.0	75599.0	230.7
BGO 17DR	56407.0	75604.0	232.9
BGO 18D	56711.0	75600.0	231.9
BGO 19D	56997.0	75350.0	232.1
BGO 20D	57113.0	74962.0	234.1
BGO 21D	57470.0	74688.0	234.7
BGO 22D	57817.0	74482.0	232.4
BGO 22DR	57831.0	74471.0	237.9
BGO 23D	58133.0	74238.0	235.9
BGO 24D	58438.0	74012.0	236.7
BGO 26D	55015.0	76128.0	227.7
BGO 27D	54680.0	75677.0	227.4
BGO 28D	54457.0	75348.0	226.1
BGO 29D	54099.0	75592.0	227.5

Table A7. (cont'd)

Well Label	SRS East (ft)	SRS North (ft)	Head (ft)			
BGO 30D	54499.0	75187.0	225.7			
BGO 31D	54841.0	74985.0	226.6			
BGO 32D	55250.0	74727.0	227.5			
BGO 33D	55695.0	74468.0	230.2			
BGO 34D	56082.0	74228.0	232.8			
BGO 35D	56556.0	73946.0	234.3			
BGO 36D	56888.0	73743.0	236.4			
BGO 37D	57292.0	73490.0	237.7			
BGO 38D	57557.0	73329.0	235.3			
BGO 39D	57831.0	73583.0	235.0			
BGO 40D	54638.0	76125.0	223.6			
BGO 44D	57910.0	76759.0	232.7			
BGO 45D	54585.0	75854.0	228.8			
BGO 46D	54420.0	75033.0	226.4			
BGO 47D	54922.0	74739.0	227.4			
BGO 48D	55121.0	74586.0	227.8			
BGO 49D	56198.0	73931.0	235.8			
BGO 50D	54209.0	75181.0	226.2			
BGX 1D	58608.0	76809.0	230.0			
BGX 9D	59522.0	76936.0	227.3			
BGX 10D	59765.0	76183.0	226.6			
BGX 11D	59581.0	75300.0	236.8			
BGX 12D	59674.0	74410.0	240.4			
BRR 1D	50588.0	77365.0	216.6			
BRR 2D	50306.0	77431.0	215.4			
BRR 3D	50203.0	77398.0	215.1			
BRR 4D	50104.0	77360.0	214.8			
BRR 5D	50009.0	77266.0	215.1			
FAC 3	55322.0	78018.0	230.5			
FAC 4	55472.0	78223.0	228.9			
FAC 5	55241.0	77960.0	224.3			
FAC 5P	55314.0	78175.0	230.6			
FAC 7	55356.0	78123.0	221.8			
FAC 8	55366.0	78090.0	226.5			
FAL 1	53756.0	78115.0	218.7			
FAL 2	53757.0	78231.0	217.1			
FCA 1N				53675.0	79037.0	299.2
FCA 2C				53712.0	78296.0	298.0
FCA 2D	53715.0	78295.0	225.4			
FCA 9D	53733.0	78600.0	225.6			
FCA 10A	53571.0	78640.0	225.3			
FCA 10C				53717.0	78642.0	302.3
FCA 10D	53732.0	78640.0	226.5			
FCA 16A	53568.0	78899.0	225.2			
FCA 16D	53719.0	78898.0	225.2			
FCA 16T				53579.0	78898.0	297.6
FCA 19D	53719.0	78271.0	217.0			
FCB 2	55046.0	76679.0	231.0			
FCB 3	54874.0	76427.0	223.2			
FCB 5	54773.0	76492.0	228.5			
FCB 6	54733.0	76582.0	228.9			
FET 1D	53299.0	76165.0	223.4			
FET 2D	52981.0	76045.0	222.0			

Table A7. (cont'd)

Well Label	SRS East (ft)	SRS North (ft)	Head (ft)
FET 3D	53025.0	75961.0	222.0
FET 4D	53149.0	75959.0	222.6
FSB 76	51388.0	76141.0	218.3
FSB 77	50713.0	75129.0	212.7
FSB 78	50164.0	74764.0	209.2
FSB 79	50139.0	73663.0	202.0
FSB 87D	50081.0	75586.0	213.5
FSB 88D	51527.0	75621.0	215.5
FSB 89D	51335.0	75548.0	214.9
FSB 90D	51140.0	75376.0	214.5
FSB 91D	50946.0	75207.0	212.9
FSB 92D	50557.0	75045.0	211.5
FSB 93D	50452.0	74888.0	210.8
FSB 94DR	50162.0	74869.0	210.6
FSB 95D	50008.0	74977.0	209.7
FSB 95DR	49996.0	74991.0	210.6
FSB 97D	49975.0	75188.0	210.5
FSB 98D	50111.0	75371.0	212.9
FSB 99D	50326.0	75691.0	211.8
FSB104D	49255.0	73865.0	203.7
FSB105D	49833.0	75244.0	208.5
FSB105DR	49841.0	75258.0	211.4
FSB106D	50636.0	74193.0	206.9
FSB107D	51149.0	75177.0	213.2
FSB108D	51142.0	76260.0	217.2
FSB109D	50488.0	75855.0	213.1
FSB110D	50141.0	74193.0	205.1
FSB111D	51515.0	75382.0	214.5
FSB112D	48780.0	74223.0	206.7
FSB113D	51098.0	74154.0	208.0
FSB114D	52018.0	75278.0	217.4
FSB115D	49728.0	72504.0	191.8
FSB116D	50629.0	72727.0	192.2
FSB117D	50486.0	74070.0	205.5
FSB118D	51276.0	74697.0	211.5
FSB119D	50600.0	74599.0	208.9
FSB120D	49163.0	75568.0	210.4
FSB121DR	48429.0	75151.0	208.5
FSB122D	48201.0	73865.0	204.3
FSB123D	51734.0	74562.0	212.7
FSL 1D	52992.0	79063.0	225.2
FSL 2D	52790.0	78636.0	226.7
FSL 3D	52465.0	77765.0	224.2
FSL 4D	52230.0	77452.0	218.9
FSL 5D	51903.0	77047.0	222.4
FSL 6D	51727.0	76733.0	221.2
FSL 7D	51485.0	76327.0	220.5
FSL 8D	51513.0	76054.0	219.7
FSL 9D	51543.0	75768.0	218.6
FSS 1D	53897.0	75257.0	223.5
FSS 2D	53918.0	75103.0	223.0
FSS 3D	53548.0	74960.0	220.7
FSS 4D	52876.0	75537.0	218.3

Table A7. (cont'd)

Well Label	SRS East (ft)	SRS North (ft)	Head (ft)
FTF 1	53179.0	77413.0	229.4
FTF 2	53275.0	77336.0	225.3
FTF 3	53244.0	77235.0	224.1
FTF 4	53268.0	77132.0	224.4
FTF 5	53168.0	77035.0	225.1
FTF 6	53062.0	77151.0	224.1
FTF 8	53059.0	77336.0	227.5
FTF 9	52769.0	77482.0	223.6
FTF 10	52905.0	77336.0	223.8
FTF 11	52748.0	77180.0	225.2
FTF 12	52648.0	77321.0	226.8
FTF 13	53098.0	76637.0	224.7
FTF 15	53230.0	76732.0	226.1
FTF 16	52879.0	76758.0	223.1
FTF 17	52884.0	76872.0	223.0
FTF 18	52879.0	76955.0	222.8
FTF 19	52670.0	77139.0	222.2
FTF 20	52500.0	77015.0	221.8
FTF 21	52498.0	76866.0	222.8
FTF 22	52494.0	76751.0	221.6
FTF 23	52660.0	76611.0	222.0
FTF 25A	52868.0	77308.0	223.3
FTF 26	52875.0	77250.0	223.3
FTF 27	52823.0	77227.0	223.4
HAC 1	61415.0	72171.0	269.1
HAC 2	61366.0	72220.0	268.6
HAC 3	61313.0	72183.0	268.9
HAC 4	61372.0	72120.0	269.2
HAP 1	63398.0	71209.0	270.7
HAP 2	63519.0	71122.0	270.1
HC 1E	61864.0	71746.0	275.0
HC 2E	61861.0	71784.0	270.5
HC 2F	61861.0	71780.0	274.3
HC 4B	63408.0	71596.0	268.0
HC 5B	61705.0	73266.0	256.1
HC 6B	62070.0	72150.0	268.9
HC 11C	62131.0	74496.0	236.6
HCA 1	63109.0	72521.0	268.9
HCA 3	63108.0	72651.0	268.7
HCA 4	62942.0	72523.0	268.6
HCB 1	63921.0	71426.0	262.9
HCB 2	63797.0	71289.0	267.8
HCB 3	63919.0	71098.0	266.1
HET 1D	60546.0	71948.0	267.4
HET 2D	60094.0	72006.0	258.2
HET 3D	60110.0	72093.0	258.6
HET 4D	60166.0	72178.0	259.0
HR3 11	60146.0	71402.0	259.3
HR3 13	60065.0	71649.0	258.1
HR8 11	59559.0	71945.0	245.8
HR8 12	59330.0	71780.0	239.3
HR8 13	59300.0	71559.0	237.8
HR8 14	59612.0	71431.0	244.0

Table A7. (cont'd)

Well Label	SRS East (ft)	SRS North (ft)	Head (ft)
HSB 65	58432.0	72425.0	234.3
HSB 65C	58447.0	72439.0	233.2
HSB 66	56928.0	72429.0	226.9
HSB 67	58424.0	71505.0	225.2
HSB 68	56901.0	71528.0	224.4
HSB 69	56475.0	71546.0	220.7
HSB 70	55758.0	72606.0	227.5
HSB 71	55279.0	72875.0	225.1
HSB 83D	58601.0	71628.0	225.8
HSB 84D	56349.0	71583.0	219.8
HSB 85C	58947.0	73802.0	239.0
HSB 86D	55996.0	72522.0	225.9
HSB100D	58796.0	72073.0	233.3
HSB101D	58594.0	71997.0	230.8
HSB102D	58393.0	71952.0	228.0
HSB103D	58315.0	71588.0	226.0
HSB104D	58075.0	71370.0	225.4
HSB105D	57877.0	71454.0	225.8
HSB106D	57644.0	71727.0	226.3
HSB107D	57412.0	71696.0	225.1
HSB108D	57145.0	71688.0	223.9
HSB109D	56885.0	71685.0	223.4
HSB110D	56672.0	71785.0	222.8
HSB111D	56494.0	71926.0	222.6
HSB111E	56487.0	71932.0	222.7
HSB112D	56408.0	72161.0	223.7
HSB112E	56399.0	72166.0	223.6
HSB113D	56164.0	72302.0	223.6
HSB114D	56104.0	72474.0	224.6
HSB115D	56039.0	72662.0	225.5
HSB116D	55988.0	72898.0	226.4
HSB117D	55155.0	72747.0	224.8
HSB125D	58584.0	71498.0	221.6
HSB126D	57169.0	70633.0	204.9
HSB127D	56788.0	71218.0	218.5
HSB129D	55103.0	71837.0	208.5
HSB130D	54651.0	70757.0	200.1
HSB131D	56891.0	70365.0	205.2
HSB132D	58799.0	71469.0	221.7
HSB133D	59102.0	71943.0	234.8
HSB134D	58296.0	71217.0	222.5
HSB135D	56552.0	71396.0	218.6
HSB136D	55941.0	71906.0	221.5
HSB137D	55696.0	72278.0	223.0
HSB138D	55260.0	73160.0	224.0
HSB139D	57384.0	71133.0	223.3
HSB140D	56560.0	70036.0	215.4
HSB141D	59170.0	71184.0	243.5
HSB142D	53493.0	73113.0	198.3
HSB143D	52774.0	73754.0	213.9
HSB145D	57753.0	71088.0	221.7
HSB146D	58493.0	70469.0	223.0
HSB147D	55804.0	73827.0	234.0

Table A7. (cont'd)

Well Label	SRS East (ft)	SRS North (ft)	Head (ft)
HSB148D	55355.0	70160.0	214.9
HSB149D	57286.0	71338.0	224.5
HSB150D	58692.0	71692.0	228.1
HSB151D	54026.0	72997.0	208.0
HSB152D	54362.0	72011.0	206.4
HSL 1D	58925.0	72179.0	235.6
HSL 2D	59423.0	72190.0	242.1
HSL 3D	59770.0	72251.0	250.0
HSL 4D	60171.0	72453.0	261.5
HSL 5D	60339.0	72562.0	263.8
HSL 6D	60531.0	72659.0	260.6
HSL 7D	60723.0	72674.0	260.3
HSL 8D	61117.0	72688.0	261.5
HSS 1D	64675.0	67610.0	268.6
HSS 2D	64785.0	67355.0	267.2
HSS 3D	64709.0	68257.0	281.5
HTF 1	62067.0	71745.0	271.8
HTF 2	62175.0	71610.0	273.0
HTF 4	61942.0	71630.0	272.5
HTF 5	62110.0	71390.0	277.6
HTF 6	62228.0	71259.0	276.4
HTF 7	62112.0	71130.0	275.6
HTF 8	61965.0	71270.0	274.5
HTF 9	61698.0	71652.0	271.5
HTF 10	61838.0	71520.0	270.8
HTF 11	61722.0	71398.0	271.6
HTF 12	61593.0	71520.0	270.7
HTF 13	61586.0	71856.0	273.4
HTF 14	61462.0	71858.0	273.2
HTF 15	61353.0	71700.0	272.8
HTF 16	61950.0	72150.0	269.0
HTF 17	61188.0	72600.0	262.8
HTF 18	61223.0	71771.0	270.5
HTF 19	61079.0	71902.0	268.5
HTF 20	61086.0	72073.0	267.3
HTF 21	61261.0	71998.0	268.5
HTF 22	62553.0	71363.0	273.9
HTF 23	62670.0	71363.0	274.1
HTF 24	62775.0	71362.0	273.9
HTF 25	62902.0	71224.0	273.9
HTF 26	62815.0	71090.0	274.0
HTF 27	62660.0	71057.0	274.2
HTF 28	62515.0	71080.0	275.7
HTF 29	62414.0	71229.0	274.2
HTF 31	62662.0	70747.0	274.6
HTF 32	62807.0	70880.0	273.9
HTF 34	61978.0	71144.0	272.6
MGA 36	57891.0	73904.0	238.4
MGC 9	55610.0	75372.0	229.6
MGC 11	55770.0	75252.0	232.2
MGC 23	56726.0	74528.0	236.4
MGC 32	57448.0	73982.0	245.7
MGE 9	55489.0	75215.0	229.7

Table A7. (cont'd)

Well Label	SRS East (ft)	SRS North (ft)	Head (ft)
MGE 21	56446.0	74487.0	235.1
MGG 15	55851.0	74699.0	233.1
MGG 19	56174.0	74456.0	232.9
MGG 23	56491.0	74214.0	235.8
MGG 28	56895.0	73905.0	237.2
MGG 36	57541.0	73413.0	238.8
NBG 1	53879.0	79300.0	224.1
NBG 2	53958.0	79099.0	224.8
NBG 3	54068.0	78939.0	218.1
NBG 4	54329.0	78942.0	217.1
NBG 5	54515.0	78943.0	217.6
P 27D	64008.0	70376.0	266.9
SBG 1	63749.0	74619.0	237.8
SBG 2	64939.0	74570.0	237.6
SBG 3	65265.0	73699.0	236.9
SBG 4	65010.0	72399.0	240.6
SBG 5	64499.0	72208.0	249.1
SBG 6	63860.0	73599.0	244.2
SCA 2	64697.0	73850.0	242.2
SCA 3	64571.0	73959.0	241.3
SCA 3A	64571.0	73965.0	270.9
SCA 4	64563.0	73856.0	241.7
SCA 4A	64567.0	73855.0	269.1
SCA 5	64630.0	74092.0	242.0
SCA 6	64637.0	73706.0	242.2
SLP 1	64449.0	72958.0	244.8
SLP 2	64529.0	72863.0	244.4
YSC 1C	65855.0	78186.0	217.5
YSC 2D	66130.0	78320.0	217.1
Z 2	53181.0	74785.0	218.1
Z 3	51328.0	75086.0	212.2
Z 8	51584.0	76640.0	218.0
Z 9	50570.0	77732.0	214.8
Z 11	61750.0	72539.0	296.4
Z 12	61400.0	71198.0	274.4
Z 13	62203.0	70785.0	274.6
Z 15	63419.0	72802.0	263.7
ZBG 1	65584.0	76584.0	234.1
ZBG 1A	65598.0	76588.0	279.7
ZBG 2	67472.0	76170.0	221.5
ZDT 1	65114.0	71644.0	239.5
ZDT 2	65059.0	71696.0	241.1
ZW 4	56556.0	77667.0	232.6
ZW 5	54708.0	75767.0	227.5
ZW 7	60300.0	72399.0	265.8
ZW 8	63801.0	70800.0	270.8
ZW 9	61400.0	73198.0	251.9
ZW 10	63401.0	73212.0	249.7
CC-9	54065.0	73295.0	214.9
CC-13	54390.0	73060.0	216.4
CC-17	54710.0	72820.0	220.0
GG-17	54470.0	72495.0	207.8
GG-21	54793.0	72260.0	211.8

Table A7. (cont'd)

Well Label	SRS East (ft)	SRS North (ft)	Head (ft)
M-5	54690.0	74820.0	228.6
M-9	55020.0	74590.0	228.0
M-17	55650.0	74100.0	235.0
M-21	55985.0	73870.0	237.9
Q-5	54470.0	74500.0	226.0
Q-9	54775.0	74260.0	226.9
Q-13	55100.0	74020.0	227.4
Q-17	55425.0	73780.0	241.6
Q-21	55745.0	73540.0	233.1
S-3	54070.0	74492.0	224.0
S-4	53678.0	74319.0	222.1
S-5	53370.0	73913.0	221.0
S-6	53222.0	73440.0	204.6
S-9	53785.0	74919.0	226.1
S-15	53930.0	75381.0	231.5
S-16	53491.0	75223.0	226.2
U-5	54219.0	74176.0	223.0
U-9	54540.0	73945.0	223.8
U-13	54863.0	73700.0	232.4
U-17	55185.0	73470.0	226.2
U-21	55506.0	73225.0	227.3
Y-7	54140.0	73730.0	218.2
Y-9	54300.0	73615.0	220.8
Y-13	54625.0	73380.0	223.2
Y-17	54950.0	73140.0	224.7
Y-21	55270.0	72900.0	224.0
4Mile_Br	49884.0	72820.2	180.0
4Mile_Br	49963.2	72807.8	180.1
4Mile_Br	50029.3	72800.3	180.3
4Mile_Br	50094.4	72804.4	180.4
4Mile_Br	50156.5	72814.8	180.5
4Mile_Br	50213.9	72829.3	180.6
4Mile_Br	50266.4	72845.2	180.7
4Mile_Br	50312.7	72847.3	180.8
4Mile_Br	50359.3	72852.2	180.9
4Mile_Br	50404.7	72852.2	181.0
4Mile_Br	50481.1	72869.6	181.1
4Mile_Br	50570.8	72884.1	181.3
4Mile_Br	50615.8	72896.9	181.4
4Mile_Br	50670.4	72916.1	181.5
4Mile_Br	50729.8	72931.6	181.6
4Mile_Br	50781.0	72948.4	181.7
4Mile_Br	50847.4	72971.2	181.8
4Mile_Br	50896.9	72994.3	181.9
4Mile_Br	50926.4	73005.5	182.0
4Mile_Br	50974.7	73032.5	182.1
4Mile_Br	51021.0	73058.6	182.2
4Mile_Br	51076.3	73086.1	182.3
4Mile_Br	51118.2	73101.0	182.4
4Mile_Br	51156.1	73111.9	182.4
4Mile_Br	51209.5	73113.9	182.5
4Mile_Br	51254.2	73116.1	182.6
4Mile_Br	51301.0	73117.6	182.7

Table A7. (cont'd)

Well Label	SRS East (ft)	SRS North (ft)	Head (ft)
4Mile_Br	51341.6	73101.1	182.8
4Mile_Br	51373.5	73094.0	182.8
4Mile_Br	51403.9	73091.6	182.9
4Mile_Br	51442.9	73074.4	183.0
4Mile_Br	51488.1	73063.5	183.1
4Mile_Br	51559.4	73057.5	183.2
4Mile_Br	51616.1	73055.1	183.3
4Mile_Br	51653.2	73057.8	183.4
4Mile_Br	51685.0	73062.6	183.4
4Mile_Br	51747.9	73052.1	183.6
4Mile_Br	51788.8	73046.8	183.6
4Mile_Br	51843.4	73032.0	183.7
4Mile_Br	51895.0	73023.1	183.8
4Mile_Br	51944.1	73011.2	183.9
4Mile_Br	51982.2	73008.6	184.0
4Mile_Br	52022.8	73008.2	184.1
4Mile_Br	52085.0	72993.5	184.2
4Mile_Br	52149.6	72979.0	184.3
4Mile_Br	52225.0	72969.6	184.4
4Mile_Br	52263.9	72959.8	184.5
4Mile_Br	52296.2	72960.0	184.6
4Mile_Br	52329.5	72945.9	184.6
4Mile_Br	52365.2	72944.7	184.7
4Mile_Br	52398.7	72934.2	184.7
4Mile_Br	52439.4	72932.9	184.8
4Mile_Br	52472.9	72918.5	184.9
4Mile_Br	52537.9	72904.4	185.0
4Mile_Br	52584.6	72891.5	185.1
4Mile_Br	52619.1	72874.2	185.1
4Mile_Br	52679.8	72832.6	185.3
4Mile_Br	52747.9	72774.8	185.4
4Mile_Br	52776.4	72737.6	185.5
4Mile_Br	52819.9	72699.6	185.6
4Mile_Br	52847.2	72675.8	185.7
4Mile_Br	52890.9	72658.5	185.7
4Mile_Br	52936.6	72630.3	185.8
4Mile_Br	52995.8	72593.8	186.0
4Mile_Br	53019.6	72583.0	186.0
4Mile_Br	53045.9	72575.7	186.2
4Mile_Br	53084.2	72564.0	186.6
4Mile_Br	53122.8	72540.2	187.0
4Mile_Br	53163.8	72527.4	187.4
4Mile_Br	53198.7	72513.9	187.7
4Mile_Br	53230.4	72500.8	188.0
4Mile_Br	53270.5	72484.4	189.1
4Mile_Br	53300.4	72471.1	190.0
4Mile_Br	53365.3	72423.0	190.2
4Mile_Br	53422.6	72372.8	190.3
4Mile_Br	53442.4	72354.9	190.4
4Mile_Br	53480.7	72340.3	190.4
4Mile_Br	53529.7	72301.9	190.6
4Mile_Br	53585.3	72258.2	190.7
4Mile_Br	53652.3	72204.3	190.9

Table A7. (cont'd)

Well Label	SRS East (ft)	SRS North (ft)	Head (ft)
4Mile_Br	53697.4	72172.5	191.0
4Mile_Br	53741.1	72133.4	191.1
4Mile_Br	53780.8	72088.7	191.2
4Mile_Br	53796.6	72069.9	191.3
4Mile_Br	53803.6	72040.7	191.3
4Mile_Br	53832.5	71977.4	191.4
4Mile_Br	53841.1	71943.6	191.5
4Mile_Br	53860.6	71911.3	191.6
4Mile_Br	53863.9	71899.7	191.6
4Mile_Br	53884.0	71886.7	191.7
4Mile_Br	53900.2	71857.0	191.7
4Mile_Br	53942.3	71808.9	191.8
4Mile_Br	53976.6	71778.1	191.9
4Mile_Br	54002.5	71758.8	192.0
4Mile_Br	54043.1	71735.9	192.1
4Mile_Br	54060.4	71721.0	192.2
4Mile_Br	54099.0	71701.8	192.3
4Mile_Br	54156.8	71663.4	192.5
4Mile_Br	54213.0	71634.9	192.7
4Mile_Br	54272.0	71591.5	192.9
4Mile_Br	54343.1	71563.3	193.1
4Mile_Br	54409.3	71534.9	193.3
4Mile_Br	54479.6	71493.9	193.5
4Mile_Br	54555.6	71446.2	193.7
4Mile_Br	54605.3	71415.0	193.9
4Mile_Br	54633.1	71395.7	194.0
4Mile_Br	54705.9	71347.9	194.3
4Mile_Br	54762.3	71307.2	194.6
4Mile_Br	54793.7	71285.1	194.7
4Mile_Br	54855.2	71193.5	195.1
4Mile_Br	54889.4	71144.6	195.3
4Mile_Br	54935.9	71089.0	195.6
4Mile_Br	54989.8	71037.5	195.9
4Mile_Br	55013.0	71014.5	196.0
4Mile_Br	55061.7	70959.2	196.2
4Mile_Br	55126.7	70934.2	196.5
4Mile_Br	55159.8	70917.8	196.7
4Mile_Br	55215.6	70874.7	196.9
4Mile_Br	55280.0	70848.4	197.2
4Mile_Br	55372.3	70857.5	197.5
4Mile_Br	55450.6	70862.4	197.8
4Mile_Br	55498.7	70863.0	198.0
4Mile_Br	55557.6	70871.5	198.1
4Mile_Br	55603.8	70880.6	198.2
4Mile_Br	55659.9	70875.0	198.3
4Mile_Br	55713.8	70852.4	198.4
4Mile_Br	55782.9	70848.1	198.5
4Mile_Br	55859.7	70814.2	198.6
4Mile_Br	55912.6	70790.3	198.7
4Mile_Br	56015.1	70771.7	198.9
4Mile_Br	56090.8	70749.1	199.0
4Mile_Br	56143.7	70735.9	199.1
4Mile_Br	56177.0	70737.8	199.2

Table A7. (cont'd)

Well Label	SRS East (ft)	SRS North (ft)	Head (ft)
4Mile_Br	56234.0	70721.8	199.3
4Mile_Br	56330.0	70688.2	199.4
4Mile_Br	56400.8	70660.8	199.6
4Mile_Br	56463.6	70629.9	199.7
4Mile_Br	56555.9	70592.3	199.9
4Mile_Br	56634.3	70562.1	200.0
4Mile_Br	56712.4	70542.6	200.2
4Mile_Br	56793.6	70519.6	200.5
4Mile_Br	56865.3	70507.2	200.6
4Mile_Br	56906.4	70491.2	200.8
4Mile_Br	56954.6	70484.6	200.9
4Mile_Br	56993.1	70458.7	201.0
4Mile_Br	57092.5	70386.0	201.4
4Mile_Br	57149.5	70338.1	201.6
4Mile_Br	57171.6	70317.5	201.6
4Mile_Br	57205.8	70287.9	201.8
4Mile_Br	57249.5	70271.1	201.9
4Mile_Br	57287.6	70266.0	202.0
4Mile_Br	57309.4	70257.2	202.1
4Mile_Br	57322.4	70242.9	202.2
4Mile_Br	57353.6	70227.2	202.3
4Mile_Br	57361.0	70205.9	202.5
4Mile_Br	57370.3	70178.8	202.7
4Mile_Br	57366.4	70141.3	203.0
4Mile_Br	57359.6	70127.9	203.1
4Mile_Br	57341.9	70107.2	203.2
4Mile_Br	57330.0	70070.4	203.5
4Mile_Br	57325.5	70039.9	203.7
4Mile_Br	57317.1	69997.5	204.0
4Mile_Br	57314.1	69982.7	204.1
4Mile_Br	57305.0	69951.2	204.2
4Mile_Br	57309.5	69899.4	204.4
4Mile_Br	57318.6	69840.3	204.7
4Mile_Br	57329.0	69773.8	205.0
4Mile_Br	57339.4	69739.5	205.1
4Mile_Br	57361.8	69707.9	205.3
4Mile_Br	57376.4	69663.2	205.5
4Mile_Br	57390.7	69643.3	205.6
4Mile_Br	57408.3	69624.4	205.7
4Mile_Br	57422.9	69599.6	205.8
4Mile_Br	57447.1	69577.4	205.9
4Mile_Br	57456.1	69563.2	206.0
4Mile_Br	57471.1	69544.1	206.0
4Mile_Br	57516.6	69519.2	206.2
4Mile_Br	57551.2	69490.2	206.3
4Mile_Br	57603.3	69477.5	206.4
4Mile_Br	57668.6	69451.4	206.5
4Mile_Br	57729.7	69426.7	206.7
4Mile_Br	57765.0	69415.5	206.7
4Mile_Br	57805.5	69410.8	206.8
4Mile_Br	57843.9	69392.5	206.9
4Mile_Br	57939.8	69374.1	207.1
4Mile_Br	57992.1	69368.5	207.2

Table A7. (cont'd)

Well Label	SRS East (ft)	SRS North (ft)	Head (ft)
4Mile_Br	58043.2	69353.3	207.3
4Mile_Br	58097.9	69345.3	207.4
4Mile_Br	58145.1	69312.3	207.6
4Mile_Br	58174.9	69265.3	207.7
4Mile_Br	58201.5	69217.7	207.8
4Mile_Br	58230.9	69163.8	207.9
4Mile_Br	58260.3	69114.8	208.0
4Mile_Br	58301.1	69033.0	208.2
4Mile_Br	58328.3	68965.3	208.4
4Mile_Br	58364.6	68892.5	208.6
4Mile_Br	58392.6	68824.5	208.7
4Mile_Br	58416.4	68737.0	208.9
4Mile_Br	58438.7	68695.9	209.1
4Mile_Br	58472.3	68657.1	209.2
4Mile_Br	58492.1	68611.0	209.3
4Mile_Br	58531.2	68551.2	209.4
4Mile_Br	58567.9	68490.5	209.6
4Mile_Br	58597.2	68415.0	209.8
4Mile_Br	58622.8	68330.8	210.0
4Mile_Br	58626.5	68244.6	210.2
4Mile_Br	58626.3	68151.2	210.5
4Mile_Br	58624.3	68075.4	210.7
4Mile_Br	58632.7	68006.0	210.9
4Mile_Br	58643.2	67964.6	211.0
4Mile_Br	58681.6	67926.2	211.2
4Mile_Br	58705.2	67886.7	211.3
4Mile_Br	58760.0	67817.2	211.6
4Mile_Br	58799.1	67776.5	211.7
4Mile_Br	58863.3	67747.2	211.9
4Mile_Br	58911.9	67733.9	212.0
Old_Eff	53093.4	72547.3	189.9
Old_Eff	53115.3	72575.5	190.0
Old_Eff	53122.5	72604.9	190.0
Old_Eff	53135.1	72630.4	190.0
Old_Eff	53156.6	72658.3	190.2
Old_Eff	53189.8	72679.7	190.4
Old_Eff	53221.2	72700.6	190.5
Old_Eff	53261.6	72723.4	190.8
Old_Eff	53283.4	72739.2	190.9
Old_Eff	53286.7	72764.2	191.0
Old_Eff	53278.6	72839.3	192.0
Old_Eff	53289.0	72907.8	193.0
Old_Eff	53299.9	72970.1	194.0
Old_Eff	53327.3	73072.9	195.0
Old_Eff	53346.3	73112.7	196.0
Old_Eff	53399.8	73172.6	197.0
Old_Eff	53427.1	73199.9	198.0
Old_Eff	53451.5	73223.8	199.0
Old_Eff	53463.3	73234.7	200.0
Old_Eff	53494.1	73266.7	201.0
Old_Eff	53535.4	73299.6	202.0
Old_Eff	53553.9	73310.0	203.0
Old_Eff	53568.1	73317.5	204.0

Table A7. (cont'd)

Well Label	SRS East (ft)	SRS North (ft)	Head (ft)			
Old_Eff	53582.5	73325.9	205.0			
Old_Eff	53645.6	73353.1	206.0			
Old_Eff	53783.5	73384.2	207.0			
Old_Eff	53876.6	73425.9	208.0			
Old_Eff	53967.2	73477.9	208.8			
Old_Eff	53981.3	73505.4	209.0			
Old_Eff	53997.3	73560.0	209.5			
Old_Eff	53998.1	73622.6	210.0			
Old_Eff	54006.0	73647.6	211.0			
Old_Eff	54017.8	73687.4	212.0			
Old_Eff	54017.9	73716.3	213.0			
Old_Eff	54015.3	73740.4	214.0			
Old_Eff	54018.4	73756.6	215.0			
Old_Eff				54026.7	73786.6	216.0
Old_Eff				54029.8	73811.1	217.0
Old_Eff				54033.8	73833.6	218.0
Old_Eff				54032.6	73857.3	219.0
Old_Eff				54028.4	73873.2	220.0
Old_Eff				54028.6	73896.5	221.0
Old_Eff				54034.0	73938.8	222.0
Old_Eff				54044.2	73976.3	222.5
Old_Eff				54040.3	74018.4	223.0
Old_Eff				54042.9	74064.2	224.0
Old_Eff				54047.6	74081.6	225.0
Old_Eff				54059.0	74108.1	226.0
Old_Eff				54068.8	74131.7	227.0
Old_Eff				54102.1	74202.2	228.0
Old_Eff				54132.3	74247.2	229.0
Old_Eff				54151.7	74273.4	230.0
Old_Eff				54166.8	74294.2	231.0
Old_Eff				54193.1	74322.5	232.0
Old_Eff				54216.4	74345.7	233.0
Old_Eff				54302.4	74423.3	234.0
Old_Eff				54363.2	74495.6	235.0
Old_Eff				54374.1	74518.0	236.0
Old_Eff				54374.7	74568.8	237.0
Old_Eff				54366.0	74614.9	238.0
Old_Eff				54365.5	74683.2	239.0
Old_Eff				54352.0	74721.4	240.0
Old_Eff				54296.5	74853.3	241.0
Old_Eff				54282.2	74904.8	242.0
Old_Eff				54233.1	74984.7	243.0
Old_Eff				54208.0	75036.3	244.0
Old_Eff				54201.4	75051.8	245.0
Old_Eff				54194.6	75065.1	246.0
Old_Eff				54181.4	75094.6	247.0
Old_Eff				54147.6	75134.8	248.0
Old_Eff				54119.4	75179.7	249.0
Old_Eff				54112.9	75198.5	250.0
NewRock1	53463.3	73234.7	200.0			
NewRock1	53470.1	73271.3	201.0			
NewRock1	53469.4	73317.2	202.0			
NewRock1	53468.9	73358.5	203.0			

Table A7. (cont'd)

Well Label	SRS East (ft)	SRS North (ft)	Head (ft)			
NewRock1	53473.5	73393.1	204.0			
NewRock1	53481.6	73413.7	205.0			
NewRock1	53514.1	73467.5	208.0			
NewRock1	53527.0	73527.9	210.0			
NewRock1	53549.6	73567.7	215.0			
NewRock1	53592.2	73621.4	220.0			
NewRock1				53617.0	73707.2	225.0
NewRock1				53640.2	73784.2	230.0
NewRock1				53664.9	73870.0	240.0
NewRock1				53678.9	73915.9	242.5
NewRock2	53493.5	73266.9	201.0			
NewRock2	53532.7	73308.3	202.0			
NewRock2	53554.3	73349.1	203.0			
NewRock2	53564.6	73394.2	204.0			
NewRock2	53568.4	73424.3	205.0			
NewRock2	53570.1	73450.3	210.0			
NewRock2	53571.7	73527.3	215.0			
NewRock2	53591.9	73621.9	220.0			
NewConcr				53682.5	73922.9	244.7
NewConcr				54095.2	75317.4	247.7
PseudoDa	51750.	72850.	185.	185.		
PseudoDa	51942.	72740.	186.	187.5		
PseudoDa	52100.	72600.	187.5	190.		
PseudoDa	52368.	72425.	191.	191.25		
PseudoDa	52690.	72190.	194.	192.5		
PseudoDa	52966.	71990.	195.	193.75		
PseudoDa	53300.	71750.	196.	195.		
PseudoDa	53589.	71523.	197.	196.25		
PseudoDa	53917.	71285.	198.	197.5		
PseudoDa	54270.	71031.	199.	198.75		

Table A8. Hydraulic head data used to create a head contour map for the "lower" aquifer zone (Figure 15).

Well Label	SRS East (ft)	SRS North (ft)	Head (ft)
BG 91	56649.0	78031.0	219.1
BG 92	56828.0	79019.0	209.0
BG 93	57160.0	79930.0	201.1
BG 94	57494.0	80867.0	191.4
BG 95	58407.0	80059.0	193.3
BG 96	58297.0	79396.0	198.5
BG 101	59277.0	78740.0	195.7
BG 103	59752.0	77883.0	200.4
BG 122	56789.0	78581.0	211.3
BGO 5C	58794.0	76476.0	216.6
BGO 6B	58346.0	76553.0	219.7
BGO 6C	58307.0	76487.0	220.1
BGO 8C	57618.0	76579.0	225.4
BGO 10B	56978.0	76982.0	220.9
BGO 10C	57041.0	76805.0	220.2
BGO 12C	56241.0	76805.0	220.0
BGO 12CR	56215.0	76806.0	222.4
BGO 13DR	55840.0	76824.0	232.2
BGO 14C	55839.0	76367.0	221.0
BGO 14CR	55789.0	76337.0	224.9
BGO 16B	56183.0	75767.0	220.3
BGO 27C	54671.0	75666.0	220.3
BGO 29C	54099.0	75577.0	223.9
BGO 30C	54512.0	75181.0	219.1
BGO 31C	54816.0	74978.0	225.5
BGO 33C	55681.0	74479.0	224.9
BGO 35C	56545.0	73953.0	228.3
BGO 37C	57279.0	73498.0	229.1
BGO 42C	55522.0	76404.0	224.4
BGO 43CR	56237.0	77035.0	226.6
BGO 43D	56238.0	77056.0	232.3
BGO 44B	57865.0	76756.0	221.9
BGO 44C	57894.0	76757.0	221.7
BGO 45B	54563.0	75840.0	220.6
BGO 45C	54577.0	75835.0	223.9
BGO 46B	54444.0	75012.0	218.9
BGO 46C	54433.0	75022.0	221.1
BGO 47C	54933.0	74752.0	223.7
BGO 48C	55124.0	74599.0	224.5
BGO 49C	56202.0	73917.0	229.0
BGO 50C	54197.0	75190.0	219.5
BGX 1C	58599.0	76820.0	216.9
BGX 2B	58256.0	77203.0	213.3
BGX 2D	58265.0	77192.0	216.3
BGX 3D	57780.0	77577.0	216.1
BGX 4C	57202.0	77886.0	215.9
BGX 4D	57186.0	77893.0	217.0
BGX 5D	57308.0	78402.0	210.6
BGX 6D	57524.0	78740.0	207.6
BGX 7D	58312.0	78349.0	207.7
BGX 8DR	58942.0	77589.0	206.5
BGX 12C	59675.0	74427.0	235.7

Table A8. (cont'd)

Well Label	SRS East (ft)	SRS North (ft)	Head (ft)
FAC 4	55472.0	78223.0	228.9
FBP 1A	51080.0	78893.0	206.8
FBP 4	51368.0	79320.0	211.6
FNB 1	54271.0	80151.0	210.8
FNB 2	54362.0	80442.0	207.0
FNB 3	54105.0	80553.0	209.2
FNB 4	53843.0	80409.0	213.1
FSB 76C	51396.0	76112.0	212.7
FSB 78C	50170.0	74772.0	207.7
FSB 79C	50171.0	73668.0	196.6
FSB 87C	50093.0	75591.0	208.4
FSB 88C	51518.0	75619.0	211.9
FSB 89C	51345.0	75553.0	211.4
FSB 90C	51148.0	75382.0	210.3
FSB 91C	50953.0	75213.0	210.3
FSB 93C	50458.0	74897.0	208.4
FSB 94C	50180.0	74869.0	207.7
FSB 95C	50016.0	74971.0	205.9
FSB 95CR	49987.0	75001.0	208.2
FSB 97C	49970.0	75179.0	207.7
FSB 98C	50116.0	75381.0	209.2
FSB 99C	50320.0	75683.0	209.2
FSB102C	50834.0	73582.0	195.1
FSB103C	49651.0	74210.0	202.3
FSB104C	49248.0	73872.0	200.5
FSB105C	49828.0	75234.0	207.2
FSB106C	50651.0	74190.0	201.1
FSB107C	51158.0	75184.0	209.7
FSB110C	50150.0	74190.0	201.6
FSB111C	51526.0	75383.0	211.1
FSB112C	48794.0	74227.0	202.6
FSB113C	51084.0	74160.0	203.1
FSB114C	52033.0	75288.0	213.8
FSB115C	49736.0	72515.0	184.2
FSB116C	50645.0	72725.0	189.6
FSB120C	49171.0	75549.0	206.8
FSB121C	48413.0	75155.0	205.0
FSB122C	48195.0	73881.0	200.5
FSB123C	51750.0	74566.0	210.8
HC 1B	61877.0	71745.0	254.9
HC 2C	61872.0	71784.0	254.2
HC 2D	61866.0	71784.0	256.3
HC 4A	63409.0	71606.0	244.7
HC 5A	61710.0	73265.0	213.8
HC 6A	62060.0	72150.0	252.2
HC 10B	61600.0	75801.0	208.4
HC 12B	59488.0	73186.0	241.6
HMD 1D	56973.0	78731.0	210.9
HMD 2D	57269.0	79665.0	202.3
HMD 3D	57745.0	79578.0	201.8
HMD 4D	58188.0	79160.0	201.9
HSB 65B	58439.0	72445.0	224.7
HSB 68B	56882.0	71525.0	217.8

Table A8. (cont'd)

Well Label	SRS East (ft)	SRS North (ft)	Head (ft)	
HSB 68C	56872.0	71524.0	218.6	
HSB 70C	55757.0	72597.0	223.9	
HSB 71C	55281.0	72866.0	223.1	
HSB 83B	58594.0	71639.0	223.2	
HSB 83C	58614.0	71636.0	225.1	
HSB 84B	56352.0	71603.0	211.2	
HSB 84C	56360.0	71597.0	214.5	
HSB 85B	58953.0	73789.0	233.9	
HSB 86B	55976.0	72519.0	223.0	
HSB 86C	55984.0	72529.0	225.8	
HSB100C	58806.0	72077.0	226.3	
HSB101C	58604.0	72001.0	225.3	
HSB102C	58399.0	71960.0	224.6	
HSB103C	58323.0	71593.0	223.6	
HSB104C	58082.0	71376.0	220.6	
HSB105C	57883.0	71447.0	219.7	
HSB106C	57651.0	71720.0	221.8	
HSB107C	57432.0	71698.0	219.5	
HSB108C	57155.0	71688.0	218.9	
HSB109C	56895.0	71684.0	219.0	
HSB110C	56680.0	71779.0	219.4	
HSB111C	56501.0	71919.0	220.7	
HSB112C	56417.0	72156.0	222.1	
HSB113C	56160.0	72312.0	222.6	
HSB114C	56107.0	72464.0	224.4	
HSB115C	56043.0	72653.0	225.2	
HSB116C	55989.0	72888.0	225.8	
HSB117C	55162.0	72740.0	222.6	
HSB125C	58592.0	71503.0	223.4	
HSB126C	57178.0	70627.0	203.6	
HSB127C	56792.0	71210.0	210.1	
HSB129C	55110.0	71830.0	205.4	
HSB130C	54643.0	70762.0	215.	199.7 <-- original data
HSB131C	56894.0	70374.0	203.4	
HSB132C	58787.0	71472.0	222.1	
HSB133C	59110.0	71949.0	230.4	
HSB134C	58289.0	71210.0	220.8	
HSB135C	56560.0	71390.0	206.5	
HSB136C	55949.0	71900.0	217.8	
HSB137C	55700.0	72269.0	220.9	
HSB139C	57374.0	71129.0	214.5	
HSB140C	56551.0	70049.0	206.2	
HSB141C	59170.0	71196.0	229.6	
HSB142C	53505.0	73119.0	198.9	
HSB143C	52773.0	73738.0	210.0	
HSB145C	57769.0	71098.0	214.0	
HSB146C	58473.0	70471.0	210.2	
HSB148C	55344.0	70151.0	215.0	202.0 <-- original data
HSB151C	54014.0	72997.0	208.7	
HSB152C	54346.0	72012.0	199.2	
P 27C	64004.0	70391.0	245.2	
SBG 2	64939.0	74570.0	237.6	
YSC 4C	65901.0	77059.0	227.5	

Table A8. (cont'd)

Well Label	SRS East (ft)	SRS North (ft)	Head (ft)	
ZW 2	54388.0	80701.0	207.1	
ZW 3	57078.0	80746.0	201.1	
S-6	53222.0	73440.0	204.6	
4Mile_Br	50029.3	72800.3	185.3	180.3 added 5'
4Mile_Br	50312.7	72847.3	185.8	180.8 |
4Mile_Br	50615.8	72896.9	186.4	181.4 |
4Mile_Br	50896.9	72994.3	186.9	181.9 v
4Mile_Br	51118.2	73101.0	187.4	182.4
4Mile_Br	51341.6	73101.1	187.8	182.8
4Mile_Br	51559.4	73057.5	188.2	183.2
4Mile_Br	51788.8	73046.8	188.6	183.6
4Mile_Br	52022.8	73008.2	189.1	184.1
4Mile_Br	52296.2	72960.0	189.6	184.6
4Mile_Br	52472.9	72918.5	189.9	184.9
4Mile_Br	52747.9	72774.8	190.4	185.4
4Mile_Br	52936.6	72630.3	190.8	185.8
4Mile_Br	53122.8	72540.2	193.0	187.0
4Mile_Br	53300.4	72471.1	195.0	190.0
4Mile_Br	53529.7	72301.9	195.6	190.6
4Mile_Br	53780.8	72088.7	196.2	191.2
4Mile_Br	53860.6	71911.3	196.6	191.6
4Mile_Br	53976.6	71778.1	196.9	191.9
4Mile_Br	54156.8	71663.4	197.5	192.5
4Mile_Br	54479.6	71493.9	198.5	193.5
4Mile_Br	54762.3	71307.2	199.6	194.6
4Mile_Br	54989.8	71037.5	200.9	195.9
4Mile_Br	55215.6	70874.7	201.9	196.9
4Mile_Br	55557.6	70871.5	203.1	198.1
4Mile_Br	55859.7	70814.2	203.6	198.6
4Mile_Br	56177.0	70737.8	204.2	199.2
4Mile_Br	56555.9	70592.3	204.9	199.9
4Mile_Br	56906.4	70491.2	205.8	200.8
PseudoDa	51750.	72850.	190.	185.
PseudoDa	51942.	72740.	195.	187.5
PseudoDa	52100.	72600.	205.	190.
PseudoDa	52368.	72425.	215.	191.25
PseudoDa	52690.	72190.	215.	192.5
PseudoDa	52966.	71990.	215.	193.75
PseudoDa	53300.	71750.	215.	195.
PseudoDa	53589.	71523.	215.	196.25
PseudoDa	53917.	71285.	215.	197.5
PseudoDa	54270.	71031.	215.	198.75

Table A9. Hydraulic head data used to create a head contour map for the Gordon aquifer (Figure 16).

Well Label	SRS East (ft)	SRS North (ft)	Head (ft)
BGO 6A	58316.0	76487.0	159.0
BGO 8A	57618.0	76569.0	160.5
BGO 8AR	57617.0	76598.0	160.2
BGO 9AA	57371.0	76975.0	157.7
BGO 10A	57050.0	76805.0	169.0
BGO 10AA	56990.0	76997.0	157.9
BGO 10AR	57063.0	76806.0	158.6
BGO 12A	56250.0	76804.0	181.0
BGO 12AR	56259.0	76803.0	158.0
BGO 14A	55838.0	76377.0	157.7
BGO 14AR	55788.0	76351.0	159.7
BGO 16A	56194.0	75757.0	160.7
BGO 16AR	56217.0	75743.0	161.3
BGO 18A	56699.0	75599.0	160.8
BGO 25A	55668.0	76158.0	160.3
BGO 26A	55014.0	76144.0	159.5
BGO 29A	54103.0	75560.0	159.5
BGO 41A	55403.0	76469.0	158.6
BGO 43A	56253.0	77061.0	158.5
BGO 43AA	56268.0	77066.0	156.8
BGO 44A	57851.0	76755.0	158.6
BGO 44AA	57880.0	76757.0	158.7
BGO 45A	54550.0	75830.0	160.9
BGO 47A	54914.0	74728.0	162.7
BGO 49A	56205.0	73902.0	165.6
BGO 50A	54179.0	75201.0	160.1
BGX 1A	58590.0	76831.0	161.5
BGX 4A	57215.0	77879.0	155.4
FSB 76A	51391.0	76131.0	154.6
FSB 76B	51394.0	76122.0	151.1
FSB 78A	50172.0	74757.0	155.3
FSB 78B	50178.0	74765.0	153.7
FSB 79A	50149.0	73664.0	157.4
FSB 79B	50159.0	73666.0	157.2
FSB 87A	50115.0	75601.0	153.3
FSB 87B	50104.0	75597.0	150.4
FSB 96A	49778.0	74882.0	152.1
FSB 96AR	49746.0	74914.0	153.1
FSB 97A	49965.0	75171.0	151.6
FSB 98A	50121.0	75389.0	150.4
FSB 98AR	50105.0	75362.0	152.0
FSB 99A	50314.0	75675.0	150.2
FSB100A	50958.0	75534.0	150.9
FSB101A	51191.0	75719.0	151.0
FSB112A	48809.0	74231.0	153.6
FSB113A	51068.0	74167.0	158.6
FSB114A	52046.0	75297.0	155.5
FSB120A	49175.0	75538.0	148.3
HC 1A	61867.0	71755.0	175.8
HC 2A	61866.0	71794.0	176.3
HC 2B	61876.0	71785.0	176.0
HSB 65A	58436.0	72436.0	170.4

Table A9. (cont'd)

Well Label	SRS East (ft)	SRS North (ft)	Head (ft)
HSB 68A	56892.0	71526.0	171.0
HSB 69A	56465.0	71549.0	171.4
HSB 83A	58606.0	71648.0	172.5
HSB 84A	56359.0	71586.0	171.2
HSB 85A	58943.0	73791.0	168.3
HSB 86A	55985.0	72520.0	167.8
HSB117A	55170.0	72733.0	166.3
HSB118A	55775.0	72696.0	166.8
HSB119A	56100.0	73082.0	166.2
HSB120A	56431.0	73395.0	165.6
HSB121A	57389.0	72024.0	170.8
HSB122A	57747.0	72195.0	170.5
HSB123A	58124.0	72189.0	171.8
HSB124A	58514.0	72199.0	191.7
HSB124AR	58531.0	72202.0	172.4
HSB139A	57365.0	71127.0	172.8
HSB140A	56535.0	70050.0	175.8
HSB141A	59168.0	71213.0	175.0
HSB144A	56200.0	71892.0	170.9
HSB146A	58454.0	70478.0	176.1
P 27B	64000.0	70405.0	181.2
YSC 1A	65438.0	78039.0	161.3
YSC 2A	66100.0	78311.0	162.6
YSC 5A	67134.0	74295.0	180.5

Table A10. Hydraulic head targets used to calibrate flow model and residuals.

Upper Three Runs aquifer; "upper" aquifer zone:

Well ID	FACT	Data	Residual
BG52	229.87	229.50	0.37
BG53	229.05	229.30	-0.25
BG54	227.97	228.50	-0.53
BG55	226.60	227.10	-0.50
BG56	224.85	227.60	-2.75
BG57	226.09	225.90	0.19
BG58	228.14	227.30	0.84
BG59	229.09	230.00	-0.91
BG60	229.24	231.00	-1.76
BG61	232.26	233.10	-0.84
BG62	233.27	234.30	-1.03
BG63	238.66	236.60	2.06
BG64	241.48	239.40	2.08
BG65	242.26	237.40	4.86
BG66	242.06	236.50	5.56
BG67	241.68	236.70	4.98
BG104	outside	224.60	
BG107	outside	235.80	
BG108	outside	238.80	
BG109	outside	240.40	
BG110	outside	241.40	
BGO1D	outside	238.60	
BGO2D	outside	238.60	
BGO3D	outside	235.80	
BGO4D	outside	232.40	
BGO5D	outside	231.30	
BGO6D	outside	231.50	
BGO7D	outside	234.20	
BGO8D	outside	234.40	
BGO9D	outside	231.80	
BGO10D	outside	231.90	
BGO10DR	outside	232.50	
BGO11D	outside	231.00	
BGO12D	outside	230.80	
BGO13D	outside	230.00	
BGO14DR	outside	231.70	
BGO15D	230.53	229.60	0.93
BGO16D	230.63	230.70	-0.07
BGO17D	231.42	230.70	0.72
BGO17DR	231.45	232.90	-1.45
BGO18D	outside	231.90	
BGO19D	outside	232.10	
BGO20D	233.46	234.10	-0.64
BGO21D	236.14	234.70	1.44
BGO22D	235.55	232.40	3.15
BGO22DR	240.16	237.90	2.26
BGO23D	241.92	235.90	6.02
BGO24D	outside	236.70	
BGO26D	228.83	227.70	1.13
BGO27D	227.05	227.40	-0.35
BGO28D	225.27	226.10	-0.83

Table A10. (cont'd)

Upper Three Runs aquifer; "upper" aquifer zone:

Well ID	FACT	Data	Residual
BGO29D	224.33	227.50	-3.17
BGO30D	224.87	225.70	-0.83
BGO31D	226.15	226.60	-0.45
BGO32D	227.86	227.50	0.36
BGO33D	229.14	230.20	-1.06
BGO34D	229.30	232.80	-3.50
BGO35D	233.76	234.30	-0.54
BGO36D	238.84	236.40	2.44
BGO37D	241.46	237.70	3.76
BGO38D	241.61	235.30	6.31
BGO39D	241.99	235.00	6.99
BGO40D	227.39	223.60	3.79
BGO44D	outside	232.70	
BGO45D	226.86	228.80	-1.94
BGO46D	223.72	226.40	-2.68
BGO47D	225.19	227.40	-2.21
BGO48D	225.38	227.80	-2.42
BGO49D	230.29	235.80	-5.51
BGO50D	223.28	226.20	-2.92
BGX1D	outside	230.00	
BGX9D	outside	227.30	
BGX10D	outside	226.60	
BGX11D	outside	236.80	
BGX12D	outside	240.40	
BRR1D	outside	216.60	
BRR2D	outside	215.40	
BRR3D	outside	215.10	
BRR4D	outside	214.80	
BRR5D	outside	215.10	
FAC3	outside	230.50	
FAC4	outside	228.90	
FAC5	outside	224.30	
FAC5P	outside	230.60	
FAC7	outside	221.80	
FAC8	outside	226.50	
FAL1	outside	218.70	
FAL2	outside	217.10	
FCA1N	outside	299.20	
FCA2C	outside	298.00	
FCA2D	outside	225.40	
FCA9D	outside	225.60	
FCA10A	outside	225.30	
FCA10C	outside	302.30	
FCA10D	outside	226.50	
FCA16A	outside	225.20	
FCA16D	outside	225.20	
FCA16T	outside	297.60	
FCA19D	outside	217.00	
FCB2	230.27	231.00	-0.73
FCB3	228.38	223.20	5.18
FCB5	228.75	228.50	0.25
FCB6	228.90	228.90	0.00
FET1D	223.02	223.40	-0.38

Table A10. (cont'd)

Upper Three Runs aquifer; "upper" aquifer zone:

Well ID	FACT	Data	Residual
FET2D	221.55	222.00	-0.45
FET3D	221.41	222.00	-0.59
FET4D	221.83	222.60	-0.77
FSB76	outside	218.30	
FSB77	outside	212.70	
FSB78	outside	209.20	
FSB79	outside	202.00	
FSB87D	outside	213.50	
FSB88D	216.17	215.50	0.67
FSB89D	215.35	214.90	0.45
FSB90D	214.17	214.50	-0.33
FSB91D	213.08	212.90	0.18
FSB92D	outside	211.50	
FSB93D	outside	210.80	
FSB94DR	outside	210.60	
FSB95D	outside	209.70	
FSB95DR	outside	210.60	
FSB97D	outside	210.50	
FSB98D	outside	212.90	
FSB99D	outside	211.80	
FSB104D	outside	203.70	
FSB105D	outside	208.50	
FSB105DR	outside	211.40	
FSB106D	204.59	206.90	-2.31
FSB107D	213.37	213.20	0.17
FSB108D	outside	217.20	
FSB109D	outside	213.10	
FSB110D	205.42	205.10	0.32
FSB111D	215.27	214.50	0.77
FSB112D	outside	206.70	
FSB113D	203.99	208.00	-4.01
FSB114D	216.11	217.40	-1.29
FSB115D	outside	191.80	
FSB116D	outside	192.20	
FSB117D	204.09	205.50	-1.41
FSB118D	210.73	211.50	-0.77
FSB119D	208.45	208.90	-0.45
FSB120D	outside	210.40	
FSB121DR	outside	208.50	
FSB122D	outside	204.30	
FSB123D	210.96	212.70	-1.74
FSL1D	outside	225.20	
FSL2D	outside	226.70	
FSL3D	outside	224.20	
FSL4D	outside	218.90	
FSL5D	outside	222.40	
FSL6D	outside	221.20	
FSL7D	outside	220.50	
FSL8D	218.79	219.70	-0.91
FSL9D	217.05	218.60	-1.55
FSS1D	222.13	223.50	-1.37
FSS2D	221.48	223.00	-1.52
FSS3D	219.21	220.70	-1.49

Table A10. (cont'd)

Upper Three Runs aquifer; "upper" aquifer zone:

Well ID	FACT	Data	Residual
FSS4D	219.27	218.30	0.97
FTF1	224.73	229.40	-4.67
FTF2	224.52	225.30	-0.78
FTF3	224.25	224.10	0.15
FTF4	224.37	224.40	-0.03
FTF5	224.06	225.10	-1.04
FTF6	223.88	224.10	-0.22
FTF8	224.27	227.50	-3.23
FTF9	223.95	223.60	0.35
FTF10	223.80	223.80	0.00
FTF11	223.21	225.20	-1.99
FTF12	223.22	226.80	-3.58
FTF13	223.45	224.70	-1.25
FTF15	223.85	226.10	-2.25
FTF16	222.95	223.10	-0.15
FTF17	223.11	223.00	0.11
FTF18	223.20	222.80	0.40
FTF19	222.87	222.20	0.67
FTF20	222.32	221.80	0.52
FTF21	222.26	222.80	-0.54
FTF22	222.38	221.60	0.78
FTF23	222.19	222.00	0.19
FTF25A	223.69	223.30	0.39
FTF26	223.61	223.30	0.31
FTF27	223.47	223.40	0.07
HAC1	outside	269.10	
HAC2	outside	268.60	
HAC3	outside	268.90	
HAC4	outside	269.20	
HAP1	outside	270.70	
HAP2	outside	270.10	
HC1E	outside	275.00	
HC2E	outside	270.50	
HC2F	outside	274.30	
HC4B	outside	268.00	
HC5B	outside	256.10	
HC6B	outside	268.90	
HC11C	outside	236.60	
HCA1	outside	268.90	
HCA3	outside	268.70	
HCA4	outside	268.60	
HCB1	outside	262.90	
HCB2	outside	267.80	
HCB3	outside	266.10	
HET1D	outside	267.40	
HET2D	outside	258.20	
HET3D	outside	258.60	
HET4D	outside	259.00	
HR311	outside	259.30	
HR313	outside	258.10	
HR811	outside	245.80	
HR812	outside	239.30	
HR813	outside	237.80	

Table A10. (cont'd)

Upper Three Runs aquifer; "upper" aquifer zone:

Well ID	FACT	Data	Residual
HR814	outside	244.00	
HSB65	outside	234.30	
HSB65C	outside	233.20	
HSB66	227.09	226.90	0.19
HSB67	outside	225.20	
HSB68	outside	224.40	
HSB69	220.26	220.70	-0.44
HSB70	220.08	227.50	-7.42
HSB71	218.12	225.10	-6.98
HSB83D	outside	225.80	
HSB84D	217.10	219.80	-2.70
HSB85C	outside	239.00	
HSB86D	220.29	225.90	-5.61
HSB100D	outside	233.30	
HSB101D	outside	230.80	
HSB102D	outside	228.00	
HSB103D	outside	226.00	
HSB104D	outside	225.40	
HSB105D	outside	225.80	
HSB106D	outside	226.30	
HSB107D	outside	225.10	
HSB108D	outside	223.90	
HSB109D	outside	223.40	
HSB110D	outside	222.80	
HSB111D	220.86	222.60	-1.74
HSB111E	220.85	222.70	-1.85
HSB112D	220.94	223.70	-2.76
HSB112E	220.89	223.60	-2.71
HSB113D	220.41	223.60	-3.19
HSB114D	220.86	224.60	-3.74
HSB115D	221.28	225.50	-4.22
HSB116D	223.58	226.40	-2.82
HSB117D	217.26	224.80	-7.54
HSB125D	outside	221.60	
HSB126D	outside	204.90	
HSB127D	outside	218.50	
HSB129D	209.75	208.50	1.25
HSB130D	201.64	200.10	1.54
HSB131D	outside	205.20	
HSB132D	outside	221.70	
HSB133D	outside	234.80	
HSB134D	outside	222.50	
HSB135D	outside	218.60	
HSB136D	215.67	221.50	-5.83
HSB137D	217.19	223.00	-5.81
HSB138D	220.63	224.00	-3.37
HSB139D	outside	223.30	
HSB140D	outside	215.40	
HSB141D	outside	243.50	
HSB142D	198.24	198.30	-0.06
HSB143D	208.60	213.90	-5.30
HSB145D	outside	221.70	
HSB146D	outside	223.00	

Table A10. (cont'd)

Upper Three Runs aquifer; "upper" aquifer zone:

Well ID	FACT	Data	Residual
HSB147D	228.22	234.00	-5.78
HSB148D	outside	214.90	
HSB149D	outside	224.50	
HSB150D	outside	228.10	
HSB151D	208.84	208.00	0.84
HSB152D	205.56	206.40	-0.84
HSL1D	outside	235.60	
HSL2D	outside	242.10	
HSL3D	outside	250.00	
HSL4D	outside	261.50	
HSL5D	outside	263.80	
HSL6D	outside	260.60	
HSL7D	outside	260.30	
HSL8D	outside	261.50	
HSS1D	outside	268.60	
HSS2D	outside	267.20	
HSS3D	outside	281.50	
HTF1	outside	271.80	
HTF2	outside	273.00	
HTF4	outside	272.50	
HTF5	outside	277.60	
HTF6	outside	276.40	
HTF7	outside	275.60	
HTF8	outside	274.50	
HTF9	outside	271.50	
HTF10	outside	270.80	
HTF11	outside	271.60	
HTF12	outside	270.70	
HTF13	outside	273.40	
HTF14	outside	273.20	
HTF15	outside	272.80	
HTF16	outside	269.00	
HTF17	outside	262.80	
HTF18	outside	270.50	
HTF19	outside	268.50	
HTF20	outside	267.30	
HTF21	outside	268.50	
HTF22	outside	273.90	
HTF23	outside	274.10	
HTF24	outside	273.90	
HTF25	outside	273.90	
HTF26	outside	274.00	
HTF27	outside	274.20	
HTF28	outside	275.70	
HTF29	outside	274.20	
HTF31	outside	274.60	
HTF32	outside	273.90	
HTF34	outside	272.60	
MGA36	241.57	238.40	3.17
MGC9	230.68	229.60	1.08
MGC11	230.75	232.20	-1.45
MGC23	232.25	236.40	-4.15
MGC32	242.18	245.70	-3.52

Table A10. (cont'd)

Upper Three Runs aquifer; "upper" aquifer zone:

Well ID	FACT	Data	Residual
MGE9	231.15	229.70	1.45
MGE21	232.06	235.10	-3.04
MGG15	231.42	233.10	-1.68
MGG19	231.41	232.90	-1.49
MGG23	233.62	235.80	-2.18
MGG28	239.75	237.20	2.55
MGG36	242.68	238.80	3.88
NBG1	outside	224.10	
NBG2	outside	224.80	
NBG3	outside	218.10	
NBG4	outside	217.10	
NBG5	outside	217.60	
P27D	outside	266.90	
SBG1	outside	237.80	
SBG2	outside	237.60	
SBG3	outside	236.90	
SBG4	outside	240.60	
SBG5	outside	249.10	
SBG6	outside	244.20	
SCA2	outside	242.20	
SCA3	outside	241.30	
SCA3A	outside	270.90	
SCA4	outside	241.70	
SCA4A	outside	269.10	
SCA5	outside	242.00	
SCA6	outside	242.20	
SLP1	outside	244.80	
SLP2	outside	244.40	
YSC1C	outside	217.50	
YSC2D	outside	217.10	
Z2	216.76	218.10	-1.34
Z3	213.40	212.20	1.20
Z8	outside	218.00	
Z9	outside	214.80	
Z11	outside	296.40	
Z12	outside	274.40	
Z13	outside	274.60	
Z15	outside	263.70	
ZBG1	outside	234.10	
ZBG1A	outside	279.70	
ZBG2	outside	221.50	
ZDT1	outside	239.50	
ZDT2	outside	241.10	
ZW4	outside	232.60	
ZW5	227.28	227.50	-0.22
ZW7	outside	265.80	
ZW8	outside	270.80	
ZW9	outside	251.90	
ZW10	outside	249.70	
CC9	outside	214.90	
CC13	212.76	216.40	-3.64
CC17	214.84	220.00	-5.16
GG17	210.68	207.80	2.88

Table A10. (cont'd)

Upper Three Runs aquifer; "upper" aquifer zone:

Well ID	FACT	Data	Residual
GG21	212.30	211.80	0.50
M5	224.75	228.60	-3.85
M9	226.14	228.00	-1.86
M17	228.17	235.00	-6.83
M21	230.83	237.90	-7.07
Q5	221.39	226.00	-4.61
Q9	223.07	226.90	-3.83
Q13	224.20	227.40	-3.20
Q17	231.63	241.60	-9.97
Q21	226.93	233.10	-6.17
S3	219.14	224.00	-4.86
S4	216.51	222.10	-5.59
S5	outside	221.00	
S6	206.49	204.60	1.89
S9	220.06	226.10	-6.04
S15	222.82	231.50	-8.68
S16	220.23	226.20	-5.97
U5	218.20	223.00	-4.80
U9	219.12	223.80	-4.68
U13	220.77	232.40	-11.63
U17	222.17	226.20	-4.03
U21	223.06	227.30	-4.24
Y7	213.68	218.20	-4.52
Y9	214.42	220.80	-6.38
Y13	215.84	223.20	-7.36
Y17	217.75	224.70	-6.95
Y21	219.18	224.00	-4.82

Upper Three Runs aquifer; "lower" aquifer zone:

Well ID	FACT	Data	Residual
BG91	outside	219.10	
BG92	outside	209.00	
BG93	outside	201.10	
BG94	outside	191.40	
BG95	outside	193.30	
BG96	outside	198.50	
BG101	outside	195.70	
BG103	outside	200.40	
BG122	outside	211.30	
BGO5C	outside	216.60	
BGO6B	outside	219.70	
BGO6C	outside	220.10	
BGO8C	outside	225.40	
BGO10B	outside	220.90	
BGO10C	outside	220.20	
BGO12C	outside	220.00	
BGO12CR	outside	222.40	
BGO13DR	outside	232.20	
BGO14C	outside	221.00	
BGO14CR	outside	224.90	
BGO16B	220.89	220.30	0.59
BGO27C	222.86	220.30	2.56

Table A10. (cont'd)

Upper Three Runs aquifer; "lower" aquifer zone:

Well ID	FACT	Data	Residual
BGO29C	221.01	223.90	-2.89
BGO30C	220.53	219.10	1.43
BGO31C	220.62	225.50	-4.88
BGO33C	222.06	224.90	-2.84
BGO35C	224.77	228.30	-3.53
BGO37C	226.81	229.10	-2.29
BGO42C	outside	224.40	
BGO43CR	outside	226.60	
BGO43D	outside	232.30	
BGO44B	outside	221.90	
BGO44C	outside	221.70	
BGO45B	223.22	220.60	2.62
BGO45C	223.57	223.90	-0.33
BGO46B	218.71	218.90	-0.19
BGO46C	219.49	221.10	-1.61
BGO47C	220.39	223.70	-3.31
BGO48C	220.51	224.50	-3.99
BGO49C	224.01	229.00	-4.99
BGO50C	219.27	219.50	-0.23
BGX1C	outside	216.90	
BGX2B	outside	213.30	
BGX2D	outside	216.30	
BGX3D	outside	216.10	
BGX4C	outside	215.90	
BGX4D	outside	217.00	
BGX5D	outside	210.60	
BGX6D	outside	207.60	
BGX7D	outside	207.70	
BGX8DR	outside	206.50	
BGX12C	outside	235.70	
FAC4	outside	228.90	
FBP1A	outside	206.80	
FBP4	outside	211.60	
FNB1	outside	210.80	
FNB2	outside	207.00	
FNB3	outside	209.20	
FNB4	outside	213.10	
FSB76C	outside	212.70	
FSB78C	outside	207.70	
FSB79C	outside	196.60	
FSB87C	outside	208.40	
FSB88C	213.23	211.90	1.33
FSB89C	212.65	211.40	1.25
FSB90C	212.43	210.30	2.13
FSB91C	210.63	210.30	0.33
FSB93C	outside	208.40	
FSB94C	outside	207.70	
FSB95C	outside	205.90	
FSB95CR	outside	208.20	
FSB97C	outside	207.70	
FSB98C	outside	209.20	
FSB99C	outside	209.20	
FSB102C	194.63	195.10	-0.47

Table A10. (cont'd)

Upper Three Runs aquifer; "lower" aquifer zone:

Well ID	FACT	Data	Residual
FSB103C	outside	202.30	
FSB104C	outside	200.50	
FSB105C	outside	207.20	
FSB106C	201.62	201.10	0.52
FSB107C	211.50	209.70	1.80
FSB110C	201.73	201.60	0.13
FSB111C	213.44	211.10	2.34
FSB112C	outside	202.60	
FSB113C	201.00	203.10	-2.10
FSB114C	213.63	213.80	-0.17
FSB115C	outside	184.20	
FSB116C	outside	189.60	
FSB120C	outside	206.80	
FSB121C	outside	205.00	
FSB122C	outside	200.50	
FSB123C	207.94	210.80	-2.86
HC1B	outside	254.90	
HC2C	outside	254.20	
HC2D	outside	256.30	
HC4A	outside	244.70	
HC5A	outside	213.80	
HC6A	outside	252.20	
HC10B	outside	208.40	
HC12B	outside	241.60	
HMD1D	outside	210.90	
HMD2D	outside	202.30	
HMD3D	outside	201.80	
HMD4D	outside	201.90	
HSB65B	outside	224.70	
HSB68B	outside	217.80	
HSB68C	outside	218.60	
HSB70C	216.71	223.90	-7.19
HSB71C	215.21	223.10	-7.89
HSB83B	outside	223.20	
HSB83C	outside	225.10	
HSB84B	212.88	211.20	1.68
HSB84C	214.35	214.50	-0.15
HSB85B	outside	233.90	
HSB86B	215.95	223.00	-7.05
HSB86C	220.36	225.80	-5.44
HSB100C	outside	226.30	
HSB101C	outside	225.30	
HSB102C	outside	224.60	
HSB103C	outside	223.60	
HSB104C	outside	220.60	
HSB105C	outside	219.70	
HSB106C	outside	221.80	
HSB107C	outside	219.50	
HSB108C	outside	218.90	
HSB109C	outside	219.00	
HSB110C	outside	219.40	
HSB111C	217.84	220.70	-2.86
HSB112C	218.50	222.10	-3.60

Table A10. (cont'd)

Upper Three Runs aquifer; "lower" aquifer zone:

Well ID	FACT	Data	Residual
HSB113C	217.39	222.60	-5.21
HSB114C	220.65	224.40	-3.75
HSB115C	221.43	225.20	-3.77
HSB116C	221.88	225.80	-3.92
HSB117C	213.52	222.60	-9.08
HSB125C	outside	223.40	
HSB126C	outside	203.60	
HSB127C	outside	210.10	
HSB129C	211.28	205.40	5.88
HSB131C	outside	203.40	
HSB132C	outside	222.10	
HSB133C	outside	230.40	
HSB134C	outside	220.80	
HSB135C	outside	206.50	
HSB136C	213.45	217.80	-4.35
HSB137C	214.02	220.90	-6.88
HSB139C	outside	214.50	
HSB140C	outside	206.20	
HSB141C	outside	229.60	
HSB142C	204.36	198.90	5.46
HSB143C	206.63	210.00	-3.37
HSB145C	outside	214.00	
HSB146C	outside	210.20	
HSB151C	208.15	208.70	-0.55
HSB152C	206.00	199.20	6.80
P27C	outside	245.20	
SBG2	outside	237.60	
YSC4C	outside	227.50	
ZW2	outside	207.10	
ZW3	outside	201.10	

Gordon aquifer:

Well ID	FACT	Data	Residual
BGO6A	outside	159.00	
BGO8A	outside	160.50	
BGO8AR	outside	160.20	
BGO9AA	outside	157.70	
BGO10A	outside	169.00	
BGO10AA	outside	157.90	
BGO10AR	outside	158.60	
BGO12A	outside	181.00	
BGO12AR	outside	158.00	
BGO14A	outside	157.70	
BGO14AR	outside	159.70	
BGO16A	161.27	160.70	0.57
BGO16AR	161.28	161.30	-0.02
BGO18A	outside	160.80	
BGO25A	159.18	160.30	-1.12
BGO26A	159.09	159.50	-0.41
BGO29A	159.54	159.50	0.04
BGO41A	outside	158.60	
BGO43A	outside	158.50	

Table A10. (cont'd)

Gordon aquifer:

Well ID	FACT	Data	Residual
BGO43AA	outside	156.80	
BGO44A	outside	158.60	
BGO44AA	outside	158.70	
BGO45A	159.53	160.90	-1.37
BGO47A	161.87	162.70	-0.83
BGO49A	164.73	165.60	-0.87
BGO50A	160.12	160.10	0.02
BGX1A	outside	161.50	
BGX4A	outside	155.40	
FSB76A	outside	154.60	
FSB76B	outside	151.10	
FSB78A	outside	155.30	
FSB78B	outside	153.70	
FSB79A	outside	157.40	
FSB79B	outside	157.20	
FSB87A	outside	153.30	
FSB87B	outside	150.40	
FSB96A	outside	152.10	
FSB96AR	outside	153.10	
FSB97A	outside	151.60	
FSB98A	outside	150.40	
FSB98AR	outside	152.00	
FSB99A	outside	150.20	
FSB100A	outside	150.90	
FSB101A	151.19	151.00	0.19
FSB112A	outside	153.60	
FSB113A	157.72	158.60	-0.88
FSB114A	156.06	155.50	0.56
FSB120A	outside	148.30	
HC1A	outside	175.80	
HC2A	outside	176.30	
HC2B	outside	176.00	
HSB65A	outside	170.40	
HSB68A	outside	171.00	
HSB69A	171.45	171.40	0.05
HSB83A	outside	172.50	
HSB84A	171.24	171.20	0.04
HSB85A	outside	168.30	
HSB86A	168.23	167.80	0.43
HSB117A	167.02	166.30	0.72
HSB118A	167.59	166.80	0.79
HSB119A	166.80	166.20	0.60
HSB120A	166.16	165.60	0.56
HSB121A	outside	170.80	
HSB122A	outside	170.50	
HSB123A	outside	171.80	
HSB124A	outside	191.70	
HSB124AR	outside	172.40	
HSB139A	outside	172.80	
HSB140A	outside	175.80	
HSB141A	outside	175.00	
HSB144A	170.21	170.90	-0.69
HSB146A	outside	176.10	

Table A10. (cont'd)

Gordon aquifer:

Well ID	FACT	Data	Residual
P27B	outside	181.20	
YSC1A	outside	161.30	
YSC2A	outside	162.60	
YSC5A	outside	180.50	